Band **54** (2008)

Late Neoproterozoic – Early Palaeozoic volcano-sedimentary successions of the Teplá-Barrandian unit (Bohemian Massif)

GEOLOGICA SAXONICA
Journal of Central European Geology

Drost, K.

Sources and geotectonic setting of Late Neoproterozoic – Early Palaeozoic volcano-sedimentary successions of the Teplá-Barrandian unit (Bohemian Massif): Evidence from petrographical, geochemical, and isotope analyses

GEOLOGICA SAXONICA
Journal of Central European Geology 54 (2008) 1–168

Sources and geotectonic setting of Late Neoproterozoic – Early Palaeozoic volcano-sedimentary successions of the Teplá-Barrandian unit (Bohemian Massif): Evidence from petrographical, geochemical, and isotope analyses

Petrographische, geochemische und isotopengeochemische Analysen zur Ermittlung von Provenance und geotektonischem Setting spätneoproterozoisch - frühpaläozoischer vulkano-sedimentärer Abfolgen des Teplá-Barrandiums (Böhmisches Massiv)

Kerstin Drost

Staatliche Naturhistorische Sammlungen Dresden, Museum für Mineralogie und Geologie
Königsbrücker Landstraße 159, D-01109 Dresden, Germany
tbu2008@gmx.de

Summary

The Teplá-Barrandian unit is situated in the centre of the Bohemian Massif at the eastern termination of the European Variscides. The geological history of the Teplá-Barrandian unit started in the late Neoproterozoic, when volcanic, pyroclastic and – chiefly siliciclastic – sedimentary rocks formed in a magmatic arc setting at the margin of Gondwana. The Neoproterozoic basement is unconformably overlain by Early Cambrian to Mid-Devonian volcano-sedimentary successions. Both the Neoproterozoic basement and the Palaeozoic cover sequence were dislocated from their original tectonostratigraphic frame during long-term plate tectonic processes and became incorporated into the Variscan orogenic belt.

In this study, Early Palaeozoic siliciclastic sedimentary rocks were investigated by means of geochemical, whole rock Nd-Sr-Pb, and detrital zircon U-Pb analyses, respectively, to constrain their provenance and the geotectonic setting in which they were deposited. Since Neoproterozoic rocks and Early Palaeozoic volcanics represent potential source rocks for the Cambrian and Ordovician detrital sediments, samples from these complexes were included. Furthermore, the geochemical composition of volcanic rocks was interpreted with regard to magma sources and geotectonic setting of the volcanism.

The Neoproterozoic siliciclastic rocks of the Teplá-Barrandian unit were deposited in various basins within a magmatic arc setting at the NW-African Gondwana margin and show a clear relation with the Cadomian terranes of Central and Western Europe. Whole rock Nd-Sr-Pb isotope compositions and U-Pb detrital zircon ages of the petrographically and geochemically immature detrital sediments point to considerable involvement of old crustal detritus for all analysed rocks. A sample from the Blovice Formation (= older part of the Neoproterozoic succession) yielding a maximum sedimentation age of 592±4 Ma revealed the oldest T_{DM} (2.2 Ga), a maximum in pre-Ediacaran detrital zircon (~670–630 Ma), and a substantial amount of Palaeoproterozoic and Archean detrital zircon (38 %). Cathodoluminescence images and datings of cores and overgrowth domains of the Archean grains, however, revealed that they were

not delivered by pristine Archean rocks. Instead, Palaeoproterozoic and Neoproterozoic overprint is characteristic. In combination with previously published characteristics, these rocks can be interpreted to represent deposits of an incipient marginal basin that were derived from recycled Pan-African lithologies of the Trans-Saharan mobile belt. Neoproterozoic greywackes of the (presently) neighbouring unit have younger T_{DM} (1.5–1.8 Ga) and are associated with volcanics of MORB affinity, which is compatible with derivation of the detrital material from a magmatic arc that developed on NW-African continental crust and deposition of the greywackes in a back-arc basin that was floored by oceanic crust. The youngest analysed rocks of the Teplá-Barrandian Neoproterozoic basement are represented by shales and greywackes of the Štěchovice Group. Homogenous whole rock Nd-Sr-Pb isotope signatures and geochemical compositions in combination with a maximum in Ediacaran detrital zircon ages (~68 %) point to redeposition processes of immature, magmatic arc derived siliciclastic material prior to sedimentation of the sampled siliciclastics. The maximum sedimentation age of 565±5 Ma that was obtained from greywackes associated with coarse conglomerates, may represent an estimate for the onset of back-arc basin inversion in the Teplá-Barrandian unit. Also the detrital sediments of the Štěchovice Group show considerable involvement of old crustal material, which emphasises the continental nature of the basement of the Cadomian magmatic arc.

Cambrian sediments lying unconformably above Neoproterozoic basement were deposited in a transtensional setting. Sedimentation did not start prior to 529±3 Ma as is indicated by the concordia age calculated from the youngest detrital zircon grains of the basal Cambrian Žitec-Hluboš Formation. Petrographic and geochemical features as well as U-Pb detrital zircon ages of the Cambrian siliciclastics display derivation from the deeply weathered Neoproterozoic magmatic arc and from young mafic rocks represented by extension-related magmatic suites. Whole rock Pb isotope characteristics and detrital zircon ages from older Lower Cambrian siliciclastics suggest contributions from old crustal domains during this time. However, from the upper part of the continental, Lower Cambrian sequence to the Middle Cambrian, there is not much evidence for old crustal material in the source area. The distinctly reduced proportion of Neoproterozoic and pre-Neoproterozoic detrital zircon in the Middle Cambrian siliciclastics suggests a change of the drainage system due to crustal tilting and related screen off of the basin from the old crustal source. Upper Cambrian volcanic rocks are characterised as continental tholeiites and effusive equivalents of A-type granites by means of their geochemical compositions. They were generated during a rifting event that is tracable in many peri-Gondwanan terranes and eventually led to the opening of the Rheic Ocean.

Tremadocian siliciclastics are chiefly derived from the Upper Cambrian volcanic complex as is indicated by their petrographic compositions and their detrital zircon age spectrum. Lower Ordovician sandstones and conglomerates display a volcanic rifted margin provenance. This in combination with the distinct proportion of >620 Ma old Neoproterozoic detrital zircon may be taken as the first indicator of a change in the geotectonic setting from rift basin to passive margin. Younger Ordovician samples display intense weathering of rather felsic, NW-African sources and effective mixing of the detritus prior to deposition at the passive Gondwana margin, which is in sharp contrast to the Cambrian siliciclastics that were derived from rather mafic source rocks. Considerable contributions from old continental crust are revealed by whole rock Nd-Sr-Pb isotope signatures and detrital zircon age spectra of Lower/Middle and Upper Ordovician shale and sandstone samples. Ordovician magmatism is represented by chiefly alkaline basaltoids with intra-plate signature. The magma was derived from low degrees of partial melting of a garnet bearing mantle source, whereas garnet remained as a residue in the source. This style of volcanism occurred until the Devonian and is therefore interpreted to have originated in a stress-related fracture zone within the Gondwanan lithosphere.

Altogether, the new data suggest that the Teplá-Barrandian unit remained at least until the end of the Ordovician – but probably during the entire pre-Variscan Palaeozoic – at the NW-African Gondwana

margin and, therefore, formed part of the southern margin of the Rheic Ocean.

Zusammenfassung

Das Teplá-Barrandium im Zentrum des Böhmischen Massivs befindet sich am östlichen Ende der europäischen Variszide. Das Basement des Teplá-Barrandiums entstand bei einer älteren – der Cadomischen – Gebirgsbildung, die sich im späten Neoproterozoikum am Rand des Superkontinents Gondwana abspielte. Kambrische bis mitteldevonische sedimentäre und vulkanische Gesteine des Teplá-Barrandiums liegen diskordant auf cadomischem Basement.

In vorliegender Arbeit wurden neoproterozoische und frühpaläozoische siliziklastische Gesteine hinsichtlich ihrer petrographischen, geochemischen und isotopengeochemischen Zusammensetzung sowie bezüglich ihrer Altersspektren von detritischen Zirkonen untersucht, um Hinweise auf Liefergebiet und geotektonisches Setting zu erlangen. Proben von paläozoischen Vulkaniten wurden in die Studie einbezogen, da sie potentielle Liefergesteine darstellen und ihre chemische Zusammensetzung das geotektonische Regime ihrer Entstehung wiedergibt.

Die kompositionell und texturell unreifen detritischen Sedimente neoproterozoischen Alters wurden in verschiedenen Becken am NW-afrikanischen Gondwana-Rand abgelagert. Obwohl die Isotopensignaturen aller bearbeiteten Proben auf Eintrag von alter kontinentaler Kruste hinweisen, lassen sich zwei Provenance-Typen unterscheiden. Einerseits lieferte der Kontinent detritisches Material, welches sich vor allem an der kontinentwärtigen Seite des back-arc-Beckens bzw. in einem Riftbecken ablagerte. Andererseits hat Subduktion und damit verbundenes back-arc-Rifting am Kontinentalrand zur Ausbildung eines kontinentalen magmatischen Bogens geführt, der zum Teil aus der gleichen Kruste besteht, wie der Kontinent, aber durch den anhaltenden subduktionsbezogenen Magmatismus auch deutlich jüngere Gesteine enthält. Dieser kontinentale magmatische Bogen repräsentiert im Durchschnitt ein jüngeres Liefergebiet als der Kontinent, was sich in den Isotopensignaturen der Abtragungsprodukte widerspiegelt.

Im frühen Kambrium waren die neoproterozoischen Becken bereits geschlossen, die Subduktion hatte aufgehört und das geotektonische Regime war auf Transtension umgestellt. Die Sedimentation der diskordant auf neoproterozoisch deformiertem Basement liegenden kambrischen Ablagerungen begann bei ~530 Ma. Das Liefergebiet der Konglomerate, Sand-, Silt- und Tonsteine bestand aus dem neoproterozoischen magmatischen Bogen und aus magmatischen Komplexen kambrischen Alters. Letztere stellen Rift-bezogene Magmatite dar, was anhand der geochemischen Signaturen oberkambrischer Vulkanite gezeigt werden konnte. Das kambrische Rifting ist in vielen Gebieten Europas und Nordamerikas nachweisbar und führte zur Entstehung des Rheic Ocean. Das Teplá-Barrandium war ab dem Unteren Ordovizium Teil des südlichen Randes dieses Ozeans. Ordovizische Sand-, Silt- und Tonsteine bestehen aus stark verwittertem Abtragungsmaterial, welches vom NW-afrikanischen Teil Gondwanas stammt und auf dem Schelf des passiven Kontinentalrandes abgelagert wurde. Die geochemischen Signaturen weisen auf felsische Ausgangsgesteine hin, die Isotopendaten auf alte Kruste. Solche Liefergesteine stehen im Gegensatz zu denen der kambrischen Sedimente, die von im Durchschnitt jüngeren und mafischeren Ausgangsgesteinen hergeleitet werden müssen. Sie stimmen aber mit denen einiger neoproterozoischer Sedimente überein, die vom Kontinent geliefert wurden. Die hauptsächlich alkalischen Vulkanite des Ordoviziums haben Intraplatten-Signaturen und stehen wahrscheinlich im Zusammenhang mit tiefen Brüchen in der Lithosphäre, die als Reaktion auf Änderungen des globalen Spannungsfeldes entstehen bzw. reaktiviert werden. Ein Rift-Setting ist für die Generation der Schmelzen nicht wahrscheinlich.

Insgesamt deuten die neuen Daten darauf hin, dass das Teplá-Barrandium bis zum Ende des Ordoviziums – aber wahrscheinlich während seiner gesamten prä-varistischen Entwicklung – mit dem NW-afrikanischen Gondwanarand assoziiert war.

1 Introduction

The Teplá-Barrandian Unit (TBU) of the Bohemian Massif was a part of the Avalonian-Cadomian tectonostratigraphic belt at the margin of West Gondwana during the Late Neoproterozoic – Earliest Cambrian. In the Palaeozoic, the TBU was dislocated from its original tectono-sedimentary position by long-term plate tectonic processes and incorporated in the Variscan (Hercynian) orogen that extends from North America over large parts of Europe to the Urals.

This work is mainly focussed on the Cambro-Ordovician volcano-sedimentary successions of the TBU. Additionally, parts of the Neoproterozoic basement were studied to identify potential sources for Palaeozoic detrital sediments and to highlight changes in the compositions of the siliciclastic sediments, which are caused by shifting geotectonic conditions. Key sections and outcrops were studied during about 3 months of field work and by means of:

- 250 thin sections
- 138 geochemical analyses of sedimentary whole rocks
- 42 geochemical analyses of (sub)volcanic whole rocks
- 22 Nd-Sr-Pb isotopic analyses of sedimentary whole rocks
- 750 U-Pb isotopic analyses of single zircon crystals

Field investigations of sedimentological features such as primary sedimentary structures and grain size distributions were evaluated in terms of depositional mechanisms and environments. Subsequently petrographical and geochemical compositions as well as detrital zircon age spectra and Nd-Sr-Pb isotopic signatures of siliciclastic sediments were analysed to identify sources of the detrital components and to deduce the provenance. Cambrian and Ordovician volcanic complexes were studied geochemically to distinguish their magma sources.

This combination of methods allows the interpretation of the Teplá-Barrandian Late Neoproterozoic to Palaeozoic volcano-sedimentary successions with respect to the geotectonic regime during the Latest Neoproterozoic and Early Palaeozoic and in the context of the peri-Gondwanan terranes.

2 Geological framework

2.1 Boundaries and components

The Neoproterozoic basement of the Teplá-Barrandian Unit (TBU) represents a fragment of Cadomian crust (Chlupáč 1993, Kříbek et al. 2000) that originally formed part of the Avalonian-Cadomian tectono-stratigraphic belt at the margin of West Gondwana (Nance et al. 1991, Nance & Murphy 1994; Fig. 2.1). Palaeozoic overstep sequences (Cambrian and Ordovician to Middle Devonian) unconformably overlie the Cadomian basement. The deposition of sedimentary rocks in two superposed basins was accompanied by magmatic activity and took place in the Cambrian and from the Ordovician to the Givetian (Chlupáč 1993; Fig. 2.3). Long-term plate-tectonic processes caused the dislocation of the TBU from the original tectono-stratigraphic frame and its incorporation into the Variscan (Hercynian) belt of Central Europe. Today the TBU represents a tectono-stratigraphic terrane within the Bohemian Massif (Matte et al. 1990; Fig. 2.2).

Although surrounded by high-grade units of the Moldanubian and Saxothuringian zones (Fig. 2.2), the TBU is preserved as a supracrustal complex that largely escaped Carboniferous high-grade metamorphism. Increasing metamorphism within the TBU towards the west and northwest (e.g., Vejnar 1966) is predominantly related to Cadomian orogenic processes as shown by Pašava & Amov (1993), Dörr et al. (1998), and Zulauf et al. (1999, and references therein). The eastern and south-eastern parts of the TBU are composed of very low-grade to low-grade Neoproterozoic and unmetamorphosed Palaeozoic overstep sequences.

The western and southern boundaries to the adjacent high-grade units are crustal scale shear zones intruded by Variscan granitoids (West Bohemian shear zone, Hoher Bogen shear zone, Central Bohe-

GEOLOGICA SAXONICA
Journal of Central European Geology 54 (2008) 1–168

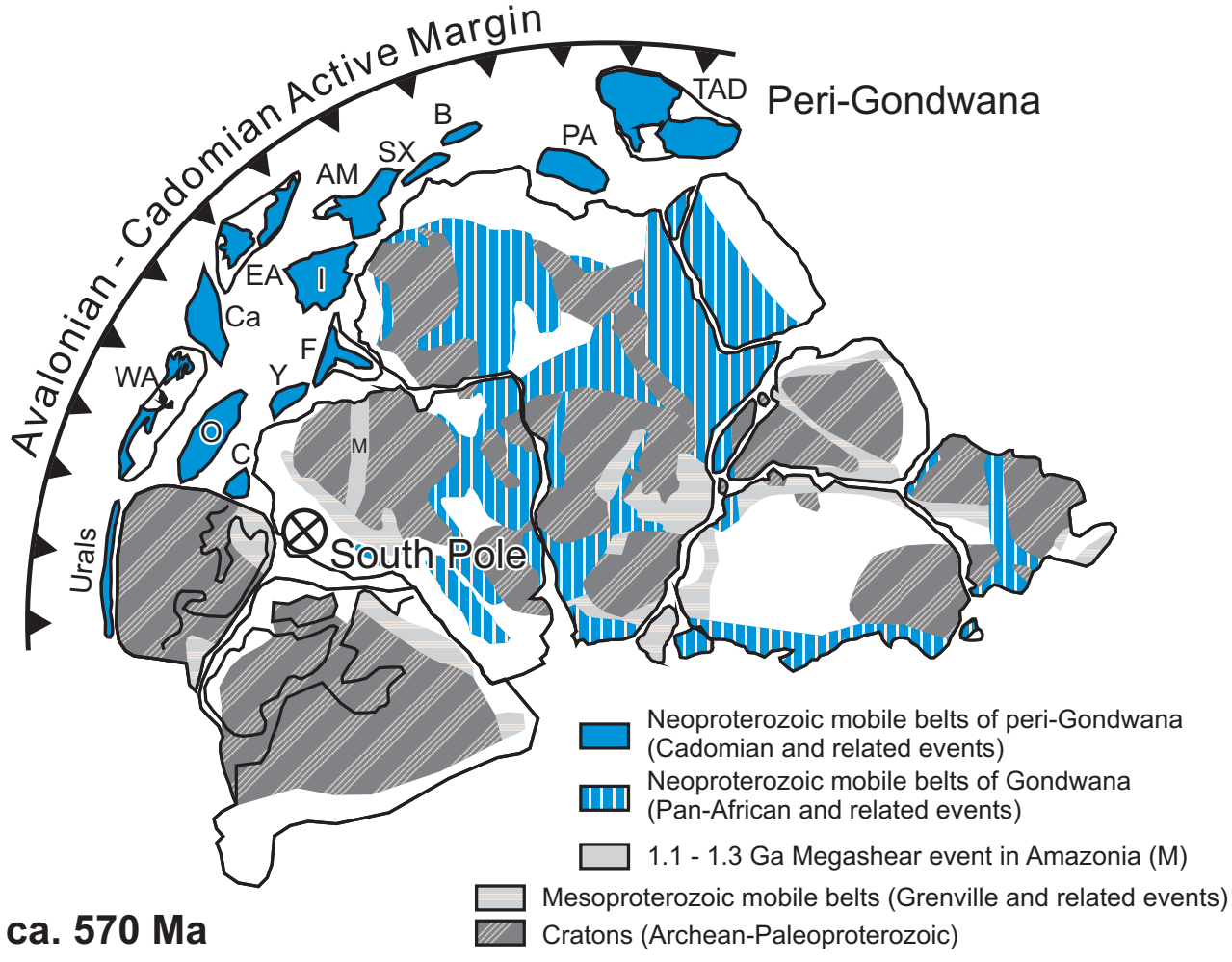

Fig. 2.1: Palaeogeography of the Avalonian-Cadomian arc and related peri-Gondwanan crustal fragments (modified after Nance & Murphy 1994; Murphy et al. 2000; Linnemann et al. 2004). **AM** – Armorican Massif, **B** – Teplá Barrandian, **C** – Chortis, **Ca** – Carolina, **EA** – East Avalonia, **F** – Florida, **I** – Iberia, **O** – Oaxaquia, **PA** – Proto-Alps, **SX** – Saxo-Thuringia, **TAD** – Turkish Plate/Aegean/Dobrogea, **WA** – West Avalonia, **Y** – Yucatan.

Abb. 2.1: Paläogeographie der zum Avalonisch-Cadomischen Orogen gehörenden peri-gondwanischen Krustenblöcke im späten Neoproterozoikum (verändert nach Nance & Murphy 1994; Murphy et al. 2000; Linnemann et al. 2004). **AM** – Armorikanisches Massiv, **B** – Teplá Barrandium, **C** – Chortis, **Ca** – Carolina, **EA** – Ost-Avalonia, **F** – Florida, **I** – Iberia, **O** – Oaxaquia, **PA** – Proto-Alpen, **SX** – Saxo-Thuringia, **TAD** – Türkische Platte/Ägäis/Dobrogea, **WA** – West-Avalonia, **Y** – Yucatan.

mian shear zone; Zulauf et al. 1997b, Zulauf et al. 2002a, and references therein). The Mariánské Lázně Complex in the north-west is overthrusted by the Teplá Crystalline Complex of the TBU (Štědrá in Vraná & Štědrá 1997). In the north, the low-grade to very low-grade Neoproterozoic rocks of the TBU are separated from the Saxothuringian Erzgebirge Mountains by the North Bohemian shear zone (Zulauf et al. 2002b, and references therein) that is largely masked by Cenozoic volcanics and sediments of the Ohře-Graben. Eastern and north-eastern parts of the TBU are largely covered by post-orogenic Late Palaeozoic and marine Late Cretaceous deposits. Nevertheless, the Neoproterozoic and Palaeozoic rocks exposed in

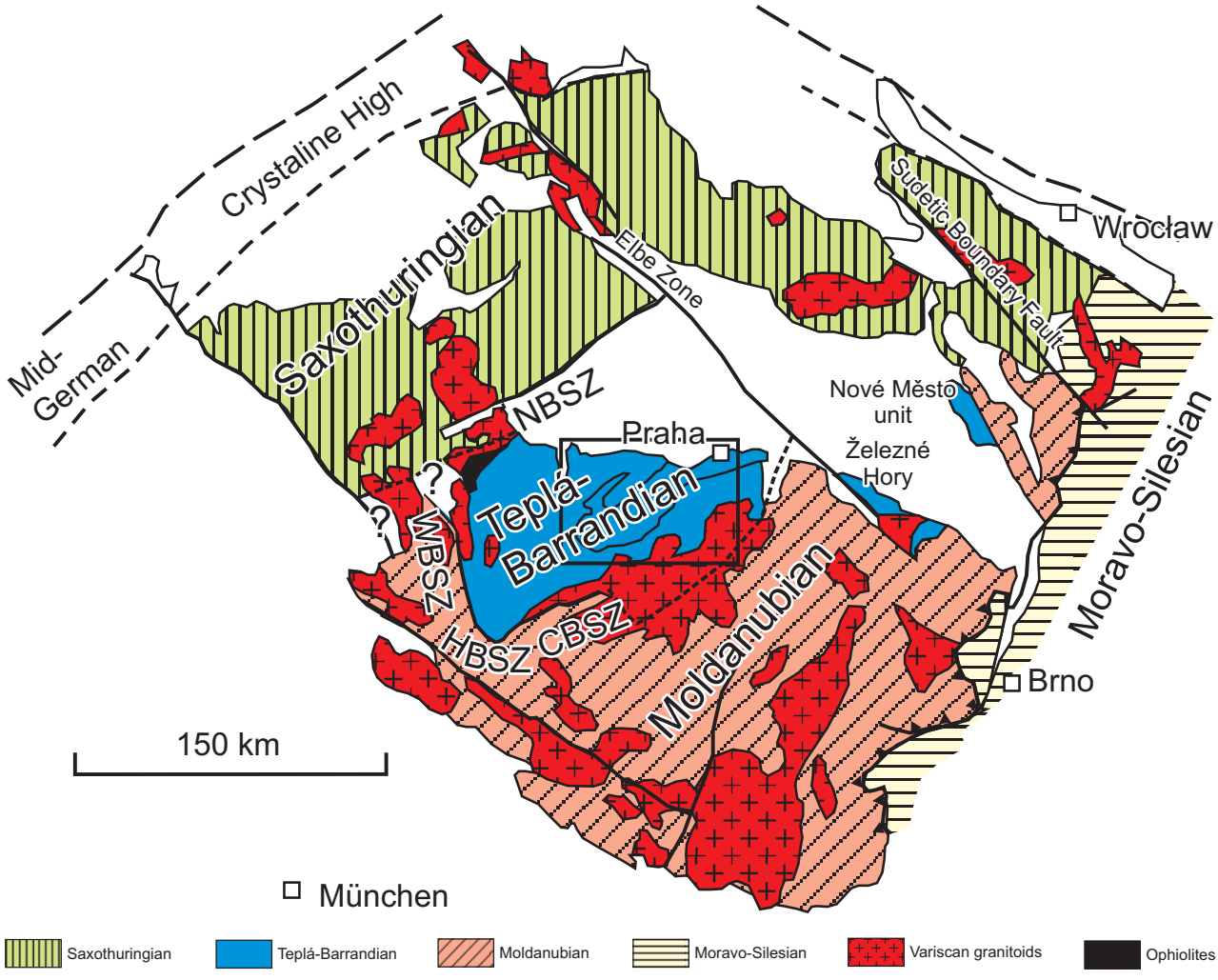

Fig. 2.2: Sketch map of the Bohemian Massif with the TBU in the central part (modified after Dallmeyer et al. 1995; Zulauf et al. 2002a; Mazur et al. 2005). CBSZ – Central Bohemian shear zone, **HBSZ** – Hoher Bogen shear zone, **NBSZ** – North Bohemian shear zone, **WBSZ** – West Bohemian shear zone. Box indicates the extract shown in Fig. 2.3.

Abb. 2.2: Schematische Karte des Böhmischen Massivs mit dem Teplá-Barrandium im Zentrum (verändert nach Dallmeyer et al. 1995; Zulauf et al. 2002a; Mazur et al. 2005). **CBSZ** – Zentralböhmische Scherzone, **HBSZ** – Hoher Bogen Scherzone, **NBSZ** – Nordböhmische Scherzone, **WBSZ** – Westböhmische Scherzone. Kasten markiert den in Abb. 2.3 dargestellten Ausschnitt.

the Železné hory represent the eastward continuation of the Teplá-Barrandian unit (e.g., Havlíček 1998a; Fig. 2.2). The easternmost outcrops of Teplá-Barrandian type crust were recognized in the Nové Město unit (Orlica Mountains/Sudetes), where low-grade rocks are separated from (most likely Moldanubian) high-grade rocks by a shear zone (Mazur et al. 2005).

2.2 Outline of the regional geology

2.2.1 Neoproterozoic

The Neoproterozoic volcano-sedimentary sequences of the TBU reach a thickness of several thousand meters and were accumulated at the northern periphery

GEOLOGICA SAXONICA
Journal of Central European Geology 54 (2008) 1–168

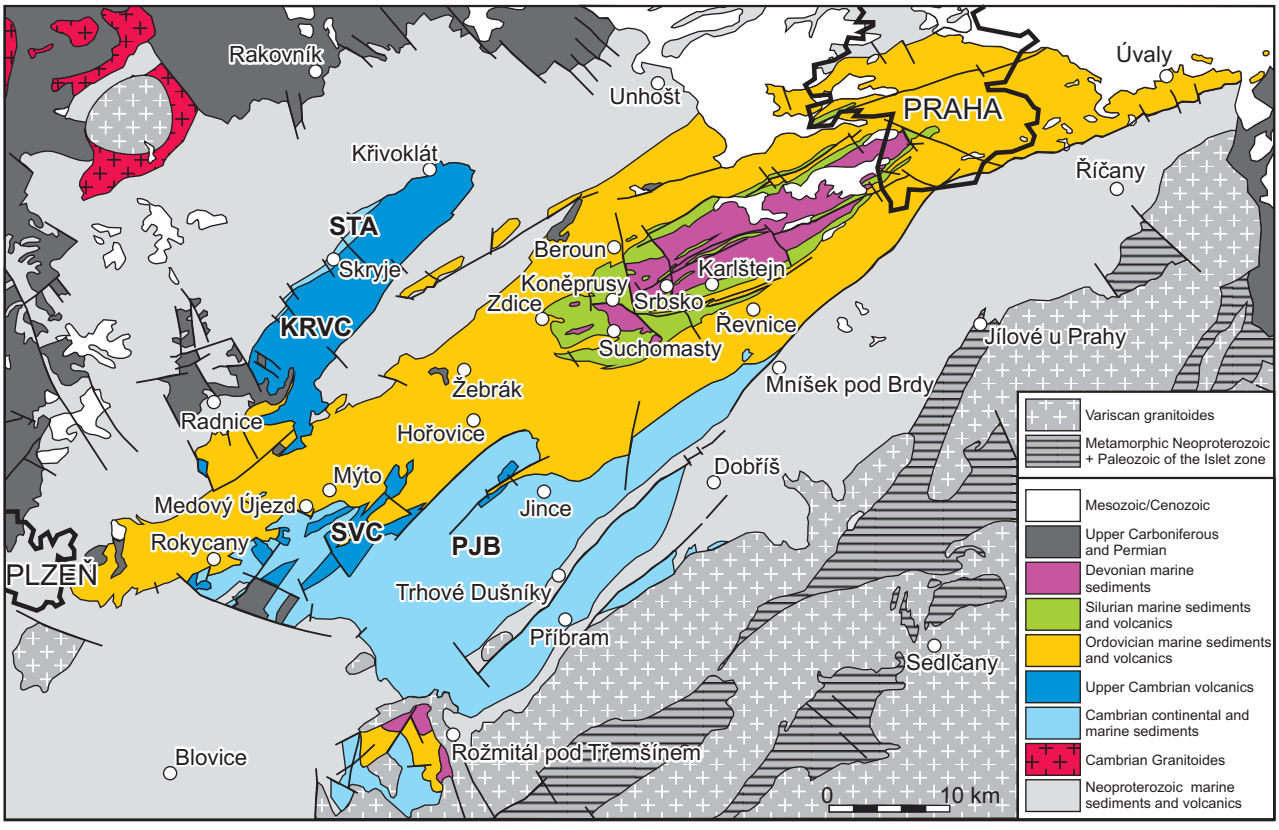

Fig. 2.3: Sketch map of the TBU (slightly modified after Chlupáč et al. 1998). **KRVC** – Křivoklát-Rokycany volcanic complex, **SVC** – Strašice volcanic complex, **PJB** – Příbram-Jince basin, **STA** – Skryje-Týřovice area.

Abb. 2.3: Karte des Teplá-Barrandiums (leicht verändert nach Chlupáč et al. 1998). **KRVC** – Křivoklát-Rokycany-Vulkanitkomplex, **SVC** – Strašice-Vulkanitkomplex, **PJB** – Příbram-Jince-Becken, **STA** – Skryje-Týřovice-Gebiet.

of Gondwana. Siliciclastic rocks were deposited as turbidites and gravity flows (Chlupáč 1993). The Neoproterozoic successions are lithostratigraphically subdivided into two major units: the Kralupy-Zbraslav Group and the Štěchovice Group (Chlupáč 1993; Fig. 2.5). Microfossils confirm an Upper Riphaean to Vendian age (corresponding to the Ediacaran in the current terminology of Gradstein et al., 2005) for both groups and allow a correlation with the Brioverian of the Armorican Massif in NW France (Konzalová 1981, 2000; Pacltová 1990, 2000; Fatka & Gabriel 1991). The Kralupy-Zbraslav Group is composed of the Blovice and the Davle formations, which are built up by alternating shales, siltstones, and sandstones with interbedded volcanics and cherts. While basic volcanics are widespread in the thick Blovice Formation in the lower part of the Kralupy-Zbraslav Group, intermediate to acidic volcanics and appropriate pyroclastics are typical for the overlying Davle Formation. The top of the Davle Formation is represented by silicified black shales. Volcanic rocks of the Kralupy-Zbraslav Group are arranged in NE-SW trending belts and belong to three major series with tholeiitic (oldest), transitional and alkaline (youngest) geochemistry, respectively. The Jílové Zone in the SE of the TBU comprises tholeiitic volcanics in the lower part and rocks of a calcalkaline association in the upper part. Geochemical signatures of the igneous rocks of the Kralupy-Zbraslav Group correspond to volcanic arc and back-arc geotectonic settings (Fiala 1977, 1978; Pelc & Waldhausrová 1994; Waldhausrová 1984, 1997a, 1997b).

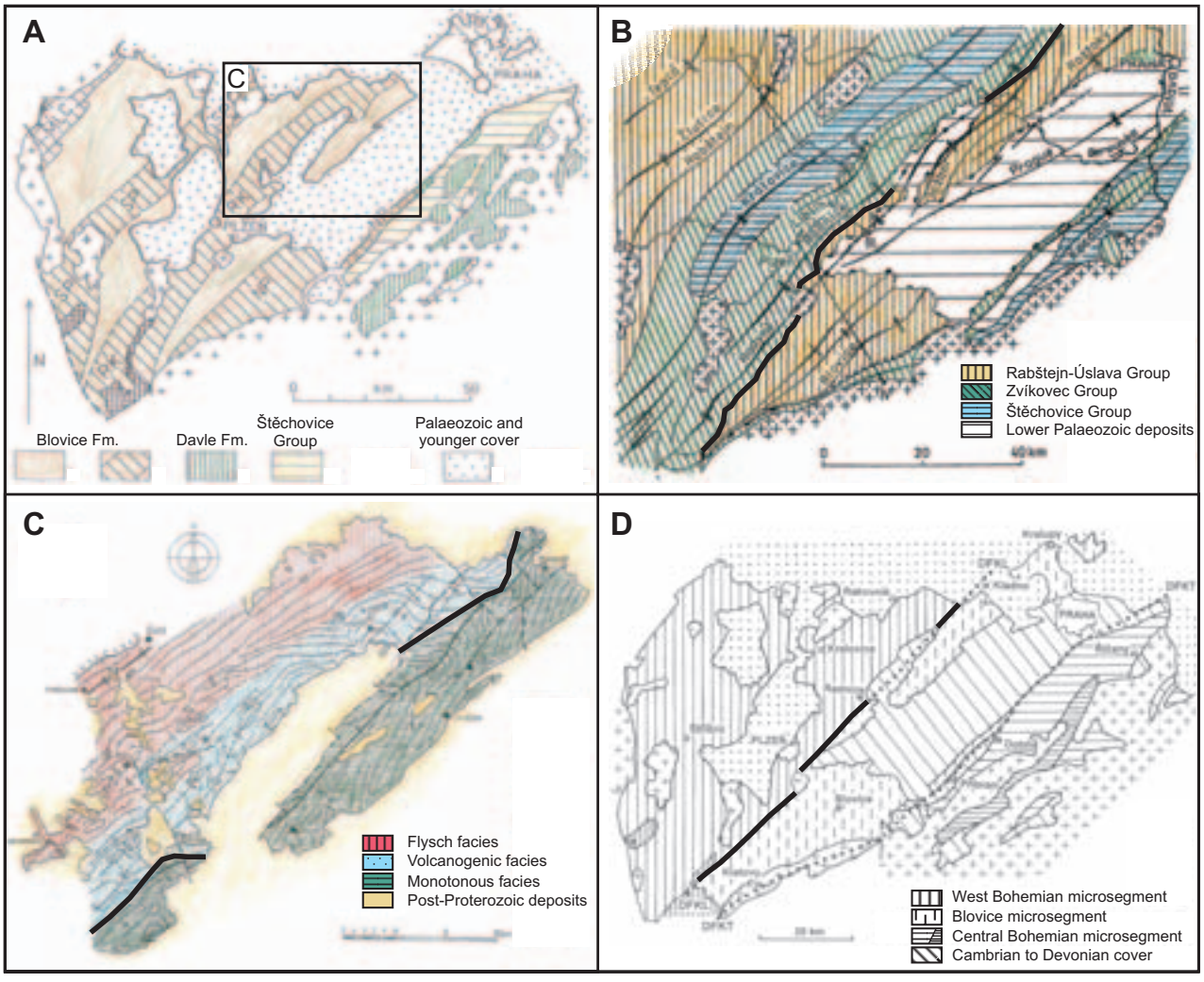

Fig. 2.4: Different lithostratigraphic concepts for the Neoproterozoic volcano-sedimentary successions of the Teplá-Barrandian unit. **A**: From Chaloupsky et al. (1995). **B**: From Holubec (1995). **C**: From Cháb and Pelc (1968). **D**: From Röhlich (2000). [For the discussion in chapter 8.1.2: The sampling localities BL and DB are separated by a major boundary (black line) in B to D.]

Abb. 2.4: Verschiedene lithostratigraphische Konzepte für die neoproterozoischen vulkano-sedimentären Einheiten des Teplá-Barrandiums. **A**: Nach Chaloupsky et al. (1995). **B**: Nach Holubec (1995). **C**: Nach Cháb and Pelc (1968). **D**: Nach Röhlich (2000). [Für die Diskussion in Kapitel 8.1.2: Die Probenahmepunkte BL und DB sind in B bis D durch eine bedeutende Grenze (schwarze Linie) voneinander getrennt.]

Alternating shales, siltstones, and greywackes are characteristic for the succeeding Štěchovice Group, which was deposited concordantly above the Davle Formation. Layers of tuffs and tuffites are revealing of continuing magmatic activity. Intercalations of conglomerates appear in the middle part of the Štěchovice Group (Fig. 2.5).

Due to the tectonic conditions as well as the lack of reliable marker horizons and precise geochronological data, the stratigraphic subdivision of the Teplá-Barrandian Neoproterozoic is still problematic and, chiefly based on the presence or absence and the character of synsedimentary volcanic rocks (e.g., Kettner 1918, Röhlich 1965, Cháb

1993). Lithostratigraphic subdivisions of the Teplá-Barrandian Neoproterozoic successions differing from the one described above were proposed (Fig. 2.4), e.g., by Röhlich (2000), who identified three micro-segments with individual lithostratigraphic features separated by NE-SW-trending major faults, by Cháb & Pelc (1968), who divide the Blovice Formation from NW to SE in flysch facies, volcanogenic facies and monotonous facies, or by Holubec (1995), who proposed a lithostratigraphic classification into the Rabštejn-Úslava (base), Zvíkovec and Štěchovice groups (top), respectively, whereas these groups are separated by unconformities.

Tentative geotectonic models for the Cadomian evolution of the TBU assume subduction accompanied by the formation of oceanic island arc, back-arc basin, and remnant arc basin (Cháb 1993, Kříbek et al. 2000). Greywacke and chert pebbles in the middle and upper parts of the Štěchovice Group, as well as radiometric age data obtained from rhyolite pebbles are interpreted to document accretion, uplift and erosion of the Cadomian arc (Zulauf et al. 1999, Dörr et al. 2002).

The rocks of the Blovice Formation underwent at least two deformation stages during Cadomian orogenic processes (Zulauf 1997, Zulauf et al. 1999, Kříbek et al. 2000; and references therein): D_1 with unknown kinematics and D_2 with top-to-the-N shearing. The peak of a LP-HT metamorphic event accompanying D_2 is dated around 550-540 Ma (Th-U-Pb model ages of metamorphic monazite) and interpreted to be related to collisional processes and slab break off (Zulauf et al. 1999). The following collapse of the thickened crust around the Precambrian/Cambrian boundary is expressed by normal faulting causing exhumation of amphibolite facies rocks in the western and northwestern part of the TBU and crustal tilting before 523 Ma (Zulauf et al. 1997a, 1999).

2.2.2 Cambrian

Cambrian rocks are preserved in the northern Skryje-Týřovice area and in the southern Příbram-Jince basin (Fig. 2.3).

The thick, mainly continental, Lower Cambrian sediments of the Příbram-Jince basin are lithostratigraphically subdivided into five formations (Havlíček 1971, 1998a). Conglomerates of the Žitec-Hluboš Formation unconformably overlie Cadomian deformed basement (Fig. 2.5). This basal Formation of the Palaeozoic overstep sequence is characterized by relatively immature conglomerates and sandstones with pebbles that are interpreted to be derived from the adjacent Neoproterozoic units (Kukal 1971). However, most of the Lower Cambrian sediments are highly mature but partly mixed with material derived from synsedimentary volcanism (Kukal 1971, Drost et al. 2004). The components of the Lower Cambrian sediments were transported by fluvial and mud flow mechanisms, respectively, and accumulated in a fault bounded basin with internal structure (Kukal 1971, Havlíček 1971). Magmatic activity around 523-511 Ma is proved by U-Pb zircon datings of calc-alkaline plutons having been emplaced in dextral NE-SW- to ENE-WSW trending transtensive shear zones (Zulauf 1997, Zulauf et al. 1997a, Dörr et al. 1998, 2002; and references therein) exposed in the western and northwestern parts of the TBU. Furthermore Venera et al. (2000) reported the presence of a ~505 Ma old (Pb-Pb, zircon) granitoid within Neoproterozoic metasediments in the northern part of the TBU.

Continuing subsidence caused a marine transgression in the Middle Cambrian (Jince Formation). In the Skryje-Týřovice area the marine Jince Formation unconformably overlies deformed Neoproterozoic successions. Lower Cambrian rocks are not present. In the Příbram-Jince basin there is a transition from the coarser-grained, continental Chumava-Baština Formation to the fine-grained, marine Jince Formation. The sediments of the overlying Ohrazenice Formation have been deposited during a regression (Kukal 1971, Havlíček 1971). The fauna of the Jince Formation shows relations to that of southwestern Europe (e.g., Ossa-Morena Zone: Fatka et al. 1998).

The Upper Cambrian is predominantly represented by subaerial volcanism preserved in the southern Strašice Volcanic Complex (SVC) and in the northern Křivoklát-Rokycany Volcanic Complex (KRVC; Fig. 2.5). The volcanic rocks of the SVC are in general more basic than those of the northern

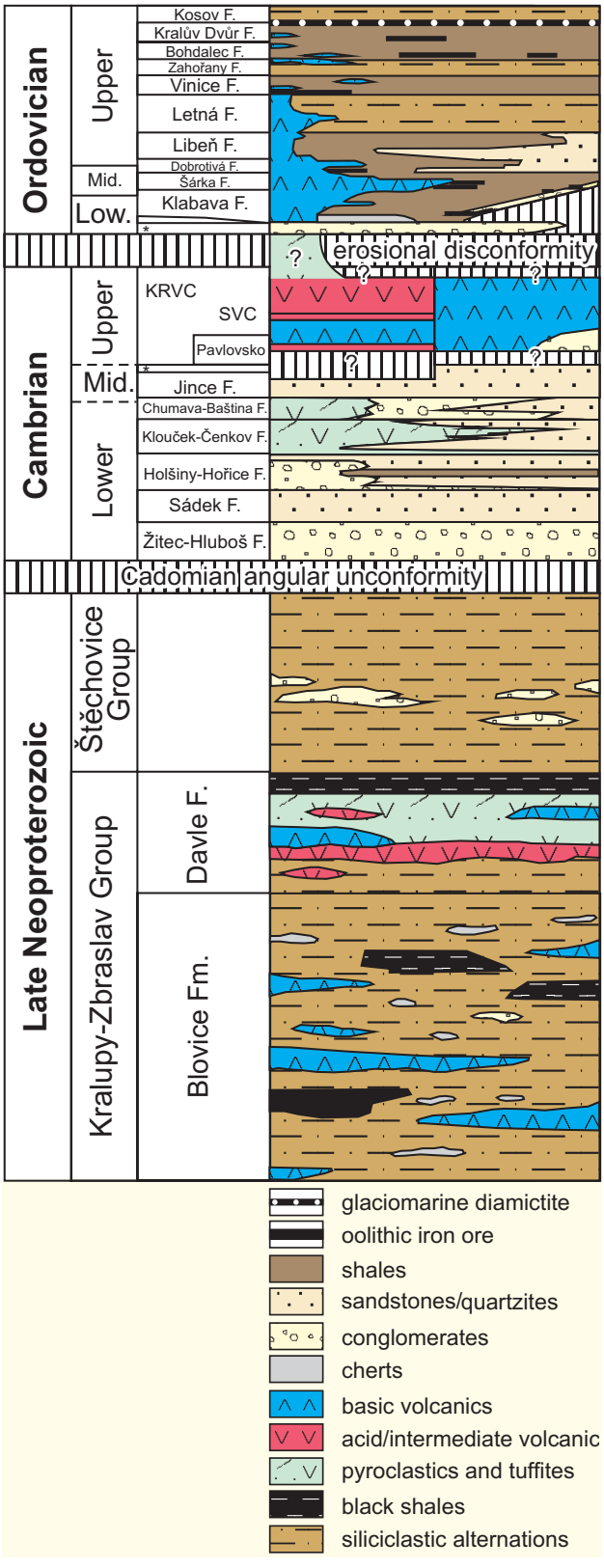

volcanic belt (Waldhausrová 1971). In the KRVC four groups of volcanics are distinguished differing in geochemistry and corresponding to discrete eruption stages (Waldhausrová 1971). Rb-Sr isotopic studies by Vidal et al. (1975) revealed a Rb/Sr whole rock age of ~490 Ma and an initial $^{87}Sr/^{86}Sr$ ratio of ~0.703 (recalculated to $\lambda_{Rb}=1.42\times10^{-11}$ recommended by IUGS, Steiger & Jäger 1977). Geochemical and Nd isotope data recently acquired by Pin et al. (2007) substantiate a mantle and/or lower crust origin of the magma.

The Upper Cambrian gap in sedimentation is only locally disrupted by undated continental siliciclastics of the Pavlovsko Formation (Kukal 1971, Havlíček 1971).

2.2.3 Ordovician

The Early Ordovician is marked by a major transgression. Tremadocian marine siliciclastics unconformably overlie deeply eroded Neoproterozoic basement or rest disconformably on Cambrian rocks (e.g., Chlupáč 1993).

Ordovician siliciclastic sediments and pyroclastic rocks with intercalations of oolithic iron ores reach a thickness of more than 2500 m (Havlíček 1998b, Fig. 2.5). A „Mediterranean Province“ fauna indicates cold or cool water and can be correlated with other peri-Gondwanan regions, such as Iberia, France, Sardinia, and the Italian-Austrian Carnic Alps (Havlíček & Vaněk 1966, Havlíček & Fatka 1992, Štorch et al. 1993). Terrigenous siliciclastic sequences are developed as shallow-water sandy facies and deeper-water dark shales (e.g., Chlupáč 1993). Detrital white

Fig. 2.5: Lithostratigraphy of the Teplá-Barrandian Neoproterozoic and Early Palaeozoic (compiled from Havlíček 1971; Vidal et al. 1975; Havlíček 1982; Chlupáč 1993, 1995; Štorch et al. 1999; Mašek 2000; Kraft et al. 2004).

Abb. 2.5: Lithostratigraphische Gliederung des Neoproterozoikums und Frühpaläozoikums des Teplá-Barrandiums (zusammengestellt nach Havlíček 1971; Vidal et al. 1975; Havlíček 1982; Chlupáč 1993, 1995; Štorch et al. 1999; Mašek 2000; Kraft et al. 2004).

mica fractions from Lower to Upper Ordovician siliciclastic sedimentary rocks yielded K-Ar ages of 612-585 Ma and suggest a crystalline source of Late Neoproterozoic (Ediacaran) age, which was probably represented by the deeply eroded Cadomian magmatic arc (Neuroth 1997, Ahrendt et al., 1998, Drost et al. 2003).

The Ordovician sequence contains volcanic products represented by pyroclastics, effusives and subvolcanic bodies (Štorch 1998). These effusives and pyroclastics can reach a thickness of up to 1000 m near the eruption centres (Fiala 1971). Patočka et al. (1993) characterized the Lower and Upper Ordovician submarine effusives as alkaline basic to intermediate igneous rocks with within-plate signature.

In the TBU the late Ordovician glaciation in the Hirnantian is recorded by two horizons of glaciomarine diamictites at the base of the Kosov Formation and by a prominent glacio-eustatic regression resulting in storm-influenced sediments in higher parts of the Kosov Formation (Štorch 1986, Brenchley & Štorch 1989, Štorch 1990). The diamictites were interpreted to be distal deposits of floating glacier ice or deposits of seasonal ice (Brenchley & Štorch 1989).

The Ordovician-Silurian boundary is petrographically and palaeontologically well documented. Upper Ordovician sediments of the Kosov Formation were replaced by Lower Silurian black graptolite shales of the Želkovice Formation (Havlíček & Vaněk 1966, Kříž 1998, and references therein). In the TBU there is locally a gap in sedimentation between uppermost Ordovician and upper Llandovery (Štorch 1986).

Ordovician to Devonian rocks form a complex that is often referred to as the Prague Basin (e.g., Havlíček 1998b). However, Melichar (2004) demonstrated that the present-day synformal structure is the result of Givetian to Frasnian folding and thrusting followed by Early Carboniferous (?)extensional flexing into a large synform. Furthermore this author shows that – though the Lower and Middle Ordovician deposits are (par)autochthonous – from the Bohdalec Formation of the Upper Ordovician there is a lower allochthonous unit comprising deeper water deposits and an upper allochthonous unit with shallower water sediments. Therefore, the term Prague Synform is to be preferred over the term Prague Basin.

2.3 Palaeomagnetic and palaeobiogeographic data

On the base of brachiopod and trilobite faunas in combination with palaeomagnetic data for the Bohemian Massif (obtained by Krs et al. 1986, 1987), Havlíček et al. (1994) defined the microcontinent Perunica comprising the Moldanubian, the Teplá-Barrandian and the Saxothuringian-Lugian. According to this study Perunica was situated in intermediate palaeolatitudes during the Cambrian (Lower Cambrian 39° S → Upper Cambrian 29° S) and moved to low southern latitudes until the Early Devonian (~5 to 9°). Assemblages of benthic faunas preserved in Middle Cambrian, Tremadocian and uppermost Ordovician (~Ashgill in the timescale of McKerrow & van Staal 2000) rocks are regarded by Havlíček et al. (1994) to indicate migrations of some faunal elements from Baltica and led to the interpretation that Perunica represented a separate microcontinent between Gondwana and Baltica during the Ordovician. In general, however, the Teplá-Barrandian Early Palaeozoic biota share many significant features with fossil assemblages to be found in North Africa, Armorica and Iberia and are therefore assigned to the Mediterranean Province or referred to as peri-Gondwanan (e.g., Vavrdová 1974, Havlíček 1989, Paris & Robardet 1990; Havlíček et al. 1994, Servais & Fatka 1997, Álvaro et al. 2003, Fatka 2003, Vecoli & Le Hérissé 2004). Also the Silurian and Devonian lithological and faunal development of the Barrandian shows many similarities with that of Gondwana, i.e. northern Africa (e.g., Chlupáč 1998, Kříž 1998, Hladil & Bek 1998, Plusquellec & Hladil 2001).

Tait et al. (1994a, b, 1995) acquired paleomagnetic data (even though differing from those by Krs et al. 1986,1987), which suggest that the Barrandian moved from high southern latitudes (76°) in the Lower Ordovician to intermediate palaeolatitudes in the Upper Ordovician (40° S) to low latitudes (23° S)

in the Upper Silurian. Although this would require large drift rates (~11 cm/y only in north direction), it is in agreement with geological facts, such as the occurrence of glaciomarine sediments corresponding to the Upper Ordovician glaciation and the larger-scale appearance of limestones in the Upper Silurian. However, the interpretation that the Teplá-Barrandian as a constituent of the "Armorican Terrane Assemblage" (comprises Variscan Europe south of the Rhenohercynian Zone: Tait et al. 1997) had rifted from Gondwana during the Ordovician and drifted northward independently from the supercontinent (e.g., Tait et al. 1997, 2000; Cocks 2000; and references therein) has not been demonstrated convincingly. Since palaeobiogeographical and lithological features of the Teplá-Barrandian and the other components of the "Armorican terrane Assemblage" show significant similarities with northern Africa during the Palaeozoic, it is unlikely that they were separated from Gondwana-mainland by a major ocean during this time. The main problem is the interpretation of the palaeomagnetic data concerning the apparent polar wander path (APWP) and the latitudinal evolution of Gondwana (see comprehensive review by Robardet, 2003, and the references therein). If the Silurian south pole is assumed to be in northern Africa following Bachtadse & Briden (1991), the palaeomagnetic data obtained by Tait et al. (1994a, b, 1995) for the Teplá-Barrandian necessitate individual drift histories for Gondwana and the "Armorican Terrane Assemblage". However, using the APWP derived from lithological and palaeoclimatic indicators (Scotese & Barrett 1990) or from palaeomagnetic studies placing the Silurian South Pole into southern South America (Bachtadse & Briden 1990, Schmidt et al. 1990, McElhinny et al. 2003) does not require separation of the "Armorican Terrane Assemblage" from Gondwana (Tait et al. 1994, Robardet 2003, Linnemann et al. 2004).

3 Lithologic, petrographic and sedimentological features of the Early Palaeozoic siliciclastics

In this chapter, the Early Palaeozoic siliciclastics of the Teplá-Barrandian unit that were studied in selected key sections and outcrops are described to characterise the geological context of the samples taken for geochemical, Nd-Sr-Pb isotopic and detrital zircon analyses, respectively. Furthermore, detrital modes of the siliciclastic rocks are used to draw inferences on the geotectonic setting of the source area(s) and the depositional environments. Selected photomicrographs of the analysed sedimentary rocks are presented in Plates III and IV in the Appendix.

For further information, see Chlupáč et al. (1998) and the references therein. This publication represents the most recent summary of sedimentological, stratigraphical, and palaeontological studies within all subunits and areas of the Teplá-Barrandian Palaeozoic volcano-sedimentary succession.

3.1 Cambrian

Lower Cambrian rocks of the Příbram-Jince Basin were studied and sampled in the area between Jince to the N, Trhové Dušníky to the S and Buková u Příbrame to the E (Fig. 3.1). Here all of the five Lower Cambrian lithostratigraphic units defined by Havlíček (1971) are exposed. The majority of the investigated outcrops is situated in a ca. 8 km long section at the eastern slope of the Litavka valley between Jince and Trhové Dušníky as well as on the hills and along the tributaries to the E of the Litavka River. The thickness of the Lower Cambrian sequence is around 3000 m in this area. However, since there is almost no internal stratigraphic control within the individual formations, it cannot be excluded that the succession is in places thinned or thickened by fault tectonics.

GEOLOGICA SAXONICA
Journal of Central European Geology 54 (2008) 1–168

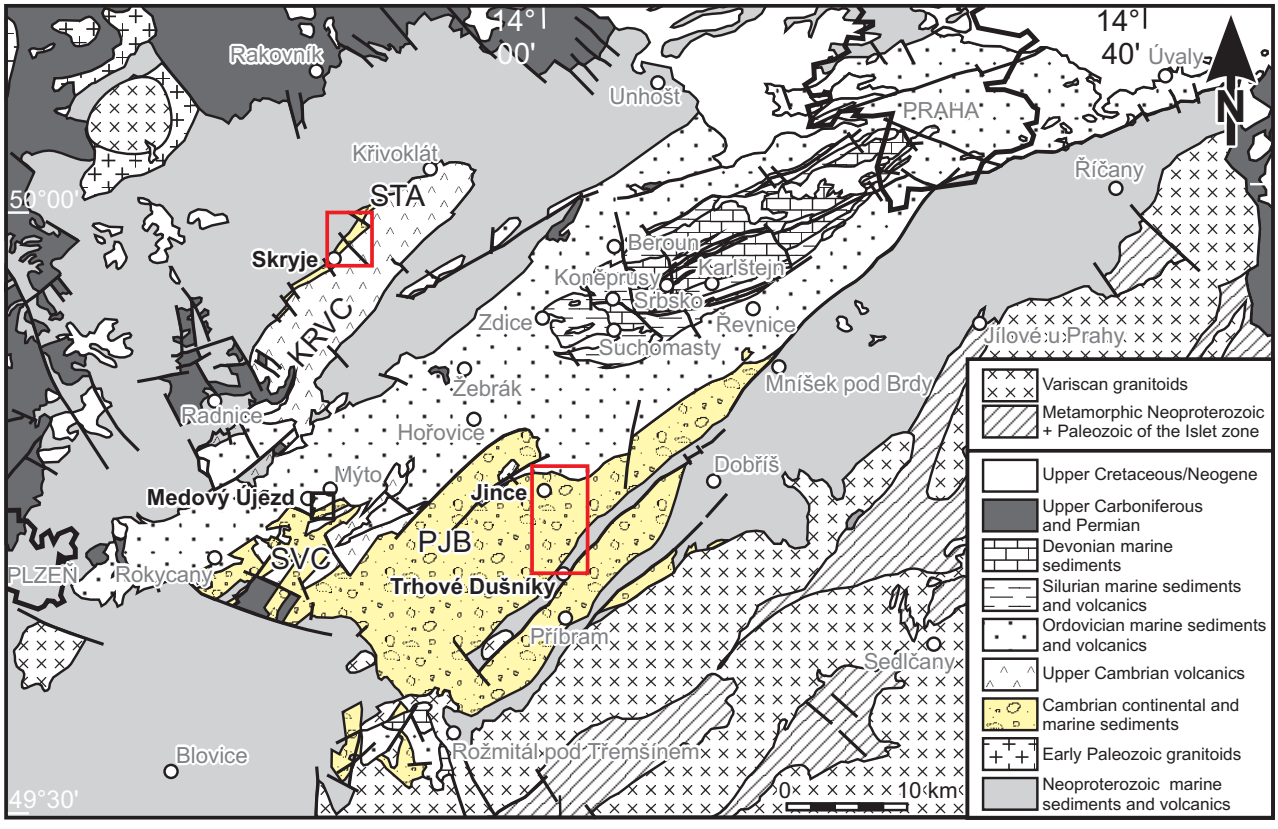

Fig. 3.1: Sketch map showing the position of the investigated outcrops and sections within the major range of Cambrian deposits in the Teplá-Barrandian unit.

Abb. 3.1: Lage der untersuchten Aufschlüsse und Profile im Hauptverbreitungsgebiet der kambrischen Gesteine.

Middle Cambrian rocks of the Příbram-Jince Basin were studied and sampled close to Jince at the locality Vinice – a ca. 1.1 km long slope at the Eastern bank of the Litavka River (Fig. 3.1). The rocks of the Jince and Ohrazenice formations have a thickness of around 500 to 550 m. The Middle Cambrian in the Skryje-Týřovice area was dealt with in several sections and outcrops in the Berounka valley and at Mileč hill in the vicinity of the villages Skryje and Týřovice (Fig. 3.1). Only the lower part of the Jince Formation is preserved in this part of the Barrandian.

The siliciclastic deposits of the Pavlovsko Formation regarded as Upper Cambrian in age are not considered here. For information on the Upper Cambrian volcanic rocks see chapter 4.

3.1.1 Lithologies, sedimentary structures and depositional environments

In the Trhové Dušníky locality of the Litavka valley the basal Žitec-Hluboš Formation is separated from cataclastic Neoproterozoic slates by a brittle strike-slip fault (orientation of the fault plane[1]: 321/84; subhorizontal slickensides) and is made up by the Žitec and Hluboš conglomerates. The reddish **Hluboš conglomerates** form 10 to 280 cm thick beds, are for the most part matrix supported and

[1] Structural data are given in the form: dip direction/dip angle in degree.

Fig. 3.2: Sedimentary features in the Sádek Formation. **A**: Current ripples indicating transport to the NE. **B**: Finely laminated unit is overlain by sandy beds with in bedding aligned mud clasts. **C**: Alternating siltstones and sandstones. **D**: Flood plain deposits represented by sandy and muddy layers and laminae showing lamination, small-scale cross bedding and discontinuous lenticular bedding. In the upper part mud clasts are preserved within sandy layer. **E**: Cross bedded sandstones of a point bar. **F**: Sandstone beds that wedge out within outcrop and represent channel fills. Locality: Dominikální Paseky.

poorly sorted. They contain predominantly subangular to subrounded granules, pebbles and less frequent cobbles. The matrix is composed of sand-sized grains of similarly subangular to subrounded appearance and finer particles. A maximum size of 20 cm was observed for individual cobbles, whereas these largest components are rather well rounded and were more commonly found in the lowermost part of the succession. The number of pebbles may decrease in such a way that the rocks are to be designated as conglomeratic/pebbly sandstones or coarse-grained sandstones. Although the fabric is often ungraded and disorganised, planar bedding and planar cross bedding as well as trough cross bedding were observed in several places. The studied sediments of the Žitec-Hluboš Formation represent medial parts of alluvial fans and were deposited by debris flows and stream flows.

The overlying **Sádek Formation** is made up by siltstones and fine- to medium-grained sandstones of chiefly reddish and subordinate greenish or greyish colour. Conglomeratic intercalations are rare in the vicinity of the Litavka valley. Matrix content and sorting vary. The roundness of the grains is questionable due to considerable recrystallisation. The observed sedimentary features (Fig. 3.2) of the chiefly thin to medium thick beds[1] are manifold and comprise planar, finely laminated beds, planar, trough and ripple cross bedding, current and wave ripples, mud clasts of few cm to few mm size, lenticular bedding and possibly badly preserved mud cracks. The variation of sedimentary structures and the predominantly small grain size suggest deposition in the lower course of a fluvial system including flood plain, river channels and lake(s).

The succeeding **Holšíny-Hořice Formation** is chiefly made up by sandstones and conglomerates being composed of predominantly subangular clasts. The fabric of the conglomerates varies from clast-supported to matrix supported. Clasts are mostly between 0.5 and 2 cm and usually do not exceed a size of 4 cm. Sandstones often contain individual pebbles that may be aligned in bedding or cross bedding (Fig. 3.3A). But also fine-grained sandstones to sandy siltstones occur occasionally. Planar bedding and cross bedding as well as massive beds are the prevailing sedimentary features. The lateral extent of the beds is often only up to few meters – then they are cut by younger ones. Sedimentary structures as well as grain size and grain distribution point to deposition by a fluvial system.

Within the Litavka valley section of the Holšíny-Hořice Formation a sequence is developed, where the reddish and greyish sandstones and conglomerates are replaced by yellowish-brown sandstones and eventually by few meters of silt- and claystones, the so-called Paseky shales (Fig. 3.3B). The Paseky shales pass into sandstone-shale alternations showing thickening upwards of the sandstone beds. Finally the yellowish-brown sandstones are replaced by grey wedge-shaped sandstones most probably representing channel fills and indicating aggradation of a lake or lagoon[2].

The Litavka valley deposits of the **Klouček-Čenkov Formation** are largely akin to those of the preceding Holšíny-Hořice Formation with respect to

[1] Thickness of the beds is given according to the terminalogy of Ingram (1954)

[2] In fact, comprehensive previous studies combining sedimentological, palaeontological, and geochemical features were ambiguous with regard to the depositional environment of the Paseky shales. A brackish, lagoonal environment is, however, preferred by Kukal (1995).

Abb. 3.2: Sedimentstrukturen in der Sádek Formation. **A**: Strömungsrippeln, die Transport nach NE anzeigen. **B**: Sandige Schichten mit in die Schichtung eingeregelten Tonsteinklasten folgen auf fein laminierte Schichten. **C**: Schluffstein-/Sandstein-Wechsellagerung. **D**: Sandige und tonig-siltige Lagen zeigen Lamination, kleinräumige Schrägschichtung sowie diskontinuierliche linsenförmige Schichtung und repräsentieren flood plain Ablagerungen. Im oberen Teil sind mud clasts innerhalb sandiger Lagen erhalten. **E**: Schräggeschichtete Sandsteine einer Sandbank. **F**: Rinnenfüllungen, die durch innerhalb des Aufschlusses auskeilende Sandsteinschichten repräsentiert werden. Lokalität: Dominikální Paseky.

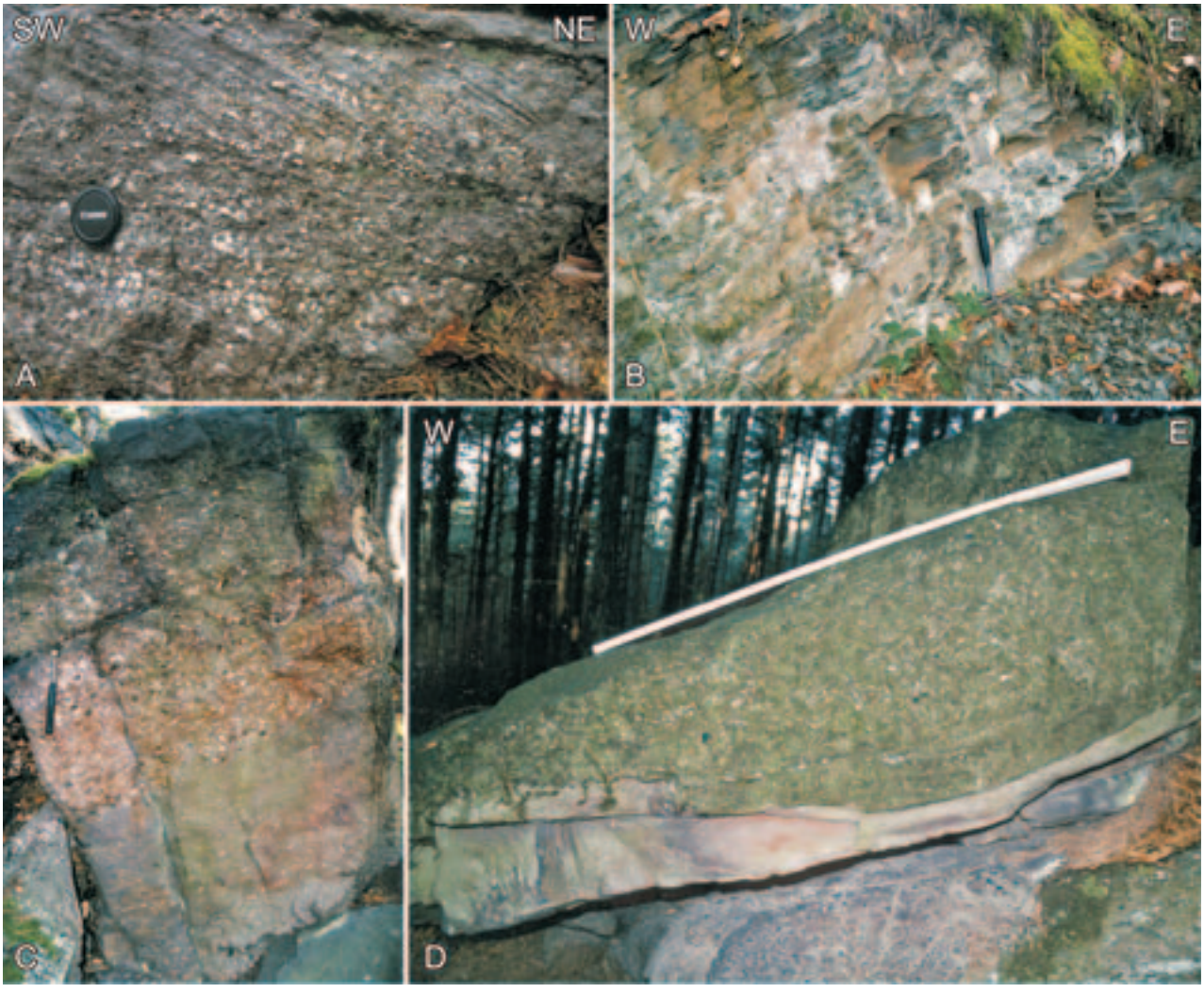

Fig. 3.3: Lithologies and sedimentary features in the Holšíny-Hořice Formation (**A**, **B**) and in the Klouček-Čenkov Formation (**C**, **D**). **A**: Small cliff consisting of massive and bedded conglomerates overlain by cross-bedded granule- and pebble-bearing sandstones. **B**: Outcrop of the Paseky shales at Medalův Mlyn. **C**: Cross-bedded sandstones with granules and pebbles arranged in internal stratification are overlain by matrix- to clast-supported conglomerates (loose block). **D**: Sandy beds are overlain by conglomerates representing a channel fill (folding rule is 60 cm).

Abb. 3.3: Lithologie und Sedimentstrukturen der Holšíny-Hořice Formation (**A**, **B**) und der Klouček-Čenkov Formation (**C**, **D**). **A**: Kleine Klippe, in der massive und geschichtete Konglomerate von schräggeschichteten, geröllführenden Sandsteinen überlagert werden. **B**: Aufschluss des Paseky-Schiefers in der Lokalität Medalův Mlyn. **C**: Schräggeschichtete Sandsteine mit in die interne Schichtung eingeregelten Geröllen werden von matrix- bis klastengestützten Konglomeraten überlagert (loser Block). **D**: Sandige Schichten werden von konglomeratischen Rinnenfüllungen überlagert (Zollstock ist 60 cm lang).

grain size, roundness and fabrics. Medium to very thick beds of sandstones and conglomerates show planar bedding, cross bedding and trough cross bedding or are of massive appearance. These sediments were accumulated in a fluvial environment, too. Lake or lagoonal deposits, however do not occur in the Klouček-Čenkov Formation of the Litavka valley.

Outcrops with rocks of the **Chumava-Baština Formation** are not numerous in the Litavka valley. Larger blocks of this formation were found in the

GEOLOGICA SAXONICA
Journal of Central European Geology 54 (2008) 1–168

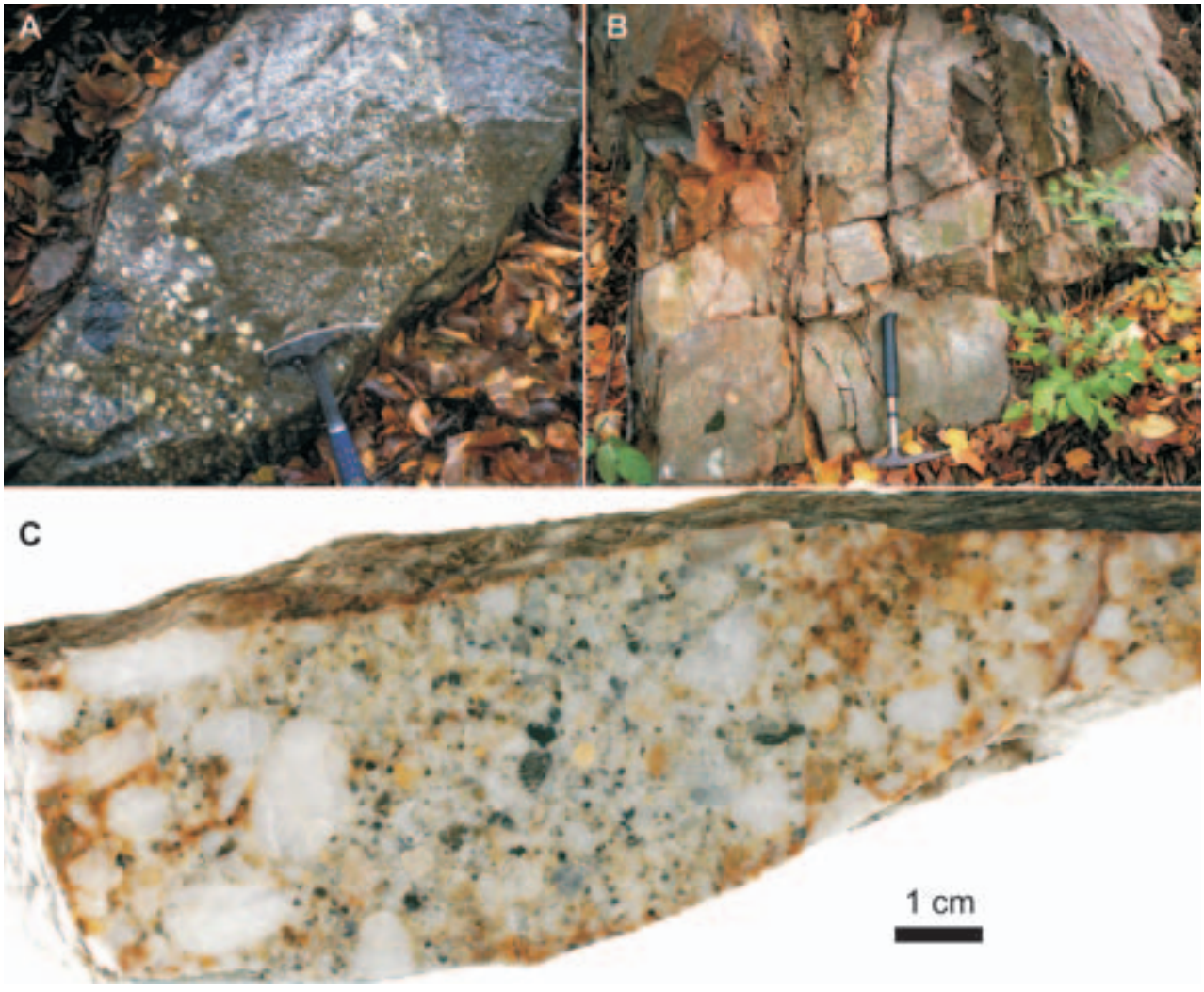

Fig. 3.4: Chumava-Baština Formation. **A**: Matrix-supported conglomerate with chiefly stable clasts. Pebbles are partly rounded, partly aligned. The large black pebble in the lower left part is 8 cm in size. **B**: Medium-grained sandstones within the uppermost part of the Chumava-Baština Formation. **C**: Polished specimen (picked sample) showing both subangular clasts and well rounded pebbles. Localities: **A**, **C** – brook NE of Čenkov, **B** – Jince Vinice.

Abb. 3.4: Chumava-Baština Formation. **A**: Matrixgestützte Konglomerate mit vorwiegend stabilen Klasten. Die Gerölle sind zum Teil gerundet und zum Teil eingeregelt. Das große schwarze Geröll unten links ist 8 cm groß. **B**: Mittelkörnige Sandsteine im obersten Teil der Chumava-Baština Formation. **C**: Poliertes Handstück (Lesestein) in dem sowohl kantengerundete als auch gut gerundete Gerölle sichtbar sind. Lokalitäten: **A**, **C** – Bach NE' von Čenkov, **B** – Jince Vinice.

bed of an unnamed brook NE of the village Čenkov. Here matrix-supported conglomerates partly contain rounded clasts or pebbles that are aligned in bedding (Fig. 3.4A, C). Pebbles reach a size of 8 cm. Planar cross bedding may occur. The uppermost part of the Chumava-Baština Formation crops out in the Jince Vinice locality and is represented by chiefly medium-grained sandstones (Fig. 3.4B). A small cliff shows questionable hummocky cross-bedding. The Chumava-Baština Formation of the Litavka valley was most probably deposited in an environment at base level representing a gradual transition between the continental Lower Cambrian deposits and the marine Jince Formation.

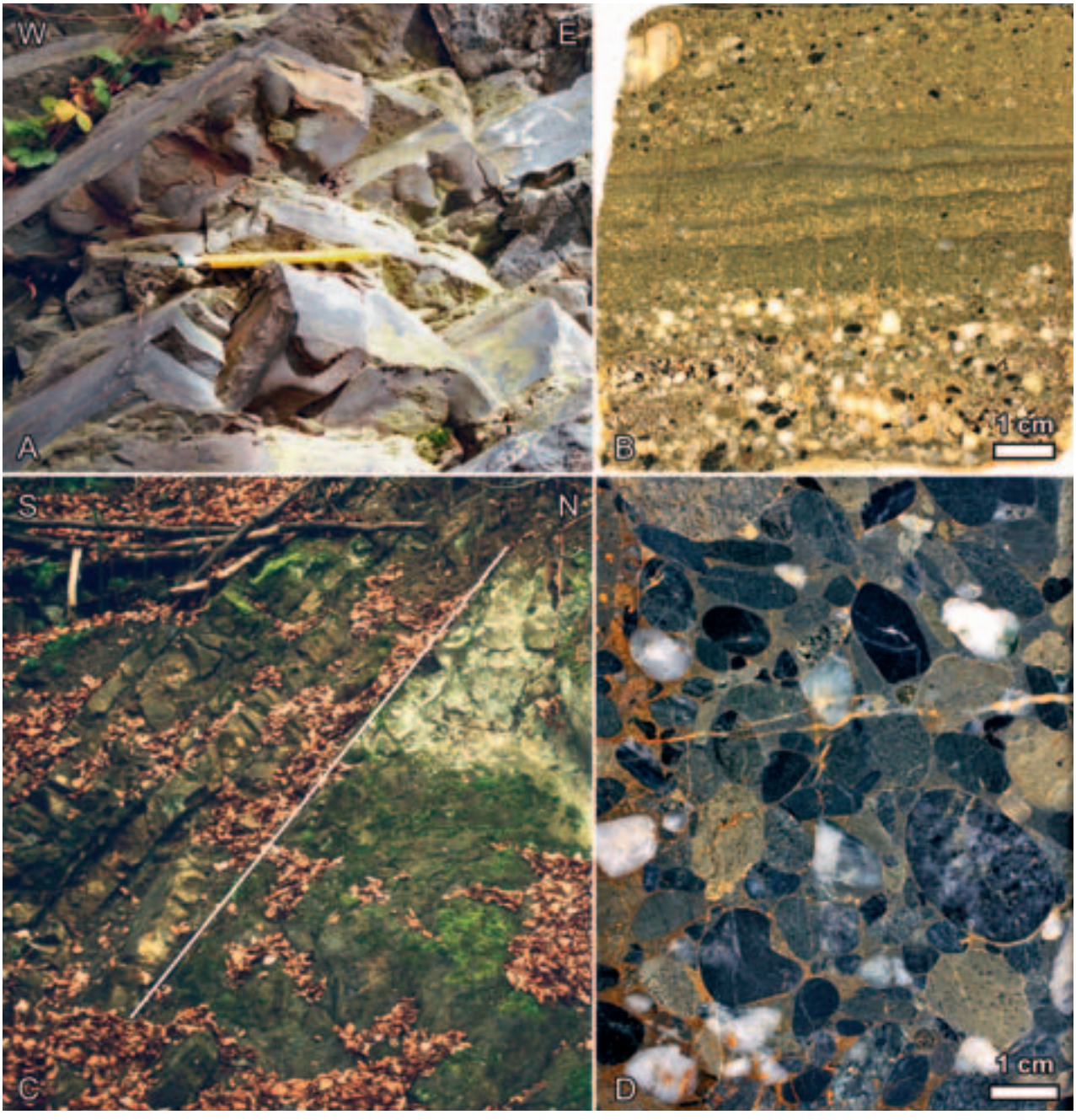

Fig. 3.5: Jince Formation. **A**: Alternation of sandstones and mudstones in the middle part of the Jince Formation in the Litavka valley (Příbram-Jince basin). Bases of the sandstone beds show scour marks. **B**: Hand specimen with conglomeratic layers. **C**: Cadomian unconformity (white line) in the Skryje-Týřovice area. Poly-deformed Neoproterozoic greywackes (N) are overlain by Middle Cambrian sandstone beds alternating with thin shale layers (S). Thickness of the visible Middle Cambrian beds is c. 120 cm. **D**: Middle Cambrian conglomerate with subangular to well rounded clasts of Neoproterozoic greywackes, volcanics and silicites. Localities: **A**, **B** – Jince Vinice, **C**, **D** – Road cut N of Týřovice, W-bank of the Berounka river.

The complete succession of the marine **Jince Formation** is preserved in the vicinity of the village Jince in the Příbram-Jince Basin. It is composed of sandstone-mudstone alternations, whereas grain-size and thickness of the sandstones largely decrease with time resulting in deposition of chiefly silty and clayey sediments in the middle part of the formation. The occurrence of water escape structures and slumping suggest rapid sedimentation and/or tectonic activity. Sole marks are developed on bases of sandstone beds (Fig. 3.5A). In the upper third of the Jince Formation number and thickness of the sandstone beds increase. Even conglomeratic layers with individual pebbles up to 1.5 cm in size occur (Fig. 3.5B). The middle part of the Jince Formation can be interpreted in terms of prodelta deposits; then progradation of the delta lead to deposition of distal to proximal delta front sediments finally replaced by channel deposits.

In the Skryje-Týřovice area the lower part of the Jince Formation is preserved. Here Middle Cambrian marine sediments lie unconformably above intensely deformed Neoproterozoic greywackes (Fig. 3–5C). In places the Early Palaeozoic sedimentation starts with highly mature, light sandstones and conglomerates occasionally showing hummocky cross-bedding. The latter and the presence of marine fauna (Havlíček 1971) point to deposition in a shallow marine environment. The largest part of the Middle Cambrian sequence of the Skryje-Týřovice area is made up by shales and immature sandstones as well as matrix or clast supported conglomerates with pebbles chiefly around 1–2 cm (Fig. 3.5D) but occasionally up to 30 cm in size. The shales occur as intercalations between sandstone and conglomerate beds, respectively, or form up to tens of meters thick sequences. The latter is in contrast to the deposits of the Příbram-Jince Basin, where also the fine-grained rocks show distinct alternations of sediments with differing grain size.

In the Příbram-Jince Basin there is a gradual transition from the marine Jince Formation to the succeeding, chiefly continental Ohrazenice Formation. At the Medový Újezd locality, where only the uppermost part of the Jince Formation crops out, lens shaped sandstone beds show thickening and coarsening upwards and represent channel fills of an initially submarine fan that is overlain by massive sandstone and conglomerate beds of the Ohrazenice Formation. Similarly in the Jince Vinice locality the increase of sandy and conglomeratic layers in the Jince Formation marks the fall of the relative sea level. The overlying **Ohrazenice Formation** is made up by conglomerates and sandstones. Sedimentary features include channels fills and cross bedding.

3.1.2 Clast types

As determined in the field and in thin section, components of the **Hluboš conglomerates** are represented by fine-grained volcanics (partly with fluidal texture), reddish aplites, cherts, granitoids, metaquartzites (partly with deformation bands), mica schists, mylonitic gneiss, and quartz (partly with bubble trains and embayments, partly with highly undulous extinction and/or transition to sub-grain formation). Undoubtfully sedimentary lithic fragments and feldspar are rare. Although the proportion of stable/unstable clasts is variable, the stable clasts tend to prevail.

Compositions of the fine- to medium-grained sandstones of the overlying **Sádek Formation**

Abb. 3.5: Jince Formation. **A**: Wechsellagerung von Sandsteinen mit Silt- und Tonsteinen im mittleren Teil der Jince Formation im Litavka-Tal (Příbram-Jince-Becken). Die Schichtunterseiten der Sandsteinschichten zeigen Belastungsmarken. **B**: Handstück mit konglomeratischen Lagen. **C**: Cadomische Diskordanz (weiße Linie) im Skryje-Týřovice-Gebiet. Mehrfach deformierte neoproterozoische Grauwacken (N) werden von mittelkambrischen Sandsteinen überlagert, welche mit dünnen Schieferlagen alternieren (S). Die Mächtigkeit der sichtbaren mittelkambrischen Schichten beträgt ca. 120 cm. **D**: Mittelkambrisches Konglomerat mit schwach bis gut gerundeten Geröllen neoproterozoischer Grauwacken, Vulkanite und Silizite. Lokalitäten: **A**, **B** – Jince Vinice, **C**, **D** – Straßenanschnitt N' von Týřovice, W-Ufer der Berounka.

were determined from thin sections and are quartzo-feldspathic. Lithic fragments are extremely rare or hardly identifiable, which might reflect the primary composition but could also be related to the small grain size and/or the state of recrystallisation. Only a few altered volcanic rock fragments could be detected. Although highly variable the content of feldspar, particularly that of plagioclase, is distinctly higher than in the underlying and succeeding Lower Cambrian formations. Furthermore many thin sections of samples from the Sádek Formation revealed a considerable amount of both opaque and transparent heavy minerals.

The siliciclastic rocks of the **Holšiny-Hořice Formation** are more mature than those of the Sádek Formation. Chert and polycrystalline quartz are the prevailing lithic fragments. Only in distinct levels clasts of volcanic rocks are frequent. For the rest unstable clasts as volcanic rock fragments and feldspar occur in distinctly lower proportions. Cathodoluminescence microscopy revealed that quartz of magmatic origin is an important component of the investigated samples. Many quartz grains do not show undulous extinction but contain trains with inclusions and show embayments. Nevertheless, also mylonitic quartz showing grain-size reduction and elongated grains occurs among the polycrystalline quartz fragments. Recrystallisation had an influence on the present appearance of the siliciclastics as is clear from authigenic quartz that forms rims around detrital quartz grains and occurs in the spaces between the grains in several thin sections.

Some of the conglomerates and sandstones of the **Klouček-Čenkov Formation** have similar petrographic compositions than those of the previous Holšiny-Hořice Formation with quartz and stable lithic fragments as the dominating components. However, volcanic detritus is extremely frequent in the samples from one locality in the upper part of the Klouček-Čenkov Formation. The clasts of these samples are almost exclusively represented by quartz-free trachytic, porphyritic or fine-grained volcanics and feldspar (plagioclase + ?alkali-feldspar) crystals.

The sandstones and conglomerates of the **Chumava-Baština Formation** are similar to those of the underlying Holšiny-Hořice and Klouček-Čenkov formations with respect to the stable clasts. In the investigated thin sections quartz, polycrystalline quartz and chert are most frequent. Additionally few volcanic lithic fragments and altered feldspar clasts may occur.

The marine siliciclastics of the **Jince Formation** are variable in composition. The spectrum of possible clasts is well visible in the conglomerates of the Skryje-Týřovice Cambrian containing granules, pebbles and even cobbles of mafic volcanics, (meta)cherts, greywackes, slates, quartzites and quartz-feldspar aggregates of probably plutonic origin (Fig. 3.5D). Metamorphic lithic fragments comprise phyllites, SC'-mylonites and polycrystalline quartz with clear indications of dynamic recrystallisation (grain-size reduction, flattening). The majority of the sedimentary rocks constituting the Jince Formation is however rather pelitic and psammitic, whereas the greywacke-like psammitic siliciclastics are made up by mono- and polycrystalline quartz of both metamorphic and magmatic origin, feldspar, chert as well as smaller proportions of volcanic and sedimentary lithic fragments.

In the continental **Ohrazenice Formation** stable components prevail again. Clasts of mono- and polycrystalline quartz and chert are most frequent. Occasionally fragments of volcanic rocks and quartz-feldspar aggregates (?granitoid pebbles) are preserved.

3.1.3 Detrital modes of the siliciclastics and implications on provenance

For 31 thin sections from Lower and Middle Cambrian siliciclastic rocks the point-counting method after Dickinson (1970, 1985) was applied to assess the provenance of the detritus. Strong recrystallisation is common in the Cambrian rocks as is indicated by authigenic rims around detrital quartz grains and by multi-grained quartz that originated from mobilisation. Therefore thin sections for modal analyses were selected according to the preservation of the original fabric. Rather immature rocks of Lower Cambrian age are probably underrepresented in this data set, because for several thin sections it was impossible to distinguish between altered rock

GEOLOGICA SAXONICA
Journal of Central European Geology 54 (2008) 1–168

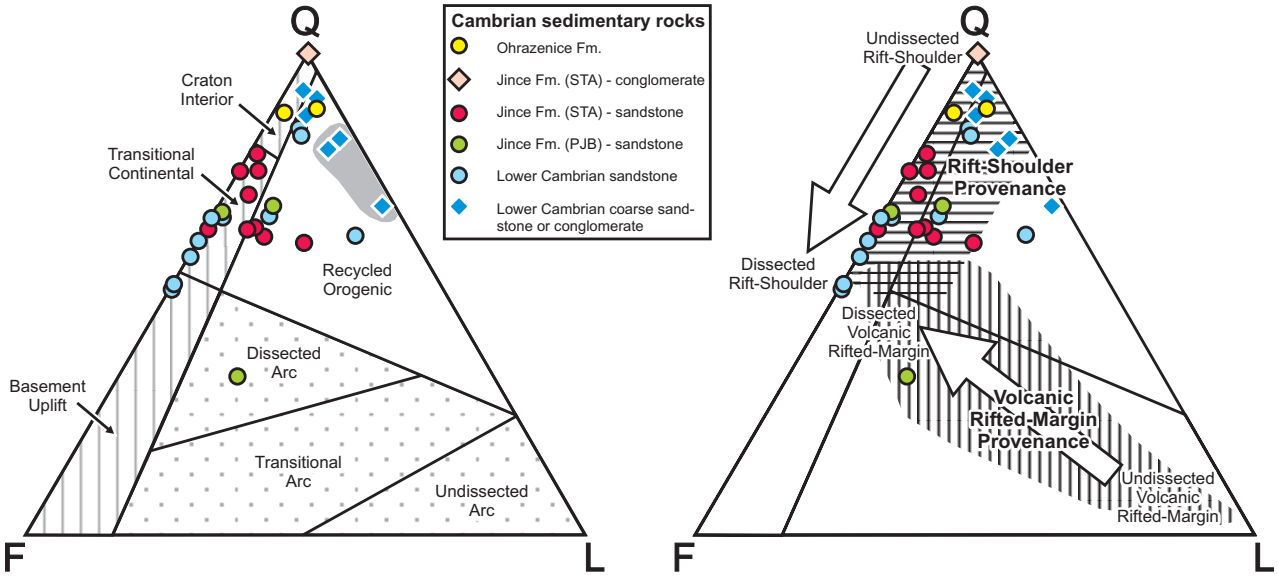

Fig. 3.6: Provenance diagrams. **F** – feldspar, **Q** – quartz, **L** – lithic fragments. **A**: Q-F-L diagram after Dickinson (1985). Detrital modes of the samples indicate a continental block and recycled orogen provenance, respectively. Grey field encloses the samples from the basal Lower Cambrian Žitec-Hluboš Formation. **B**: Q-F-L diagram showing the fields of rift shoulder provenance and volcanic rifted-margin provenance obtained by Garzanti et al. (2001) from analyses of modern sands of the Red Sea and Gulf of Aden. A rift shoulder provenance is indicated for the majority of the Cambrian samples from the Teplá-Barrandian unit.

Abb. 3.6: Provenace-Diagramme. **F** – Feldspat, **Q** – Quarz, **L** – Gesteinsbruchstücke. **A**: Q-F-L-Diagramm nach Dickinson (1985). Die Modalbestände der kambrischen Proben fallen in die Felder continental block provenance bzw. recycled orogen provenance. Das graue Feld hinterlegt die Proben von der basalen unterkambrischen Žitec-Hluboš Formation. **B**: Garzanti et al. (2001) ermittelten anhand von Analysen rezenter Sande des roten Meeres und des Golf von Aden die im Q-F-L-Diagramm dargestellten Felder rift shoulder provenance und volcanic rifted margin provenance. Eine Herkunft von gehobenen Riftschultern ist für die Mehrheit der kambrischen Proben des Teplá-Barrandiums angezeigt.

fragments ("pseudo-matrix") and detrital matrix. Also the grain-categories (**Q** – quartz, **F** – feldspar, **L** – lithic fragments) are not further subdivided to avoid additional sources of error. The results of point-counting are given in Table 2 of the Appendix.

Fig. 3.6A shows the samples within the Q-F-L diagram with the provenance fields of Dickinson (1985). Due to the scarcity or absence of unstable lithic fragments, the majority of the samples plots close to the Q-F axis and therefore, within or close to the field of continental block provenance. Varying proportions of quartz and feldspar cause alignment between the sub-fields of craton interior provenance and transitional continental provenance. The chiefly fine- to medium-grained sandstones of the Sádek and Jince formations have modal compositions that are transitional between craton interior provenance – as is to be expected on passive continental margins or in intracratonic basins – and basement uplift provenance – as is usually revealed by detrital sediments associated with rifting or transform ruptures (Dickinson & Suczek 1979, Dickinson 1980). Craton interior provenance is displayed by mature sandstones and conglomerates occurring within the entire Cambrian siliciclastic succession from the Sádek to the Ohrazenice Formation, respectively. The conglomerates and sandstones of the basal Lower Cambrian Žitec-Hluboš Formation contain larger amounts of unstable lithic fragments (cf., Kukal 1971). The modal analyses of three samples from this formation plot in the field of recycled orogen provenance. Moreover for one sandstone with lower

quartz content but distinct amounts of feldspar and lithic fragments a derivation from magmatic complexes is indicated.

Fig. 3.6A furthermore shows that recycled orogen provenance and magmatic arc provenance are not very likely. The high proportion of stable clasts implies that periods of temporary storage and redeposition under relatively warm climatic conditions provided the prerequisite for effectively operating chemical weathering (cf., Kukal 1971). Only the compositions of the rocks of the basal Žitec-Hluboš Formation suggest lower weathering intensity and faster transport to the basin. Siliciclastics containing feldspar and volcanic rock fragments seem to be derived from a mixed source providing highly weathered detritus and products of more or less syn-sedimentary volcanism. This is not in agreement with a passive margin or intracontinental setting[1] as suggested by the diagram (Fig. 3.6A) but compatible with a transtensional or extensional setting.

In fact, the modal compositions of the Cambrian sandstones and conglomerates of the Teplá-Barrandian unit resemble modern rift-related sands, e.g. those from Lake Tanganyika (East African rift system; Soreghan & Cohen 1993), from the Cerro Prieto geothermal field near the Colorado River delta (Salton Trough - Baja California rift basin system; Lyons & van der Kamp 1980) and from the Red Sea and Gulf of Aden rifted margins (Garzanti et al. 2001). Recent studies by Garzanti et al. (2001, 2006) revealed that rifted margin sands can be subdivided due to their petrographic composition into rift shoulder derived sands and sands with provenance from volcanic rifted margins (Fig. 3.6B). Sands coming from undissected rift-shoulders are mature and reflect intense weathering of a chiefly sedimentary cover. The more of the cover sequence becomes eroded, the more basement rocks become available resulting in a trend along the Q-F axis from the Q-pole to higher feldspar contents. The influence of rift-related volcanism is reflected by the volcanic rifted-margin provenance. Depending on transport distance and mechanism as well as on the nature of the volcanism and the proportions of rift-shoulder derived material there is a trend from the L-pole of the Q-F-L-diagram to quartzofeldspathic compositions. The variable modal compositions of the Cambrian samples from the Teplá-Barrandian are in good agreement with this provenance scheme (Fig. 3.6B), whereas the majority of the analysed samples is assigned to the rift-shoulder provenance. It is therefore assumed that the Cambrian siliciclastics of the Teplá-Barrandian represent rift basin deposits.

3.2 Ordovician

Ordovician rocks were studied and sampled in several individual outcrops and sections (Fig. 3.7), whereas Lower and Middle Ordovician siliciclastics were investigated chiefly in the SW' part of the Prague synform and those of Upper Ordovician age in the NE' part.

3.2.1 Lithologies, sedimentary structures and depositional environments

In the investigated localities conglomerates and sandstones of the Tremadocian **Třenice Formation** lie disconformably above Cambrian siliciclastics (Fig. 3.8A) or unconformably above Neoproterozoic sedimentary rocks (Fig. 3.8B). The former was observed in the Medový Újezd locality, where the SW

[1] Previous studies (Kukal 1971, Havlíček 1971) have suggested that the Cambrian siliciclastics represent molasse sequences that were deposited in intramontane troughs. The detritus was interpreted to be derived from local sources represented by Late Neoproterozoic rock units of the Cadomian orogen. However, the clast inventory of the Cambrian detrital sediments showing prevalence of stable clasts is not in agreement with that of molasse deposits, i.e. short and fast transport of detritus from recently accreted island arc and back-arc complexes to an intramontane basin. Enhanced chemical weathering would be required to modify the primary compositions of such source rocks in a suitable way. Kukal (1971) suggests a tropical or subtropical, continental climate and the formation of thick residual gravel covers that were reworked and transported to the basin. Yet the latter requires a morphology that is not well compatible with an intramontane basin and the deposition of molasse sequences.

GEOLOGICA SAXONICA
Journal of Central European Geology 54 (2008) 1–168

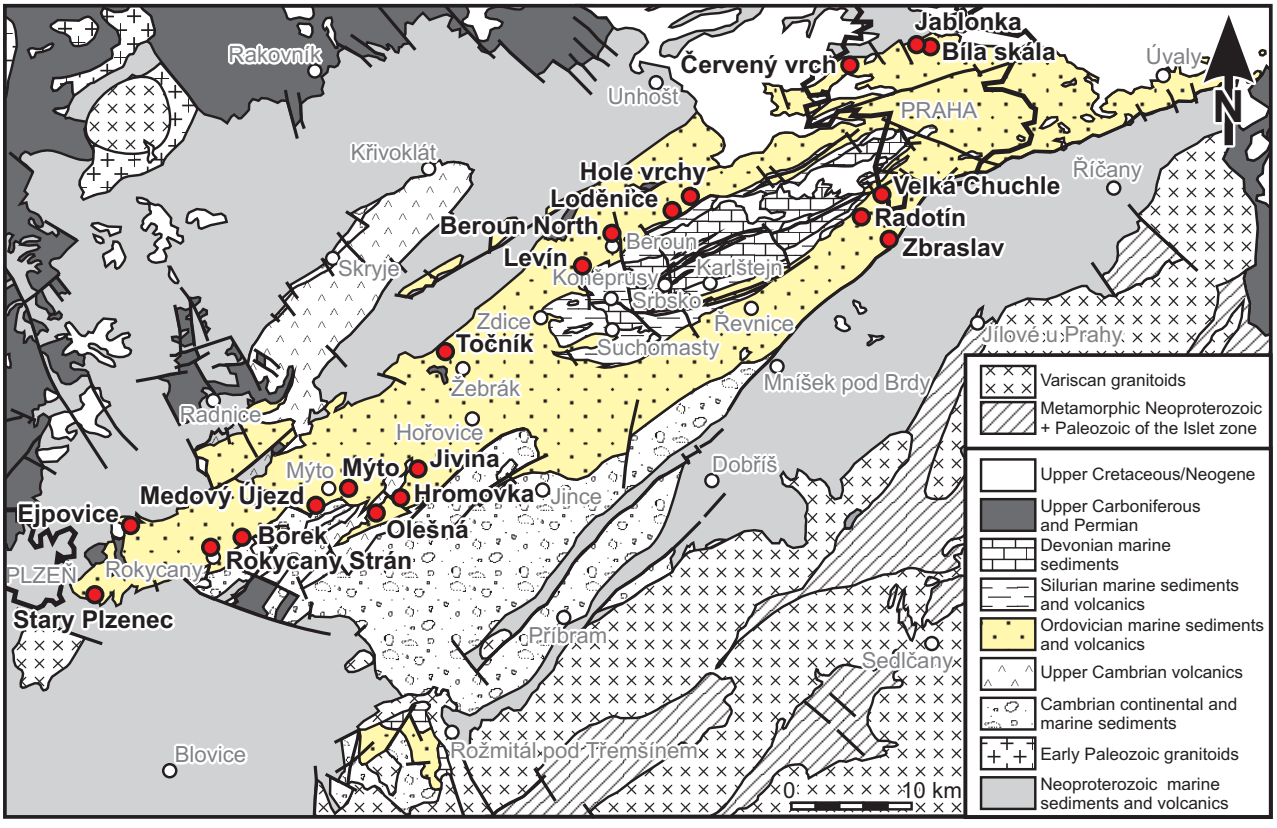

Fig. 3.7: Sketch map showing the location of the investigated outcrops and sections within the major range of Ordovician deposits in the Teplá-Barrandian unit. Names of the localities are given in black and correspond to those listed in Table 1 of the Appendix.

Abb. 3.7: Schematische Karte mit der Lage der untersuchten Aufschlüsse und Profile im Hauptverbreitungsgebiet ordovizischer Gesteine im Teplá-Barrandium. Die Namen der Lokalitäten sind in schwarz eingetragen und entsprechen denen in Tab. 1 des Anhangs.

limb of an anticline crops out. Here Middle Cambrian siliciclastics of the Jince and Ohrazenice formations are overlain by conglomerates and sandstones of the Lower Ordovician Třenice Formation, which in turn is succeeded by a basal conglomerate and shales of the Klabava Formation. Orientation of the bedding planes is similar for the Middle Cambrian and Lower Ordovician rocks (Fig. 3.8A inset) ruling out an angular unconformity between Cambrian and Ordovician (at least in this place). The hiatus between the Ohrazenice Formation and the Třenice Formation corresponds to a time span of approximately 20 My.

The Tremadocian Třenice Formation (Fig. 3.8C) is represented by marine conglomerates and sandstones. A basal conglomerate with rounded to subangular pebbles and occasionally boulders and cobbles is overlain by moderately to well sorted conglomerates, sandstones and less frequent siltstones. Although obscured by recrystallisation due to diagenetic and hydrothermal processes, particles seem to be subangular to subrounded. Thickness of the massive or internally laminated beds is highly variable and ranges between few centimetres to > 1 m. Trough cross bedding and hummocky cross bedding are the prevailing sedimentary structures. Furthermore in places coarser particles were observed at the base of sandstone or conglomerate beds. According to grain size, sorting and sedimentary structures a shoreface environment can be inferred for the sediments of the Třenice Formation.

Fig. 3.8: **A**: Erosional disconformity between the Middle Cambrian Ohrazenice Formation (massive bed to the left, orientation 135/47) and the Tremadocian Třenice Formation (orientation 140/45) at the locality Medový Újezd. Hammer lies on the basal conglomerate of the Třenice Formation. Inset: Poles of the bedding planes in Schmidt net. Black circles stand for Middle Cambrian, white ones for Lower Ordovician rocks, respectively. **B**: Angular unconformity between Neoproterozoic shales (to the right) and the Tremadocian Třenice Formation. The discordance plane dips to the left in the back (orientation: 152/57). Locality: Točnik. **C**: Shallow-water sediments of the Třenice Formation at Jivina old quarries. **D**: Klabava Formation at Medový Újezd with basal conglomerate (left) overlain by shales. **E**: Silicified silty shales of the Klabava Formation at Točnik.

In the locality Točnik the Třenice Formation is overlain by silicites of the **Klabava Formation**[1] (Fig. 3.8E), whereas the contact between the sandstones/conglomerates and the cherts is not clearly traceable. Rocks of both formations were effected by silicification. In contrast fine-grained conglomerates and sandstones of the Třenice Formation are overlain by a basal conglomerate and by red and green shales of the Klabava Formation in the Medový Újezd locality (Fig. 3.8D). The effect of hydrothermal fluids is less obviously in this outcrop.

The Klabava Formation reaching from the Tremadocian to the lower Middle Ordovician comprises a large variety of siliciclastics, pyroclastics and oolitic iron ores that were formed in laterally differing environments. Particularly the now active Komárov volcanic complex had a considerable impact on the sedimentary facies. On the one hand tuffitic rocks of various colours were observed in the localities Mýto, Borek and Ejpovice (Fig. 3.7). In the latter place also ooids of iron compounds, carbonaceous beds and tuffs occur. Red and partly green shales and sandstones as well as silicites are preserved in somewhat easterly located outcrops (Jivina, Hrmovka, Olešna). On the other hand few hundred meters of monotonous yellowish-green to greyish-brown shales without obvious influence from magmatic and tectonic activity are exposed N of Rokycany (Fig. 3.7). The presence of glauconite and phosphatic particles in the sandstones and conglomerates points to a shelf environment that is – as shown by carbonatised tuffs and tuffites as well as by iron oolites[2] – controlled by volcanic and hydrothermal activity.

Rocks of the succeeding **Šárka Formation** are Darriwillian in age and comprise brownish grey to dark grey shales as well as few siltstones and fine-grained sandstones. In places siliceous concretions occur, e.g., in the Červeny vrch locality within the city of Prague, where the lowermost part of the Šárka Formation was exposed in a temporary excavation. Oolitic iron ores are a common feature in the localities Ejpovice and Mýto. The iron ooids are preserved in a matrix that is composed of shale/siltstone and/or carbonatised tuff or tuffite. The variability of kind and proportion of the matrix between the ooids and the formation of ooids around older ones point to involvement of redeposition processes.

The **Dobrotivá Formation** is made up by shale-siltstone-sandstone successions (Fig. 3.9). The shales and siltstones are mostly dark (occasionally yellowish brown or light grey), contain varying amounts of white mica and may enclose concretions. The sandstones are rather fine-grained and well sorted. The sandstone beds are between ~10 cm and > 1.5 m thick, thickness of the shale and siltstone intercalations varies from

[1] The silicites were until recently assigned to the Milina Formation. They were interpreted to result from biochemical sedimentation in a very shallow water environment during a regression (e.g., Havlíček & Vaněk 1966, Havlíček 1998). Kukal (1963), however, suggested formation of the silicites in relation to volcanic activity. Recent interpretations (Kraft & Chlupáč 2004) also assume silicification due to volcanic activity but consider the shales, sandstones and cherts formerly assigned to the Milina Formation to be part of the Klabava Formation. The latter is followed in this studie.

[2] Ooids are up to 4 mm in size. They are composed of chamosite and/or hematite and usually formed around a nucleus. The nuclei are represented by detrital minerals or rock fragments, biogenic detritus and older ooids. Sturesson et al. (1999, 2000) have shown that the formation of such ooids is associated with volcanic ash falls, emanations of Fe, Al and Si enriched fluids and/or to rapid weathering of fresh volcanic rocks. These authors furthermore underline the relation of iron ooids with relative low stands of the sea level and with low sedimentation rates.

Abb. 3.8: **A**: Erosionsdiskordanz zwischen der mittelkambrischen Ohrazenice Formation (massive Bank links, Fallrichtung/Fallwinkel: 135/47) und der tremadozischen Třenice Formation (140/45) in der Lokalität Medový Újezd. Der Hammer liegt auf den basalen Konglomeraten der Třenice Formation. Schmidtsches Netz: Pole der Schichtflächen der mittelkambrischen (schwarze Kreise) und tremadozischen Gesteine (weiße Kreise). **B**: Winkeldiskordanz zwischen neoproterozoischen Schiefern (rechts) und der tremadozischen Třenice Formation in der Lokalität Točnik. Die Diskordanzfläche fällt nach links hinten ein (152/57). **C**: Flachwassersedimente der Třenice Formation in den alten Steinbrüchen Jivina. **D**: Klabava Formation in der Lokalität Medový Újezd. Basale Konglomerate (links) werden von Tonsteinen überlagert. Silizifizierte siltige Tonsteine der Klabava Formation in der Lokalität Točnik.

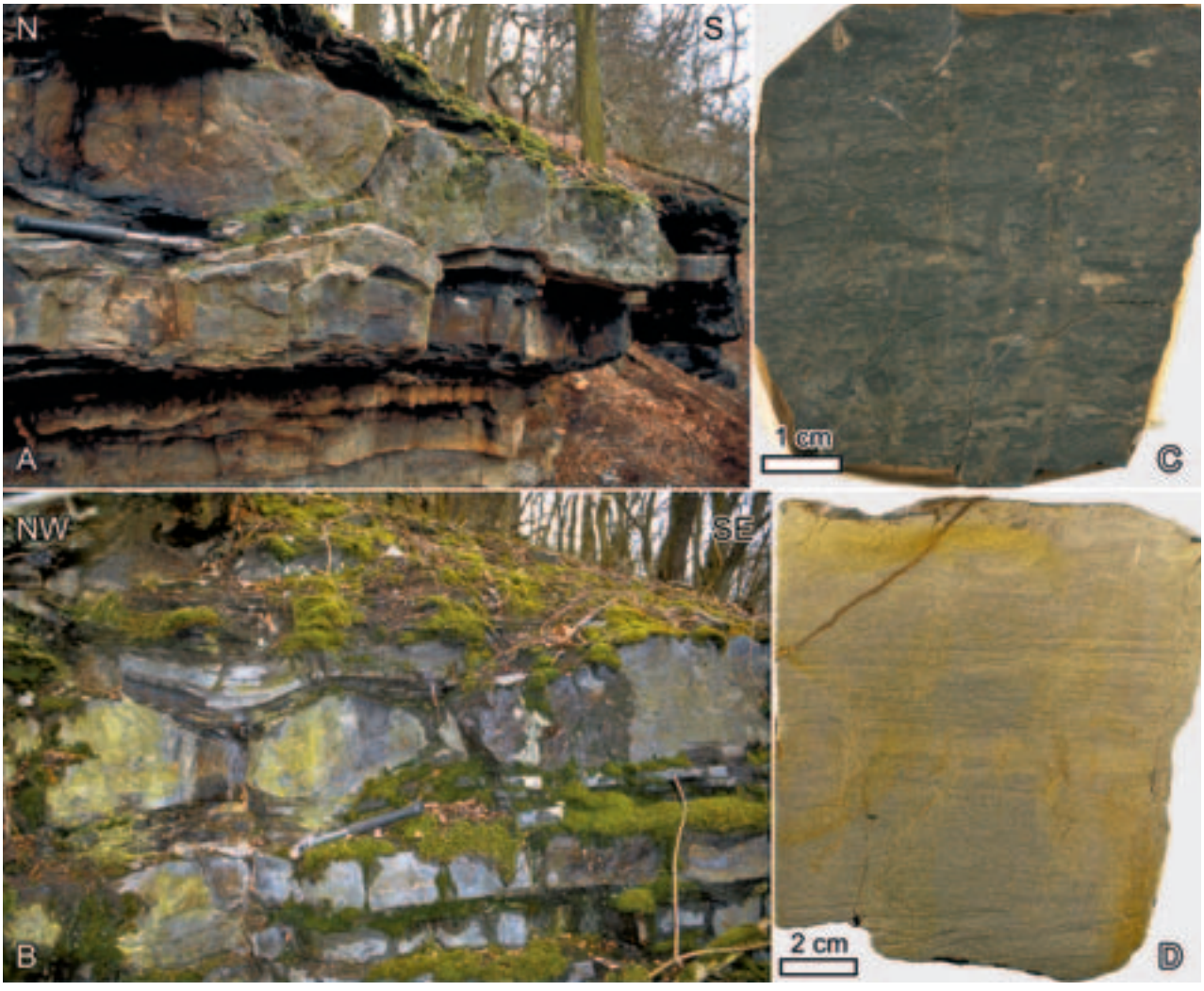

Fig. 3.9: Dobrotivá Formation. **A** and **B**: Outcrops in the Starý Plzenec locality showing alternations of sandstone, siltstone and shale. Pinch and swell structure of a thick sandstone bed is well visible in **B**. **C**: Polished hand specimen of a siltstone from the Jablonka locality exhibiting highly turbate texture. **D**: Polished hand specimen of a siltstone from the Jablonka locality showing horizontal and ripple cross lamination, respectively. In the uppermost part convolute bedding is observable.

Abb. 3.9: Dobrotivá Formation. **A** und **B**: Aufschlüsse in der Lokalität Starý Plzenec in denen Wechsellagerungen von Sand-, Silt- und Tonsteinen angeschnitten sind. Eine mächtige Sandsteinbank zeigt pinch-and-swell-Strukturen. **C** und **D**: Polierte Handstücke von Siltsteinen aus der Lokalität Jablonka. Der dunkle Siltstein in **C** zeigt ein stark turbates Gefüge, während die Probe in **D** horizontale und Rippelschrägschichtung sowie im obersten Teil convolute bedding aufweist.

few mm to several dm (Fig. 3.9A, B). Hummocky cross bedding (mostly dm-scale), small- to medium-scale ripple cross bedding, horizontal lamination and amalgamated beds are the prevailing sedimentary structures in the sandstone beds. Shale and siltstone beds contain starved ripples and thin sandstone layers. They have partly turbate textures (Fig. 3.9C) but may also show fine horizontal lamination, ripple cross bedding as well as convolute bedding (Fig. 3.9D). In the Starý Plzenec locality pinch and swell structures were observed in the sandstone beds (Fig. 3.9B) that may have formed in the semi-consolidated rock

GEOLOGICA SAXONICA
Journal of Central European Geology 54 (2008) 1–168

Fig. 3.10: Libeň Formation at Bíla Skála locality. **A**: Medium and thick sandstone beds with thin to very thin shale intercalations. **B**: Wavy (dm- to m-scale) upper bedding surface of a sandstone bed. **C**: Base of a sandstone bed showing sole marks. **D**: Ripple marks on upper bedding surface of a sandstone bed.

Abb. 3.10: Libeň Formation in der Lokalität Bíla Skála. **A**: Sandsteinschichten mittlerer bis großer Mächtigkeit mit dünnen bis sehr dünnen Tonsteineinschaltungen. **B**: Wellige (dm- bis m-Maßstab) Oberseite einer Sandsteinschicht. **C**: Unterseite einer Sandsteinschicht mit Sohlmarken. **D**: Rippelmarken auf der Oberseite einer Sandsteinschicht.

during slumping processes. The sediments of the Dobrotivá Formation were deposited in a storm-influenced transitional zone to shelf environment.

The studied rocks of the **Libeň Formation** are largely similar to those of the Dobrotivá Formation being composed of sandstone-siltstone-shale alternations (Fig. 3.10A). The sandstones tend to have somewhat larger grainsize (fine- to medium sand). The occurrence of Skolithos ichnofossils, hummocky cross stratification (dm- to m-scale; Fig. 3.10B) as well as current and oscillation ripples chiefly on top of the sandstone beds (Fig. 3.10D) and sole marks on the base of sandstone beds (Fig. 3.10C) are characteristic for storm-induced deposits, whereas the depositional environment is somewhat more proximal to the coast (inner shelf to shoreface) than that of the investigated rocks of the underlying Dobrotivá Formation. Rapid sedimentation of individual beds is indicated by water escape structures in the shale-siltstone proportions of the Libeň Formation.

The **Letná Formation** was studied in a ca. 250 m long road cut in Prague Zbraslav. Chiefly thin to medium thick sandstone beds alternate with silty and clayey mudstones (Fig. 3.11). The rocks occasionally show sole marks, horizontal lamination, small-scale cross bedding and ripple marks, turbate

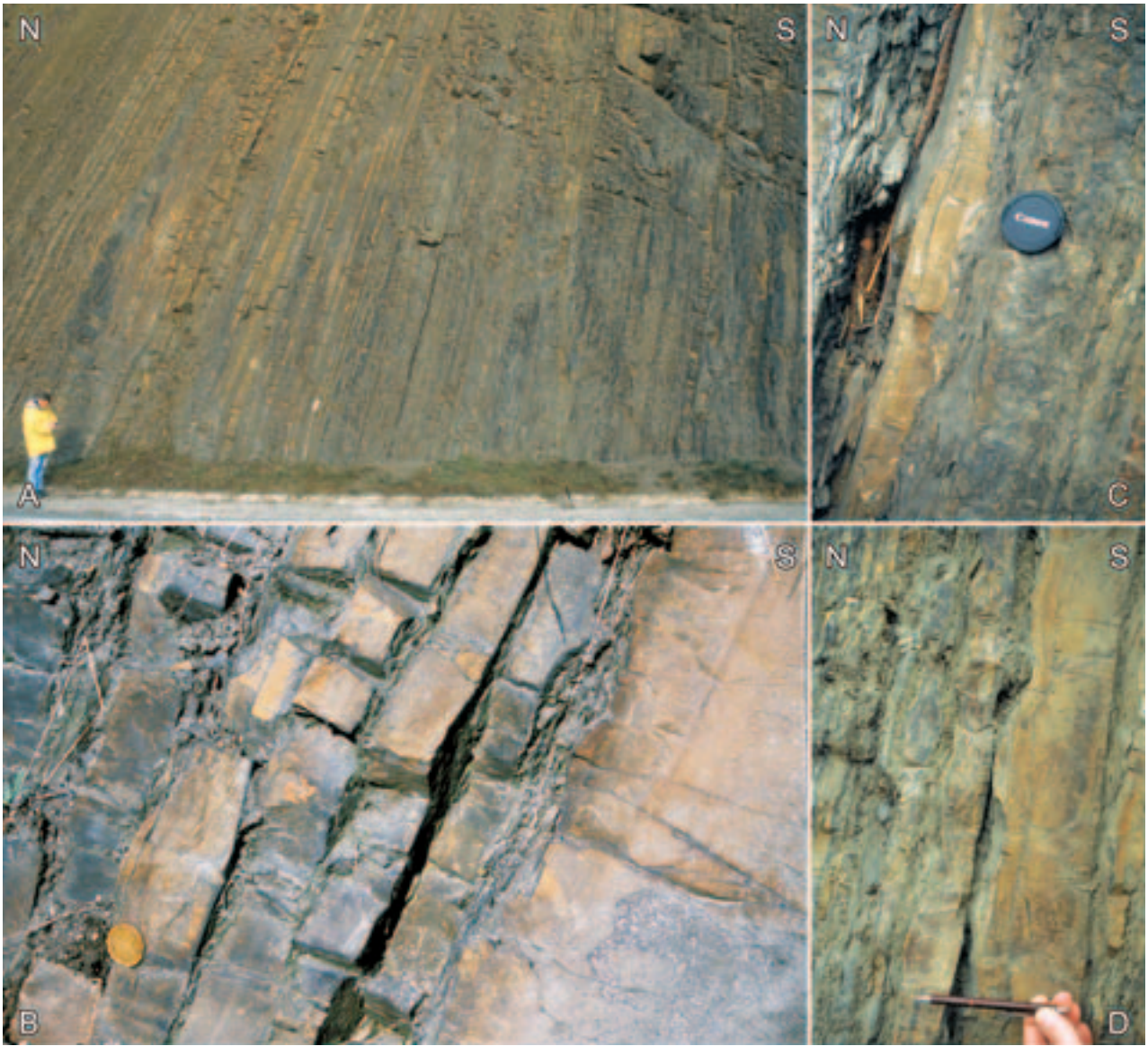

Fig. 3.11: Letná Formation in the locality Zbraslav. **A**: Steeply NNW-dipping, thin to medium beds of the Letná Formation. **B**: Sandstone bed with erosive base. **C**: Sandstone/mudstone alternation. Sandstones show ripples on upper bedding surface (thick bed to the right), sole mark (first thin bed to the right) and cross bedding (bed with coin). **D**: Ripple marks (15–20 cm amplitude) on upper bedding surfaces.

Abb. 3.11: Letná Formation in der Lokalität Zbraslav. **A**: Steil nach NNW einfallende, Schichten geringer bis mittlerer Mächtigkeit. **B**: Sandsteinschicht mit erosiver Basis. **C**: Sandstein-Tonstein-Wechellagerung. Die Sandsteine zeigen Rippeln auf den Scichtoberseiten (mächtige Bank rechts), Sohlmarken (erste dünne Bank rechts) und Schrägschichtung (Bank mit der Münze). **D**: Rippelmarken (15–20 cm Amplitude) auf Schichtoberseiten.

textures/convolute bedding, fading ripples as well as ichnofossils. Small-scale (few cm) pinch and swell structures in matrix-rich sandstones are most probably caused by water escape processes and point to rapid sedimentation (at least for individual beds) and/or tectonic activity. The sedimentary structures

GEOLOGICA SAXONICA
Journal of Central European Geology 54 (2008) 1–168

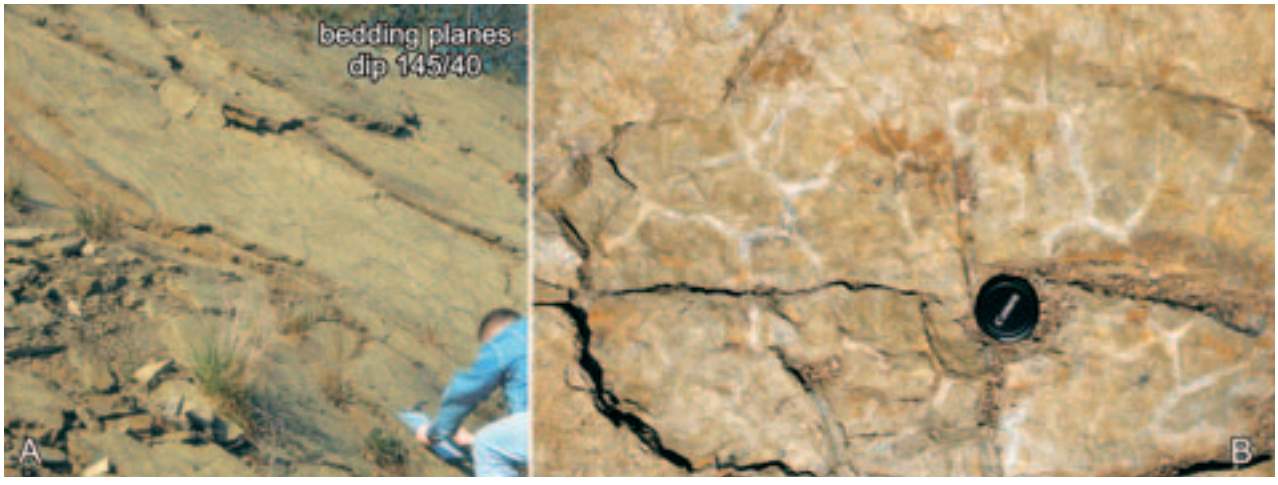

Fig. 3.12: Siltstones of the Zahořany Formation. Upper bedding surfaces of the chiefly thin beds showing ripple marks (**A**) and ichnofossils (**B**). Locality: Loděnice vinice.

Abb. 3.12: Siltsteine der Zahořany Formation. Die Schichtoberseiten der meist geringmächtigen Schichten zeigen Rippelmarken (**A**) und Ichnofossilien (**B**). Lokalität: Loděnice vinice.

in the high frequency alternation of shales, siltstones and sandstones imply a deposition by turbidity currents. However, the observed sedimentary structures together with the lack in graded bedding, the relatively good sorting of the sandstone beds and the presence of a Cruziana ichnofacies[1], rather point to a fluvial dominated shelf environment.

The **Vinice Formation** is made up by shales deposited in a distal environment. Samples were taken in the locality Beroun North (Fig. 3.7). The overlying siltstone-dominated **Zahořany Formation** was investigated in the localities Loděnice and Hole vrchy (Fig. 3.7). The thinly bedded siltstones show horizontal lamination, small-scale cross bedding, or bioturbation. Ripple marks may be preserved on upper bedding surfaces (Fig. 3.12A). The siltstones yield witnesses of the Zoophycus and Cruziana ichnofacies (Mikuláš 1990) that are indicative of outer shelf and continental slope environments, respectively (Bromley 1999).

Samples of the **Bohdalec** and **Králův Dvůr formations** were taken from shales that crop out in the Velká Chuchle and Levín localities (Fig. 3.7), respectively. In the uppermost part of the Králův Dvůr Formation a c. 15 cm thick carbonate bed is overlain by c. 1 m shales containing several horizons with carbonaceous lenses. These shales are in turn overlain by a 0.15 m thick glaciomarine diamictite bed, the base of which represents the base of the **Kosov Formation**. After c. 2.5 m shales another horizon with glaciomarine diamictites occurs, which has a thickness of c. 2.4 m in the locality Levín (Fig. 3.13A). The diamictites are partly massive and partly show fine lamination (Fig. 3.13B). They are made up by a fine-grained matrix in which sand-sized grains and pebbles are included. In the investigated outcrop maximum pebble size was 3.5 cm, whereas pebbles up to 1.5 cm were relatively frequent (Fig. 3.13B). Clasts are rounded to angular. The diamictites are overlain by shales and thin sandstone beds that are in turn followed by fining and thinning upward sandstone-shale sequences. The sandstones show tool marks and scour marks on lower bedding surfaces, small-scale cross bedding, ripple marks and hummocky cross stratification. In the Radotín locality the higher part of the Kosov Formation is accessible. There similar storm-influenced shelf sediments are preserved (Fig. 3.13C, D).

[1] The Cruziana ichnofacies was identified by Chlupáč & Kukal (1988). Bromley (1999) assignes this ichnofacies to proximal to distal shelf environments.

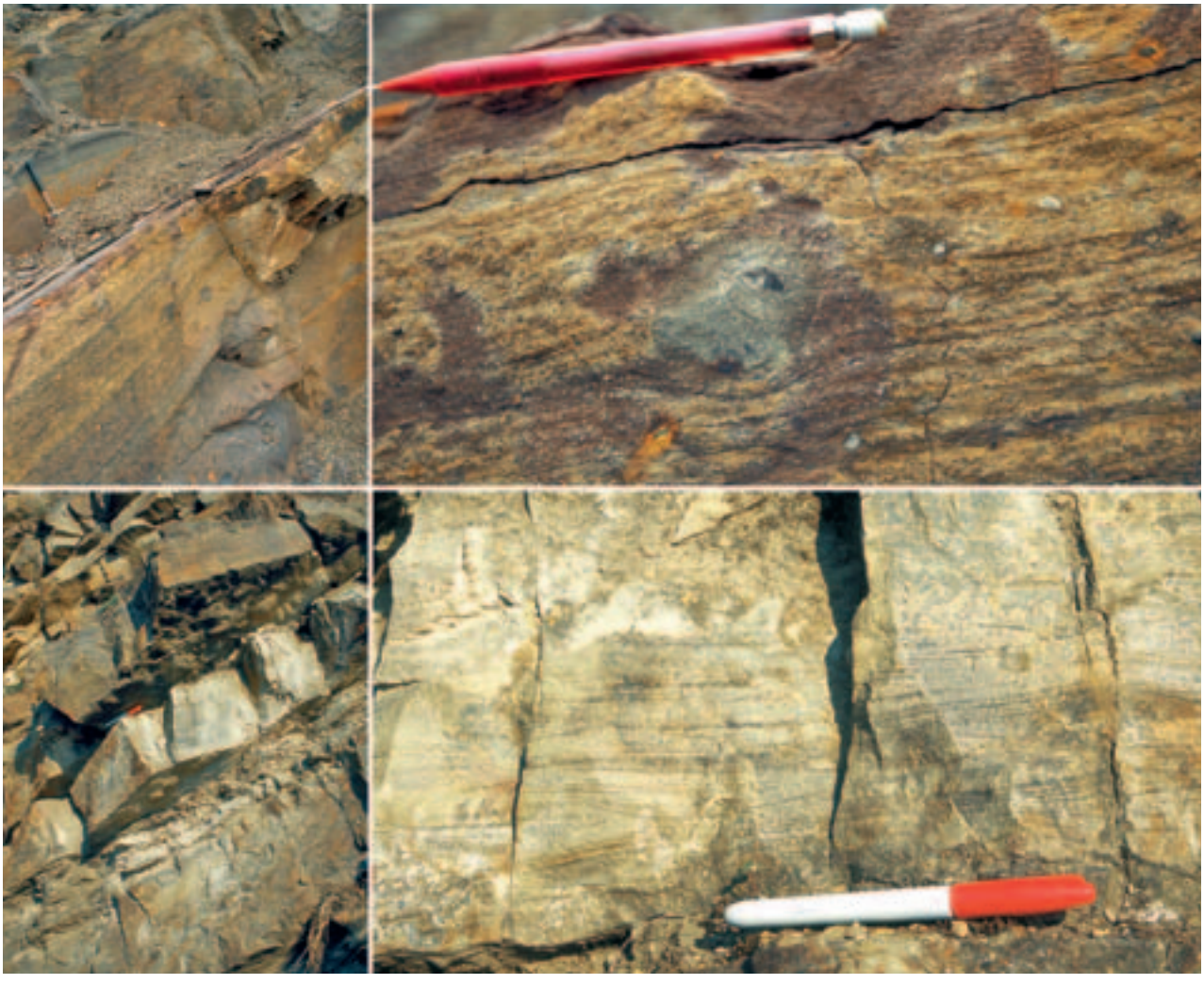

Fig. 3.13: Kosov Formation. **A**: Upper horizon of the glaciomarine diamictite. B: Dropstones in finely laminated part of the upper diamictite horizon. **C**: Storm-induced alternation of sandstones and shales. Lower bedding surfaces of the sandstone beds may show flute casts. **D**: Internal lamination of the sandstone beds may be plane or wavy. Localities: **A**, **B** – Levín, **C**, **D** – Radotín.

Abb. 3.13: Kosov Formation. **A**: Oberer Horizont des glazoimarinen Diamiktits. **B**: Dropstones in fein laminiertem Teil des oberen Diamiktithorizonts. **C**: Sturm-induzierte Wechsellagerung von Sand- und Tonsteinen. Die Schichtunterseiten der Sandsteinbänke zeigen zum Teil flute casts. **D**: Interne Lamination von Sandsteinbänken, welche eben oder wellig sein kann. Lokalitäten: **A**, **B** – Levín, **C**, **D** – Radotín.

3.2.2 Clast types

The sandstones and conglomerates of the **Třenice Formation** contain stable clasts – such as quartz (often rhyolite-derived, some vein quartz with vermicular chlorite), chert as well as quartzose tectonite fragments – intensely altered feldspars and clasts of chiefly felsic volcanics, pyroclastics and siliciclastic sedimentary rocks in highly variable proportions. Feldspars are chiefly represented by kaolinitised orthoclase and sericitized plagioclase, whereas the latter were only recognised through comparison with the phenocrysts in the Upper Cambrian porphyritic rhyolites (cf., chapter 4.1). A further characteristic feature is the occurrence of glauconite in partly considerable abundance.

The basal conglomerate of the **Klabava Formation** shows a similar clast inventory as the underlying Třenice Formation. The volcanogenic clasts are, however, prevailing and comprise rhyolite pebbles (partly with fluidal texture, often porphyritic with large quartz phenocrysts, sometimes with completely decomposed feldspar phenocrysts) and strongly altered and recrystallised fine-grained groundmass fragments of silicic volcanics. Fragments of basic and/or intermediate volcanics are rare. Also in the Klabava Formation glauconite is an important mineral. Apart from the basal conglomerate it was found in a sandstone and a conglomerate from the locality Borek and in the shales at Medový Újezd. Furthermore chamosite and hematite ooids were observed in shales.

Silt and fine sand grains in the siliciclastics of the **Šárka Formation** are represented by quartz, white mica and rare plagioclase. Intrabasinal and possibly in few cases in-situ formed hematitic and chamositic iron oolites are an important component within this formation.

The clast spectra of the sandstones and siltstones of the **Dobrotivá and Libeň formations** are dominated by monocrystalline quartz. Detrital white mica may be frequent as may be stable heavy minerals (zircon, rutile, monazite, tourmaline). Orthoclase and plagioclase are extremely rare or absent. Undoubtfully identifiable lithic fragments were not observed. Nevertheless it can not be excluded that few of the matrix domains are not detrital but derived from diagenetic decomposition of fine-grained lithic fragments. The proportion of these questionable domains is, however, low and – if any – originated most likely from intraformational shale clasts.

In the fine-grained sandstones and siltstones of the **Letná and Zahořany formations** the clast inventory is similar except for the fact that fresh plagioclase occurs in small but distinct amounts. Additionally few quartz-feldspar aggregates and few quartz-white mica composites were observed in the sandstones from the Letná Formation.

The observed sand- to pebble-sized clasts of the glaciomarine diamictite of the **Kosov Formation** are chiefly represented by quartz and fine-grained rock fragments (shales, siltstones, altered volcanics), feldspar is rare. The succeeding fine-grained sandstones are largely similar to those of the Dobrotivá and Libeň formations but additionally include a small proportion of carbonate clasts, feldspar and glauconite.

3.2.3 Detrital modes of the siliciclastics

Determination of the detrital modes of the Ordovician siliciclastics is difficult due to advanced recrystallisation. Particularly the Lower Ordovician sandstones and conglomerates were furthermore subject to silicification. The detrital modes of 15 maintainable thin sections from Ordovician sandstones and conglomerates were determined after Dickinson (1970, 1985) and are given in Table 2 of the Appendix.

Lower/Middle Ordovician rocks have varying Q:F:L ratios, which results in two small clusters within the recycled orogenic and transitional arc fields of the provenance diagram after Dickinson (1985; Fig. 3.14A). Both suggested provenances are not very likely because of the character of the underlying and overlying rocks. It is proved that the majority of the detritus is derived from rift-related felsic volcanic rocks of Cambrian age and from deeply weathered Neoproterozoic basement (cf., Kukal 1963; chapters 3.2.2, 4.3 and 7.3.2 of this study). Therefore a rifted margin provenance is to be expected. In Fig. 3.14B the plotted data for Lower/Middle Ordovician sandstones and conglomerates, however, do only partly match the field of volcanic rifted margin provenance. The remaining three sandstones have a deficiency in feldspar. Since feldspar phenocrysts are intensely altered even within the preserved equivalents of the supposed volcanic source rocks (cf., chapter 4.1) it is not surprising that the feldspars are not identifiable after sedimentary reworking[1].

[1] The intense alteration of feldspar was not only caused by weathering but enhanced by hydrothermal fluids released during the Upper Cambrian /Lower Ordovician volcanic stage. This is obvious from the occurrence of silicification in Lower Ordovician detrital sediments and from altered geochemical compositions of samples from several localities. Similar alteration by hydrothermal fluids was recognized in recent sands from Lake Tanganyika (East African rift system; Soreghan & Cohen 1993) resulting in a clear shift of the detrital modes away from the Q-F-axis and towards the Q-L-axis.

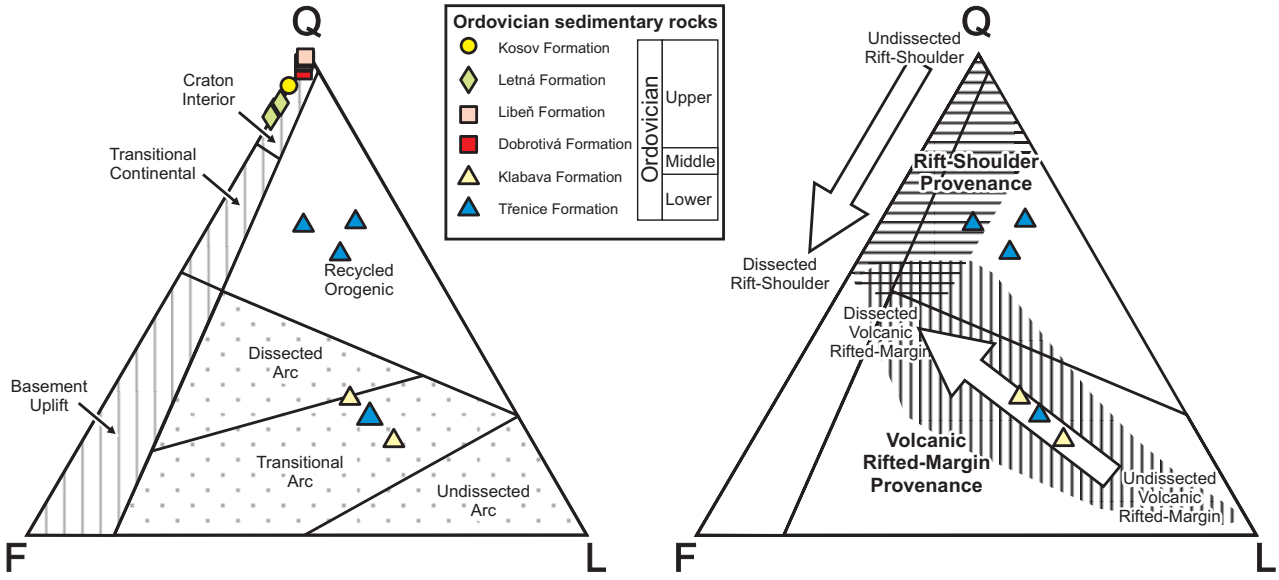

Fig. 3.14: Provenance diagrams for the Ordovician sandstones and conglomerates. **Q** – quartz, **F** – feldspar, **L** – lithic fragments. **A**: Q-F-L diagram after Dickinson (1985). Detrital modes of the Lower/Middle Ordovician samples indicate a magmatic arc or recycled orogen provenance, respectively. The Middle/Upper Ordovician samples fall into the field of craton interior provenance. **B**: Q-F-L diagram after Garzanti et al. (2001) showing the fields of rift shoulder and volcanic rifted-margin provenance, respectively. Because of the low feldspar contents the Lower/Middle Ordovician sandstones and conglomerates of the Teplá-Barrandian unit do only partly fall in the specified fields.

Abb. 3.14: Provenace-Diagramme. **F**: Feldspat, **Q**: Quarz, L: Gesteinsbruchstücke. **A**: Q-F-L-Diagramm nach Dickinson (1985). Die Modalbestände der unter-/mittelordovizischen Proben fallen in die Felder magmatic arc provenance bzw. recycled orogen provenance. Für die mittel-/oberordovizischen Proben wird eine craton interior provenance angezeigt. **B**: Q-F-L diagram nach Garzanti et al. (2001) mit den Feldern rift shoulder provenance und volcanic rifted-margin provenance. Aufgrund ihres niedrigen Feldspatgehaltes fallen die unter-/mittelordovizischen Sandsteine und Konglomerate des Teplá-Barrandiums nur zum Teil in die vorgesehenen Felder.

In contrast, Middle/Upper Ordovician fine- to medium-grained sandstones have high quartz contents at slightly varying feldspar proportions which lets them plot close to the Q-pole, in the field of craton interior provenance (Fig. 3.14A). Such compositionally mature sediments accumulate in several settings including platforms, continental margins and rifted margins (Dickinson and Suczek 1979), whereas a passive continental margin setting is most favourable for the Middle/Upper Ordovician siliciclastics.

3.3 Geotectonic setting of the Early Palaeozoic detrital sediments

Altogether the fluvial and marine depositional environments as well as the modal compositions of the Cambrian sandstones and conglomerates can be interpreted in terms of a rift-related setting. Derivation of the detritus from deeply weathered pre-rift sedimentary and crystalline rocks as well as from syn-rift magmatic suites is in agreement with the quartzolithic to arkosic compositions of the samples and with deposition in a transtensional setting. The latter is confirmed by structural geologic analyses and geochronological data of Zulauf et al. (1997) and Dörr et al. (2002) proving emplacement of Lower Cambrian plutons in the W' and NW' parts of the

Teplá-Barrandian unit within N- to NNW-dipping, dextral, oblique-slip shear zones. Furthermore these authors proved tilting of the Neoproterozoic basement prior to 523 Ma.

In the Upper Cambrian there is a prominent hiatus within most of the Teplá-Barrandian unit. Only minor sedimentary deposits of small areal extent are assigned to the Upper Cambrian. Similarly, an Upper Cambrian hiatus is, e.g., known in the neighbouring Saxothuringian terrane (e.g., Linnemann & Romer 2002) and in the Moroccan Souss Basin (Waters & Schofield 2004).

In the Tremadoc there was a major transgression as is also correlatable over North Africa and the Arabian plate (Carr 2002, and references therein). In the Teplá-Barrandian unit conglomerates, sandstones and later shales were deposited during and after the individual stages of this transgression event. For the Lower/Middle Ordovician marine sediments a rifted margin setting is most likely. The depositional environments were influenced by magmatic and post-magmatic activity. From the higher Middle Ordovician to the lower Upper Ordovician sedimentation was dominated by storm-related reworking of siliciclastic material pointing to a relative low stand of the sea level during this time. After a repeated deepening of the sedimentary environment from the higher Upper Ordovician and the deposition of the glaciomarine diamictite in the Hirnantian another regression led to deposition of further storm sediments in the Uppermost Ordovician. The increased compositional maturity of the Middle/Upper Ordovician siliciclastic rocks points to a passive margin setting and the occurrence of the glaciomarine diamictite clearly relates the Teplá-Barrandian unit to the Cadomian-type terranes (sensu Murphy et al. 2006).

Comparing the thicknesses of the Lower, Middle and Upper Ordovician sedimentary rocks it seems that sedimentation rate increases dramatically in the Upper Ordovician (ranges of thickness of the individual formations are given by Havlíček 1998). However, Melichar (2004) has shown that at least the Bohdalec, Kralův Dvůr and Kosov formations were subject to tectonic thickening during early stages of the Variscan orogeny. Probably further tectonic studies will find evidence for additional duplications of the stratigraphic sequences in older Upper Ordovician rocks.

4 Volcanic rocks

Samples of Cambrian and Ordovician volcanic rocks were taken to get information on their petrography and geochemistry, which allows to draw inferences on the magma sources as well as on the respective geotectonic setting. A further reason for including these rocks is the fact that they represent potential sources for the Early Palaeozoic siliciclastics. Three Neoproterozoic samples and 3 samples from a Silurian volcanic sequence were added for comparison with the Cambrian and Ordovician volcanic series, i.e. to highlight changes or permanence of the geotectonic conditions.

Selected photomicrographs and a hand specimen photograph of the analysed volcanic rocks are presented in Plates I and II in the Appendix. Sampling localities are shown in Fig. 4.1 and listed in Table A1 in the Appendix.

4.1 Samples

The Neoproterozoic samples were collected in the Skryje-Týřovice area, where Middle Cambrian marine sediments lie unconformably above Neoproterozoic volcano-sedimentary successions. The samples belong to the Kralupy-Zbraslav Group (sensu Mašek 2000; see Fig. 2.4) and were subject to Cadomian deformation and metamorphism. They are grey to dark grey, fine-grained and only thin sections reveal a micro(glomero)porphyritic texture with altered phenocrysts up to a size of 1.0 mm in sample DB1/0 as well as very rare and smaller phenocrysts in samples DB6/12 and DB6/13. Phenocrysts may have originally included plagioclase, clinopyroxene, orthopyroxene, and olivine, but are largely altered and were replaced by carbonate, sericite, albite, quartz, and other phases. The groundmass has a microspherulitic texture as a result of devitrivication of the originally glassy matrix and may contain fine, disperse opaque minerals.

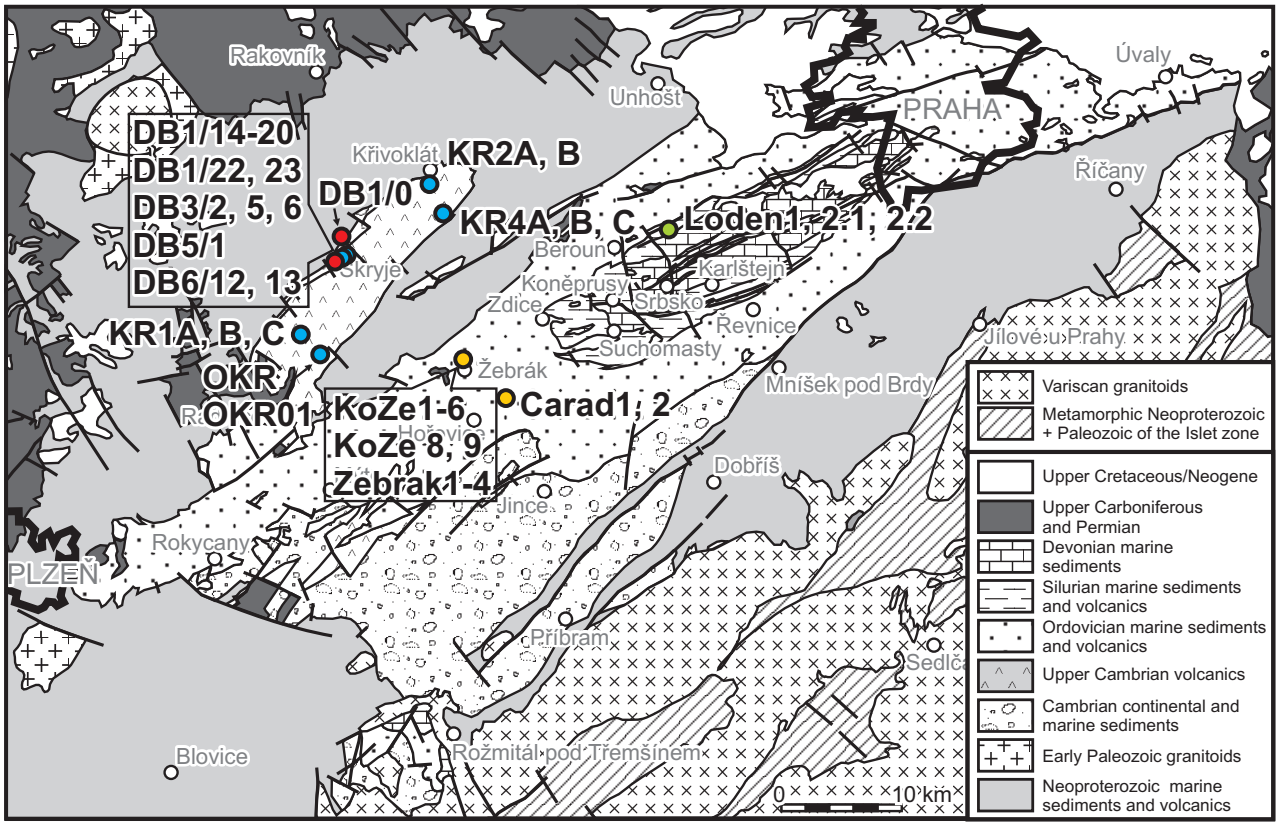

Fig. 4.1: Sketch map with sampling localities

Abb. 4.1: Schematische Karte mit Probenahmepunkten.

The Upper Cambrian Křivoklát-Rokycany volcanic complex formed above Neoproterozoic basement or Middle Cambrian marine sediments, respectively. Palaeozoic rocks of the TBU are unmetamorphosed but may be altered to various extents. Samples comprise 10 mafic and 13 siliceous effusive rocks. Thin sections of the dark grey, fine-grained basaltoids display predominantly trachytic and in a few cases porphyritic textures, respectively. Plagioclase phenocrysts, although commonly strongly altered (carbonatisation, albitisation, epidotisation), may show zonation. Few samples contain phenocrysts of pyroxene that were replaced by chlorite, carbonate and hematite. Also amygdales that are filled by carbonate and quartz-chlorite occur in one sample. The primary groundmass was glassy or composed of orthopyroxene, clinopyroxene, plagioclase and opaque minerals and is largely altered to carbonate, chlorite and fine opaque substance. Samples of the siliceous members of the Upper Cambrian volcanic complex include grey and light, fine-grained rocks with trachytic texture (sometimes with rare plagioclase phenocrysts) and light porphyritic rhyolites with phenocrysts of quartz, K-feldspar and plagioclase. Feldspars are intensely kaolinised, carbonatised or sericitized. Quartz crystals often show effects of resorption. The majority of the phenocrysts is up to 2.5 mm in size, larger grains may occur.

The 12 analysed Lower/Middle Ordovician rocks of the Komárov volcanic complex comprise dark brownish- to greenish-grey, amygdaloidal and microporphyritic to porphyritic lavas – often with glomeroporphyritic clusters – and brownish-green breccias as well as greenish-grey tuffs. Phenocrysts are largely altered to carbonate, chlorite, serpentine, ?albite and tiny opaque minerals and may have included plagio-

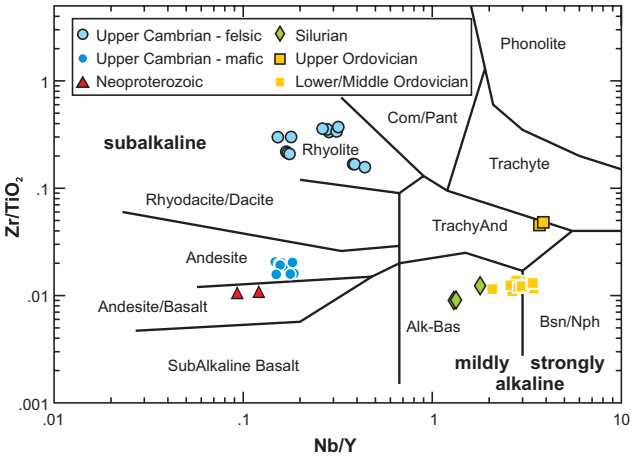

Fig. 4.2: Zr/TiO_2 vs. Nb/Y diagram after Winchester & Floyd (1977).

Abb. 4.2: Zr/TiO_2 vs. Nb/Y Diagramm nach Winchester & Floyd (1977).

clase and pyroxene (?and olivine). Amygdales are filled with carbonate and/or chlorite-quartz. Besides altered mafic minerals the matrix contains large amounts of fine, ±isometric or acicular, opaque phases. The brecciated rocks consist of scoriaceous clasts in a matrix of carbonate. The amygdales and phenocrysts within the clasts are filled/replaced by quartz-chlorite or carbonate and outlined by a very fine-grained, opaque mineral. Tuff samples contain altered glass shards, carbonate, plagioclase, and anhedral quartz. The relative abundance of quartz is also expressed by elevated SiO_2 contents, however, the HFSE and REE characteristics of these rocks appear not noticeably affected by possible additions of sedimentary material. Chiefly fine and dispersed, opaque minerals are common in all samples from the Komárov complex.

Two samples from the Upper Ordovician volcanic stage have an intersertal texture with chlorite and carbonate between alkali-feldspar and plagioclase laths. Although the feldspar crystals are altered, zonation and twinning are well observable in many of them. Large phenocrysts of other minerals (?orthopyroxene) are rare and were replaced predominantly by carbonate. Spaces between the feldspar laths are chiefly filled with chlorite, carbonate and magnetite, whereas the former two phases may represent fillings of amygdales and products of alteration and mineral replacement.

Dark grey to black, fine-grained volcanics of Silurian (Wenlock) age were sampled in the northwestern part of the Silurian deposits within the Prague synform. Thin sections of the 3 samples reveal a porphyritic to glomeroporphyritic texture with matrix grains showing alignment around phenocrysts. Phenocrysts and matrix grains include altered olivine, plagioclase (occasionally with corroded rims, zoning or sieve textures) and pyroxene (partly with sector zoning). Plagioclase may appear relatively fresh, however pyroxene is largely altered and olivine crystals are preserved only as pseudomorphs. Opaque minerals are common.

4.2 Geochemistry

Sample preparation and analytical methods are described in the Appendix. Geochemical analyses of the volcanic rocks are listed in Tables A3 to A5 of the Appendix; sampling localities are shown in Fig. 4.1 and listed in Table A1 of the Appendix. For diagrams using major elements the analyses were recalculated to 100% by compensating the loss on ignition (LOI).

4.2.1 Geochemical classification

Since particularly the alkaline earth elements are likely to be mobilized during alteration and metamorphism the total alkalis vs. silica (TAS) diagram as recommended for the chemical classification of volcanic rocks by the IUGS Subcommission on the Systematics of Igneous Rocks (LeMaitre 1988) is of limited use for the classification of altered or metamorphosed volcanics (e.g., Winchester & Floyd 1977, Rollinson 1993). An alternative approach for sample classification is the Zr/TiO_2 vs. Nb/Y diagram introduced by Winchester & Floyd (1977, Fig. 4.2) using HFSE. These are considered to be relatively immobile during alteration and low- to medium-grade metamorphism. The Zr/TiO_2 ratio acts as a

Table 4.1: Discriminatory incompatible element ratios for different reservoirs. Values for N-MORB and OIB from Sun & McDonough (1989), those for the continental crust from Rudnick & Gao (2003). * Ti/V ratios for N-MORB and OIB from Shervais (1982).

Tab. 4.1: Verhältnisse inkompatibler Spurenelemente für verschiedene Reservoire. N-MORB und OIB aus Sun & McDonough (1989), für die kontinentale Kruste aus Rudnick & Gao (2003). * Ti/V-Verhältnisse für N-MORB und OIB aus Shervais (1982).

	Th/La	Th/Nb	Zr/Nb	Y/Nb	Yb/Ta	Ti/V
N-MORB	0.05	0.05	32	12.0	23.1	20–50*
OIB	0.11	0.08	5.8	0.6	0.8	≥50*
lower continental crust	0.15	0.24	13.6	3.2	2.5	25.1
bulk continental crust	0.28	0.7	16.5	2.4	0.5	31.3

differentiation index and the Nb/Y ratio as an alkalinity index. In this diagram (Fig. 4-2) samples cluster in clear groups. Neoproterozoic and Upper Cambrian mafic volcanics are classified as basaltic andesites and andesites, respectively. Samples of Upper Cambrian age having higher SiO_2-contents (65.8–78.7 wt.%)[1] are classified as rhyolites by their HFSE patterns. Both, Neoproterozoic and Upper Cambrian volcanics, have a subalkaline signature. In contrast, Ordovician and Silurian effusives are alkaline and correspond to alkali-basalts – basanites/nephelinites (Lower/Middle Ordovician), trachyandesites (Upper Ordovician), and alkali-basalts (Silurian).

4.2.2 Trace elements

Concentrations of trace elements and REE in samples are usually normalised to a common reference standard and presented in multi-element diagrams. In this work the trace element data of all studied volcanic rocks are shown as chondrite-normalized patterns (Fig. 4.3) with normalizing values from Thompson (1982) as recommended by Rollinson (1993). Elements are arranged by decreasing incompatibility in oceanic basalts from left to right (Sun & McDonough 1989).

LIL elements such as Cs, Rb, Ba, K and Sr were excluded from the multi-element plots. Since particularly Neoproterozoic and Cambrian volcanics – and to a lesser extend also Ordovician and Silurian effusives – were subject to metamorphism (only Neoproterozoic rocks) and alteration (all units), respectively, the redistribution of the mobile LILE caused strong enrichment/depletion of these elements in the samples and render their patterns useless for interpretation of the magma source. The HFSE (including REE and some transitional elements), however, are assumed to reflect the primary magmatic concentrations. Furthermore ratios of incompatible elements (Tab. 4.1) yield information on the nature of the mantle source and potential crustal contamination.

Neoproterozoic: Neoproterozoic volcanics are about 5- to 10-times enriched in incompatible elements when compared to chondrite (Fig. 4.3A). The multi-element pattern is slightly inclined with highly incompatible elements less enriched than less incompatible elements. LREE are depleted when compared to MREE

[1] Upper Cambrian silicic volcanics were found to be fresh enough (LOI 1.1 to 3.7 wt%) to take into consideration their major element compositions. Silicic volcanics with trachytic texture have lower SiO_2 contents (65.8–71.3 wt%) than those with porphyritic texture (75.8–78.7 wt%). In the TAS diagram (not shown) three of the samples with trachytic texture are classified as dacites, the remaining rocks represent rhyolites. To simplify matters all the silicic rocks are termed rhyolites according to the classification diagram of Winchester & Floyd (1977). Upper Cambrian silicic volcanics represent peraluminous rocks according to the Al/(Ca+Na+K) vs. Al/(Na+K) diagram of Maniar & Piccoli (1989). Interestingly, only the samples with trachytic texture are ranked as tholeiitic rocks by the cation plot of Jensen (1976; not shown) and the AFM diagram of Irvine & Baragar (1971, not shown). Those with porphyritic texture are classified as calc-alkaline rhyolites.

GEOLOGICA SAXONICA
Journal of Central European Geology 54 (2008) 1–168

Table 4.2: Discriminatory trace element ratios of the analysed samples. Numbers represent ranges (for n≥3) or individual values (for n<3), value in brackets indicates outlier. $(La/Yb)_N$, $(Gd/Yb)_N$, Eu/Eu* were calculated with the chondritic abundances given by Boynton (1984).

Tab. 4.2: Spurenelementverhältnisse der analysierten Proben. Werte repräsentieren von-bis-Bereiche (für n≥3) oder Einzelwerte (für n<3), Wert in Klammern zeigt einen Ausreißer an. $(La/Yb)_N$, $(Gd/Yb)_N$, Eu/Eu* wurden mit den chondritischen Häufigkeiten von Boynton (1984) berechnet.

	$(La/Yb)_N$	$(Gd/Yb)_N$	Eu/Eu*	Ti/V	Th/La	Th/Nb	Zr/Nb	Y/Nb	Yb/Ta
Neoproterozoic (n=3)	0.4–0.7	0.93–1.16	0.93–1.03	24–30	0.11–0.17	0.1	20/26	8.2/10.9	11.4
Upper Cambrian, mafic (n=10)	1.8–2.3	1.13–1.33	0.87–1.11	41–50	0.15–0.19	0.26–0.38	27–32	5.4–6.8	5.5–8.4
Upper Cambrian, silicic (n=13)	3.7–8.6	1.13–1.75	0.21–0.23 0.64–0.73	–	0.21–0.60	0.63–0.99	9.4–46.8	2.3–6.6	2.7–7.4
Lower/Middle Ordovician (n=12)	12.1–16.5	2.4–2.9	0.89–1.09	76–103 (178)	0.09–0.15	0.07–0.09	2.8–3.6	0.3–0.5	0.4–0.7
Upper Ordovician (n=2)	~27	4.4/4.5	1.08/1.12	120/129	0.12/0.13	0.09	6.6	0.3	0.2/0.3
Silurian (n=3)	7.6–9.4	2.7	1.07–1.12	79–87	0.08	0.06	5.6–6.9	0.6–0.8	0.8–1.0

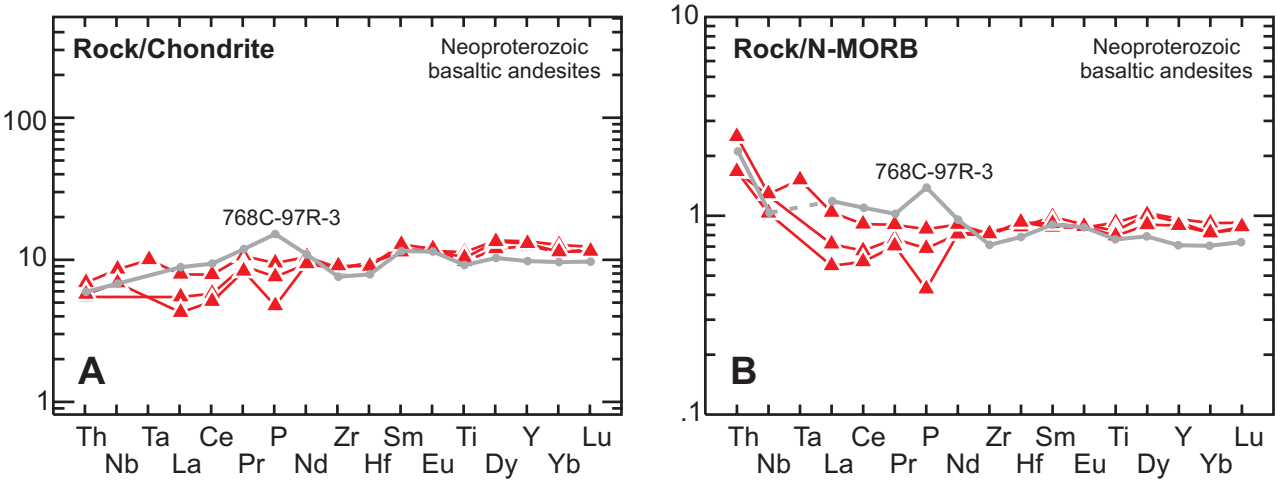

Fig. 4.3: Multi-element plots for Neoproterozoic basaltic andesites (n=3). In grey tholeiitic basalt from the Sulu Basin for comparison (768C-97R-3: Spadea et al. 1991). A) Chondrite-normalised with normalizing values from Thompson (1982). **B**: N-MORB-normalized with normalizing values from Sun & McDonough (1989).

Abb. 4.3: Multi-Element-Plots der neoproterozoischen basaltischen Andesite (n=3). In grau ein tholeiitischer Basalt des Sulu-Beckens (768C-97R-3: Spadea et al. 1991) zum Vergleich. **A**: Chondrit-normiert mit Normierungswerten von Thompson (1982). **B**: N-MORB-normiert mit Normierungswerten von Sun & McDonough (1989).

and HREE (Fig. 4.3A). $(La/Yb)_N$ ratios range between 0.4 and 0.7 (Tab. 4.2). These features, together with the absence of an Eu-anomaly[1], are characteristic for relatively primitive MOR basalts. MORB-

[1] The Eu-anomaly was calculated by the equation:

$$\frac{Eu}{Eu*} = \frac{Eu_N}{0.5 \times (Sm_N + Gd_N)}$$

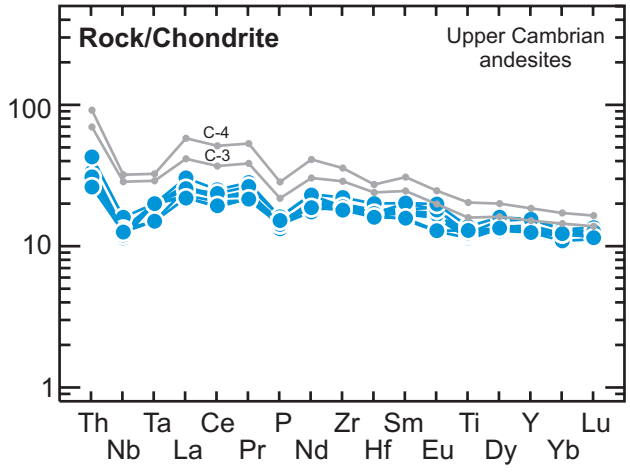

Fig. 4.4: Multi-element diagram for Upper Cambrian basaltic andesites (n=10) normalized to chondrite (Thompson 1982). In grey continental tholeiites (C-3, C-4: Dostal et al. 2003) for comparison.

Abb. 4.4: Chondrit-normierte (Thompson 1982) Multi-Element-Plots der oberkambrischen basaltischen Andesite (n=3). In grau kontinentale Tholeiite (C-3, C-4: Dostal et al. 2003) zum Vergleich.

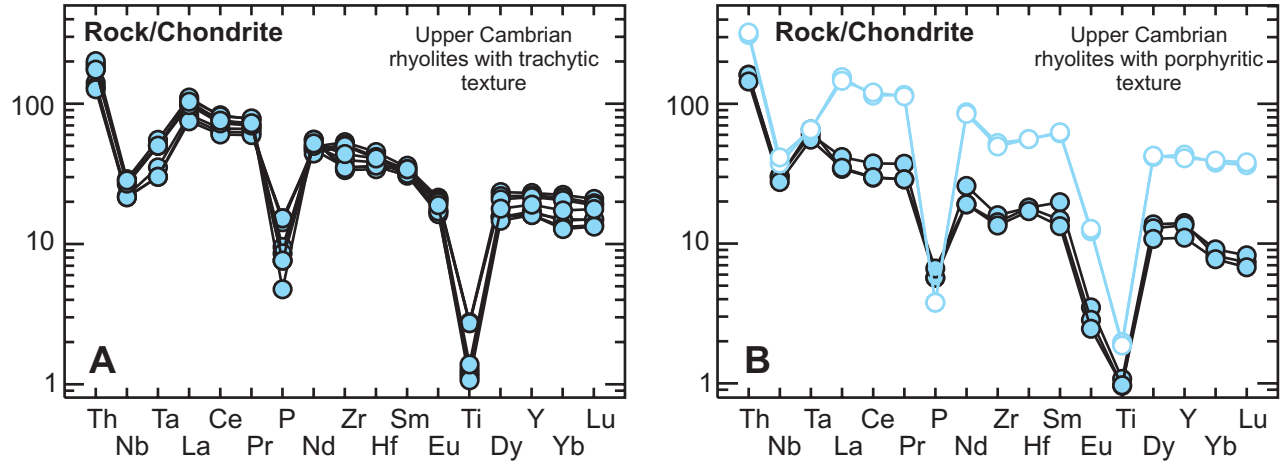

Fig. 4.5: Chondrite-normalized (Thompson 1982) plots of Upper Cambrian rhyolitoids. **A**: Rhyolites with trachytic texture (n=8). **B**: Rhyolites with porphyritic texture (n=5).

Abb. 4.5: Chondrit-normierte (Thompson 1982) Multi-Element-Plots der oberkambrischen Rhyolithoide. **A**: Rhyolithe mit trachytischer Textur (n=8). **B**: Rhyolithe mit porphyrischer Textur (n=5).

normalized multi-element patterns (Fig. 4.3B) of the Neoproterozoic basaltic andesites are flat (around 1) with regard to the less incompatible elements. The largest deviation from MORB is displayed by Th, which is enriched (1.9- to 2.4-times MORB) in all 3 samples. Nb was detected in two samples and Ta in one sample. In these cases Nb and Ta are enriched. However, sample DB1/0 having yield the only complete multi-element pattern, displays a negative Nb peak with regard to Th and Ta. Ti/V ratios of 24 to 30 are in the range of MORB (Shervais, 1982). Zr/Nb ratios (20 to 26) are somewhat lower than in average N-MORB and Th/La (0.11 to 0.17) as well as Th/Nb ratios (0.10) are slightly elevated when compared to N-MORB (for comparison with different sources see Tab. 4.1) pointing to a modification of the depleted mantle source or contamination of the melt by crustal material. A small variation among the Neoproterozoic samples comes from La, Ce, Pr and P (Fig. 4.3), which are slightly depleted in samples DB6/12 and DB6/13 when compared to MORB and to sample DB1/0 (Fig. 4.4A).

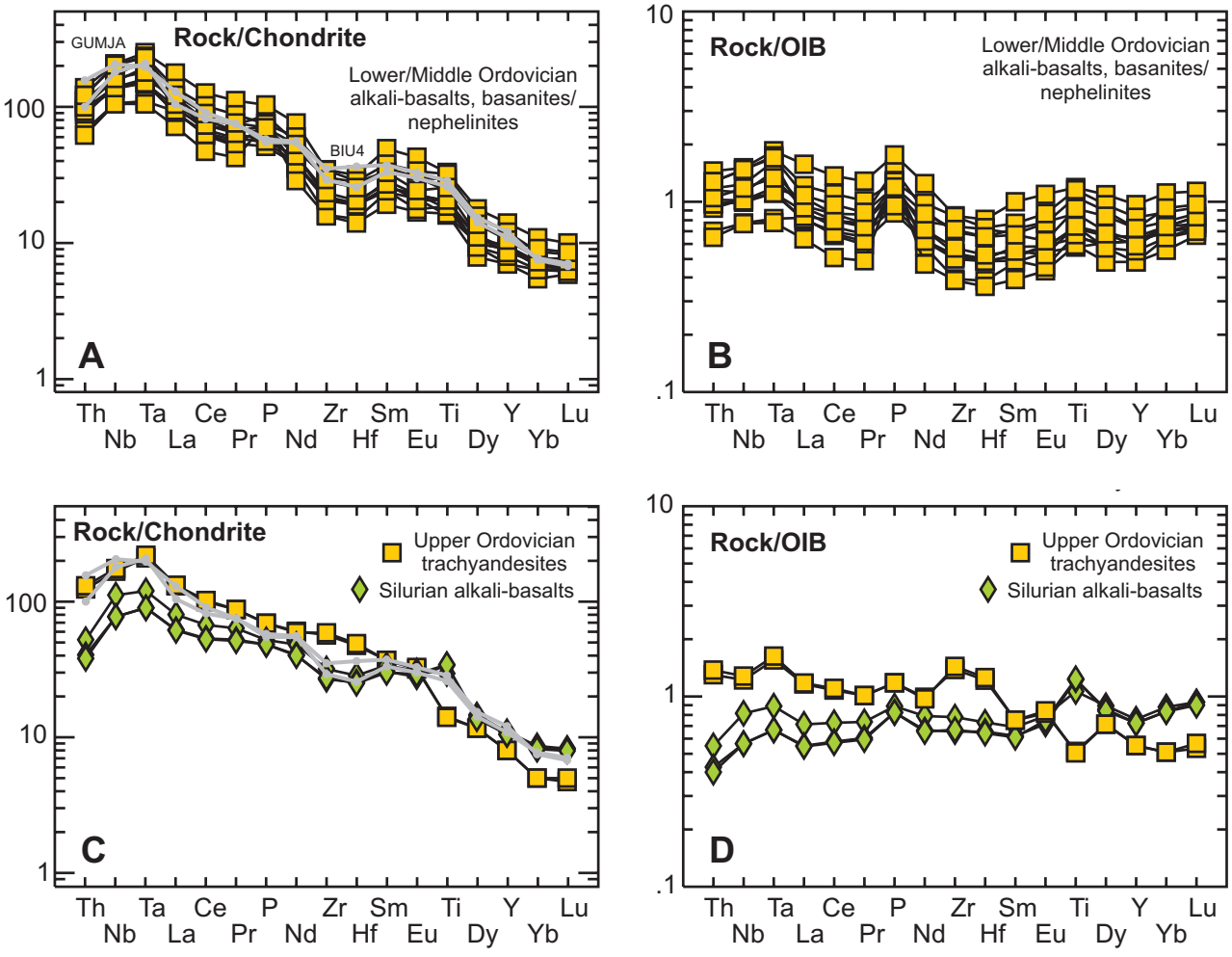

Fig. 4.6: Multi-element plots of Ordovician and Silurian volcanics. In grey two samples from the Cameroon volcanic line (BIU4, GUMJA: Rankenburg et al. 2005) for comparison. **A**: Lower/Middle Ordovician alkaline basaltoids (n = 12) normalised to chondrite (Thompson 1982). **B**: Same data normalised to OIB (Sun & McDonough 1989). **C**: Upper Ordovician (n = 2) and Silurian (n = 3) alkaline volcanics normalised to chondrite (Thompson 1982). **D**: Same data normalised to OIB (Sun & McDonough 1989).

Abb. 4.6: Multi-Element-Plots der ordovizischen und silurischen Vulkanite. In grau zwei Proben von der Cameroon Volcanic Line (BIU4, GUMJA: Rankenburg et al. 2005) zum Vergleich. **A**: Unter-/mittelordovizische alkalische Basaltoide (n = 12) normiert auf Chondrite (Thompson 1982). **B**: Die gleichen Daten normiert auf OIB (Sun & McDonough 1989). **C**: Oberordovizische (n = 2) und silurische (n = 3) alkalische Vulkanite normiert auf Chondrit (Thompson 1982). **D**: Die gleichen Daten normiert auf OIB (Sun & McDonough 1989).

Upper Cambrian: Chondrite-normalised multi-element patterns of the andesites (Fig. 4.4) are slightly inclined with an enrichment of most highly incompatible elements over less incompatible elements ($[La/Yb]_N$=1.8–2.3). The Eu-anomaly varies from weakly negative to absent to weakly positive (0.87–1.11). Flat HREE-patterns either imply melt generation in the spinel stability field or a high degree of partial melting that does not leave garnet as a residue. Nb and Ta being distinctly depleted when compared to the neighbouring elements Th and La (Fig. 4.4), indicate involvement of a crustal component. This is also suggested by the Th/La (0.15 to 0.19) and Th/Nb ratios (0.26 to 0.38), respectively, which are elevated

when compared to mantle values (Tab. 4.1). Zr/Nb ratios of 27 to 35 are in the range of N-MORB. All these features are shared with those of continental tholeiites (Dupuy and Dostal 1984).

Although the ternary diagram of Meschede (1986; Fig. 4.7B) is ambiguous since field C comprises both volcanic arc basalts and continental tholeiites, Ti/V ratios of 41 to 50 are transitional between typical N-MORB and alkaline rocks but distinctly higher than in island arc tholeiites (Shervais 1982).

Upper Cambrian silicic volcanics are not similar to each other. Their geochemical compositions on the one hand differs in accordance with their differing textures and on the other hand rhyolites with porphyritic texture vary among each other. Although all samples have, steeply inclined multi-element patterns (Fig. 4.5) their $(La/Yb)_N$ range between 3.7 and 8.6. The negative Eu-anomaly varies with the SiO_2 content reaching values of 0.21–0.23 for the samples with porphyritic texture and ranging from 0.64 to 0.73 in less siliceous rocks with trachytic texture. When normalised to chondrite the silicic samples exhibit Nb and Ta depletion as well as Th enrichment in accordance with the mafic rocks. Three of the porphyritic rhyolites show relatively low concentrations of REE, Zr and Hf as well as a depletion in Yb and Lu, whereas their patterns for the most incompatible elements Th, Nb and Ta are similar to those of the remaining silicic rocks.

The Cambrian rhyolites are classified as extrusive equivalents of A-type granites by the diagram of Whalen et al. (1987; Fig. 4.7C). Eby (1992) subdivided A-type granitoids geochemically in A_1-type that is derived from sources similar to OIB and A_2-type, which represents magmas derived from continental crust or underplated crust that has been through a cycle of continent-continent collision or island-arc magmatism. Teplá-Barrandian silicic volcanics fall into the field of A_2-type granitoids. The Y+Nb vs. Rb diagram of Pearce et al. (1984) characterises these rocks as volcanic arc granites and within plate granites (Fig. 4.7D), respectively.

Ordovician and Silurian: Chondrite-normalised plots (Fig. 4.6A, C) show strong enrichment of the most incompatible elements over less incompatible elements. Nb and Ta concentrations are elevated when compared to neighbouring Th and La. The Eu anomaly is weak to absent (0.89–1.12). Elevated $(Gd/Yb)_N$ ratios (Tab. 4.2), i.e., fractionated HREE, suggest generation of the melts in the presence of residue garnet. In accordance with these features, established discrimination diagrams (Fig. 4.7A, B) point to derivation from an enriched mantle source and extrusion of the volcanics within an intra-plate setting. OIB-normalised multi-element patterns (Fig. 4.6B, D) reveal slight differences between samples of the individual age intervals. Upper Ordovician trachyandesites show a depletion of less incompatible elements (Sm to Lu) when compared to OIB and to Lower Ordovician and Silurian volcanics. Silurian alkali-basalts are less enriched in highly incompatible elements than Ordovician samples. Lower/Middle Ordovician volcanics have Zr/Nb ratios of 2.8–3.6 that are lower than those of average OIB, whereas the low Zr content controls the ratio (cf., Tab. 4.1). Upper Ordovician and Silurian rocks have Zr/Nb ratios (5.6–6.9) that are close/similar to average OIB.

4.3 Magma sources and implications on the geotectonic setting

The geochemistry of the Teplá-Barrandian Neoproterozoic to Silurian volcanic rocks clearly varies among samples of different age and reflects several stages of the geotectonic history of this part of the Bohemian Massif. Different geotectonic conditions are characterised by magmatism from different sources that can be identified by HFSE and REE patterns even in altered volcanic rocks.

The overall character of the Neoproterozoic volcanism in the TBU is manifold (Fiala 1977, 1978; Pelc & Waldhausrová 1994; Waldhausrová 1997a, 1997b; Pin & Waldhausrová 2007) and the number of samples taken only from the Neoproterozoic basement close to the unconformably overlying Skryje-Týřovice Cambrian deposits is far too limited to adequately constrain the complex Neoproterozoic plate-tectonic processes. However, it can be demonstrated

that the analysed basaltic andesites **1**) largely resemble N-MORB, **2**) show slightly elevated Th/Nb and Th/La ratios compared to N-MORB and **3**) have Th/Yb vs. Ta/Yb ratios (Fig. 4.7A) that are transitional between tholeiitic volcanics of oceanic island arcs and N-MORB. These geochemical features are compatible with a subduction-related modification of the depleted mantle source and generation of the magmatism in a back-arc setting. This is supported by highly radiogenic εNd_{600} values of +7.8 to +9.3 recently acquired by Pin & Waldhausrová (2007) for similar rocks of the Teplá-Barrandian Neoproterozoic.

A (sub)recent analogue of such a back-arc setting is the Sulu Sea NE of Borneo, whose opening occurred during a relatively short time interval in the Early Miocene. The basin is surrounded by island arcs and continental fragments (Silver & Rangin 1991). The basalts from the floor of the Sulu Basin show an affinity to N-MORB, whereas the mantle source was modified by subduction-related geochemical components. The latter is indicated by enriched LILE and Th contents (Spadea et al. 1991). Although LILE had to be excluded due to their mobility, Fig. 4.3 highlights the similarity of the incompatible element patterns of the Teplá-Barrandian Neoproterozoic volcanics with the sample from the Sulu Basin.

Upper Cambrian mafic volcanics are clearly different from the Neoproterozoic volcanism and largely resemble continental tholeiites (cf., Pin et al. 2007). They are similar to continental tholeiites of the Permian rifting-stage in the Central Western Carpathians (Fig. 4.4: samples C-3 and C-4 from Dostal et al. 2003). However, in contrast to the TBU, where intermediate rocks and rhyolites dominate the volcanic suite (Waldhausrová 1971) they are only represented by rare volcaniclastics and dykes in the Slovakian Carpathians. εNd_{500} values of +6.1 to +6.7 determined on five of the analysed mafic samples (Pin et al. unpublished data) are within the compositional range of the subcontinental lithosphere (compilation of Rollinson, 1993). The same is true for the initial Sr isotope relationship ($^{87}Sr/^{86}Sr_i \sim 0.704$) reported by Vidal et al. (1975). Besides the andesites also intermediate rocks (εNd = +4.5 to +5.3) and even rhyolites (εNd = +0.2 to +1.8) have positive εNd values (Pin et al. 2007). The latter demonstrates that an old crustal source is ineligible for generation of the rhyolites. Instead the classification of the felsic rocks as effusive equivalents of A_2-type granites (Fig. 4.7C) suggests derivation from the lower crust, which must have been composed of recently added island-arc-related complexes of Neoproterozoic age. Therefore the calc-alkaline signature that is indicated by some geochemical features (cf. Patočka et al. 1993) represents an inherited component. A suitable reason for melting of the lower crust is underplating by basaltic magmas similar to the Upper Cambrian continental tholeiites. Particularly the dominance of the felsic volcanics suggest storage of hot mantle material at the Moho and melting of the lower crust at high temperatures. The latter is supported by the morphologies of zircon crystals from a rhyolite sample indicative of high temperatures (cf. chapter 7.3.1) Furthermore, it cannot be excluded that some of the rhyolites evolved from or were mixed with mantle magmas. Altogether the Upper Cambrian volcanism belongs to an important rifting event at the northern Gondwana margin that is traceable across many peri-Gondwanan terranes (e.g., Ossa-Morena Zone – Sánchez-García et al. 2003, Saxothuringia – Kemnitz et al. 2002, Sudetes – Kryza & Pin 2002).

Ordovician and Silurian volcanics are much more enriched in incompatible elements than Upper Cambrian continental tholeiites and resemble alkaline basalts. High $(La/Yb)_N$ and $(Gd/Yb)_N$ (Tab. 4.2) of the Ordovician volcanics suggest low degrees of partial melting of a garnet peridotite mantle source, whereas the garnet remained as a residue in the source. Lower concentrations of highly incompatible elements (i.e., lower $[La/Yb]_N$) and similar $(Gd/Yb)_N$ in the Silurian alkalibasalts point to a larger degree of partial melting of the same source.

The Teplá-Barrandian did not represent an intra-oceanic island during the Ordovician and Silurian, but contained a basement of continental crust that formed at the latest in the Neoproterozoic (possibly in places the TBU is underlain by distinctly older basement). A recent equivalent of OIB-type magmatism that

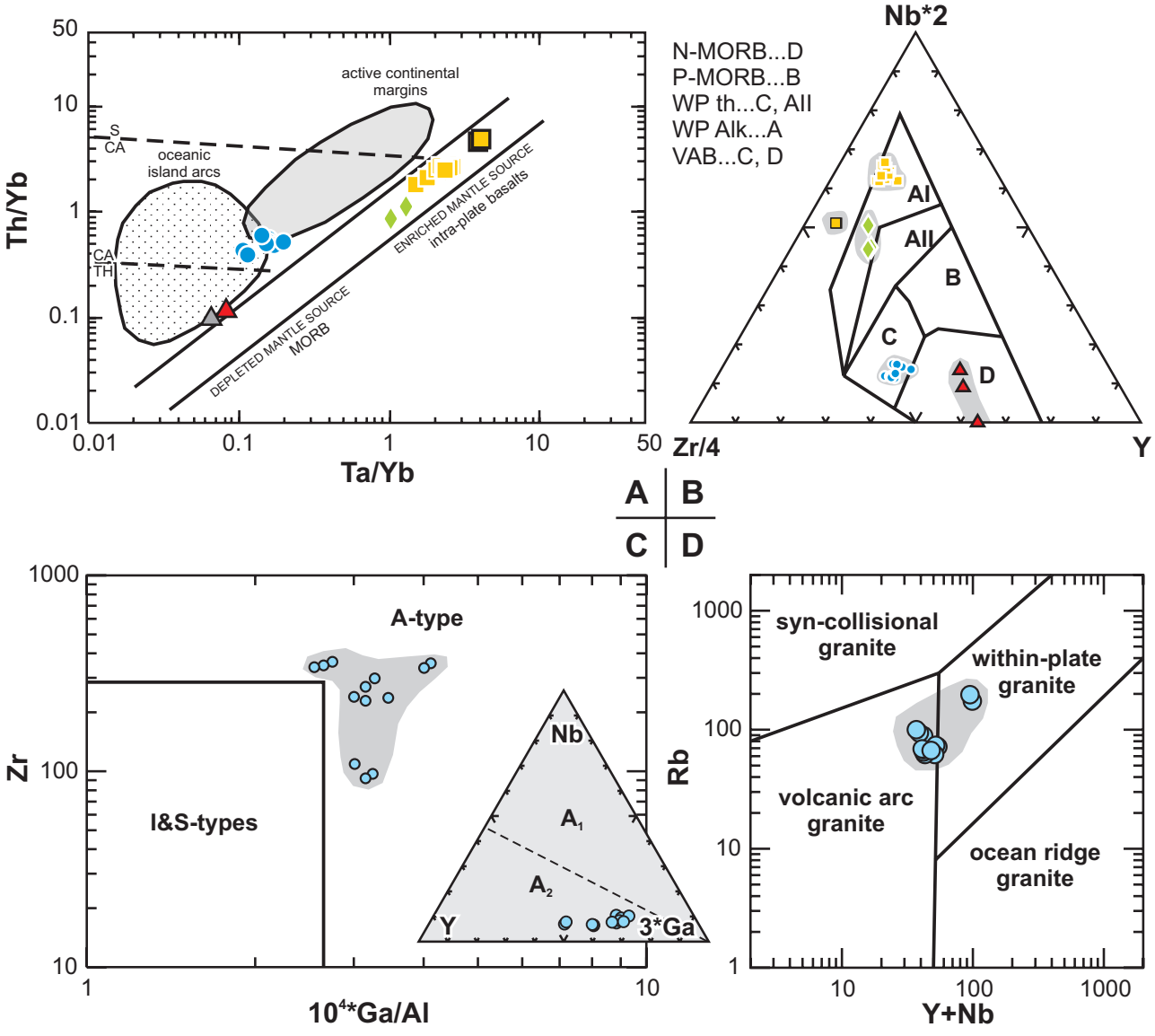

Fig. 4.7: Discrimination diagrams for Neoproterozoic – Silurian volcanics. Symbols as in Fig. 4.2. Mafic rocks: **A**: Ta/Yb vs. Th/Yb diagram after Pearce et al. (1983). Grey triangle stands for sample DB6/13, where Ta was not detected. Therefore the Ta content was estimated by Nb/14 due to Nb/Ta=14 in sample DB1/0. **B**: Nb-Zr-Y diagram after Meschede (1986). Rhyodacites and rhyolites: **C**: Granite discrimination diagram after Whalen (1987), inset: distinction of A-type granites after Eby (1992); D) Y+Nb vs. Rb diagram after Pearce et al. (1984).

Abb. 4.7: Diskriminationsdiagramme für neoproterozoische bis silurische Vulkanite. Symbole wie in Abb. 4.2. Mafische Gesteine: **A**: Ta/Yb vs. Th/Yb-Diagramm nach Pearce et al. (1983). Das graue Dreieck steht für Probe 6/13, in der Ta nicht nachgewiesen wurde. Der Ta-Gehalt wurde aber mittels Nb/14 abgeschätzt, da Nb/Ta = 14 in Probe DB1/0. **B**: Nb-Zr-Y-Diagramm nach Meschede (1986). Rhyodazite und Rhyolithes: **C**: Granit-Diskriminationsdiagramm nach Whalen (1987), Einschub: Unterscheidung der A-Typ Granite nach Eby (1992); **D**: Y+Nb vs. Rb-Diagramm nach Pearce et al. (1984).

is not restricted to oceanic islands on oceanic crust is the Cameroon Volcanic Line (CVL; Fig. 4.6) extending from the continental interior of equatorial West Africa to Annobón (formerly Pagalu) Island in the South Atlantic (actually the CVL is the NE' part of a volcanic chain that commences at the oceanic

Island of St. Helena close to the Mid-Atlantic Ridge [e.g., Halliday et al. 1988, Fairhead & Wilson 2004]). Fitton & Dunlop (1985) showed that the alkaline volcanics of the continental part of the Cameroon Line are geochemically and isotopically indistinguishable from those of the oceanic sector and hence, were not substantially affected by interaction with the continental lithosphere. A further similarity with the Barrandian alkaline volcanism is the long magmatic history (~65 Ma to recent in the CVL) during which there is lack of evidence for considerable migration of the volcanism with time. The latter is interpreted to be indicative of a relatively shallow mantle source (Fitton & Dunlop 1985). In the Barrandian Palaeozoic alkaline magmatism is known from the Ordovician and Silurian and even from the Devonian[1] (adds up to a total of ~90 Ma), whereas the thickness of the volcanic deposits and the duration of the volcanic activity decrease with time (cf., Štorch 1998). However, this is not necessarily a result of migration but may be related to the decreasing present-day spatial extent of the Palaeozoic successions, i.e., Devonian rocks are only preserved in the core of the Prague synform (Fig. 2.3). Such repeated, "stationary" intraplate volcanism can be explained by stress-related fractures that form within the lithosphere as a result of changes in absolute plate motions (e.g., Foulger 2003, Fairhead & Wilson 2004, Smith 2004). These fractures allow the formation and ascent of OIB-type magma.

5 Geochemistry of sedimentary rocks

The geochemistry of clastic sediments reflects the type and proportions of their detrital components and therefore the geotectonic setting of their source rocks. Subsequent processes such as weathering, transport and diagenesis modify the primary provenance signals of the resulting sediments (e.g., Bhatia 1983, Johnsson 1993). Particularly duration and intensity of source rock weathering, duration and mechanisms of transport, and the energy of the depositional environment control the extent of these modifications. Since land plants did probably not play an important role until the Devonian[2], their effects (e.g., slope stability, acid degradation products, capacity of soil to hold water, retain of sediment in the weathering profile or in temporary storage) on weathering are assumed to be negligible for the analysed Late Neoproterozoic to Ordovician detrital sediments.

When keeping in view possible interactions of these various factors, reliable information on source area and modifying conditions may be derived from geochemical compositions of clastic sediments.

In this chapter the analysed rocks are subdivided according to grain size and stratigraphic age into Neoproterozoic siliciclastics (marin, n=13), Lower Cambrian sandstones and conglomeratic sandstones (continental and/or transitional, n=21), Lower Cambrian shale (transitional, n=1), Middle Cambrian sandstones (marine, n=15), Middle Cambrian shales (marine, n=16), Ordovician sandstones (marine, n=14) and Ordovician shales (marine, n=28). Analytical data are given in Tables A5 to A7 of the Appendix. For diagrams using major elements the analyses were recalculated to 100% by compensating the LOI. Sample preparation and analytical methods are described in the Appendix. Most of the diagrams refer to PAAS, which is the post-Archean average Australian shale of Taylor & McLennan (1985) as well as to UCC and BCC, which are upper and bulk continental crust as given by Rudnick & Gao (2003). The averages of Teplá-Barrandian Palaeozoic

[1] A geochemical analysis of a Devonian hyaloclastite that was published by Patočka et al. (1993) is similar to those of Lower/Middle Ordovician alkali-basalts/basanites. This Devonian sample is characterised by: $[La/Yb]_N$=18.5; Th/La=0.12; Th/Nb=0.07; Zr/Nb=3.7; Y/Nb=0.34 and Yb/Ta=0.39.

[2] Although remnants of older land plants and terrestrial fungi were found (e.g., Redecker et al. 2000, Heckman et al. 2001) their impact on weathering is thought to be negligible. Particularly the fact that early land plants colonised only places close to water makes it unlikely that they advanced weathering of extensive continental areas significantly (pers. comm. Dr. Lutz Kunzmann).

Table 5.1: Major element ratios and CIA of the analysed samples of the individual age groups. * – Na_2O contents are below detection limit in four Lower Cambrian and two Middle Cambrian samples, respectively. Major element ratios of PAAS, UCC and BCC are listed for comparison.

Tab. 5.1: Hauptelementverhältnisse und CIA der analysierten Proben der einzelnen Altersabschnitte. * – Na_2O-Gehalt war für vier unterkambrische und zwei mittelkambrische Proben unter der Nachweisgrenze. Hauptelementverhältnisse für den post-archaischen australischen Durchschnittstonstein (PAAS - Taylor & McLennan 1985), die durchschnittliche obere Erdkruste (UCC) und die durchschnittliche Erdkruste (BCC - Rudnick & Gao 2003) sind zum Vergleich angegeben.

	Al_2O_3/SiO_2	K_2O/Na_2O	$Al_2O_3/(CaO+Na_2O)$	CIA
Neoproterozoic				
greywackes (n=9)	0.19–0.26	0.50–2.19	2.92–4.42 (7.32)	57–68
shales/siltstones (n=4)	0.19–0.30	0.39–0.65	(1.69) 3.01–3.53	(46) 60–64
Lower Cambrian				
sandstones - high CIA (n=11)	0.02–0.11 (0.21)	1.04–55.0*	8.04–153.5*	74–87
sandstones - low CIA (n=10)	0.06–0.32	0.06–1.05	1.75–3.78	47–62
shale (n=1)	0.39	12.6	29.2	79
Middle Cambrian				
sandstones (n=15)	0.01–0.19	0.40–6.83*	1.98–46.6*	(51) 60–82
shales/siltstones (n=16)	0.23–0.30	0.74–2.00	4.15–8.39	65–76
Ordovician				
sandstones (n=8)	0.02–0.19	1.18–30.0	6.71–29.2	72–87
sandstones, carbonaceous (n=6)	0.05–0.12	0.32–0.62	0.59–2.40	–
shales/siltstones (n=28)	0.21–0.45	1.29–45.3	6.08–122.9	72–83
PAAS	0.30	3.08	7.56	70
UCC	0.23	0.86	2.24	51
BCC	0.26	0.59	1.68	46

volcanics were calculated from the analyses in Tables A2 to A4 of the Appendix. For details on the volcanics see chapter 4.

5.1 Major elements

Major element data are useful to describe and discriminate siliciclastic sediments. The most discriminatory major element ratios of the analysed shales/siltstones and greywackes/sandstones are listed in Tab. 5.1, whereas (**1**) Al_2O_2/SiO_2 is an expression of quartz-enrichment in psammites and a measure for the content of clay minerals in pelites, respectively, (**2**) K_2O/Na_2O reflects the content of K-feldspar and mica relative to that of plagioclase, and moreover, with regard to shales and siltstones it is a measure for cation exchange in clay minerals, where the larger K^+ is retained in preference to the smaller Na^+ during intensive weathering, and (**3**) $Al_2O_3/(CaO+Na_2O)$ compares an immobile element to mobile ones (e.g., Nesbitt et al. 1980, Bhatia 1983). Another useful feature is the chemical index of alteration[1] (CIA; Nesbit & Young 1982), which effectively reflects the degradation of feldspars to clay minerals by chemical weathering.

[1] CIA was calculated using molecular proportions:

$$CIA = (Al_2O_3 / [Al_2O_3 + CaO^* + Na_2O + K_2O]) \times 100$$

GEOLOGICA SAXONICA
Journal of Central European Geology 54 (2008) 1–168

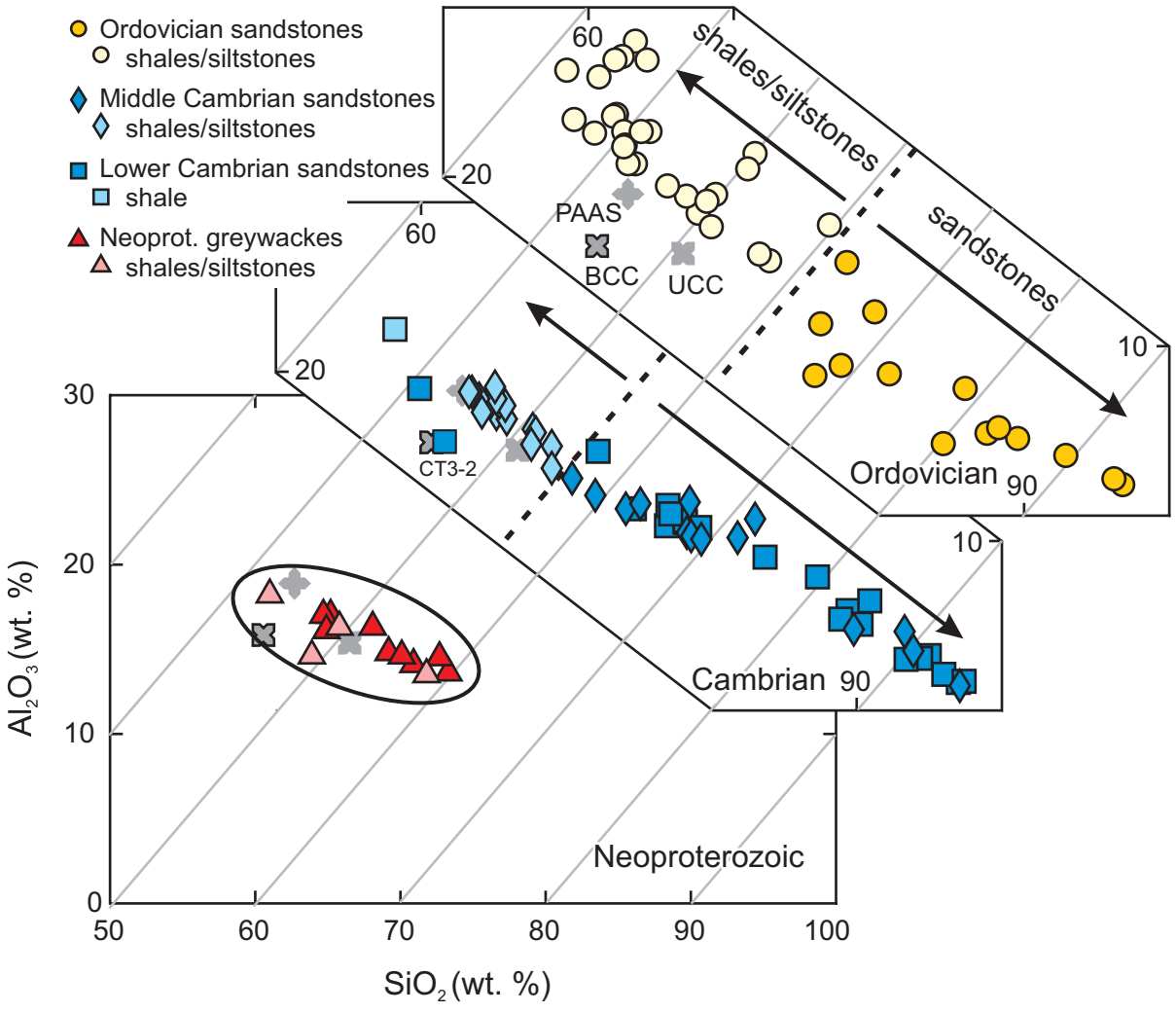

Fig. 5.1: SiO_2 vs. Al_2O_3 diagram highlighting different degrees of chemical weathering and hydrodynamic sorting during time. Neoproterozoic rocks of varying grain-sizes plot in a narrow field. Cambrian and Ordovician sedimentary rocks, however, are subdivided into Al_2O_3-rich shales/siltstones and SiO_2-rich sandstones. CT3-2 is a Lower Cambrian sandstone sample that is composed of almost entirely volcanogenic detritus.

Abb. 5.1: Das SiO_2 vs. Al_2O_3-Diagramm hebt die unterschiedlichen Grade von chemischer Verwitterung und hydrodynamischer Sortierung hervor. Die neoproterozoischen Sedimente verschiedener Korngrößen plotten in ein enges Feld. Kambrische und ordovizische Sedimente sind hingegen deutlich in Al_2O_3-reiche Ton-/Siltsteine und SiO_2-reiche Sandsteine getrennt. CT3-2 ist eine unterkambrische Sandsteinprobe die fast ausschließlich aus vulkanogenem Detritus besteht.

Neoproterozoic rocks of different grain-size have similar ranges of Al_2O_3 and SiO_2 (Fig. 5.1) as well as low CIA (Fig. 5.2). Furthermore greywackes and associated shales and siltstones are characterised by homogenous Al_2O_3/SiO_2, K_2O/Na_2O and $Al_2O_3/(CaO+Na_2O)$ ratios (Tab. 5.1, Fig. 5.3). All these features demonstrate that chemical weathering (decomposition of unstable minerals, formation of clay minerals) was not efficient during this time. Instead mechanical breakdown of the source rocks in combination with a negligible duration of transport must have dominated.

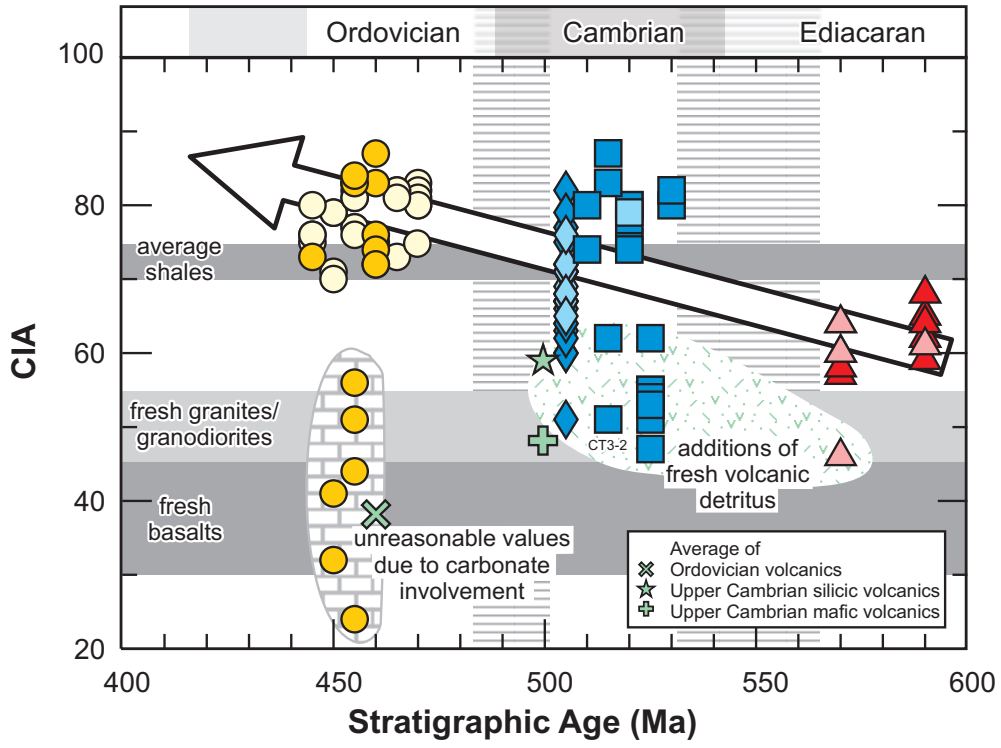

Fig. 5.2: Stratigraphic Age vs. CIA diagram showing an increasing degree of weathering from the Neoproterozoic to the Ordovician for the majority of the samples. Several Cambrian sandstones and one Late Neoproterozoic shale contain fresh detritus from synsedimentary volcanism and therefore have lower CIA values than "ordinary" sediments of these stratigraphic intervals. Six Ordovician sedimentary rocks have unreasonably low CIA values on account of carbonaceous matrix. Grey fields – typical CIA values of average shales, fresh basalts and granites/granodiorites (after Nesbit & Young, 1982). Horizontal rules – periods from which no sediments are known in the Teplá-Barrandian. Symbols as in Fig. 5.1.

Abb. 5.2: Stratigraphisches Alter vs. CIA-Diagramm, welches einen zunehmenden Verwitterungsgrad des Ausgangsgesteins vom Neoproterozoikum zum Ordovizium für den größten Teil der Proben anzeigt. Einige kambrische Sandsteine und ein spätneoproterozoischer Tonschiefer enthalten frisches Material von synsedimentärem Vulkaismus und haben daher niedrigere CIA-Werte als „normale" Proben dieser Altersabschnitte. Sechs ordovizische Proben haben zu niedrige CIA-Werte, da sie eine karbonatische Matrix aufweisen. Eine Karbonat-Korrektur der CIA-Werte kann mit den zur Verfügung stehenden Daten nicht durchgeführt werden. Graue Felder – typische CIA-Werte für durchschnittliche Tonsteine, frische Basalte und Granite/Granodiorite (nach Nesbit & Young, 1982). Die Schraffur steht für Zeitabschnitte aus denen keine Sedimente im Teplá-Barrandium bekannt sind. Symbole wie in Abb. 5.1.

In contrast, Cambrian and Ordovician siliciclastics are clearly subdivided into sandstones with high SiO_2 and shales/siltstones with high Al_2O_3 (Tab. 5.1, Fig. 5.1), which is a result of mineralogical differentiation due to size sorting of the particles, i.e., shales and siltstones are rich in clay minerals formed by chemical weathering and sandstones are enriched in quartz, which is a residue of chemical weathering. Nevertheless, the CIA values of the SiO_2-rich psammitic rocks are similar to those of the associated Al_2O_3-rich pelites (Fig. 5.2).

5.1.1 Early Palaeozoic shales/siltstones

Major element features of the shales and siltstones of the individual stratigraphic intervals are quite homogenous when compared to those of the sandstones (see below). CIA values increase from Neoproterozoic to Ordovician, whereas (1) Middle Cambrian pelites have chiefly similar or lower values than average shales and (2) the majority of the Ordovician shales and siltstones has even higher CIA than average shales (Fig. 5.2). The only

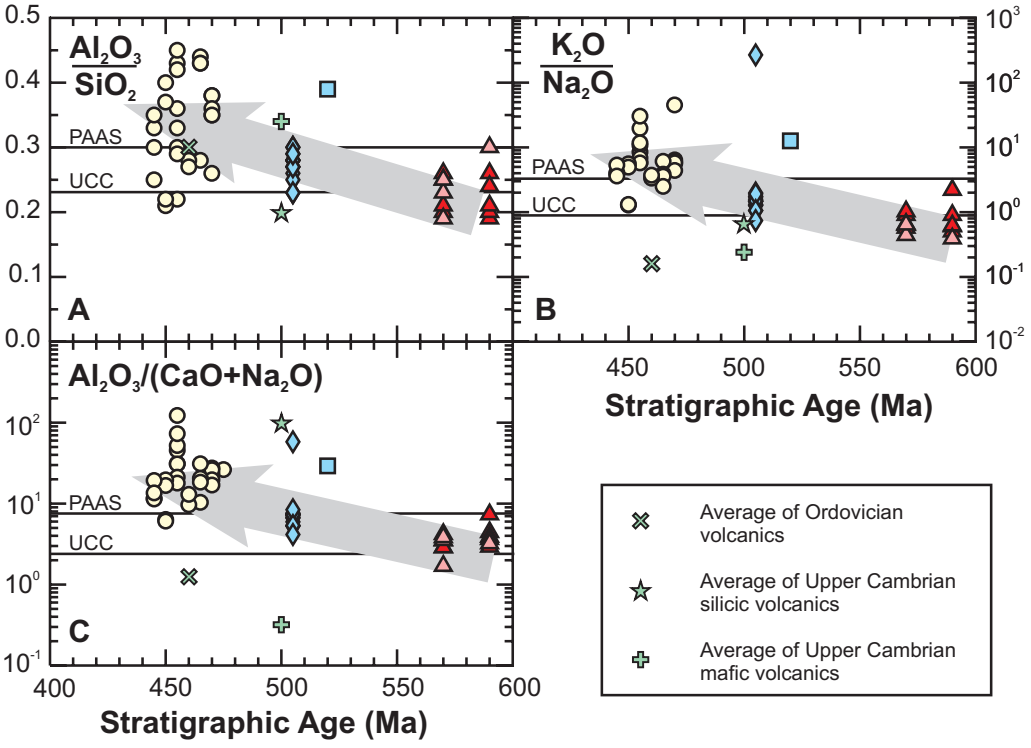

Fig. 5.3: Stratigraphic Age vs. Major Element Ratio plots for Cambrian and Ordovician shales and siltstones. For the late Neoproterozoic greywackes (red triangles) and shales/siltstones (pink triangles) are plotted to highlight the geochemical similarity of the different lithologies. Synsedimentary volcanism does not notably influence the shale/siltstone composition. A) Al_2O_3/SiO_2 ratios. B) K_2O/Na_2O ratios. C) $Al_2O_3/(CaO+Na_2O)$ ratios.

Abb. 5.3: Stratigraphisches Alter vs. Hauptelementverhältnis – Diagramme für kambrische und ordovizische Ton- und Siltsteine. Für das späte Neoproterozoikum sind sowohl die Grauwacken (rote Dreiecke) als auch die Ton-/Siltsteine (rosa Dreiecke) geplottet, um die geochemische Ähnlichkeit beider Lithologien hervorzuheben. Die chemischen Zusammensetzungen der Proben sind offenbar nicht durch synsedimentären Vulkanismus modifiziert. **A**: Al_2O_3/SiO_2-Verhältnisse. **B**: K_2O/Na_2O-Verhältnisse. **C**: $Al_2O_3/(CaO+Na_2O)$-Verhältnisse.

shale sample from the Lower Cambrian sequence is similar to the Ordovician shales with respect to its major element composition (Fig. 5.1, Fig. 5.2, Fig. 5.3). The general increase in Al_2O_3/SiO_2 ratios from Neoproterozoic to Ordovician (Fig. 5.3A) suggests diminished importance of mechanical grain size reduction but increased degradation of primary minerals accompanied by formation of clay minerals towards the Ordovician. The Ordovician rocks with Al_2O_3/SiO_2 ratios between those of UCC and PAAS represent rather siltstones, whereas these with distinctly elevated Al_2O_3/SiO_2 ratios are shales. Increasing K_2O/Na_2O and $Al_2O_3/(CaO+Na_2O)$ ratios of the pelites (Fig. 5.3B, C) are controlled by both increasing enrichment of Al_2O_3 and K_2O and progressive depletion of Na_2O and CaO. For siltstones this is related to decreasing plagioclase contents. In shales it is rather an expression of changing clay mineral composition, which is controlled by the intensity of source rock weathering.

5.1.2 Early Palaeozoic sandstones

CIA values generally increase from Neoproterozoic to Ordovician, whereas several Cambrian sandstones differ from this trend having low CIA (Fig. 5.2). Furthermore 6 Ordovician sandstones

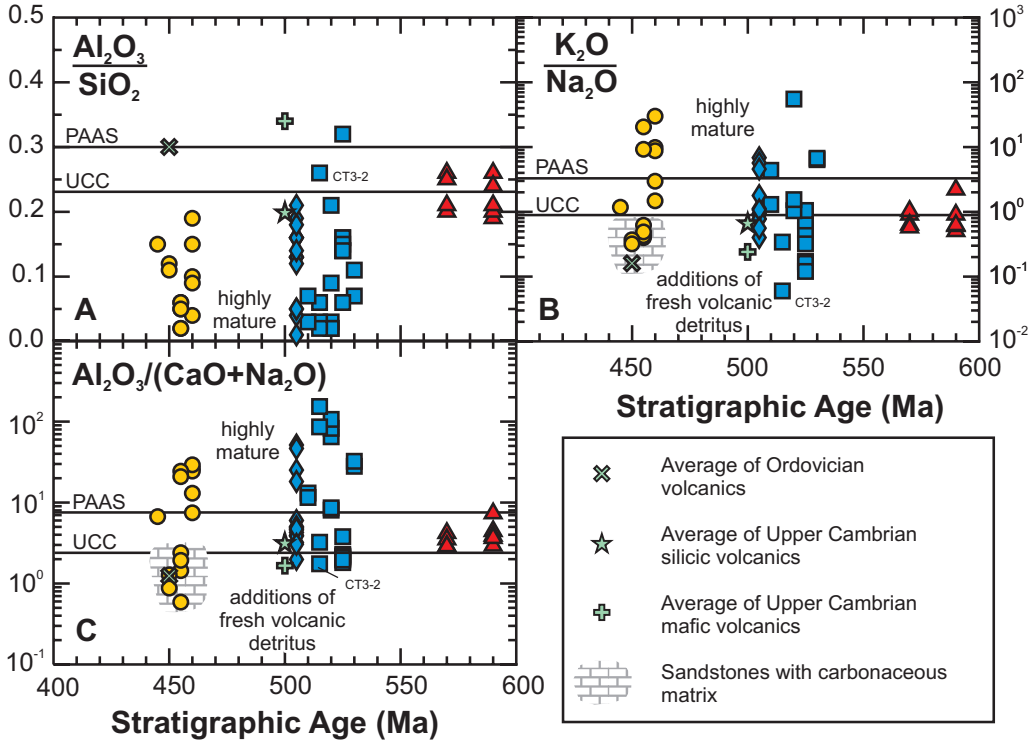

Fig. 5.4: Stratigraphic Age vs. Major Element Ratio plots for Neoproterozoic to Ordovician greywackes and sandstones indicate a general increase in chemical maturity with time. Averages of volcanic rocks of the TBU are given for an estimate of potential input from synsedimentary volcanism. **A**: Al_2O_3/SiO_2 ratios. **B**: K_2O/Na_2O ratios – four Lower Cambrian and two Middle Cambrian sandstones are not plotted because Na_2O was not detected. **C**: $Al_2O_3/(CaO+Na_2O)$ ratios.

Abb. 5.4: Stratigraphisches Alter vs. Hauptelementverhältnis – Diagramme für neoproterozoische bis ordovizische Grauwacken und Sandsteine zeigen prinzipiell eine Zunahme der chemischen Reife vom Neoproterozoikum zum Ordovizium. Außerdem sind die Durchschnittswerte für vulkanische Gesteine des Teplá-Barrandiums angegeben, da diese eine potentielle Quelle für die siliziklastischen Sedimente darstellen. **A**: Al_2O_3/SiO_2-Verhältnisse. **B**: K_2O/Na_2O-Verhältnisse; vier unterkambrische und zwei mittelkambrische Sandsteinproben sind nicht geplottet, da ihr Na_2O-Gehalt unterhalb der Nachweisgrenze ist. **C**: $Al_2O_3/(CaO+Na_2O)$-Verhältnisse.

did not yield reasonable CIA values due to their carbonaceous matrix. Similarly low K_2O/Na_2O and $Al_2O_3/(CaO+Na_2O)$ ratios of the low-CIA Cambrian sandstones and the carbonaceous Ordovician siliciclastics (Tab. 5.1, Fig. 5.4B, C) are indicative of contributions from fresh volcanic material.

The majority of the Lower Cambrian and Ordovician psammites as well as few Middle Cambrian quartzitic siliciclastics of the Skryje-Týřovice area are highly enriched in SiO_2 and correspondingly depleted in other major element oxides entailing low Al_2O_3/SiO_2 ratios. CIA values of these rocks are distinctly higher than those of the Neoproterozoic siliciclastics (Tab. 5.1, Fig. 5.2). Similarly, high K_2O/Na_2O and $Al_2O_2/(CaO+Na_2O)$ ratios, respectively, (Fig. 5.1, Fig. 5.4) are indicative of intense weathering, since Na and Ca are most rapidly removed by fluids during decomposition of plagioclase and other unstable minerals (Nesbitt et al. 1980). With regard to their major element compositions most of the Middle Cambrian sandstones show more similarities with the Neoproterozoic detrital sediments than with the highly mature Lower Cambrian and Ordovician sandstones.

GEOLOGICA SAXONICA
Journal of Central European Geology 54 (2008) 1–168

Table 5.2: Trace element characteristics[1] of the analysed samples of the individual age groups. Trace element ratios of PAAS, UCC and BCC are listed for comparison.

Tab. 5.2: Spurenelementcharakteristika[1] der analysierten Proben der einzelnen Altersabschnitte. Spurenelementverhältnisse von PAAS, UCC und BCC sind zum Vergleich angegeben.

	La/Yb_N	La/Sm_N	Eu/Eu*	Ce/Ce*	Zr/Hf	Th/U	Th/Sc	ΣREE [ppm]
Neoproterozoic								
greywackes (n=9)	5.6–9.7	3.0–4.1	0.72–0.87	0.93–1.00	33.0–39.5	1.0–4.7	0.28–0.70	94–165
shales/siltstones (n=4)	6.1–8.7	2.6–3.6	(0.64) 0.73–1.01	0.85–0.96	30.9–38.9	2.1–2.9	0.29–0.46	107–155
Lower Cambrian								
sandstones - high CIA (n=11)	4.2–15.3	2.4–7.1	0.75–0.87	0.94–1.18	29.6–41.5	1.6–5.0	0.42–1.03 (2.17)	25–97 (147)
sandstones - low CIA (n=10)	5.0–11.2	2.5–5.2	0.82–1.03	0.86–1.03	36.5–41.7	2.4–3.7	0.35–0.90	49–171
shale (n=1)	7.2	3.6	0.76	0.94	34.1	3.1	0.48	187
Middle Cambrian								
sandstones (n=15)	5.7–10.2	2.7–4.5	0.80–0.92	0.85–1.04	36.0–44.4	2.0–3.6	0.26–0.73	20–149
shales/siltstones (n=16)	5.5–8.8	3.0–4.1	0.72–0.82	0.91–1.04	34.6–39.0	2.5–3.3	0.38–0.59	140–188
Ordovician								
sandstones (n=8)	4.9–10.7	1.3–4.0	0.67–0.81	0.96–1.12	31.4–36.4	3.0–6.9	0.82–1.71	77–199
sandstones, carbonaceous (n=6)	4.9–13.8	2.6–3.7	0.68–0.83	0.97–1.04	32.2–36.1	5.0–6.3	0.88–2.55	112–222
shales/siltstones (n=28)	8.2–15.0	3.1–5.7	0.65–0.77	0.87–1.08	30.8–34.9	(2.9) 4.5–7.8	0.57–1.48	186–329
PAAS	9.1	4.3	0.64	1.01	42.0	4.7	0.91	183
UCC	10.5	4.1	0.69	0.99	36.4	3.9	0.75	148
BCC	7.1	3.2	0.87	1.02	35.7	4.3	0.26	106

5.2 Trace elements

HFSE (e.g., Zr, Hf, Nb, Th, Sc) and REE are considered to be immobile during weathering and transport and have a low residence time in sea water (summarized by Bhatia 1985, Bhatia & Crook 1986, Elderfield et al. 1990). Therefore, these elements on the one hand may represent direct provenance indicators, e.g., high Sc is characteristic for a provenance from mafic rocks, as this compatible element substitutes

[1] All REE-related values referring to a normalisation (e.g., La/Yb_N, Eu/Eu*) were calculated with the chondritic abundances given by Boynton (1984). The anomalies of Eu and Ce were calculated by the equations:

$$\frac{Eu}{Eu^*} = \frac{Eu_N}{0.5 \times (Sm_N + Gd_N)} \quad \text{and} \quad \frac{Ce}{Ce^*} = \frac{Ce_N}{0.5 \times (La_N + \mathrm{Pr}_N)}$$

On account of the steep LREE patterns of the analysed siliciclastics the application of the geometric mean did not yield reasonable values, particularly for Ce/Ce*. The values obtained by using the arithmetic mean are closer to the visual impression derived from Fig. 5.5.

into early crystallising phases, such as pyroxenes and amphiboles (e.g., McLennan 1999), high LREE and Th may be related to monazite or allanite, which point to a felsic igneous and/or to an amphibolite facies to high-grade metamorphic provenance, respectively. On the other hand HFSE and REE distributions may identify weathering processes, which in turn may be indicative of the geotectonic setting of the sedimentary basin, e.g., high LREE and Th may also be an indicator of recycled sedimentary provenance, as monazite is relatively stable during sedimentary and weathering processes and may be concentrated in siliciclastic source rocks (Mange & Maurer 1991, and references therein), high Th/U ratios may result from intense source rock weathering in a low-energy/passive margin setting, as Th is retained in particles during sedimentary and weathering processes but U is more soluble and mobile (McLennan et al. 1993). Since HFSE and REE patterns of siliciclastic sediments are predominantly controlled by heavy minerals, analyses with some obviously elevated HFSE and/or REE are to be considered with caution because mechanical sorting during transport and sedimentation may concentrate heavy minerals in particular levels/lenses of the sedimentary pile and may therefore modify the provenance signal in favour of the respective source(s).

LILE (Cs, Rb, Ba, K, Sr) abundances in detrital sediments are largely ruled by weathering processes, because all these elements are highly soluble in aqueous fluids and therefore controlled by the system: residual phases – newly formed minerals – released solutions (Mittlefehldt 1999). However, different response to weathering processes gives information on the intensity of source rock weathering, i.e. Sr is most rapidly removed, whereas Rb, Cs and Ba are fixed onto secondary clay minerals (Nesbitt et al. 1980). In contrast to the HFSE and REE, significant amounts of LILE are incorporated in rock-forming minerals, such as plagioclase, alkali-feldspar, biotite and muscovite. Consequently, if sandstones and conglomerates contain fresh grains/pebbles, these may reflect the LILE composition of the source rocks. LILE behave incompatibly during mantle melting and are therefore enriched in the upper continental crust (Rudnick 1999).

As was already indicated by the major elements, Neoproterozoic greywackes and shales are largely similar to each. This also applies to their trace element compositions (Tab. 5.2). Therefore they are treated together in 5.2.1.

5.2.1 Neoproterozoic siliciclastics and Early Palaeozoic shales/siltstones

Chondrite-normalised REE plots of the Late Neoproterozoic shales, siltstones and greywackes and Early Palaeozoic shales and siltstones (Fig. 5.5) reveal increasing abundances of REE with time. Neoproterozoic rocks have total REE contents of 94–165 ppm, La/Yb_N of 5.9–9.7 and La/Sm_N of 2.6–4.1 (Tab. 5.2, Fig. 5.5A, B). While analyses of Cambrian pelites show an overlap with those of the Neoproterozoic siliciclastics concerning their REE abundances (140 - 188 ppm) and fractionation patterns (La/Yb_N = 5.5–8.8, La/Sm_N = 3.0–4.1; Fig. 5.5C, D), most analyses of the Ordovician shales and siltstones yielded distinctly higher ∑REE (186–329 ppm), La/Yb_N (8.2–15.0), and La/Sm_N (3.1–5.7; Fig. 5.5E to H, Tab. 5-2). This is chiefly controlled by the abundance of LREE in the Ordovician sediments. While ∑LREE and ∑HREE correlate well in the Neoproterozoic and Cambrian siliciclastics, Ordovician rocks show a prominent shift towards elevated ∑LREE/∑HREE. The Eu-anomaly deepens from Neoproterozoic to Ordovician. Although calculated Ce/Ce* suggest a

Fig. 5.5: Chondrite-normalised REE patterns of Neoproterozoic siliciclastics (sample name bold for greywackes, italics for siltstone, normal for shales) and Cambrian and Ordovician siltstones (italics) and shales (normal). Normalisation values from Boynton (1984). Shaded field in C to H represents the envelope of the analysed Neoproterozoic siliciclastics.

Abb. 5.5: Chondrit-normierte SEE-Muster neoproterozoischer Siliziklastika (Probename fett für Grauwacken, kursiv für Siltsteine, normal für Tonsteine) sowie kambrischer und ordovizischer Siltsteine (kursiv) und Tonsteine (normal). Normierungswerte nach Boynton (1984). Das graue Feld in C bis H entspricht den analysierten neoproterozoischen Siliziklastika.

GEOLOGICA SAXONICA
Journal of Central European Geology
54 (2008) 1–168

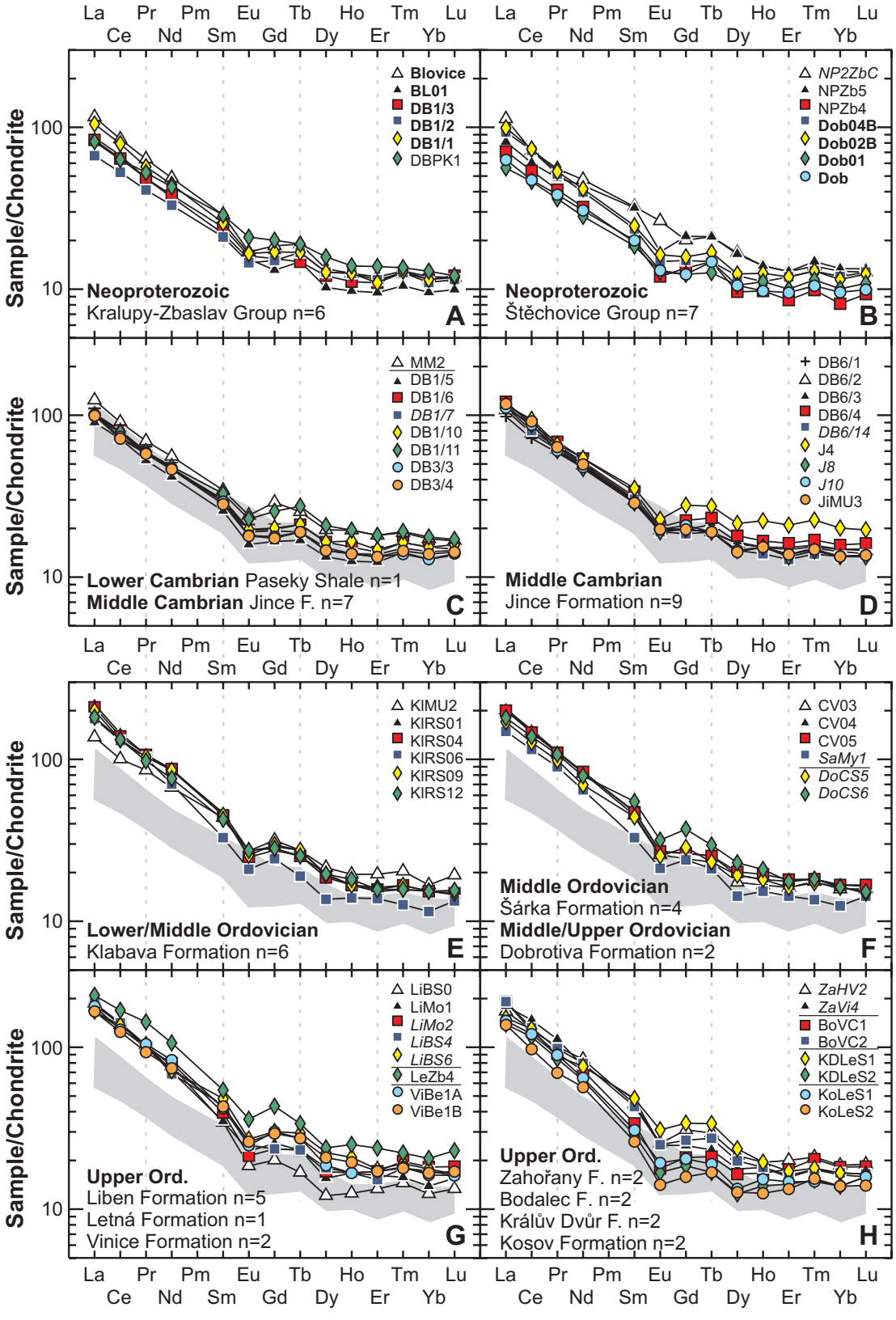

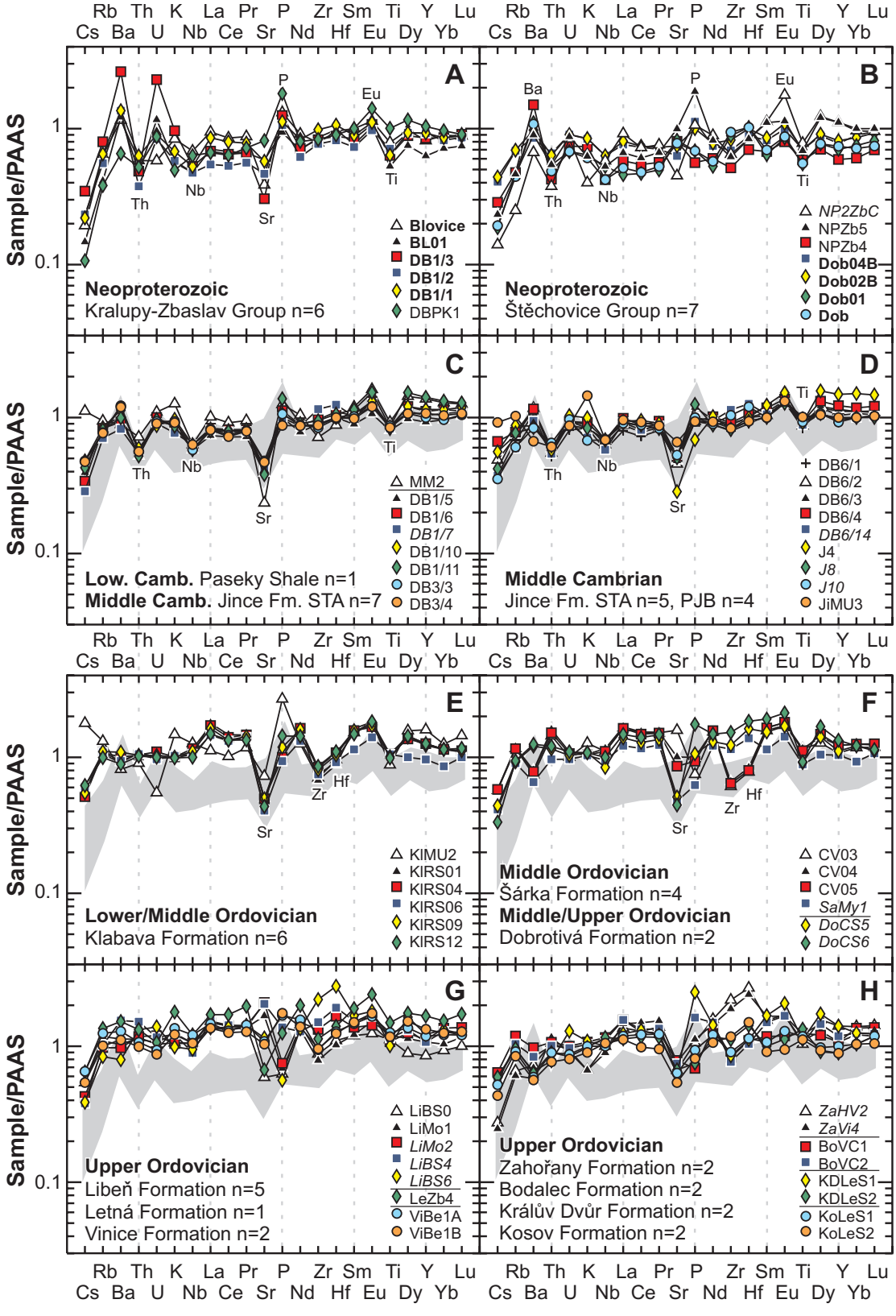
Rb Th K La Pr P Zr Sm Ti Y Lu
Cs Ba U Nb Ce Sr Nd Hf Eu Dy Yb
Sample/PAAS
1
0.1
A
Neoproterozoic
Kralupy-Zbaslav Group n=6
Blovice
BL01
DB1/3
DB1/2
DB1/1
DBPK1
B
Neoproterozoic
Štěchovice Group n=7
NP2ZbC
NPZb5
NPZb4
Dob04B
Dob02B
Dob01
Dob
C
Low. Camb. Paseky Shale n=1
Middle Camb. Jince Fm. STA n=7
MM2
DB1/5
DB1/6
DB1/7
DB1/10
DB1/11
DB3/3
DB3/4
D
Middle Cambrian
Jince Fm. STA n=5, PJB n=4
DB6/1
DB6/2
DB6/3
DB6/4
DB6/14
J4
J8
J10
JiMU3
E
Lower/Middle Ordovician
Klabava Formation n=6
KIMU2
KIRS01
KIRS04
KIRS06
KIRS09
KIRS12
F
Middle Ordovician
Šárka Formation n=4
Middle/Upper Ordovician
Dobrotivá Formation n=2
CV03
CV04
CV05
SaMy1
DoCS5
DoCS6
G
Upper Ordovician
Libeň Formation n=5
Letná Formation n=1
Vinice Formation n=2
LiBS0
LiMo1
LiMo2
LiBS4
LiBS6
LeZb4
ViBe1A
ViBe1B
H
Upper Ordovician
Zahořany Formation n=2
Bodalec Formation n=2
Králův Dvůr Formation n=2
Kosov Formation n=2
ZaHV2
ZaVi4
BoVC1
BoVC2
KDLeS1
KDLeS2
KoLeS1
KoLeS2

slight trend towards Ce enrichment during time, there are no pronounced Ce-anomalies visible in chondrite-normalised plots (Fig. 5.5).

PAAS-normalised multi-element plots for Neoproterozoic detrital sediments and Early Palaeozoic shales and siltstones are given in Fig. 5-6. Neoproterozoic rocks yielded inclined patterns with even less incompatible elements below PAAS. There are peaks in Ba, (P) and Eu and troughs in Th, Nb and Ti. All this is in line with major contributions from island arc rocks and a continental component. The U and Sr anomalies in the Neoproterozoic rocks of the Kralupy-Zbraslav Group (Fig. 5.6A) are most probably related to redistribution of these elements during deformation and metamorphism. The younger Neoproterozoic rocks (Štěchovice Group) include one sample (NP2ZbC, Fig. 5.6B) with a larger proportion of volcanic detritus. This is indicated by a distinct positive Eu-anomaly, low concentrations of LILE and Nb and elevated contents of P and HREY. The latter points to apatite involvement and applies also to sample NPZb5.

Cambrian shales and siltstones (Fig. 5.6C, D) have very homogenous trace element compositions and show incompatible element patterns that are slightly more inclined than those of Neoproterozoic sediments. At least the abundances of less incompatible elements are in the same range as PAAS. Th, Nb, Sr and Ti are distinctly depleted when normalised to PAAS. In comparison to Neoproterozoic sediments Ba and Sr are depleted, Cs, Rb and to a lesser extend Th and K are enriched. The Lower Cambrian shale sample (MM2; Fig. 5.6C) is similar to Middle Cambrian shales and siltstones concerning its multi-element pattern with two exceptions: the Cs concentration is higher and in the range of PAAS and Sr is somewhat more depleted than in Middle Cambrian rocks.

One Middle Cambrian sample (JiMU3; Fig. 5.6D) shows slightly elevated concentrations of Cs, Rb and K and was probably influenced by hydrothermal fluids during the Lower Ordovician. The same – but to a larger extent – is true for one Lower Ordovician shale (KlMU2; Fig. 5.6E) from the same locality. Additionally to distinctly elevated Cs, Rb and K concentrations, this sample is characterised by elevated P and HREY contents pointing to involvement of apatite and/or xenotime. A small Ce-anomaly (slightly positive for the Middle Cambrian sample: Fig. 5.5D; slightly negative for the Ordovician sample: Fig. 5.5E) is visible in both samples from the Medový Újezd locality.

The majority of the Ordovician shales and siltstones shows horizontal multi-element patterns and a depletion in Sr when normalised to PAAS. Although many samples display a negative Ti-anomaly, TiO_2 contents of the Ordovician shales and siltstones are similar to that of PAAS. Shales are characterised by distinct Zr-Hf troughs, whereas siltstones have rather PAAS-like contents or show Zr-Hf enrichment (Fig. 5.6E to H). This is controlled by the weathering resistant heavy mineral zircon, which occurs as a residue of weathering in the detrital silt fraction but is not quantitatively transferred to the clay fraction.

5.2.2 Early Palaeozoic sandstones

The analysed sandstones of the individual age intervals have less uniform multi-element patterns (Fig. 5.7) than the associated shales. This is to some extend attributed to highly variable SiO_2 contents (quartz dilution - McLennan et al. 1990) and related variations in heavy mineral concentration but first of all to differences in provenance and weathering conditions.

Trace element analyses of most Cambrian sandstones reveal a depletion in LREE relative to MREE and

Fig. 5.6: PAAS-normalised multi-element patterns of Neoproterozoic siliciclastics (sample name bold for greywackes, italics for siltstone, normal for shales) and Cambrian and Ordovician siltstones (italics) and shales (normal). Shaded field in **C** to **H** represents the envelope of the analysed Neoproterozoic siliciclastics. Normalisation values from Taylor & McLennan (1985).

Abb. 5.6: PAAS-normierte Multi-Element-Muster der neoproterozoischen Siliziklastika (Probename fett für Grauwacken, kursiv für Siltsteine, normal für Tonsteine) sowie kambrische und ordovizische Siltsteine (kursiv) und Tonsteine (normal). Das graue Feld in **C** bis **H** zeigt die analysierten neoproterozoischen Proben zum Vergleich. Normierungswerte aus Taylor and McLennan (1985).

HREE when normalised to PAAS. Apart from that trace element patterns are variable. Lower Cambrian sandstones may be subdivided into four types:

(**1**) Among the Lower Cambrian sandstone samples there are some rocks with multi-element patterns largely parallel to those of the Neoproterozoic sediments (PJ1/3 and HL1 in Fig. 5.7A, MM8 in Fig. 5.7C). Different trace element concentrations within this group chiefly correspond to varying SiO_2 contents. However, independent of the SiO_2 content, Sr is distinctly depleted in this group of sediments when compared to the Neoproterozoic rocks. This suggests that Lower Cambrian detrital sediments are derived from the Neoproterozoic basement or similar crust.

(**2**) A further – at least intermittently available – source is represented by young volcanic rocks. Particularly the sandstones of the Sádek (except DB B; Fig. 5.7A, B) and Klouček-Čenkov formations (Fig. 5.7D) received contributions from a young mafic and/or intermediate source. The detrital sediments of this group have PAAS-normalized patterns that are steeper inclined, i.e., show stronger depletion in incompatible elements, than those of the Neoproterozoic rocks. Furthermore these samples are – independent of their SiO_2 contents – characterised by low CIA values (see above). Th, Sr, Zr and Hf concentrations of these samples are variable due to involvement of different quantities of weathered crustal material.

(**3**) A third group of Lower Cambrian detrital sediments is represented by sandstones and conglomeratic sandstones with elevated La/Yb_N (samples of the Holšiny-Hořice Formation except MM8: Fig. 5.7C, sample DB B in Fig. 5.7A). Due to high SiO_2 contents, their trace element concentrations are distinctly lower than those of PAAS. Multi-element patterns of these detrital sediments reflect larger contributions from differentiated, weathered crust.

(**4**) The rocks of the Chumava-Baština Formation have elevated Th to Lu concentrations when compared to the remaining samples with similarly high SiO_2 contents (LS1-3 and CB3 in Fig. 5.7D). As this formation is represented by only two samples it is questionable, if these features are characteristic for the entire Chumava-Baština Formation or if the analysed samples correspond to levels with heavy mineral enrichment and therefore represent outliers[1].

Middle Cambrian sandstones of the Skryje-Týřovice area (Fig. 5-7E, F) have multi-element patterns that are slightly inclined when normalised to PAAS but largely similar to those of the Neoproterozoic siliciclastics. In comparison to the latter, elevated Zr and Hf concentrations and depletion of Sr and P may occur. In contrast, Middle Cambrian sandstones of the Příbram-Jince Basin show multi-element patterns that are - normalized to PAAS - somewhat steeper inclined than those of the Neoproterozoic detrital sediments, which suggests larger contributions from a mafic source.

[1] Thin sections of these rocks are ambiguous, too. They revealed a large number of tiny heavy mineral inclusions in quartz grains. As well smaller crystals of monazite, titanite, zircon and non-transparent heavy minerals were observed on grain boundaries within lithic fragments(?) consisting of polycrystalline quartz or quartz and feldspar. However, recrystallisation of the rocks does only rarely allow a clear identification of coarser grained lithic fragments. Furthermore the largest heavy minerals seem to be related to particular laminae/layers and are therefore interpreted to be the result of sedimentary sorting.

Fig. 5.7: PAAS-normalized multi-element patterns of Cambrian and Ordovician sandstones with highly variable SiO_2 contents. Shaded field represents the envelope of the analysed Neoproterozoic siliciclastics. Bold sample names stand for rocks with $SiO_2 \geq 90$ wt.% (volatile-free recalculated analyses). Normalisation values from Taylor and McLennan (1985).

Abb. 5.7: PAAS-normierte Multi-Element-Muster der im SiO_2-Gehalt stark variierenden, kambrischen und ordovizischen Sandsteine. Das graue Feld zeigt die analysierten neoproterozoischen Proben zum Vergleich. Fett gedruckte Probenamen stehen für Gesteine mit $SiO_2 \geq 90$ Gew.-% (wasserfrei gerechnete Analysen). Normierungswerte aus Taylor and McLennan (1985).

GEOLOGICA SAXONICA
Journal of Central European Geology
54 (2008) 1–168

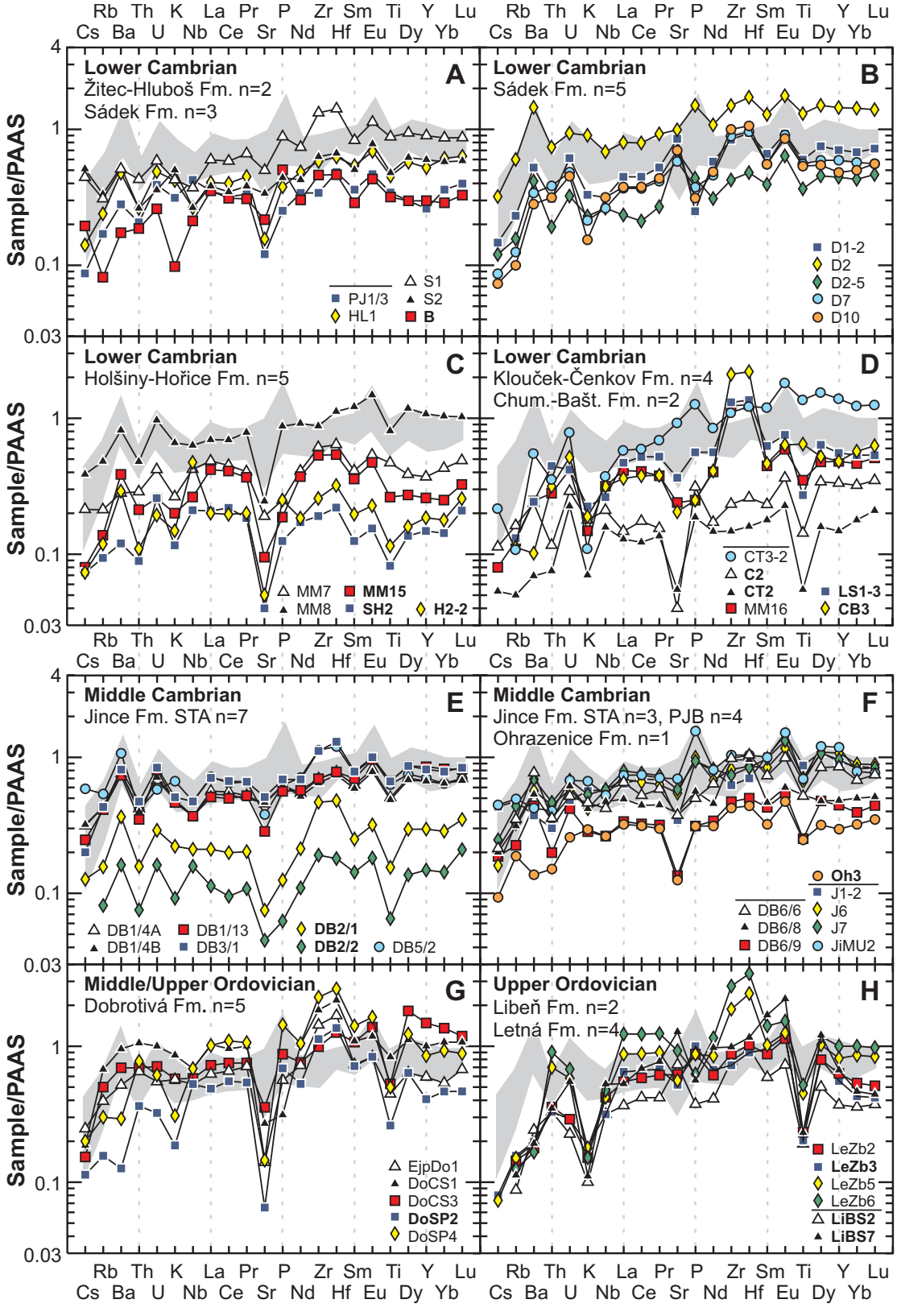

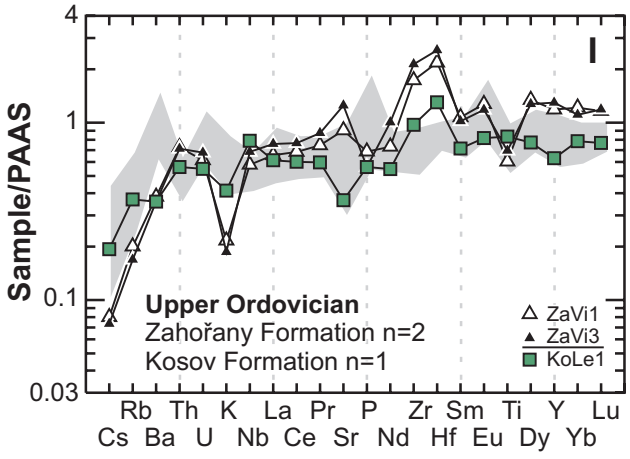

Fig. 5.7: Continued.

Fourteen sandstone samples from five Middle to Upper Ordovician formations were analysed. Although multi-element patterns of the Ordovician sandstones are variable, too, they differ from those of the Cambrian sandstones. In many samples Th and U are distinctly elevated when compared to the neighbouring elements Ba and K (Fig. 5-7G to I). In contrast to the Cambrian sandstones, Ordovician psammites show largely horizontal PAAS-normalised REE patterns, however, abundances of MREE are slightly elevated relative to LREE and HREE. Th-U, LREE and MREE are chiefly controlled by monazite, while Zr-Hf and HREE are ruled by zircon. All this is indicative of derivation from felsic igneous and/or siliciclastic sources, i.e. crustal sources that are more evolved than the Neoproterozoic basement rocks. Cs, Rb, Ba, and K are markedly below PAAS in the majority of the Ordovician samples.

The rocks of the Dobrotivá Formation (Fig. 5.7G) show depletions in Cs, Sr and Ti and enrichment in Zr and Hf when normalised to PAAS. The samples from the Ejpovice (EjpDo1) and Černá Skála (DoCS1, DoCS3) outcrops differ from those of the Starý Plzenec (DoSP2, DoSP4) locality by higher portions of Rb, Ba and K, which is related to the smaller grain-size and higher matrix and mica contents, respectively, in the former. Sample DoCS3 shows a depletion in LREE relative to MREE and HREE when normalised to PAAS. This and the higher concentrations of Sr and Na_2O (relative to the remaining samples from the Dobrotivá Formation) point to additional contributions from a mafic source.

The samples of the Libeň, Letná and Zahořany formations (Fig. 5.7H, I) do not show the pronounced negative Sr anomaly, which is observable in the rocks of the Dobrotivá Formation (Fig. 5.7I). This feature correlates with elevated CaO and Na_2O contents, which are related to carbonate matrix and plagioclase in the samples of the Letná Formation and to carbonate matrix, detrital matrix, mica and plagioclase in the sandstones of the Zahořany Formation. SiO_2-rich sandstones (SiO_2 = 96.3 / 95.8 wt%) of the Libeň Formation do neither contain significant amounts of carbonate (CaO = 0.04 / 0.09 wt%, LOI = 0.44 / 0.61 wt%) nor remarkable amounts of feldspar.

Fig. 5.7I shows two fine-grained sandstones of the Zahořany Formation that have inclined PAAS-normalised multi-element patterns with depleted LREE relative to MREE and HREE and show Sr enrichment. These rocks were obviously influenced by the Ordovician alkaline volcanism. Similarly, the sample from the uppermost Ordovician Kosov Formation (Fig. 5.7I, Fig. 5.8D) has lower La/Yb_N than the majority of the Ordovician siliciclastics.

5.3 Provenance and weathering

The analysed samples show that sandstone compositions may be sensitive to small-scale changes in provenance. Particularly the intermittent influence of synsedimentary volcanic activity or the temporary availability of an additional source is more directly reflected by sandstones than by fine-grained siliciclastics. Shales and siltstones, however, do better reflect the overall geotectonic regime of the sedimentary basin and the overall weathering conditions.

The data for the shales and siltstones show an increase in incompatible elements (Cs, Rb, K, Th, Nb, Ta, LREE, [MREE]) from the Neoproterozoic to the Ordovician. As these elements are enriched in the Earth's crust when compared to the depleted mantle,

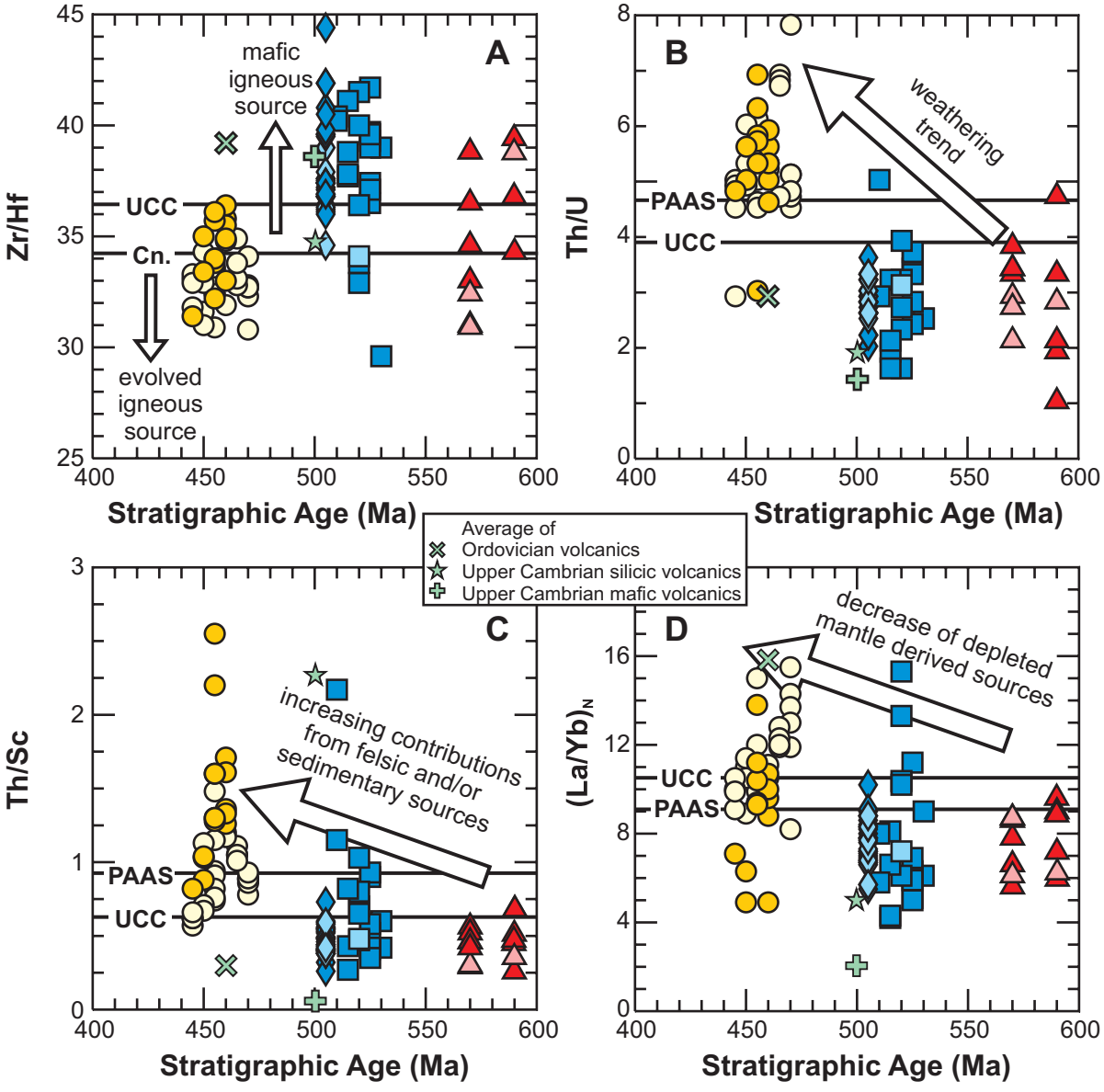

Fig. 5.8: Stratigraphic Age vs. Trace Element Ratio plots for Neoproterozoic and Early Palaeozoic detrital sediments. Symbols as in Fig. 5.1. **A**: Zr/Hf ratios of Cambrian sediments are distinctly higher than those of Ordovician rocks and point to contrasting sources. Cn. – chondritic value (Thompson 1982, Weyer et al. 2002). **B**: Th/U ratios of the Ordovician siliciclastics are markedly elevated when compared to UCC, Neoproterozoic and Cambrian sediments and indicate more intense chemical weathering. After McLennan et al. (1993) **C**: Th/Sc ratios increase from Neoproterozoic to Ordovician detrital sediments and reflect decreasing importance of mafic sources. **D**: $(La/Yb)_N$ increase from Cambrian to Ordovician indicating increasing contributions from differentiated crust.

Abb. 5.8: Stratigraphisches Alter vs. Spurenelement-Verhältnis-Diagramme für neoproterozoische und frühpaläozoische detritische Sedimente. Symbole wie in Abb. 5.1. **A**: Die Zr/Hf-Verhältnisse der kambrischen Sedimente sind deutlich höher als die der ordovizischen Gesteine, was auf unterschiedliche Ausgangsgesteine hinweist. **Cn.** – Chondrit (Thompson 1982, Weyer et al. 2002). **B**: Die Th/U-Verhältnisse der Ordovizischen Proben sind im Vergleich zur durchschnittlichen oberen Erdkruste (UCC) sowie den neoproterozoischen und kambrischen Sedimenten deutlich erhöht, was auf intensive chemische Verwitterung ihrer Ausgangsgesteine hinweist. Nach McLennan et al. (1993) **C**: Die Th/Sc-Verhältnisse nehmen vom Neoproterozoikum zum Ordovizium zu und spiegeln eine Abnahme an mafischen Ausgangsgesteinen wieder. **D**: Die $(La/Yb)_N$-Verhältnisse steigen vom Neoproterozoikum zum Ordovizium und zeigen eine Zunahme an Eintrag von differenzierter Kruste an.

this change suggests an increasing contribution of crustal sources towards the Ordovician. Although particularly LILE may be subject to redistributions during diagenesis and low-grade metamorphism (e.g., Taylor & McLennan 1985, Wronkiewicz & Condie 1987), the largely parallel Cs-Rb patterns in the spider diagrams (Fig. 5.6) suggest different intensities of source rock weathering and changing provenances (cf., Nesbitt et al. 1980) with time rather than syn- and post-depositional alterations.

Fig. 5.8 shows several trace element ratios, which discriminate the analysed rocks effectively. Differences in grain size do not have a particular influence on these ratios as is clear from the concordance of the shale/siltstone data with the sandstone data in the respective age interval.

Zr/Hf ratios of the Neoproterozoic rocks are variable, Cambrian siliciclastics have distinctly elevated Zr/Hf ratios when compared to chondrite and to the upper continental crust and Ordovician sediments exhibit distinctly lower Zr/Hf than Cambrian sediments and the upper continental crust (Fig. 5-8A). Zirconium and Hf are chiefly controlled by the heavy mineral zircon (ZrSiO4), which is the dominant reservoir of both elements. Since zircon crystals of different origin incorporate different amounts of Hf, their Zr/Hf ratios may vary considerably and allow discrimination of different host/source rocks (Hoskin & Schaltegger 2003, Miller et al. 2005; and references therein). Continental and oceanic intraplate basaltic rocks (Dupuy et al. 1992, David et al. 2000) have Zr/Hf ratios that are distinctly higher than the chondritic value of 34.2 (Thompson 1982, Weyer et al. 2002), MOR basalts (David et al. 2000) have relatively uniform Zr/Hf ratios slightly above the chondritic value and evolved igneous rocks (except some peralkaline granites/rhyolites; e.g., Linnen & Keppler 2002) show Zr/Hf ratios considerably below the chondritic value. This implies that Neoproterozoic detrital sediments of the Teplá-Barrandian unit are derived from a heterogeneous source, while the majority of the Cambrian siliciclastics got larger contributions from mafic source rocks. In contrast, Ordovician sediments are clearly separated from the Cambrian rocks by distinctly lower Zr/Hf ratios, i.e., they are derived from felsic (meta)igneous rocks and/or recycled from sedimentary rocks with an ultimate source consisting of felsic igneous rocks.

Thorium is an incompatible element for the mantle mineralogy and during sedimentary processes it is transported almost exclusively in particulate form, i.e., Th became enriched in the Earth's crust when compared to the depleted mantle. Uranium, although incompatible, too, is soluble if oxidized to U^{6+} and subsequently may be accumulated in ore deposits or incorporated in the oceanic crust during alteration. The latter finally causes recycling of U to the mantle by subduction (e.g., Taylor & McLennan 1985, Plant et al. 1999). Therefore, high Th/U ratios in detrital sediments may be an indicator of sedimentary recycling. On the other hand Th/U ratios may be controlled by accessory minerals such as monazite, xenotime, thorite, or allanite. Fig. 5-8B shows the Th/U ratios of the analysed Teplá-Barrandian sediments. The Neoproterozoic rocks of the Kralupy-Zbraslav Group have a wide range of Th/U, which is possibly not primary. Variably intense deformation and low-grade metamorphism of these rocks occurred in late Neoproterozoic times and may have allowed redistribution of U, which in turn led to modifications in the Th/U ratios. Neoproterozoic rocks of the Štěchovice Group and Cambrian siliciclastics have similar Th/U below the upper crustal value of 3.9, which is chiefly controlled by low Th abundances. An appropriate source for these siliciclastics should be made up by or include considerable amounts of (depleted-) mantle-derived igneous rocks. This is realised in undifferentiated island arc complexes, accretionary wedges containing slices of ocean floor or extensional/transtensional settings with synsedimentary tholeiitic intra-plate volcanism (e.g., McLennan et al. 1993). Ordovician shales, siltstones and sandstones have distinctly higher Th/U ratios at higher abundances of both elements when compared to the Neoproterozoic and Cambrian sediments. Such elevated Th/U ratios in combination with the high CIA (cf., Fig. 5.2) point to intensive and long-standing source rock weathering. Furthermore, involvement of Th-rich phases (probably chiefly monazite) is suggested by high Th/U ratios in combination with other trace element data (cf., Fig. 5.7G, H), which

indicates a felsic igneous, metamorphic and/or recycled siliciclastic provenance, respectively.

The Th/Sc ratio (Fig. 5.8C) compares an incompatible element to a relatively compatible one. Thorium is incorporated in the late crystallising silicate phases and therefore enriched in granites and associated accessory minerals. Scandium, in contrast, substitutes into early crystallising phases, such as pyroxenes and amphiboles. Both elements are immobile in sedimentary environments and have low residence times in sea water. Therefore, the Th/Sc ratio reflects the signature of the source rocks and distinguishes crustal/felsic source rocks and provenance from mafic complexes (Bhatia & Crook 1986, McLennan et al. 1993). All analysed Neoproterozoic siliciclastics and the majority of the Cambrian sediments have Th/Sc around or below the upper crustal value of 0.75 pointing to involvement of depleted mantle derived detritus. Several Lower Cambrian sandstones have elevated Th/Sc, which is compatible with enrichment of heavy minerals. In the SiO_2-rich samples DB B (Sádek Formation), MM15 and H2-2 (Holšiny-Hořice Formation) the Th/U ratio is controlled by the presence of monazite, as indicated by undepleted LREE (cf., Fig. 5.7A, C) and elevated La/Yb_N (samples around and above upper crustal values in Fig. 5.8D). For the SiO_2-rich samples of the Chumava-Baština Formation (LS1-3, CB3), sphene, apatite and zircon are the relevant heavy minerals, as suggested by distinctly elevated Zr and Hf in both samples, undepleted P in sample LS1-3 and undepleted Ti in sample CB3 (Fig. 5.7D). Several, particularly uppermost, Ordovician siliciclastics have Th/Sc ratios around the upper crustal value, but the majority of the Ordovician rocks has markedly elevated Th/Sc when compared to UCC and to Neoproterozoic and Cambrian siliciclastics. The high values of the sandstone samples from the Dobrotivá (DoCS1, DoSP4), Libeň (LiBS2) and Letná (LeZb2, 5, 6) formations are attributed to enrichment of heavy minerals (phosphates, sphene, zircon; cf., Fig. 5.7G, H). In general, Th/Sc ratios increase from the Lower/Middle Ordovician (Klabava Formation) to the Upper Ordovician and then decrease in the uppermost Ordovician, whereas high Th/Sc ratios indicate felsic igneous and/or siliciclastic sources or their metamorphic equivalents. Intense source rock weathering results in high Th/Sc ratios, too.

Fig. 5.8D shows the La/Yb_N ratios of the analysed samples, of UCC and PAAS. The La/Yb_N ratio compares a relatively incompatible light REE to a more compatible heavy REE. Since LREE are enriched in the crust when compared to the depleted mantle, differences in the La/Yb_N ratios of siliciclastic sediments reflect provenance from different sources. Particularly high La/Yb_N ratios of fine-grained siliciclastic sediments may also be the product of extreme chemical weathering (Cullers et al. 1975, Nesbitt et al. 1990). Neoproterozoic and the majority of the Cambrian detrital sediments of the Teplá-Barrandian have low La/Yb_N ratios (Fig. 5.8D). This is compatible with derivation from island-arc related complexes containing depleted mantle derived igneous rocks and sedimentary material. Larger contributions from older sedimentary complexes are indicated only for the rocks of the Lower Cambrian Holšiny-Hořice Formation. Lower and Middle Ordovician shales and siltstones of the Klabava and Šárka formations have distinctly elevated La/Yb_N ratios when compared to the underlying Cambrian and Neoproterozoic rocks and to UCC. Since the Teplá-Barrandian underwent a subaerial period during the Upper Cambrian and the lowermost Ordovician, it is likely that the Lower and Middle Ordovician shales reflect the denudation of a weathering crust. In the upper Middle and Upper Ordovician the La/Yb_N ratios drop to values, which are normal for the upper continental crust. However, also the younger Ordovician siliciclastics have markedly higher La/Yb_N ratios than Neoproterozoic and Cambrian sediments indicating larger contributions from crustal sources.

5.4 Summary of geochemical information

Geochemical data of the analysed rocks clearly discriminate individual groups of samples. These groups match the stratigraphic ages of the analyzed siliciclastic rocks and reflect changing sources and weathering conditions over time (Fig. 5.9), which in turn indicate shifts in the geotectonic setting.

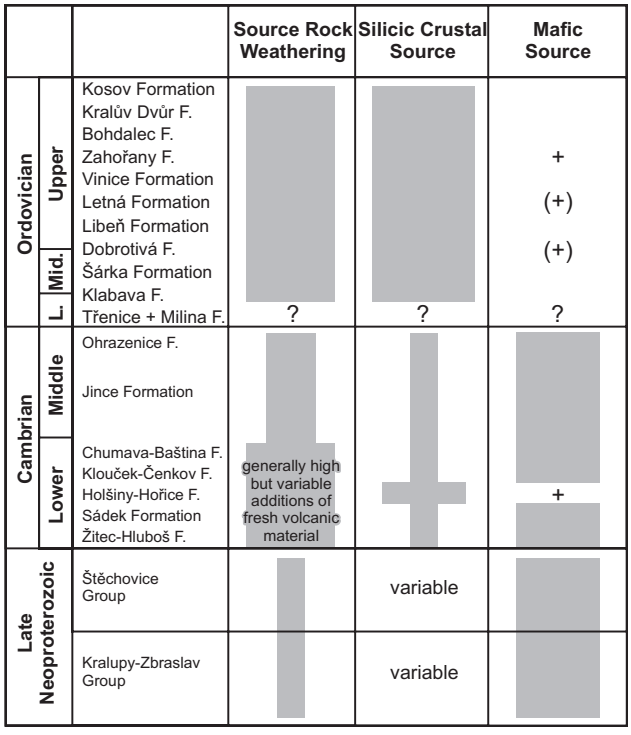

Fig. 5.9: Summary of geochemical information.

Abb. 5.9: Zusammenfassung der geochemischen Informationen.

Late Neoproterozoic siliciclastics were derived from island arc complexes and continental crust in varying proportions, which, in combination with the lack of indications for notable chemical weathering of the source rocks, points to an active geotectonic setting (active or complex continental margin). Cambrian detrital sediments are similar to the Neoproterozoic siliciclastics with regard to many geochemical features. However, chemical weathering of the source rocks was distinctly more effective during the Lower and Middle Cambrian than in the Neoproterozoic. The detritus is predominantly derived from the Neoproterozoic basement and from young mafic source rocks, but older crustal rocks contributed to the composition of the Cambrian deposits, too. All this is compatible with a transtensional/rift setting of the Cambrian basin. In contrast, geochemical compositions of the Ordovician detrital sediments indicate involvement of stable REE- and HFSE-rich phases, such as phosphates, allanite, and zircon, which may be derived from felsic igneous complexes, metamorphic rocks (chiefly metapelites), and/or from recycling of siliciclastic sediments/sedimentary rocks. The high degree of source rock weathering and the provenance from crustal source rocks suggest deposition of the Ordovician sediments in a mature rift or passive margin setting, respectively.

6 Sr-Nd-Pb isotopic compositions of sedimentary whole rocks

Nd-Sr-Pb isotopic compositions of sedimentary whole rocks from the Late Neoproterozoic Cadomian basement and from the Early Palaeozoic siliciclastic overstep sequences of the TBU were determined in order to detect changes in provenance during this period and to substantiate the results of the element geochemical analyses of the previous chapter. As different reservoirs, such as the depleted mantle, the lower continental crust, and the upper continental crust are characterised by specific geochemical and isotopic signatures, the compositions of siliciclastic sediments allow the identification of varying contributions of material derived from these contrasting sources. Furthermore, mixed isotopic compositions resulting from different reservoirs in the source area of sediments may be resolved by the combination of differently behaving isotopic systems.

6.1 Samples

A total of 22 samples was taken to analyse the Nd-Sr-Pb isotopic composition of the Neoproterozoic basement and its Early Palaeozoic overstep sequence (Fig. 6.1). Rock types, lithostratigraphic units and localities are listed in Tab. 6-1. Whole rock analyses (carried out by ACTLABS) were thoroughly examined before selection of the samples to ensure that

GEOLOGICA SAXONICA
Journal of Central European Geology 54 (2008) 1–168

Table 6.1: List of studied samples. Numbers in brackets represent estimated ages that were used for calculations of the time-integrated parameters.

Tab. 6.1: Liste der untersuchten Proben. Zahlen in Klammern sind geschätzte Alter, die für die Berechnung der initialen Isotopenverhältnisse benutzt wurden.

Sample		Rock type	Stratigraphic age	Lithostratigraphic unit
Neoproterozoic				
1	BL 01	greywacke	Neoproterozoic (590)	Kralupy-Zbraslav Group
2	DB 1/1	deformed greywacke	Neoproterozoic (590)	Kralupy-Zbraslav Group
3	DB 1/2	deformed greywacke	Neoproterozoic (590)	Kralupy-Zbraslav Group
4	NPZB 4	siltstone	Neoproterozoic (570)	Štěchovice Group
5	NPZB 5	shale	Neoproterozoic (570)	Štěchovice Group
6	DOBRIS	fine-grained greywacke	Neoproterozoic (570)	Štěchovice Group
7	DOBRIS 02B	fine-grained greywacke	Neoproterozoic (570)	Štěchovice Group
Cambrian				
8	DB S1	fine-grained sandstone	Lower Cambrian (525)	Sádek Fm.
9	DB D2	fine-grained sandstone	Lower Cambrian (525)	Sádek Fm.
10	MM2	shale	Lower Cambrian (520)	Holšiny-Hořice Fm.
11	DB 1/5	shale	Middle Cambrian (505)	Jince Fm.
12	DB 6/1	shale	Middle Cambrian (505)	Jince Fm.
13	DB 6/3	shale	Middle Cambrian (505)	Jince Fm.
14	J4	shale	Middle Cambrian (505)	Jince Fm.
15	J8	siltstone	Middle Cambrian (505)	Jince Fm.
Ordovician				
16	KIRS 01	shale	Arenig (470)	Klabava Fm.
17	LIBS 0	shale	Caradoc (455)	Libeň Fm.
18	LEZB 4	shale	Caradoc (455)	Letná Fm.
19	VIBE 1A	shale	Caradoc (455)	Vinice Fm.
20	KDLE S2	siltstone	Ashgill (445)	Králův Dvůr Fm.
21	KOLE S1	shale	Ashgill (445)	Kosov Fm.
22	KOLE S2	shale	Ashgill (445)	Kosov Fm.

the samples are representative for the stratigraphic interval.

Isotopic analyses were carried out at the Isotope Geochemistry and Geochronology Laboratories of the GeoForschungsZentrum Potsdam. Analytical procedures are described in the appendix; analytical data are listed in Table A8.

The analysed samples comprise shales, siltstones and sandstones/greywackes. Although different lithologies may carry different provenance signals, it was shown in chapter 5 that this does not apply to the Neoproterozoic siliciclastics. In the Lower Cambrian of the Teplá-Barrandian, there is a lack of shales and siltstones, thus, two fine-grained sandstones were selected in addition to one shale sample. Middle Cambrian and Ordovician detrital sediments are represented by shales and by one siltstone each. Fig. 6.2 shows that the different lithological features of the selected siliciclastics are not related to distinct geochemical characteristics. Instead, the trace element signatures strongly correlate with the depositional age of the samples. It is therefore assumed that the

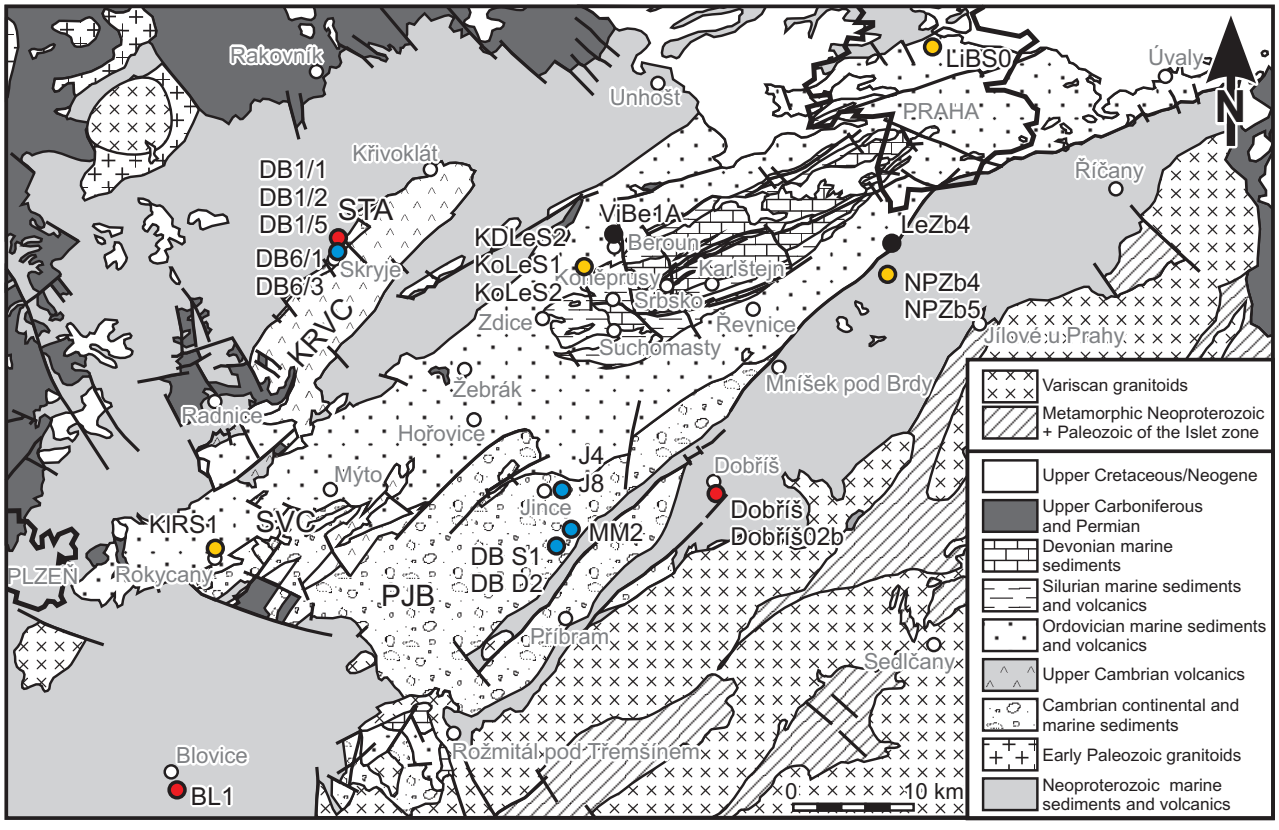

Fig. 6.1: Sketch map of sampling localities for Nd-Sr-Pb analyses of sedimentary whole rocks.

Abb. 6.1: Schematische Karte mit den Probenahmepunkten für Nd-Sr-Pb-Analysen an sedimentären Gesamtgesteinen.

variation in trace element compositions is largely attributed to provenance and weathering conditions, rather than a result of heavy mineral enrichment, sorting, or diagenetic alteration. Thus, the isotope signatures of the samples are believed to reflect the composition of the contributing sources.

6.2 Results

Six of seven **Neoproterozoic** samples yield εNd_T values of -7.2 to -3.6 and T_{DM} from 1.49 to 1.80 Ga (Fig. 6.3, Fig. 6.4, Fig. 6.5). Sample BL01 exhibits the strongest negative εNd_{590} value of -11.7 and the oldest T_{DM} (2.17 Ga). $^{87}Sr/^{86}Sr_T$ ratios of five samples range between 0.7064 and 0.7098 (Fig. 6.4); the remaining two samples (DB1/1, DB1/2) reveal anomalously low $^{87}Sr/^{86}Sr_{590}$ ratios resulting from post-depositional Rb gain or Sr loss. Rb/Sr ratios of these samples (0.90, 0.96) are slightly higher than those of the other Precambrian samples (0.37–0.74) and caused an over-correction of the in-situ formed ^{87}Sr. The Sr evolution lines of the apparently undisturbed Neoproterozoic sediments define a narrow field that is intersected by the disturbed samples in a low angle (Fig. 6.4B). Intermediate $(La/Yb)_N$ ratios (6.0.9.3; norm: chondrite – Boynton 1984) of the Neoproterozoic siliciclastic sediments are in agreement with the Nd and Sr isotopic data, demonstrating mixing of a juvenile component derived from Neoproterozoic magmatic rocks and older continental crust (Fig. 6.3A).

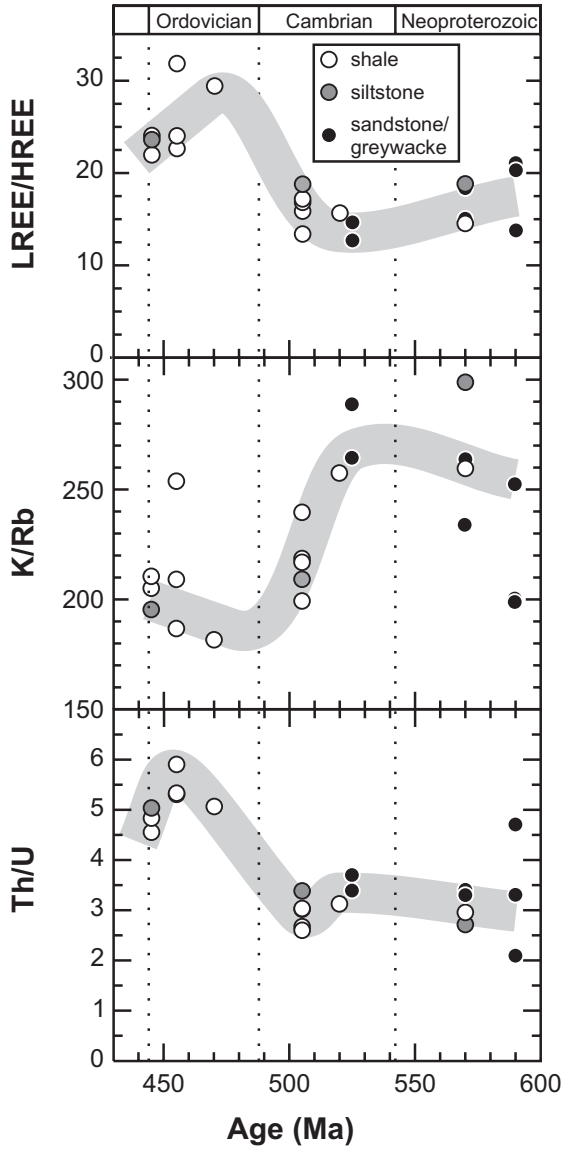

Fig. 6.2: Bivariate plots illustrating the variation of trace element signatures of the samples as a function of the stratigraphic age. Differences in the grain size (expressed by different colours of the data points) of the individual samples do not have a significant impact on the diversity of the geochemical features.

Abb. 6.2: Die Spurenelement-Signaturen der Proben variieren mit dem stratigraphischen Alter. Unterschiede in der Korngröße der einzelnen Proben haben keinen wesentlichen Einfluß auf die geochemischen Merkmale.

Cambrian siliciclastics have higher εNd_T values (-6.0 to +1.0) than Neoproterozoic ones, even attaining positive values in two Lower Cambrian samples (DB S1, DB D2), and younger T_{DM} (1.12–1.65 Ga; Fig. 6.5). $^{87}Sr/^{86}Sr_T$ ratios of five samples vary from 0.7037 to 0.7088; three analyzed shales (MM2, DB1/5, J4), however, have obviously disturbed Rb/Sr systematics as the anomalously low $^{87}Sr/^{86}Sr_T$ ratios of 0.6996 to 0.7023 indicate overcorrection of in situ ^{87}Sr-growth (Fig. 6.4B). REE characteristics, particularly of the Middle Cambrian sedimentary rocks, are similar to those of the analysed Neoproterozoic rocks (Fig. 6.3A, and chapter 5). Although major and trace element geochemical data suggest a derivation of the Cambrian siliciclastics predominantly from the Cadomian basement, the Nd (Fig. 6.3B) and Sr isotopic signatures demonstrate an additional contribution of young mantle-derived material to these rocks. Two Lower Cambrian fine-grained sandstones have the youngest T_{DM} (1.12–1.13 Ga; Fig. 6-5).

Ordovician pelites exhibit very homogenous εNd_T values of -9.6 to -8.3 and T_{DM} of 1.88-2.02 Ga (Fig. 6-3, Fig. 6-5). The latter overlap with the old crustal residence ages of Neoproterozoic sediments. The high T_{DM} and the high $^{87}Sr/^{86}Sr_T$ ratios, varying from 0.7083 to 0.7139 (Fig. 6-4), indicate a significant proportion of old continental crust in the source area. REE patterns resemble those of PAAS demonstrating a broad input of differentiated continental crust as well (cf. chapter 5).

Initial isotopic compositions of the uranogenic lead are similar for Neoproterozoic and Middle Cambrian siliciclastics. Sediment derivation from reservoirs of similar evolution may have been realized either by recycling of Neoproterozoic rocks during the Middle Cambrian or by a basically similar source area (Fig. 6-6A). Lower Cambrian and Ordovician rocks have markedly higher $^{207}Pb/^{204}Pb$ ratios that point to a source area with higher proportions of old continental crust.

Plotting $^{206}Pb/^{204}Pb_T$ vs. $^{208}Pb/^{204}Pb_T$ (Fig. 6.6B) reveals varying time-integrated Th/U ratios for samples derived from different reservoirs. Neoproterozoic and Middle Cambrian samples have similar initial Th/U ratios of ~3.0, which is in line with derivation from island arc rocks. Lower Cambrian

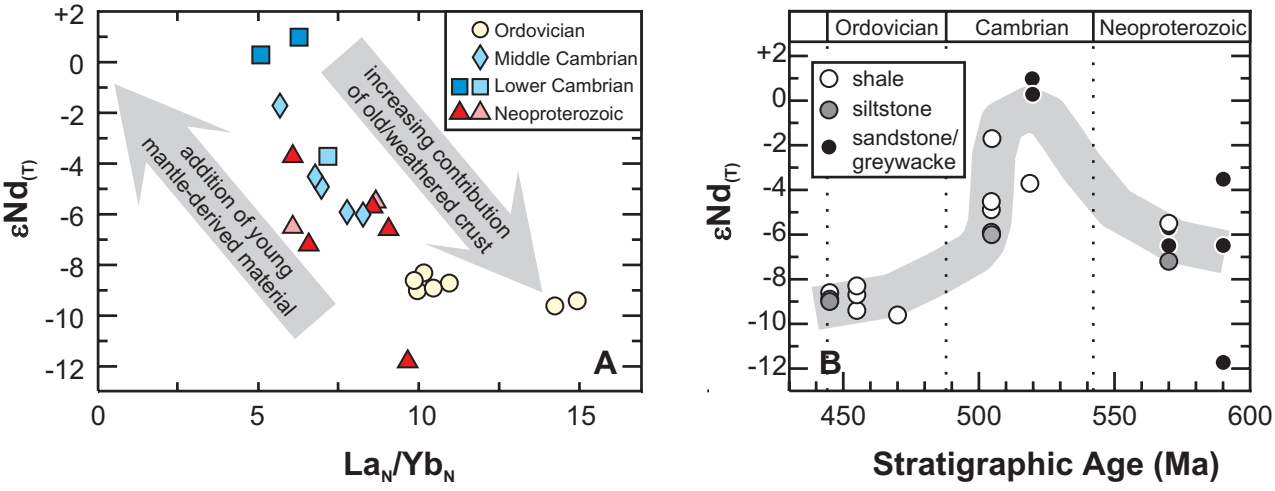

Fig. 6.3: **A**: εNd_T vs. $(La/Yb)_N$ diagram demonstrating low εNd_T values and enrichment of LREE in crustally derived rocks, which is in contrast to high εNd_T values and low LREE in material from depleted mantle-derived source rocks. Light symbols – shales/siltstones, dark symbols – greywackes/sandstones. **B**: εNd_T vs. Stratigraphic Age diagram showing elevated εNd_T in the Cambrian and a clear drop of εNd_T values in the Ordovician.

Abb. 6.3: **A**: Das εNd_T vs. $(La/Yb)_N$-Diagramm zeigt niedrige εNd_T-Werte und Anreicherung von leichten SEE für krustenderivierte Ausgangsgesteine und hohe εNd_T-Werte bei niedrigen Gehalten an leichten SEE für Ausgangsgesteine, die aus dem abgereicherten Mantel stammen. **B**: Das Stratigraphisches Alter vs. εNd_T-Diagramm zeigt erhöhte εNd_T-Werte im Kambrium und einen deutlichen Abfall der εNd_T-Werte im Ordovizium.

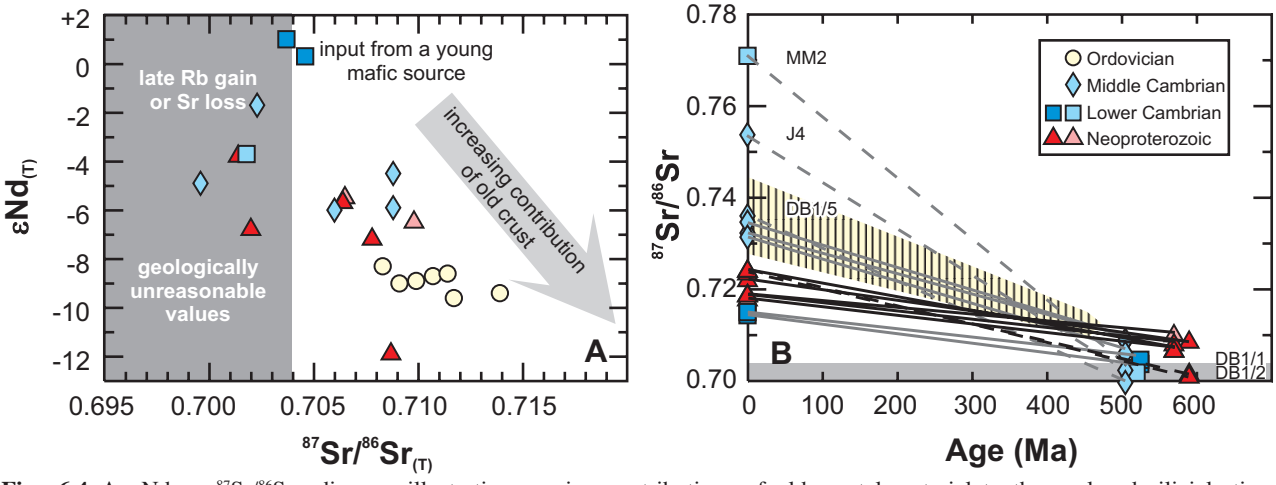

Fig. 6.4: **A**: εNd_T vs. $^{87}Sr/^{86}Sr_{(T)}$ diagram illustrating varying contributions of old crustal material to the analysed siliciclastics. Samples with disturbed Rb/Sr system have anomalously low $^{87}Sr/^{86}Sr_{(T)}$ ratios (shaded field). **B**: Sr evolution diagram reveals steeper slopes for sediments with disturbed Rb/Sr system (dashed lines). Hatched area represents the envelope of the Ordovician sediments. Light symbols – shales/siltstones, dark symbols – greywackes/sandstones.

Abb. 6.4: Das εNd_T vs. $^{87}Sr/^{86}Sr_{(T)}$-Diagramm stellt die unterschiedlichen Einträge von alter kontinentaler Kruste heraus. Proben mit gestörtem Rb/Sr-System haben unnormal niedrige $^{87}Sr/^{86}Sr_{(T)}$-Verhältnisse (graues Feld). **B**: Die Linien der Sr-Entwicklung der Proben mit gestörtem Rb/Sr-System (gestrichelte Linien) steigen steiler an, als die der ungestörten Proben gleichen stratigraphischen Alters.

siliciclastics had somewhat higher Th contents (Th/U ~ 3.4) that can be explained by additional involvement of old sedimentary rocks, as suggested by the isotopic composition of the uranogenic lead.

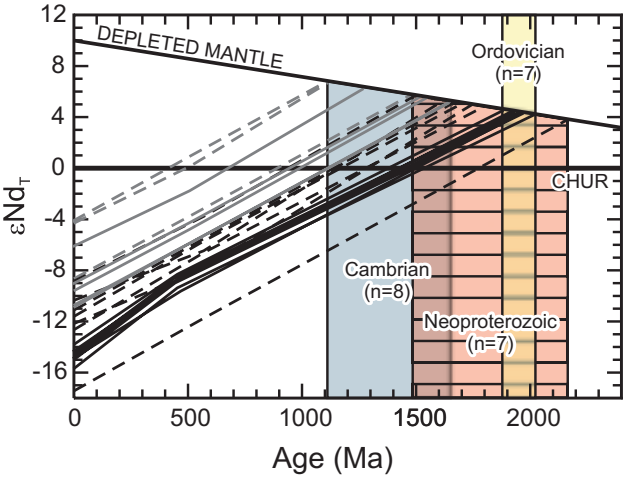

Fig. 6.5: Two-stage model ages (Liew & Hofmann 1988) of Neoproterozoic and Early Palaeozoic clastic sediments of the TBU. CHUR – chondritic uniform reservoir.

Abb. 6.5: Zwei-Phasen Modellalter (Liew & Hofmann 1988) der neoproterozoischen und frühpaläozoischen klastischen Sedimente des Teplá-Barrandiums. CHUR – chondritic uniform reservoir.

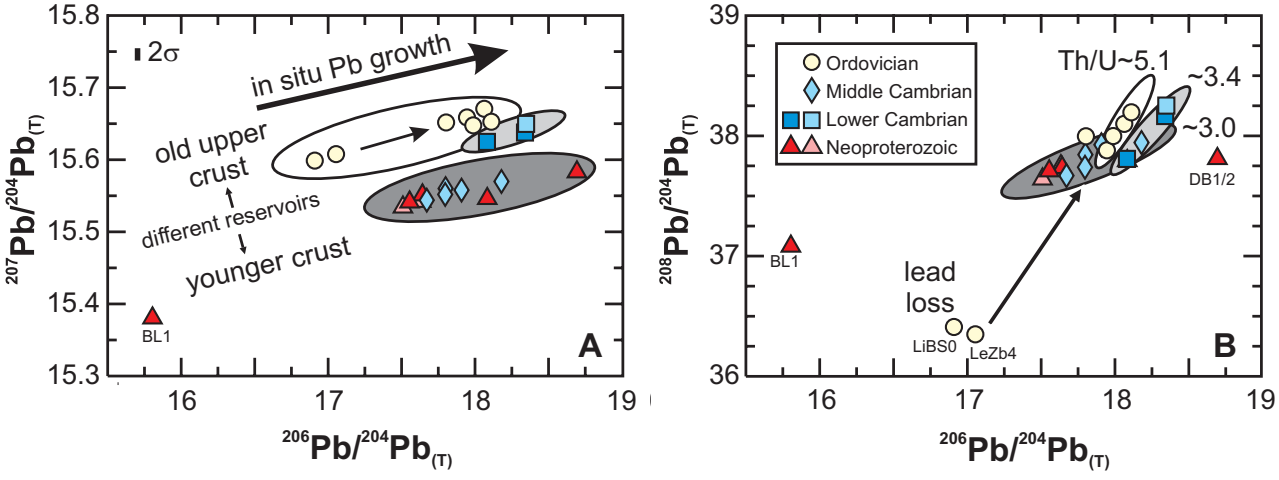

Fig. 6.6: **A**: $^{206}Pb/^{204}Pb_{(T)}$ vs. $^{207}Pb/^{204}Pb_{(T)}$ diagram detecting different reservoirs for the Neoproterozoic/Middle Cambrian and Lower Cambrian/Ordovician samples, respectively. **B**: $^{206}Pb/^{204}Pb_{(T)}$ vs. $^{208}Pb/^{204}Pb_{(T)}$ diagram indicating different reservoirs with varying time-integrated Th/U ratios. Light symbols – shales/siltstones, dark symbols – greywackes/sandstones. Note that samples LiBS0 and LeZb4 obviously experienced post-depositional lead-loss resulting in too low values when recalculated to the age of deposition.

Abb. 6.6: A: Aus dem $^{206}Pb/^{204}Pb_{(T)}$ vs. $^{207}Pb/^{204}Pb_{(T)}$-Diagramm ist ersichtlich, dass das Pb der neoproterozoischen und mittelkambrischen Siliziklastika aus einem anderen Reservoir stammt als das der unterkambrischen und ordovizischen Proben. **B**: Das $^{206}Pb/^{204}Pb_{(T)}$ vs. $^{208}Pb/^{204}Pb_{(T)}$ -Diagramm zeigt, dass verschiedene Reservoire mit unterschiedlichen alterskorrigierten Th/U-Verhältnissen geliefert haben. Helle Symbole – Silt-/Tonsteine, dunkle Symbole – Grauwacken/Sandsteine. Es ist zu beachten, dass die Proben LiBS0 und LeZb4 offenbar nach der Ablagerung Blei-Verlust erlitten haben, was zu zu niedrigen Verhältnissen führt, wenn man auf die Isotopenverhältnisse zum Zeitpunkt der Ablagerung zurückrechnet.

In contrast to Neoproterozoic and Cambrian samples, Ordovician pelites have distinctly higher initial Th/U ratios of ~5.1. This is in agreement with the generally elevated Th/U ratios in the Ordovician siliciclastics of the TBU (Fig. 6-2 and cf., chapter 5) and indicates recycling of clastic sedimentary rocks.

6.3 Variations of isotopic signatures

The isotopic compositions clearly vary among samples of different stratigraphic ages. However, regardless of the well-defined groups corresponding to

different provenances during individual stratigraphic periods, there is some variation within these groups that is attributed to initial isotopic heterogeneities and under- or over-correction for in situ growth.

The Rb-Sr system of Neoproterozoic samples DB1/1 and DB1/2, as well as of the Cambrian shales MM2, DB1/5 and J4 is disturbed. These samples yielded geologically unreasonably low $^{87}Sr/^{86}Sr_T$ ratios (<0.704) due to over-correction of in situ ^{87}Sr growth. The relatively high mobility of Rb and Sr during fluid-rock-interaction at low to medium temperature likely caused late Rb addition or Sr loss that in turn increased the Rb/Sr ratios and eventually resulted in anomalously low apparent $^{87}Sr/^{86}Sr_T$ ratios. Such a fractionation of Rb and Sr is reflected in the Sr evolution trends, which are steeper than in apparently undisturbed samples (Fig. 6.4B). For a simple two-stage Sr-evolution and the assumption that disturbed samples initially had similar Rb-Sr systematics as undisturbed samples of similar stratigraphic age, the intersections of the Sr evolution lines give a rough estimate for the time of disturbance. The intersection points of the Cambrian samples MM2 and J4 (both Příbram-Jince Basin) imply Rb gain or Sr loss between ~500 and ~400 Ma, which may be related to magmatic activity and associated crustal heating in this time interval. The remaining three samples showing disturbed Rb-Sr systematics were taken close to each other in the Skryje-Týřovice area. Their present-day $^{87}Sr/^{86}Sr$ ratios are almost similar to those of the undisturbed samples with similar stratigraphic age. Although intersecting the undisturbed samples in an acute angle the age of disturbance can be estimated to be younger than ~300 Ma, i.e., late- or post-Variscan.

Two Ordovician samples (LiBS0, LeZb4) form outliers in the $^{206}Pb/^{204}Pb_T$ – $^{207}Pb/^{204}Pb_T$ and $^{206}Pb/^{204}Pb_T$ – $^{208}Pb/^{204}Pb_T$ plots (Fig. 6.6). Their anomalous positions in the diagrams reflect over-correction of in situ Pb growth and thus indicate disturbance of the U-Th-Pb system by lead loss. They show, however, the same high $^{208}Pb/^{204}Pb_T$ ratios as the other Ordovician samples.

In contrast, the isotopic diversity of the Neoproterozoic samples cannot exclusively be attributed to alteration. The range in Pb and Nd isotopic compositions among Neoproterozoic rocks is chiefly due to the samples of the Blovice Formation (lower part of the Neoproterozoic succession – see Fig. 2.3), whereas samples from the Štěchovice Group (upper part of the Neoproterozoic succession) have more homogeneous isotopic signatures. Since the Blovice Formation was affected by a late Neoproterozoic metamorphic event (Pašava & Amov 1993), the mobility of U^{6+} during metamorphism may explain the disturbance of the U-Th-Pb system in the analysed deformed greywackes. Thus, the lead isotopic data of the samples from the Blovice Formation (BL01, DB1/2) do not necessarily reflect the provenance of these rocks but are probably the result of U redistribution during late Neoproterozoic metamorphism. However, the variations in the Nd isotope compositions of the Neoproterozoic samples indicate changing proportions of material derived from different sources. The larger the input from Neoproterozoic island arc rocks and the lower the contribution from old crustal sources, the more radiogenic is the Nd isotope signature.

Sample BL01 from the Blovice Formation differs from the younger Neoproterozoic rocks with respect to the U-Th-Pb and Sm-Nd systems. Although its $^{87}Sr/^{86}Sr_{590}$ ratio of 0.7082 is a reasonable value for detrital material from an old craton, it cannot be excluded that this sample also underwent Rb gain or Sr loss. The combined Nd-Sr isotopic data of sample BL01 indicate major input from old high-grade metamorphic crust (unradiogenic εNd_T at low $^{87}Sr/^{86}Sr_T$ ratio). This might be in agreement with lithological studies by Cháb & Pelc (1968), who identified small proportions of metamorphic rock fragments and heavy minerals within siliciclastic rocks of similar stratigraphic position. However, the heavy mineral spectrum and the petrography of sample BL01 rather suggest granitoid detritus. If the $^{87}Sr/^{86}Sr_{590}$ ratio of 0.7082 reflects over-correction of in situ Sr growth, the geochemical and Nd isotope data as well as the petrographic features may be explained by major input from Palaeoproterozoic granitoid rocks such as the Icartian basement in the Armorican Massif.

GEOLOGICA SAXONICA
Journal of Central European Geology 54 (2008) 1–168

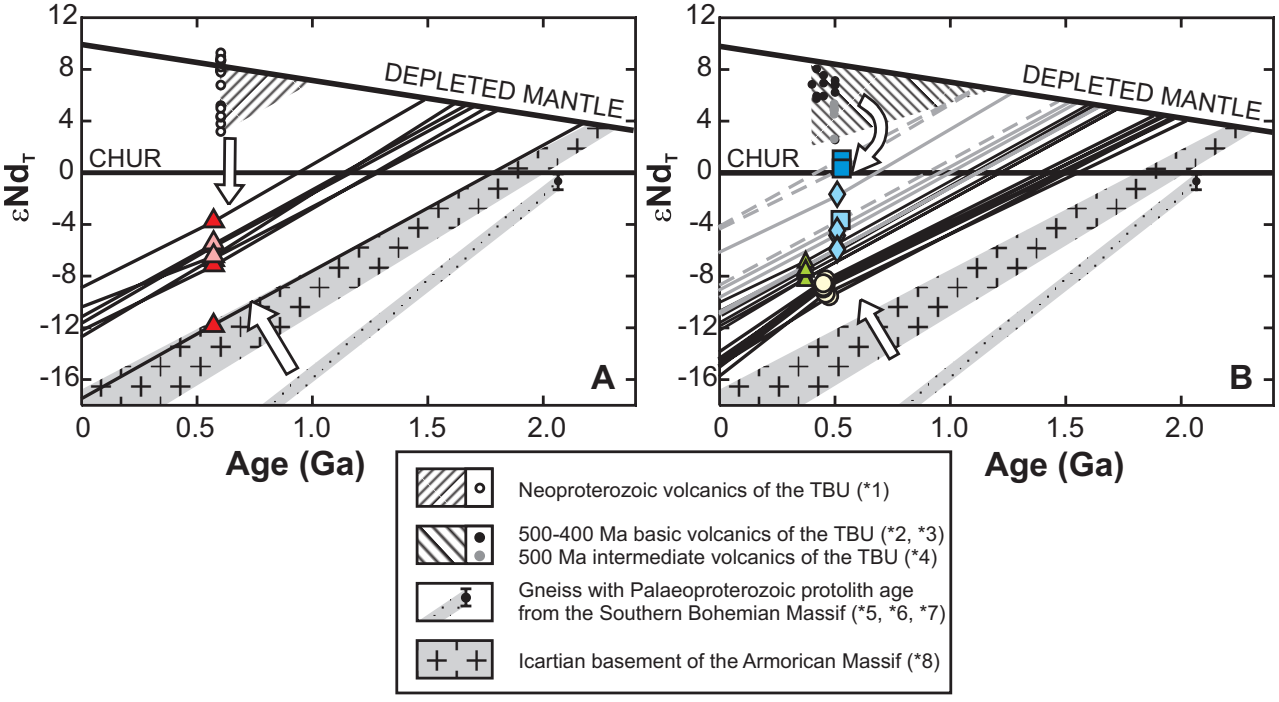

Fig. 6.7: εNd evolution diagram comparing the analysed samples and potential source rocks. **A**: Triangles represent εNd_{570} values for Neoproterozoic siliciclastic sedimentary rocks of the TBU. **B**: Large symbols represent εNd_T values of Cambrian, Ordovician and Devonian sedimentary rocks of the TBU (triangles = εNd_{380} values of Devonian greywackes; from Strnad & Mihaljevič 2005). Depleted mantle curve from Liew & Hofmann (1988). CHUR – chondritic uniform reservoir. Data sources: *1 – Pin & Waldhausrová (2007); *2 – Vokurka and Frýda (1997); *3 – Pin et al. (unpublished data); *4 – Pin et al. (2007); *5 – Liew & Hofmann (1988); *6 – Kröner et al. (1988); 7 – Wendt et al. (1993); *8 – Samson & D'Lemos (1998).

Abb. 6.7: εNd-Entwicklung der Proben im Vergleich zu potentiellen Liefergesteinen. **A**: Die Dreiecke zeigen die εNd_{570}-Werte der neoproterozoischen Proben aus dem Teplá-Barrandium. **B**: Große Symbole stehen für kambrische, ordovizische und devonische Sedimentgesteine des Teplá-Barrandiums (Dreiecke = εNd_{380}-Werte von devonischen Grauwacken; aus Strnad & Mihaljevič, 2005). Kurve für den abgereicherten Erdmantel nach Liew & Hofmann (1988). CHUR – chondritic uniform reservoir. Datenquellen: *1 – Pin & Waldhausrová (2007); *2 – Vokurka and Frýda (1997); *3 – Pin et al. (unveröffentlichte Daten); *4 – Pin et al. (2007); *5 – Liew & Hofmann (1988); *6 – Kröner et al. (1988); 7 – Wendt et al. (1993); *8 – Samson & D'Lemos (1998).

6.4 Crustal residence ages

The crustal residence age (T_{DM}) of a rock gives the time when its constituents were separated from the mantle (e.g., DePaolo 1988). In detrital sediments the T_{DM} reflects the average crustal residence time of all contributing sources, i.e., the mixing of material that was derived from the depleted mantle at different times (e.g., Arndt and Goldstein 1987). In this study, two-stage model ages were calculated using the formula of Liew & Hofmann (1988) and compared to the Nd isotope evolution of potential sources (Fig. 6.7).

The calculation of two-stage model ages is useful for estimation of the crustal residence ages of siliciclastics, because different reservoirs such as island arc terranes and old continental crust have contrasting Nd isotope signatures and distinct Sm/Nd ratios. Therefore, the $^{147}Sm/^{144}Nd$ ratio of the sample, which represents a weighted mixture of all sources, is only used for the Nd evolution of the sediment from the time of deposition until present. The pre-sedimentation history is instead estimated with a typical crustal $^{147}Sm/^{144}Nd$ value of 0.12. This correction may result in a kink in the Nd evolution lines (Fig. 6.5, Fig. 6.7) but does not have a large

impact on the Neoproterozoic and Cambrian samples. However, the crustal residence ages of the Ordovician samples having more enriched LREE and accordingly low Sm/Nd between 0.15 and 0.18 ($^{147}Sm/^{144}Nd$ from 0.088 to 0.107) are significantly underestimated when inferred from single stage model ages. Furthermore, one Neoproterozoic sample (NPZb5) with a relatively high Sm/Nd of 0.24 ($^{147}Sm/^{144}Nd$=0.142) yields an unreasonably old single stage model age. These differences in the Sm/Nd ratio result in different slopes of the $^{143}Nd/^{144}Nd$ growth line and do not correspond to the age but to the nature of the source rocks. In the case of the Ordovician samples the LREE-enrichment and associated low Sm/Nd is attributed to intense source rock weathering, monazite enrichment and/or felsic source rocks (cf. chapters 5.1 and 5.3), whereas the high Sm/Nd of the Neoproterozoic sample NPZb5 is caused by a larger content of magmatic detritus and related apatite enrichment (cf., Fig. 5.6B).

Teplá-Barrandian Neoproterozoic to Ordovician siliciclastic rocks gave T_{DM} of 1.12 to 2.17 Ga, whereas 17 of the 22 samples yield crustal residence ages > 1.5 Ga. Fig. 6.7 showing the Nd isotope evolution of Neoproterozoic – Early Palaeozoic siliciclastic sedimentary rocks of the TBU in comparison to potential source rocks illustrates that old crustal sources played an important role for the majority of the analysed rocks. Data for Devonian greywackes (Strnad & Mihaljevič 2005) were added for the sake of completeness.

Palaeoproterozoic basement rocks are known to be present in the northern Armorican Massif (Auvray et al. 1980, Samson & D'Lemos 1998, Inglis et al. 2004) and the Moldanubian domain in the southern Bohemian Massif (Wendt et al. 1993, Friedl et al. 2004). Such old crustal complexes and the Cadomian island arc contributed to the Neoproterozoic siliciclastic rocks of the TBU (Fig. 6.7A). The Nd isotopic signature of sample BL01 is similar to that of the Icartian basement of the Armorican Massif. The other 6 Neoproterozoic samples contain more prominent proportions of juvenile arc-derived material. Nevertheless, their T_{DM} (≥ 1.5 Ga), which are markedly in excess of the stratigraphic age, emphasize the involvement of old crustal sources.

The Cambrian samples have younger T_{DM} (1.12 to 1.65 Ga) than the Neoproterozoic sediments, which is compatible with major input from synsedimentary mantle-derived volcanism related to incipient rifting (Fig. 6.7B). Although Ordovician to Devonian strata of the TBU also contain volcanic rocks with quite radiogenic Nd isotopic signatures (Vokurka & Frýda 1997; Fig. 6.7B), the sedimentary record of this period seems to be less influenced by the volcanic source. Ordovician detrital sediments have T_{DM} of 1.88 to 2.02 Ga, which are distinctly older than those of the Cambrian sedimentary rocks (Fig. 6.7B) and reflect major contributions from old crustal sources. Devonian greywackes studied by Strnad & Mihaljevič (2005) have T_{DM} of 1.58 to 1.75 Ga (recalculated to the two-stage model of Liew & Hofmann 1988) that overlap those of the Neoproterozoic greywackes.

6.5 Provenance

Isotope data of the analysed rocks clearly form individual groups of samples. These groups match the stratigraphic ages of the analysed siliciclastics (Fig. 6-8) and reflect changing sources over time, which in turn indicates differences in the geotectonic regime.

The deposition of the Neoproterozoic siliciclastic rocks in an active geotectonic setting as indicated by the element geochemistry (chapter 5) is substantiated by the isotope data. Although detritus derived from a magmatic arc dominates the chemical and petrographic compositions of the Late Neoproterozoic sediments (cf. Jakeš et al. 1979, Lang 2000), Nd and Sr isotopic signatures reveal mixing of juvenile material with detritus from an old crustal source (Fig. 6-4A, Fig. 6.7A). Particularly, the fact that the T_{DM} (1.49–2.17 Ga) are far in excess of the Late Neoproterozoic stratigraphic age points to involvement of differing proportions of old continental crust. This is supported by findings of Proterozoic and Archean detrital and inherited zircon in greywackes (see chapter 7) and granitoid pebbles from conglomerates of the Neoproterozoic succession (Dörr et al.

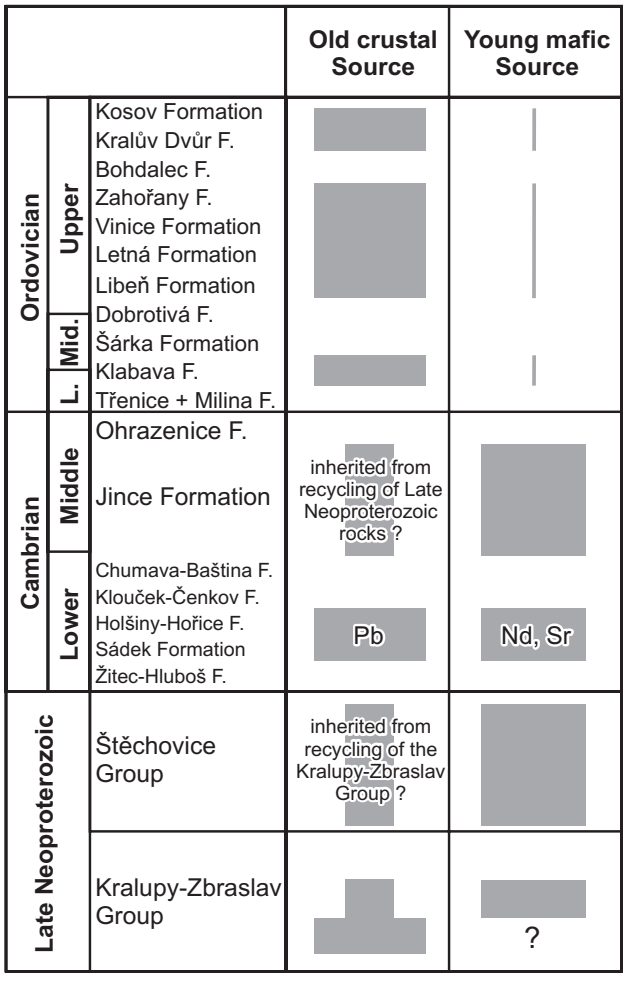

Fig. 6.8: Summary of the results obtained from whole rock Nd-Sr-Pb isotope data.

Abb. 6.8: Zusammenfassung der Ergebnisse der Nd-Sr-Pb-Analysen an Gesamtgesteinen.

2002, Sláma et al. 2003, Drost et al. 2004). Such a mixed signature is not in agreement with derivation of the detrital sediments from an oceanic island arc but requires continental crust in the source area. Such a mixed source may have been represented either by a magmatic arc that developed on continental crust or, more likely, by the Pan-African belt that involves island arc complexes and old crustal units.

Lower Cambrian, chiefly continental sediments have more radiogenic εNd_T values (-3.7 to +1.0) and younger T_{DM} (1.12–1.47 Ga) than the Neoproterozoic rocks. Likewise initial $^{87}Sr/^{86}Sr$ ratios (~0.704) mirror significant input of detritus from young mantle-derived magmatic rocks. In contrast, the uranogenic lead shows that old continental crust contributed significantly to these sedimentary rocks. The latter implies that the Lower Cambrian physiography allowed craton-derived detritus to enter the Příbram-Jince Basin (cf. chapter 7). The divergent indication of the predominant sediment source obtained from Sr and Pb isotopes is not in contradiction but it reflects the different contents of Sr and Pb in mantle-derived volcanic rocks and continental crust, respectively. Mantle-derived rocks have higher Sr concentrations and relatively low Pb contents. The continental crust, however, is lower in Sr and relatively high in Pb. In sediments containing contributions from both reservoirs, the Sr isotopic composition is dominated by the mantle-derived rocks, whereas the Pb isotopic signature is controlled by the crustal source. The marine Middle Cambrian sedimentary sequence has isotopic signatures that largely correspond to those of the analysed Neoproterozoic rocks. However, the younger T_{DM} (1.27–1.65 Ga) reveal contributions from post-Neoproterozoic magmatic rocks as a new component (Fig. 6-7B). Indications for a provenance from old crust have not been detected in the Middle Cambrian siliciclastic rocks. Isotopic features of the Cambrian sediments are in agreement with a rift-related setting.

The analysed Ordovician pelites form a very homogeneous group with respect to their isotopic compositions. εNd_T values of -9.6 to -8.3, T_{DM} of 1.88 to 2.02 Ga as well as Sr and Pb isotope data of Ordovician pelites point to an increased input of material delivered from the Gondwana hinterland (see also chapter 7). The uniform isotopic signatures of the Ordovician samples point to derivation of the sediments from a large area of stable continental crust that was mixed efficiently to average out isotopic heterogeneities of the source area.

7 U-Pb zircon ages

7.1 Intension

The Palaeozoic sequences of the Barrandian basins are well studied, in particular concerning palaeontology and palaeoecology. However, reliable geochronological data are rare. Therefore, 9 greywacke/sandstone samples for dating of detrital zircon were taken to get information on:

(**1**) Maximum sedimentation ages
- Neoproterozoic sediments are only roughly dated by microfossils. Detrital zircon from the Blovice Formation (regarded as the oldest rocks of the TBU) and from the Štěchovice Group (the youngest of the Neoproterozoic-rocks) was analysed to get an idea of the age interval preserved in the Neoproterozoic sequences of the TBU.
- The up to 2500 m Lower Cambrian continental successions are palaeontologically undatable therefore it is questionable when the Palaeozoic sedimentation started after the Cadomian deformation.

(**2**) Age spectra of the source area(s), i.e. provenance
- Which craton/unit supplies the detritus of the Neoproterozoic and Palaeozoic siliciclastic sediments of the TBU?
- Is there a traceable change of the source area between Neoproterozoic and Middle Devonian?

(**3**) Palaeozoic magmatic activity in the source area(s)
- Is there a prominent input derived from Palaeozoic magmatic activity?
- If so, are there local candidates for the derivation of the detritus or is it originated from igneous events unknown in the TBU?

Furthermore the age of the andesite-rhyolite volcanism regarded as Upper Cambrian was determined by U-Pb dating of magmatic zircon crystals from a rhyolite sample.

7.2 Samples and Methods

Samples were collected from Neoproterozoic, and Early Palaeozoic strata of the TBU. Additionally detrital zircon ages from a Middle Devonian greywacke representing the youngest pre-Variscan siliciclastics of the TBU were determined for comparison. Sampling localities are shown in Fig. 7-1. Rock types, lithostratigraphic units, method of dating, and the reference to the respective data set in the appendix are given in Tab. 7-1. Zircon from a rhyolite sample (OKR) from the Křivoklát-Rokycany volcanic complex and 17 detrital zircon grains from a Neoproterozoic greywacke (sample Dob) were dated by SHRIMP II in Perth. Additional grains of sample Dob were dated by laser LA-ICP-MS at the Institute of Mineralogy at the Johann-Wolfgang-Goethe University in Frankfurt. A further Neoproterozoic sample (BL) as well as one Cambrian (Oh3), one Ordovician (Tocnik) and one Devonian (Roblin) sandstone, respectively, were analysed with regard to their detrital zircon ages at Frankfurt University. Two Cambrian (PJ1/3, CB3) and four Ordovician sandstones (TrTo3, LiBS2, LeZb6, KoLeD1d) were analysed by LA-ICP-MS at the Natural History Museum in London. Analytical procedures for U-Pb dating of zircon by SHRIMP and LA-ICP-MS are described in the appendix.

Both LA-ICP-MS and SHRIMP apply in-situ measurement of the U, Th, and Pb isotopes, which permits analysing differently old domains within the same grain. CL-imaging of the zircon grains prior to analyses reveals such different domains and allows age determination of a specific part of the zircon. In the case that the different formation stages of the same grain are not visible in the CL-image, the time-resolved signals of the respective measurements will detect this change in the isotopic ratios. This is essential for provenance studies, because mixed ages of detrital zircon are difficult to interpret and may be misleading.

Ten sandstone/greywacke samples from 9 localities were analysed with regard to their age spectra preserved in detrital zircon. U, Th, and Pb isotopic

GEOLOGICA SAXONICA
Journal of Central European Geology 54 (2008) 1–168

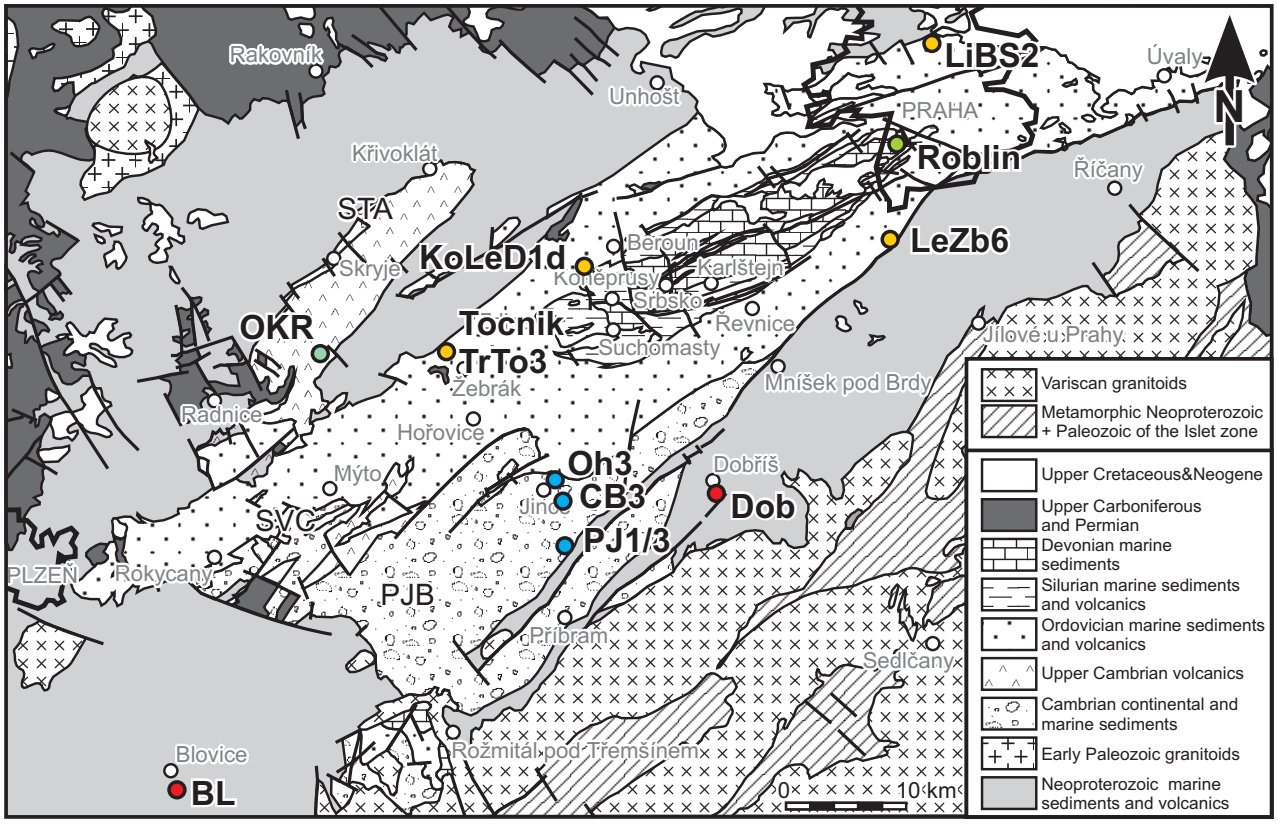

Fig. 7.1: Sketch map of sampling localities for U-Pb analyses of zircon.

Abb. 7.1: Schematische Karte mit Probenahmepunkten für U-Pb-Analysen an detritischen Zirkonen.

data of 48 to 112 analyses per sample were achieved. Time resolved signals of the LA-ICP-MS data were checked with respect to suspect features caused by inclusions, cracks or chemical zonation in subsurface parts of the polished zircon grains. Parts of analyses that show such disturbance were excluded from the age calculations. Those analyses in which all the signal is affected were rejected. Furthermore all analyses with >20% discordance between $^{206}Pb/^{238}U$ age and $^{207}Pb/^{206}Pb$ age were rejected[1].

Concordance/discordance were calculated by the equations:

concordance

$= (\ ^{206}Pb/^{238}U \text{ age} / ^{207}Pb/^{206}Pb \text{ age}) \times 100$

discordance

$= 100 - ([\ ^{206}Pb/^{238}U \text{ age} / ^{207}Pb/^{206}Pb \text{ age}] \times 100)$

Discordance may originate from Pb loss, addition of common Pb or ablation of differently old domains within the zircon. Reverse discordance can occur due to inter-element fractionation by heating of the zircon during the ablation process. Low count rates for ^{207}Pb may be a reason for both normal and reverse discordance. Features causing discordance in such a

[1] All labs using LA-ICP-MS techniques differ from each other in analytical instrumentation and have specific data processing routines. The LA-ICP-MS equipment at Frankfurt University allows a higher spatial resolution than that at NHM London and often also correction for common Pb. Therefore the rejection rate for analyses performed at Frankfurt University is somewhat lower. Nevertheless, the results obtained from the two different labs are similar. For details concerning analytical instrumentation and data processing see appendix.

Table 7.1: Rock types, lithostratigraphic units, method of dating, and reference to the respective data set in the Appendix. **F** – measured at the Institute of Mineralogy of the Johann-Wolfgang Goethe University Frankfurt, **L** – measured at the Natural History Museum in London (NHM).

Tab. 7.1: Gesteinstypen, lithostratigraphische Einheiten, Datierungsmethode und Referenz zum jeweiligen Datensatz im Anhang. **F** – am Institut für Mineralogie der Johann-Wolfgang Goethe-Universität Frankfurt gemessen, **L** – am Naturhistorischen Museum London (NHM) gemessen

Sample	Rock type	Lithostratigraphic unit	Method - nominal spot diameter [μm]	Data listed in: (Appendix)
Detrital zircon from sedimentary rocks				
Neoproterozoic				
BL	greywacke	Kralupy-Zbraslav Group	LA-ICP-MS (F) - 30	Table A12
Dob	fine-grained greywacke	Štěchovice Group	LA-ICP-MS (F) - 30 SHRIMP II - 15 to 20	Table A12 Table A10
Cambrian				
PJ1/3	sandstone/ conglomerate	Žitec-Hluboš-Fm. (Lower Cambrian)	LA-ICP-MS (L) - (18) 30/45 (60)	Table A11
CB3	sandstone	Chumava-Baština-Fm. (?Lower/ Middle Cambrian)	LA-ICP-MS (L) - (18) 30/45	Table A11
Oh3	sandstone	Ohrazenice-Fm. (?Middle/Upper Cambrian)	LA-ICP-MS (F) - 30	Table A12
Ordovician				
Tr To3 Tocnik	conglomerate/ sandstone	Třenice Fm. (Lower Ordovician)	LA-ICP-MS (L) - 30/45 LA-ICP-MS (F) - 30	Table A11 Table A12
LiBS2	sandstone	Libeň Fm. (Upper Ordovician)	LA-ICP-MS (L) - 18/30/45	Table A11
LeZb6	sandstone	Letná Fm. (Upper Ordovician)	LA-ICP-MS (L) - 18/30	Table A11
Ko Le D1d	diamictite	Kosov Fm. (Upper Ordovician)	LA-ICP-MS (L) - (18) 30/45	Table A11
Devonian				
Roblin	greywacke (carbonaceous)	Srbsko Fm. (Middle Devonian)	LA-ICP-MS (F) - 30	Table A12
Magmatic zircon from a rhyolite sample				
OKR	volcanic, felsic	Křivoklát-Rokycany volcanic complex (?Upper Cambrian)	SHRIMP II - 15 to 20	Table A10

rate that the analyses had to be rejected are discussed exemplarily for sample LeZb6.

For analyses yielding ages younger than 1 Ga, the $^{206}Pb/^{238}U$ age is referred to in the text and used for construction of the frequency-distribution plots (Fig. 7.14, Fig. 7.16), for ages ≥1 Ga the $^{207}Pb/^{206}Pb$ age is used. The errors reported in the text are 2σ. Concordia ages were calculated after Ludwig (1998).

7.3 Results

7.3.1 ?Upper Cambrian volcanic complex

Zircon crystals from the youngest effusive stage of the KRVC (sample OKR) are colourless to very light yellow, transparent and euhedral. They are medium-

GEOLOGICA SAXONICA
Journal of Central European Geology 54 (2008) 1–168

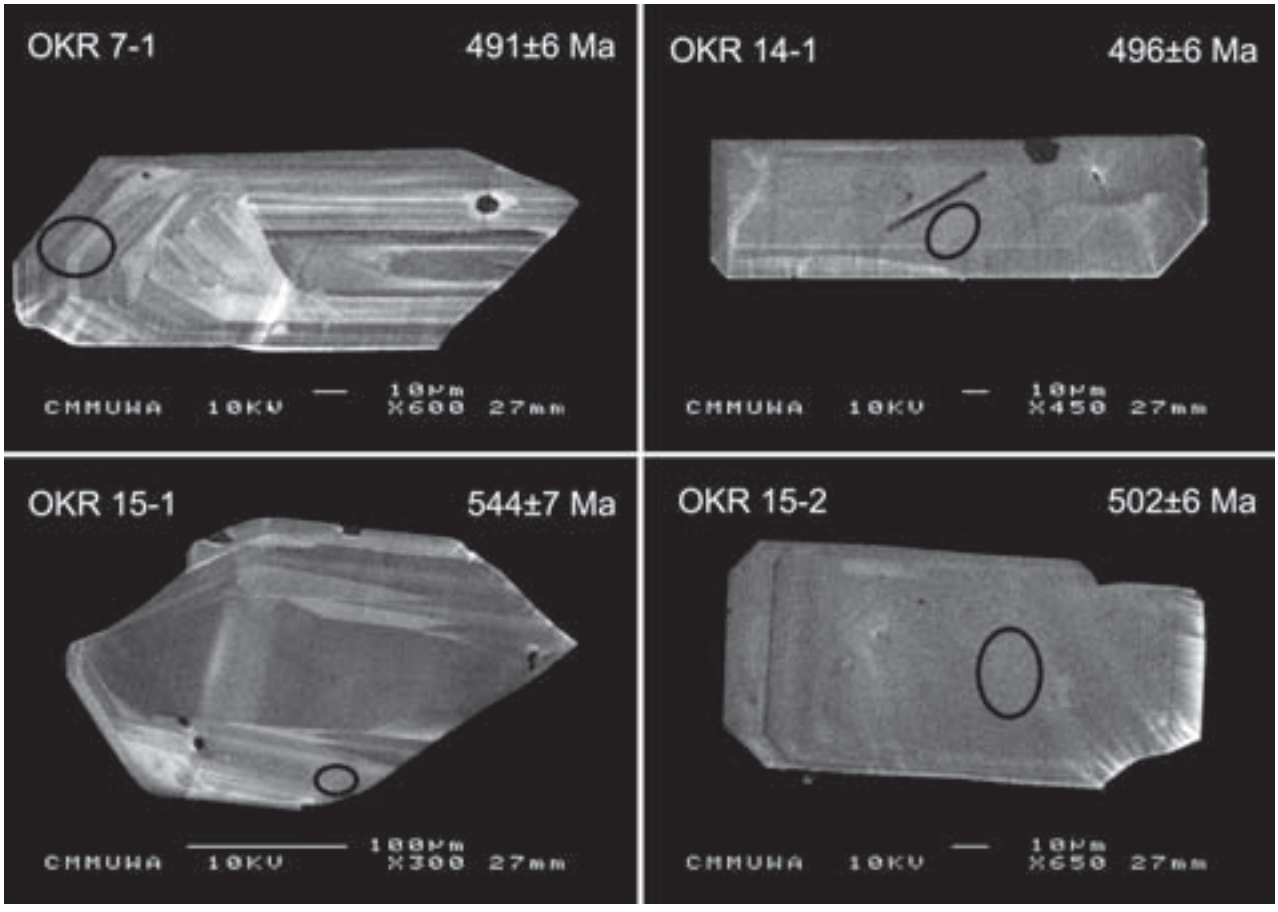

Fig. 7.2: CL images of zircon crystals from rhyolite sample OKR. Placing of the individual SHRIMP spots is indicated by black ellipses.

Abb. 7.2: Kathodoluminiszenz-Aufnahmen der Zirkonkristalle aus Rhyolithprobe OKR. Die schwarzen Ellipsen zeigen die Platzierung des SHRIMP-Spots.

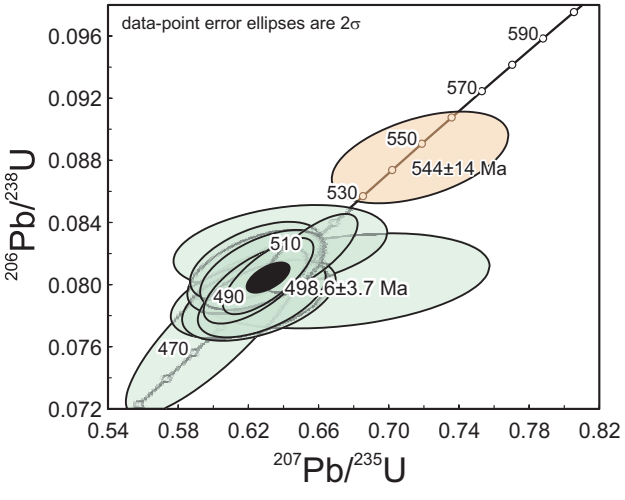

Fig. 7.3: Concordia diagram for zircon from rhyolite sample OKR. Green error ellipses indicate individual analyses, black one denotes their concordia age. Orange error ellipse represents the concordia age (544±14 Ma, 2σ, MSWD of concordance 0.23) of an inherited zircon.

Abb. 7.3: Corncordia-Diagramm für die Analysen an Probe OKR. Die grünen Fehlerellipsen stehen für Einzelanalysen, die schwarze Ellipse zeigt das Konkordia-Alter, welches aus den 12 Einzelanalysen berechnet wurde. Die orange Fehlerellipse repräsentiert das Konkordia-Alter (544±14 Ma, 2σ, MSWD = 0.23) eines ererbten Zirkons.

to long-prismatic, characterized by the {100}-prism and the {101}-pyramid only and show oscillatory, euhedral concentric zoning or a more or less homogenous structure, under CL (Fig. 7.2). Their position in the classification scheme after Pupin (1980; D, P5) corresponds to alkaline magmatism. Uranium, Th, and lead isotopes of these grains were analysed by SHRIMP. The concordia age calculated from 12 zircon grains is 499±4 Ma (2σ; Fig. 7.3, see Table A6 for results of the individual analyses), which confirms the suggestion of an Upper Cambrian age of the volcanism. Only one of the separated zircon crystals is very light yellow, transparent and shows a longitudinal zoning and a very narrow rim under CL (Fig. 7.2).This grain yielded a concordant inherited age of 544±14 Ma (2σ, concordia age).

7.3.2 Detrital zircon from sedimentary rocks

Sample BL

Sample BL from the Neoproterozoic Blovice Formation represents the oldest of the analysed rocks. Its zircon age spectrum spans ages between 579±13 Ma and 3501±16 Ma (Fig. 7.4, Table A8). Neoproterozoic detritus makes up ~62% of the zircon population. 39 of the 43 grains have $^{206}Pb/^{238}U$ ages between 579±13 Ma and 677±13 Ma, another 3 grains are around 800 Ma old, and one zircon has an age of ~1 Ga. Palaeoproterozoic zircon with $^{207}Pb/^{206}Pb$ ages between 1754±53 and 2145±22 Ma is frequent (26%) and shows a maximum at around 1.9 Ga. One grain has an age of 2485±18 Ma. Of the 8 Archean ages (~12%) 4 are between 2569±14 and 2675±32 Ma, 2 are around 2850 Ma and 1 is concordant at 3215±18 Ma. The oldest zircon of sample BL is about 20% discordant and has a $^{207}Pb/^{206}Pb$ minimum age of 3501±16 Ma.

An estimate for the depositional age of the greywacke is given by the concordia age calculated from the 9 youngest grains (579±13–602±14 Ma) with ≤10% discordance, which indicates that sedimentation took place at or is younger than 592±4 Ma (Fig. 7.4C).

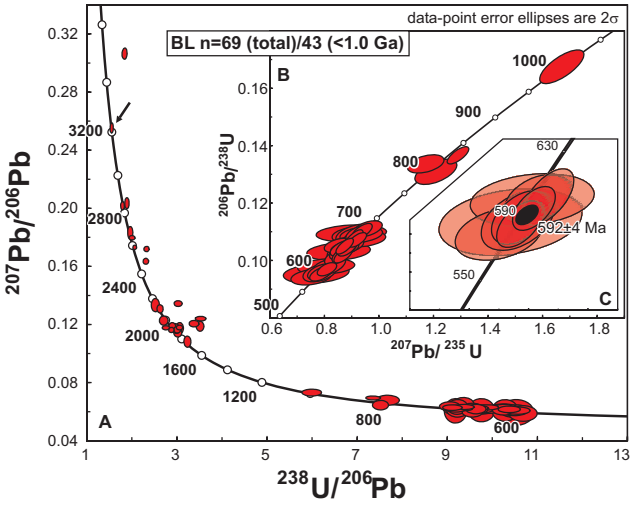

Fig. 7.4: Concordia diagrams for sample BL. **A**: All analyses ≤20% discordant in Tera-Wasserburg plot. **B**: Neoproterozoic ages in concordia plot. **C**: Concordia age (±2σ error, MSWD/probability of concordance and equivalence = 1.08/0.37) calculated from the 9 youngest ages is assumed to represent the maximum sedimentation age of the greywacke.

Abb. 7.4: Konkordia-Diagramme für Probe BL. **A**: Alle Analysen, die ≤20% diskordant sind, in Tera-Wasserburg-Diagramm. **B**: Neoproterozoische Alter in Konkordia-Diagramm. **C**: Das Konkordia-Alter (±2σ Fehler, MSWD/Wahrscheinlichkeit von Konkordanz und Äquivalenz = 1.08/0.37), welches aus den 9 jüngsten Altern berechnet wurde, gibt einen Hinweis auf das maximale Sedimentationsalter der Grauwacke.

Sample Dob

Of the 56 U-Pb analyses reported for sample Dob, 15 (+ 2 analyses that are >20% discordant) were performed by SHRIMP II in Perth and 41 by LA-ICP-MS at Frankfurt University. Since both methods yielded comparable results, the ages obtained for sample Dob are treated together. The acquired ages range between 548±12 and 2633±51 Ma (Fig. 7.5, Tables A6 and A8). Most frequent is Neoproterozoic zircon between 548±12 and 646±16 Ma (~71%). Another 3 grains have ages of 675±24 to 732±15 Ma. One 12%-reverse-discordant SHRIMP analysis gave a $^{206}Pb/^{238}U$ age of 867±26 Ma (corresponding $^{207}Pb/^{206}Pb$ age = 774±80 Ma). Palaeoproterozoic detritus between 1904±79 and 2183±39 Ma was detected in 11 cases (~20%). A maximum occurs at around 2020 Ma. The oldest grain found in sample Dob has an Archean age of 2633±51 Ma.

GEOLOGICA SAXONICA
Journal of Central European Geology 54 (2008) 1–168

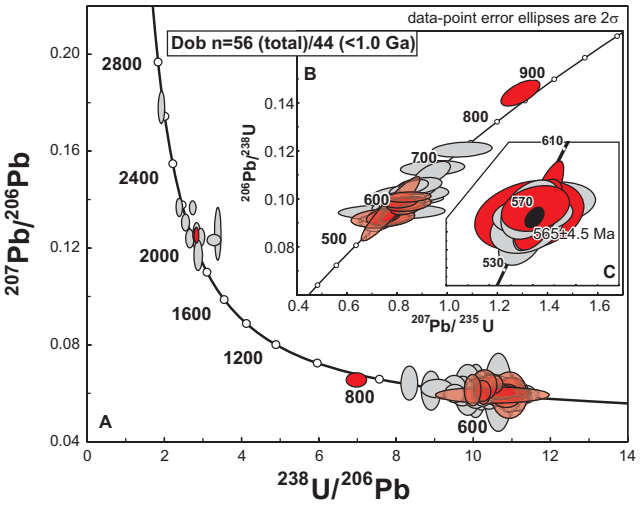

Fig. 7.5: Concordia diagrams for sample Dob. **A**: All analyses ≤20% discordant in Tera-Wasserburg plot. **B**: Neoproterozoic ages in concordia plot. C: Concordia age (±2σ error, MSWD/probability of concordance and equivalence = 0.91/0.57) calculated from the 10 youngest ages with ≤10% discordance represents the maximum sedimentation age of the greywacke. Red ellipses stand for SHRIMP analyses, grey ones for LA-ICP-MS data.

Abb. 7.5: Konkordia-Diagramme für Probe Dob. **A**: Alle Analysen, die ≤20% diskordant sind, in Tera-Wasserburg-Diagramm. **B**: Neoproterozoische Alter in Konkordia-Diagramm. **C**: Das Konkordia-Alter (±2σ Fehler, MSWD/Wahrscheinlichkeit von Konkordanz und Äquivalenz = 0.91/0.57), welches aus den 10 jüngsten Altern mit ≤10% Diskordanz berechnet wurde, gibt einen Hinweis auf das maximale Sedimentationsalter der Grauwacke. Rote Ellipsen – SHRIMP-Analysen, graue Ellipsen – LA-ICP-MS-Daten.

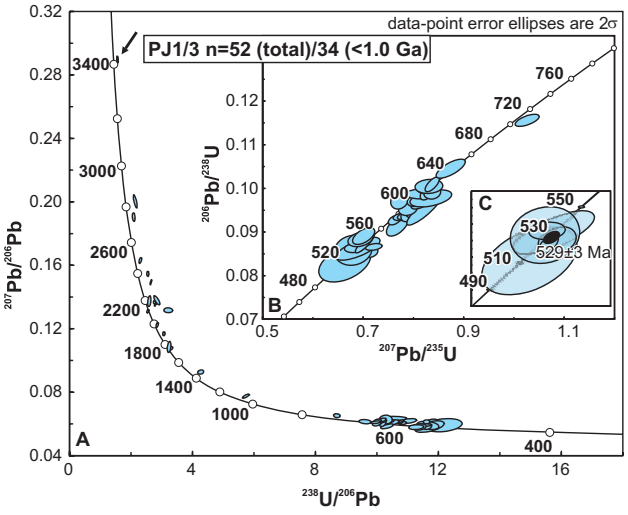

Fig. 7.6: Concordia diagrams for sample PJ1/3. **A**: All analyses ≤20% discordant in Tera-Wasserburg plot. **B**: Neoproterozoic and Early Cambrian ages in concordia plot. **C**: Concordia age (±2σ error, MSWD/probability of concordance and equivalence = 1.2/0.26) calculated from the 6 youngest ages with ≤8% discordance representing the maximum sedimentation age of the sandstone.

Abb. 7.6: Konkordia-Diagramme für Probe PJ1/3. **A**: Alle Analysen, die ≤20% diskordant sind, in Tera-Wasserburg-Diagramm. **B**: Neoproterozoische und unterkambrische Alter in Konkordia-Diagramm. **C**: Das Konkordia Alter (±2σ Fehler, MSWD/Wahrscheinlichkeit von Konkordanz und Äquivalenz = 1.2/0.26), welches aus den 6 jüngsten Altern mit ≤8% Diskordanz berechnet wurde, gibt einen Hinweis auf das maximale Sedimentationsalter des Sandsteines.

The maximum sedimentation age is around 565±4.5 Ma as indicated by the concordia age calculated from the 10 youngest near concordant analyses (Fig. 7.5C). This is in agreement with the lower intercept age of 568±3 Ma (U-Pb, zircon, ID-TIMS) obtained by Dörr et al. (2002) from a rhyolite pebble from the Štěchovice Group.

Sample PJ1/3

Zircon grains from a conglomeratic sandstone close to the base of the Palaeozoic deposits were analysed by LA-ICP-MS at NHM London. After rejection of insufficient analyses 52 ages between 504±6 and 3412±10 Ma remained. Neoproterozoic and Cambrian detrital zircon makes up ~65% of the population. Of those 34 grains, 31 have $^{206}Pb/^{238}U$ ages from 511±20 to 619±8 Ma with a small gap (Fig. 7.6B) between ~550 and ~570 Ma. Older Neoproterozoic detritus is represented by 2 grains with ages of 640±10 Ma and 705±7 Ma. One Cambrian $^{206}Pb/^{238}U$ age of 504±6 Ma is only 82% concordant and is most probably attributed to some lead loss.

Two grains of sample PJ1/3 yielded Mesoproterozoic ages (1108±28 Ma and 1466±22 Ma). Palaeoproterozoic ages between 1750±14 and 2480±16 Ma were acquired for 13 of the analysed zircon crystals (25%). Three grains yielded Archean $^{207}Pb/^{206}Pb$ ages around 2.8 Ga and 3.4 Ga.

The 6 youngest concordant and near concordant analyses, respectively, gave a concordia age of 529±3 Ma representing a maximum sedimentation age for the sandstone from the Žitec-Hluboš Formation (Fig. 7.6C).

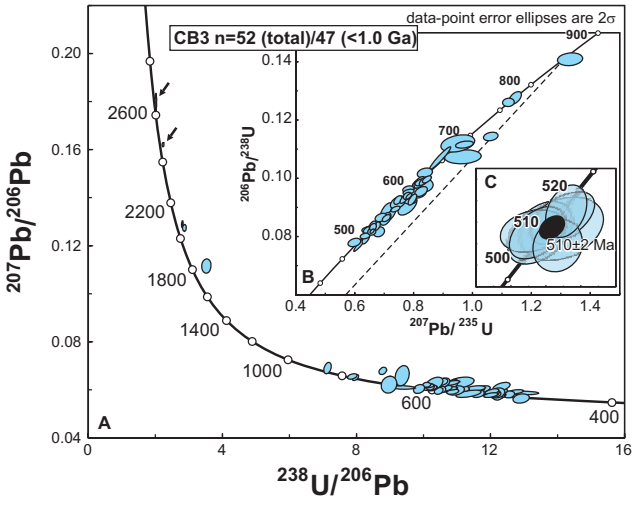

Fig. 7.7: Concordia diagrams for sample CB3. **A**: All analyses ≤20% discordant in Tera-Wasserburg plot. **B**: Neoproterozoic and Cambrian ages in concordia plot. **C**: Concordia age (±2σ error, MSWD/probability of concordance and equivalence = 1.07/0.38) calculated from 7 young ages with ≤8% discordance is assumed to represent the maximum sedimentation age of the sandstone.

Abb. 7.7: Konkordia-Diagramme für Probe CB3. **A**: Alle Analysen, die ≤20% diskordant sind, in Tera-Wasserburg-Diagramm. **B**: Neoproterozoische und kambrische Alter in Konkordia-Diagramm. **C**: Das Konkordia-Alter (±2σ Fehler, MSWD/Wahrscheinlichkeit von Konkordanz und Äquivalenz = 1.07/0.38), welches aus den 7 jüngsten Altern mit ≤8% Diskordanz berechnet wurde, gibt einen Hinweis auf das maximale Sedimentationsalter des Sandsteines.

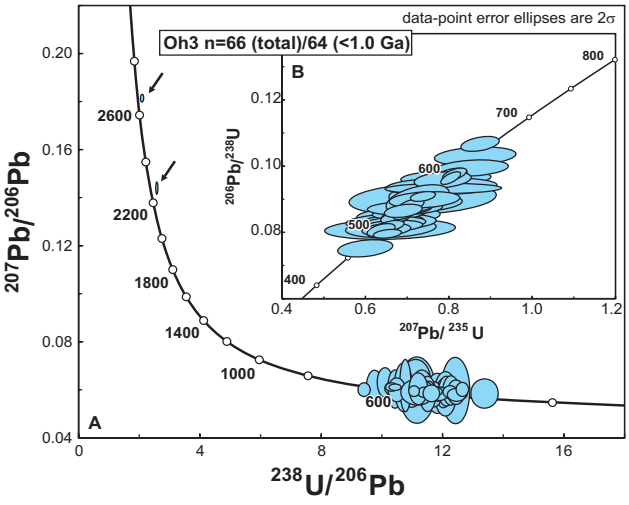

Fig. 7.8: Concordia diagrams for sample Oh3. **A**: All analyses ≤20% discordant in Tera-Wasserburg plot. **B**: Neoproterozoic and Cambrian ages in concordia plot.

Abb. 7.8: Konkordia-Diagramme für Probe Oh3. **A**: Alle Analysen, die ≤20% diskordant sind, in Tera-Wasserburg-Diagramm. **B**: Neoproterozoische und kambrische Alter in Konkordia-Diagramm.

Sample CB3

Sample CB3 was taken from the Chumava-Baština Formation, which closes the early Cambrian continental period. Zircon from sample CB3 was analysed by LA-ICP-MS at NHM London. The 52 analyses (Table A7) yielded Palaeozoic, Neoproterozoic and Palaeoproterozoic ages as well as one Archean age (Fig. 7.7). Palaeozoic detritus makes up ~36% (19 grains) of the analysed material. Of those 19 analyses 4 yielded $^{206}Pb/^{238}U$ ages that are somewhat younger than the stratigraphic age of the sample (Lower or early Middle Cambrian) and probably underwent lead loss. The associated $^{207}Pb/^{206}Pb$ ratios correspond within error (!) to Lower and Middle Cambrian ages (in the timescale of Gradstein et al., 2004) and are interpreted to be more meaningful than the $^{206}Pb/^{238}U$ ages in these particular cases (ja28a08, ja28a15, ja28e13, ja28b06 in Table A7). Seven young near concordant analyses gave a concordia age of 510±2 Ma representing a maximum sedimentation age for the sandstone from the Chumava-Baština Formation (Fig. 7-7C).

Neoproterozoic detritus has $^{206}Pb/^{238}U$ ages between 546±15 to 849±11 Ma (28 analyses – 54%), whereas ages ≤624±8 Ma are numerous and those around 655 Ma, 680 Ma, 770 Ma and 850 Ma (2 grains each) are less frequent (Fig. 7.7B). Palaeoproterozoic (~1.8, ~2.06, ~2.08, ~2.47 Ga) and Archean (~2.65 Ga) $^{207}Pb/^{206}Pb$ ages were determined on 5 grains (~10%).

Sample Oh3

Sample Oh3 was taken from the Ohrazenice Formation, which represents the beginning of the late Cambrian continental period. Analyses were performed by LA-ICP-MS at Frankfurt University and yielded 66 ages of predominantly Cambrian and Neoproterozoic origin (Fig. 7.8B). Only 2 of the 66 ages are Palaeoproterozoic (2272±23 Ma) or Archean (2664±12 Ma), respectively (Table A8, Fig. 7.8A).

Two analyses gave $^{206}Pb/^{238}U$ ages younger than the stratigraphic age of the sample (Oh25, Oh76) which is attributed to Pb-loss and indicated by a

GEOLOGICA SAXONICA
Journal of Central European Geology 54 (2008) 1–168

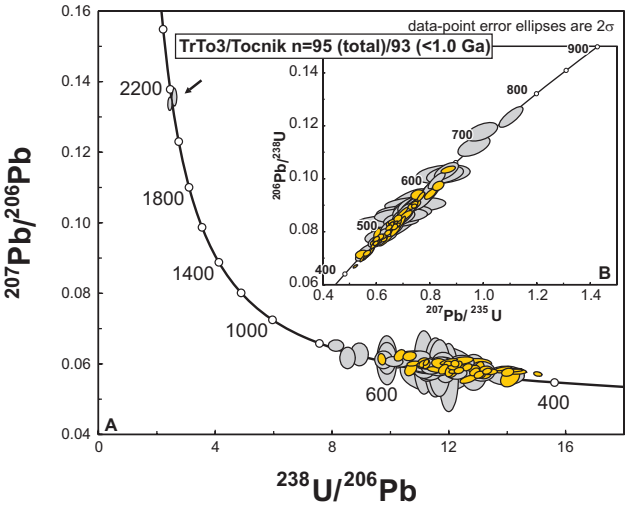

Fig. 7.9: Concordia diagrams for samples TrTo3 and Tocnik. **A**: All analyses ≤20% discordant in Tera-Wasserburg plot. **B**: Neoproterozoic and Early Palaeozoic ages in concordia plot. Yellow ellipses stand for analyses obtained by LA-ICP-MS at NHM London, grey ones for LA-ICP-MS data acquired at Frankfurt University.

Abb. 7.9: Konkordia-Diagramme für die Proben TrTo3 und Tocnik. **A**: Alle Analysen, die ≤20% diskordant sind, in Tera-Wasserburg-Diagramm. **B**: Neoproterozoische und frühpaläozoische Alter in Konkordia-Diagramm. Gelbe Ellipsen stehen für Analysen, die im NHM London gemacht wurden (TrTo3), graue Ellipsen für LA-ICP-MS-Daten die an der Universität Frankfurt aquiriert wurden (Tocnik).

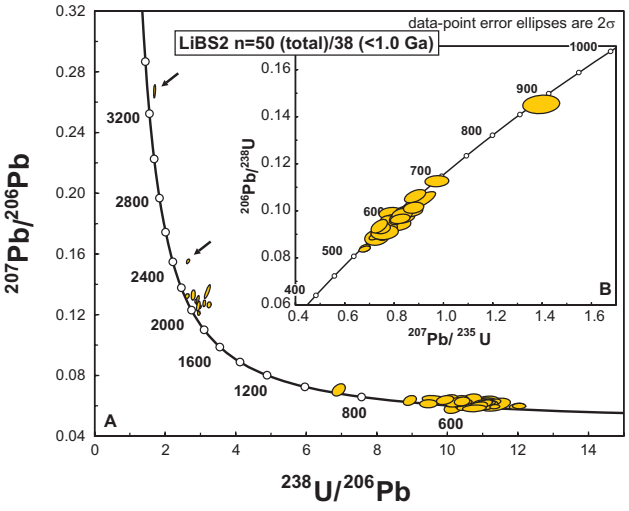

Fig. 7.10: Concordia diagrams for sample LiBS2. **A**: All analyses ≤20% discordant in Tera-Wasserburg plot. **B**: Neoproterozoic and Early Palaeozoic ages in concordia plot.

Abb. 7.10: Konkordia-Diagramme für Probe LiBS2. **A**: Alle Analysen, die ≤20% diskordant sind, in Tera-Wasserburg-Diagramm. **B**: Neoproterozoische und frühpaläozoische Alter in Konkordia-Diagramm.

higher grade of discordance (12%, 17%) between the $^{206}Pb/^{238}U$ age and the respective $^{207}Pb/^{206}Pb$ age. 38 grains with ages between 499±10 and 543±9 Ma emphasise the dominance of Cambrian detritus (~58%). Neoproterozoic ages chiefly range between 546±10 and 599±9 Ma (21 grains – 32%). Further 3 grains have older Neoproterozoic $^{206}Pb/^{238}U$ ages of 610±12, 631±13 and 653±11 Ma.

Samples TrTo3 and Točník

Samples TrTo3 and Tocnik were taken from a sequence of quartzose sandstones that were deposited during the Early Ordovician marine transgression. Data were acquired by LA-ICP-MS at NHM London (n=47, Table A7) and by LA-ICP-MS at Frankfurt University (n=48, Table A8). The results obtained in the different labs are similar and are therefore treated together.

As in sample Oh3 Early Palaeozoic and Neoproterozoic detritus prevails (Fig. 7.9B), whereas Palaeoproterozoic zircon (2145±20, 2170±26 Ma) is represented by only 2 grains (Fig. 7.9A). Of the analysed 95 grains 61 yielded Early Palaeozoic $^{206}Pb/^{238}U$ ages (67%). Neoproterozoic zircon is for the most part younger than 634±6 Ma (29 grains – 31%). Neoproterozoic $^{206}Pb/^{238}U$ ages between 685±18 and 749±18 Ma were determined for 3 crystals.

Several analyses gave $^{206}Pb/^{238}U$ ages younger than the stratigraphic age of the sample. Since the $^{207}Pb/^{206}Pb$ ages of these grains take reasonable values – also in combination with only slight discordance – this feature can be explained by Pb loss.

Sample LiBS2

For this Upper Ordovician quartzose sandstone 50 U-Pb analyses were acquired by LA-ICP-MS at NHM London (Table A7). Zircon grains are between 100 and 200 μm long and quite well rounded. The age distribution pattern of sample LiBS2 differs significantly from the previous one. Of the 50 grains only 2 yielded Early Palaeozoic ages (Fig. 7.10B). Neoproterozoic detritus with $^{206}Pb/^{238}U$ ages between 546±5 and 650±13 Ma is very frequent and makes up 68% (34 grains) of the zircon population. Older

Neoproterozoic $^{206}Pb/^{238}U$ ages of 686±11 and 874±18 Ma were determined for 2 zircon grains.

Zircon with Palaeoproterozoic and Archean ages makes up 24% of the population (Fig. 7-10A). Palaeoproterozoic $^{207}Pb/^{206}Pb$ ages from ~1.95 to ~2.15 Ga were measured on 10 grains. One zircon yielded an older Palaeoproterozoic age of 2394±14 Ma. Additionally one analysis revealed an Archean $^{207}Pb/^{206}Pb$ age of 3286±22 Ma.

Sample LeZb6

67 zircon grains from Upper Ordovician sample LeZb6 were measured by LA-ICP-MS at NHM London. Of those analyses 19 were rejected on the basis of the presence of features such as discordance >20%, high common Pb, inconsistent behaviour of U-Pb and Th-Pb ratios or elemental U-Pb fractionation. The remaining 48 analyses (Table A7) yielded ages between 506±6 and 2452±16 Ma (Fig. 7.11A). Early Palaeozoic detritus is very rare. Neoproterozoic zircon with ages between 544±16 and 669±10 Ma makes up ~46% of the population. Two grains with Mesoproterozoic $^{207}Pb/^{206}Pb$ ages of 1068±52 and 1398±64 Ma were detected. Palaeoproterozoic ages from 1842±120 to 2452±16 Ma were determined for 22 grains, whereas most of these analyses cluster between ~2.0 and ~2.2 Ga.

The high proportion of Palaeoproterozoic zircon (~46%) in sample LeZb6 is attributed to disturbance of the U-Pb system in a large number of (?Palaeozoic and) Neoproterozoic zircon grains, which led to a much higher rejection rate for analyses yielding young ages: of the 41 measured Palaeozoic and Neoproterozoic $^{206}Pb/^{238}U$ ages, 15 (37%) were rejected with respect to the following aspects. (1) One reason for insufficient analyses was common Pb contamination (Fig. 7.11B, ellipses that lie right and far right of the concordia). The $^{206}Pb/^{238}U$ ratios are often only slightly influenced by common Pb, which is due to the high isotopic abundance of the parent ^{238}U (99.2745) and associated high contents of radiogenic ^{206}Pb (compared to often negligible contributions of common ^{206}Pb). Radiogenic ^{207}Pb, however, forms from the decay of ^{235}U with a very low isotopic abundance of 0.7200 (De Bievre & Taylor 1993). In the case of common Pb contamination, the total ^{207}Pb is composed of both a radiogenic and an unradiogenic component, which results in a prominent increase of the $^{207}Pb/^{235}U$ and $^{207}Pb/^{206}Pb$ ratios and, consequently, in discordance. (2) Another reason for measuring a disturbed U-Pb system may be inter-element fractionation between U and Pb (two of the ellipses protruding above the concordia in Fig. 7.11B). Since, the zircon is heated in the course of ablation, it may occur that U and Pb isotopes are not provided to the mass spectrometer in constant ratios, i.e. increasing heating of the zircon causes increasing availability of Pb over U. Therefore, the ratios of $^{207}Pb/^{235}U$ and $^{206}Pb/^{238}U$ may increase

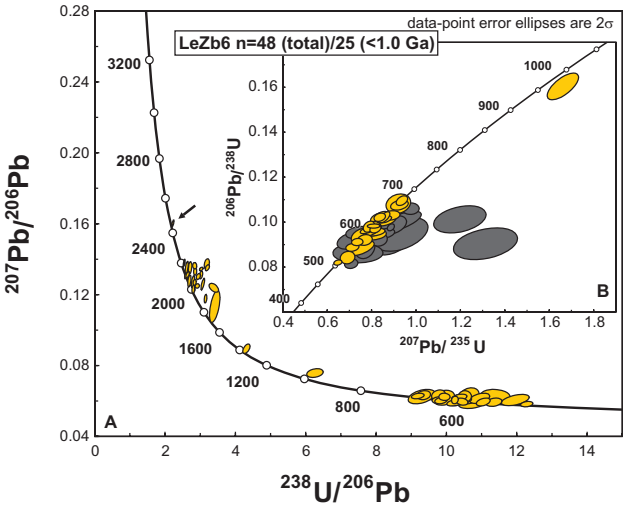

Fig. 7.11: Concordia diagrams for sample LeZb6. **A**: All analyses ≤20% discordant in Tera-Wasserburg plot. **B**: Neoproterozoic and Early Palaeozoic ages in concordia plot. Dark grey ellipses represent analyses that were rejected and illustrate common lead contamination (ellipses far to the right of the concordia), reverse discordance caused by fractionation (ellipses protruding above the concordia) and normal discordance >20% induced by Pb loss, mixed ages or disturbance by smaller amounts of common Pb.

Abb. 7.11: Konkordia-Diagramme für Probe LeZb6. **A**: Alle Analysen, die ≤20% diskordant sind, in Tera-Wasserburg-Diagramm. **B**: Neoproterozoische und frühpaläozoische Alter in Konkordia-Diagramm. Dunkelgraue Ellipsen zeigen die Analysen, die verworfen wurden. Gründe für die Ablehnung bestimmter Analysen waren: Kontamination mit gewöhnlichem Blei (Ellipsen weit rechts von der Konkordia), Laser-induzierte Interelement-Fraktionierung und damit verbundene reverse Diskordanz (Ellipsen, die oberhalb der Konkordia liegen bzw. weit nach links über die Konkordia hinausragen) sowie normale Diskordanz >20%, welche durch Pb-Verlust, Mischalter und/oder kleinere Mengen von gewöhnlichem Pb hervorgerufen werden kann.

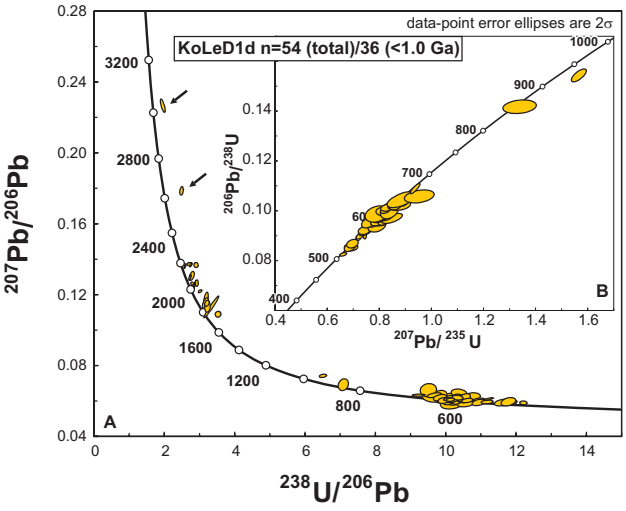

Fig. 7.12: Concordia diagrams for sample KoLeD1d. **A**: All analyses ≤20% discordant in Tera-Wasserburg plot. **B**: Neoproterozoic and Early Palaeozoic ages in concordia plot.

Abb. 7.12: Konkordia-Diagramme für Probe KoLeD1d. **A**: Alle Analysen, die ≤20% diskordant sind, in Tera-Wasserburg-Diagramm. **B**: Neoproterozoische und frühpaläozoische Alter in Konkordia-Diagramm.

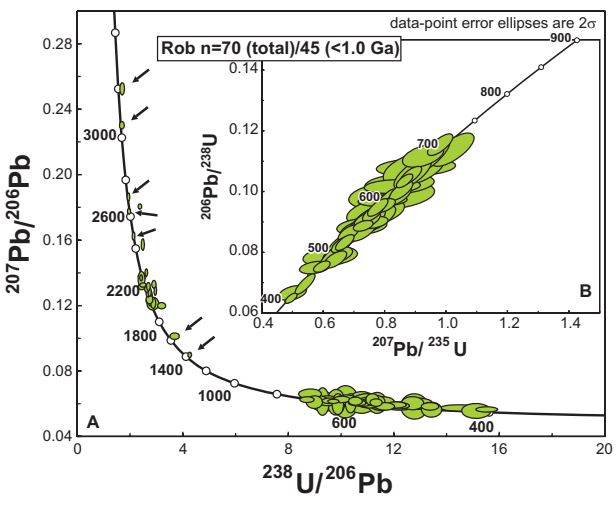

Fig. 7.13: Concordia diagrams for sample Roblín. **A**: All analyses ≤20% discordant in Tera-Wasserburg plot. **B**: Neoproterozoic and Palaeozoic ages in concordia plot.

Abb. 7.13: Konkordia-Diagramme für Probe Roblín. **A**: Alle Analysen, die ≤20% diskordant sind, in Tera-Wasserburg-Diagramm. **B**: Neoproterozoische und paläozoische Alter in Konkordia-Diagramm.

and correspond to ages that are too old. Because of the higher mass difference between ^{206}Pb and ^{238}U in comparison to ^{207}Pb and ^{235}U, the $^{206}Pb/^{238}U$ age is more concerned by the effect of fractionation than the $^{207}Pb/^{235}U$ age, which results in reverse discordance. (3) Young zircon (<1 Ga) may have relatively low ^{207}Pb contents, which results from the low isotopic abundance of the parent ^{235}U and the short time that was available for radioactive decay. Therefore, low count rates of ^{207}Pb may cause imprecise $^{207}Pb/^{206}Pb$ and $^{207}Pb/^{235}U$ ages with large errors and, accordingly, are a common reason for discordance. The zircon crystals from sample LeZb6 had a relatively small grain size (80–130 μm, few grains up to 180 μm) and were ablated with a nominal spot diameter of 18 or 30 μm, respectively, which additionally lowered the proportion of the measured ^{207}Pb (few of the ellipses that lie below the concordia in Fig. 7.11B).

Sample KoLeD1d

Sample KoLeD1d was taken from a glaciomarine diamictite of the Hirnantian glaciation. Detrital zircon was analysed by LA-ICP-MS at NHM London and yielded ages between 509±3 and 3024±22 Ma (Fig. 7.12). Cambrian ages from 509±3 to 535±8 Ma were obtained for 4 grains.

The number of measured Neoproterozoic ages is distinctly higher. Thirty grains (~56%) gave ages between 552±5 and 665±10 Ma. An older Neoproterozoic $^{206}Pb/^{238}U$ age of 853±13 Ma was achieved from 1 grain. One zircon yielded a Mesoproterozoic $^{207}Pb/^{206}Pb$ age of 1026±22 Ma. Of the 54 analysed grains, 16 gave Palaeoproterozoic ages from 1770±24 to 2182±10 Ma, which makes up ~30% of the population. Furthermore, two Archean ages of 2634±18 and 3024±22 Ma were determined.

Sample Roblín

For sample Roblín – that was taken from the youngest pre-Variscan sequence of the Teplá-Barrandian – 70 U-Pb analyses were achieved by LA-ICP-MS at Frankfurt University. Ages range from 404±9 to 3198±19 Ma (Table A8, Fig. 7.13A). Palaeozoic ages were obtained from 17 grains (24%). Neoproterozoic detritus with ages between 545±14 and 703±16 Ma is more frequent and makes up 40% of the zircon population (28 grains). One grain yielded a Mesoproterozoic $^{207}Pb/^{206}Pb$ age of 1408±30.

The record of Palaeoproterozoic ages ranges from 1635±29 Ma to 2476±21 Ma, whereas 16 of the 19 (27%) Palaeoproterozoic ages are between 1.9 and 2.2 Ga. Five grains with Archean ages were found. Of those 3 are between 2625±13 and 2706±19 Ma, one is near concordant at 3.05 Ga, and the oldest grain of sample Roblín has a $^{207}Pb/^{206}Pb$ age of 3198±19 Ma. U-Pb data acquired by LA-ICP-MS at Charles University Prague and Memorial University of Newfoundland were recently published by Strnad & Mihaljevič (2005). Their results for greywackes from the Givetian Roblín beds are similar to those obtained in this study.

7.4 Constraints on stratigraphy

Maximum sedimentation ages obtained from the Neoproterozoic samples BL (592±4 Ma) and Dob (565±4.5 Ma) give an approximation for the time interval preserved in the Neoproterozoic volcano-sedimentary successions of the Teplá-Barrandian unit. Although maximum sedimentation ages calculated from detrital zircon data are to be considered critically, the clear age difference and the prominent increase in ages younger than 600 Ma in the younger Neoproterozoic sample Dob substantiate that the deposition of the Blovice Formation (BL) took place markedly prior to sedimentation of the Štěchovice Group (Dob).

Sample PJ1/3 representing the lowermost part of the Cambrian continental sequence yielded a maximum sedimentation age of 529±3 Ma indicating that the Palaeozoic sedimentation did not start until the higher Lower Cambrian[1]. Sandstone sample CB3 taken from the strata directly underlying the Middle Cambrian marine Jince Formation gave a maximum sedimentation age of 510±2 Ma. Therefore it is highly probable that the continental successions of the TBU referred to as Lower Cambrian in fact extend into the early Middle Cambrian (timescale of Gradstein et al. 2005).

Since products of igneous events are common within the Neoproterozoic and Cambrian sequences, it is assumed that a distinct proportion of more or less synsedimentary igneous material was supplied to the siliciclastics (cf., chapter 3.1). Therefore the calculated maximum sedimentation ages of the four samples are regarded as significant chronostratigraphic contribution to the so far largely lithostratigraphic subdivision of the Teplá-Barrandian Neoproterozoic and Lower Cambrian successions. Although it cannot be excluded that the Neoproterozoic basement of the Teplá-Barrandian contains older rocks than the sampled strata of the Blovice Formation, the new data point to a deposition of the Cadomian rocks during a relatively short period within the Ediacaran period between 592±4 Ma and 565±4.5 Ma. After a hiatus in the sedimentary record spanning about 35 Ma the accumulation of the Lower Cambrian rift-related rocks started around 529±3 Ma.

7.5 Age distribution patterns of detrital zircon

A total of 612 ages was obtained from detrital zircon of 10 samples that were taken from Neoproterozoic to Upper Ordovician siliciclastic successions and a late Middle Devonian greywacke sequence. Apart from the rocks that were deposited during the Middle Cambrian to Lowermost Ordovician, all samples show similar age distributions with a maximum for Neoproterozoic ages and share following general features (Fig. 7.14):

- Archean ages are present in almost all samples but with low frequency (total 22)
- Palaeoproterozoic grains are common in most samples (total 117).
- Zircon with ages between 0.9 and 1.6 Ga is very rare or absent, respectively (total 7). None of these ages appears twice – neither per sample nor in total!

[1] Sedimentation started around the base of the Botomian after the timescale of the German Stratigraphic Commission (2002). The latest stratigraphic time scale after Gradstein et al. (2005) does not provide a subdivision of the Lower Cambrian.

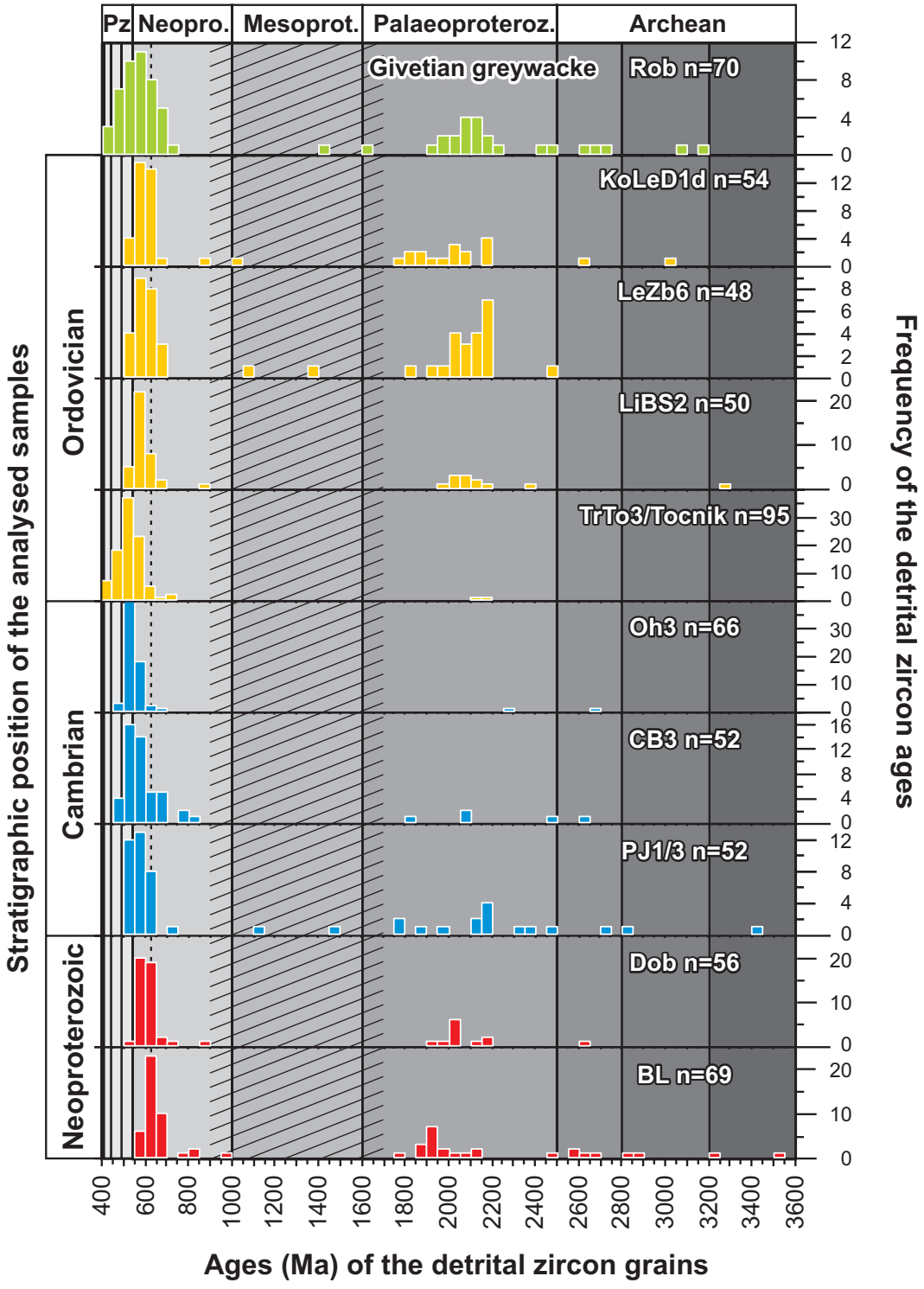

Fig. 7.14: Frequency distribution plot for detrital zircon ages of individual Neoproterozoic to Devonian samples. Bars show 50 Ma intervals. Note different scales of the y-axis for the individual samples.

Abb. 7.14: Häufigkeitsverteilungsdiagramm für die einzelnen Proben des Neoproterozoikums bis Devon. Die Balken entsprechen Intervallen von 50 Mio. Jahren. Es ist zu beachten, dass die y-Achsen für die einzelnen Proben unterschiedliche Maßstäbe aufweisen.

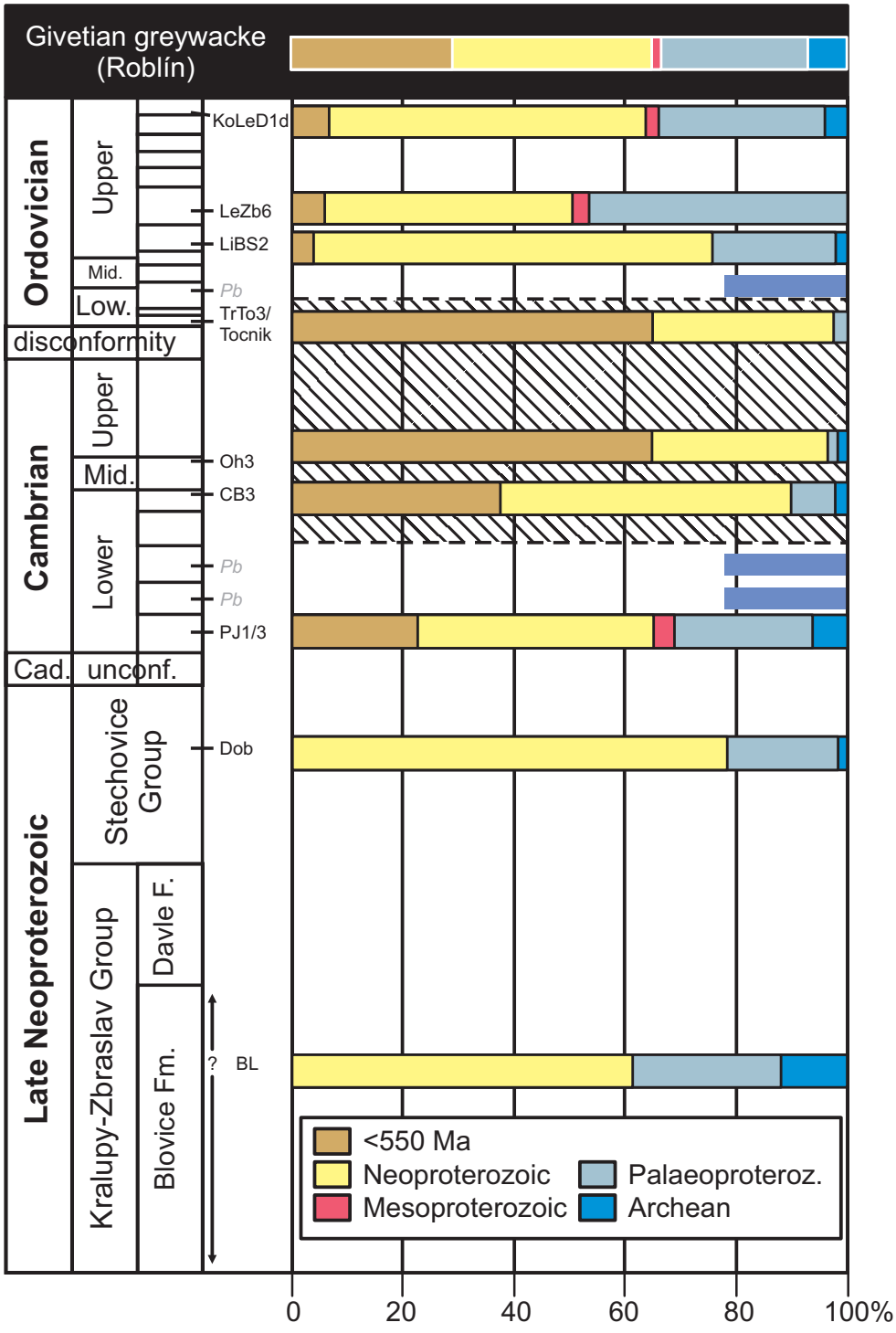

Fig. 7.15: Proportions of Archean, Proterozoic and Palaeozoic detritus in the individual samples. Results from whole rock Pb isotope analyses (cf. chapters 6.2 and 6.5) that detected contributions from old crustal material are indicated for key samples.

Abb. 7.15: Anteile von archaischem, proterozoischem und paläozoischem Detritus in den einzelnen Proben. Die Ergebnisse der Gesamtgesteins-Pb-Isotopenanalysen (s. Kapitel 6.2 und 6.5), die Eintrag von alter kontinentaler Kruste anzeigen, sind für die Schlüsselproben mit angegeben.

· Detritus of Neoproterozoic origin (<900 Ma) is frequent or prevailing in all analysed samples (total 312).

Differences in the age distribution patterns chiefly concern the proportions of Palaeozoic zircon (total 154; Fig. 7.15).

In the Neoproterozoic rocks (samples BL and Dob) and in the oldest Cambrian sample (PJ1/3) a prominent proportion of detritus from Palaeoproterozoic and older sources (22–37%) is traceable (Fig. 7.14, Fig. 7.15). Younger Lower Cambrian rocks still contain contributions from old crust, which is indicated by their whole rock Pb isotope compositions (see chapters 6.2 and 6.5). From the uppermost Lower Cambrian to the Lower Ordovician input of old zircon decreases. Instead, the contributions from sources younger than 550 Ma increase strongly. The scarcity of pre-Neoproterozoic zircon could be attributed to a dilution effect (the higher the proportion of Palaeozoic detritus, the lower the proportion of Precambrian zircon). However, when ignoring the ages younger than 550 Ma there are still low percentages of pre-Neoproterozoic zircon in these samples (CB3: 15.6%, Oh3: 8.7%, TrTo3+Točník: 6.1%). The lack of old zircon combined with common (sample CB3 - 38%) or extremely frequent (samples Oh3 and TrTo3/Tocnik - 65% each) Palaeozoic detritus in uppermost Lower Cambrian to Early Ordovician rocks might be related to crustal tilting with related change in the drainage system and therefore a change/restriction in provenance.

After the sedimentation of the Cambrian Ohrazenice Formation (sample Oh3) until the deposition of the Tremadocian Třenice Formation (samples TrTo3/Tocnik) up to 1500 m andesitic to rhyolitic volcanics were accumulated. The Upper Cambrian age of the volcanism is confirmed by U-Pb-SHRIMP dating of zircon from rhyolite sample OKR yielding a crystallisation age of 499±4 Ma. The Upper Cambrian volcanic complex and products of the older Cambrian magmatism occurring in the Teplá-Barrandian (523–505 Ma: Dörr et al. 1998, 2002; Zulauf et al. 1997; Venera et al. 2002) have to be considered as an important source for late Lower Cambrian to lowermost Ordovician siliciclastics.

From the late Lower or Middle Ordovician on the old source is available again. This is indicated by the whole rock lead isotopic signature of samples from several stratigraphic levels (cf. chapters 6.2 and 6.5) and by the abundant old zircon grains in the Upper Ordovician samples (Fig. 7.14, Fig. 7.15). Pre-Neoproterozoic detritus makes up ~24/~36% in samples LiBS2 and KoLeD1d. The high proportion of pre-Neoproterozoic detritus (50%) in the sandstone from the Upper Ordovician Letná Formation (LeZb6) results from the high rejection rate for the younger ages. Yet, when regarding all measurements (before rejection of insufficient analyses) the fraction of old zircon is in a similar dimension as in the other Upper Ordovician samples (~36%).

Palaeozoic zircon is very rare in the analysed Upper Ordovician rocks (4–7%). Thus the Cambrian and Lower Ordovician deposits must have been covered to a large extent. In contrast the Devonian greywacke yielded a distinct content of post-550 Ma detritus (24%; Fig. 7.15), which should have been associated with uplift and erosion of parts of the older Palaeozoic rocks. Apart from the more frequent Palaeozoic zircon, the age spectrum of sample Roblín largely resembles those of the Neoproterozoic to lowermost Cambrian and Upper Ordovician rocks (Fig. 7.14).

7.6 Source area

Several recent studies applied detrital zircon age spectra to deduce the ancestry of crustal fragments with Cadomian basement from one of the different cratons/units composing northern Gondwana (e.g. Fernández-Suárez et al. 1999, 2000, 2002; Friedl et al. 2000, 2004; Gutiérrez-Alonso et al. 2003; Murphy et al. 2004a, 2004b; Linnemann et al. 2004; Martínez Catalán et al. 2004). The presence of c. 0.9–1.2 Ga old and/or Mesoproterozoic zircon in Neoproterozoic and Palaeozoic rocks is used as an indicator for Amazonian provenance (e.g., Friedl et al. 2000, Gutiérrez-Alonso et al. 2005). In the – meanwhile well dated – West African craton, 0.9–1.2 Ga old or

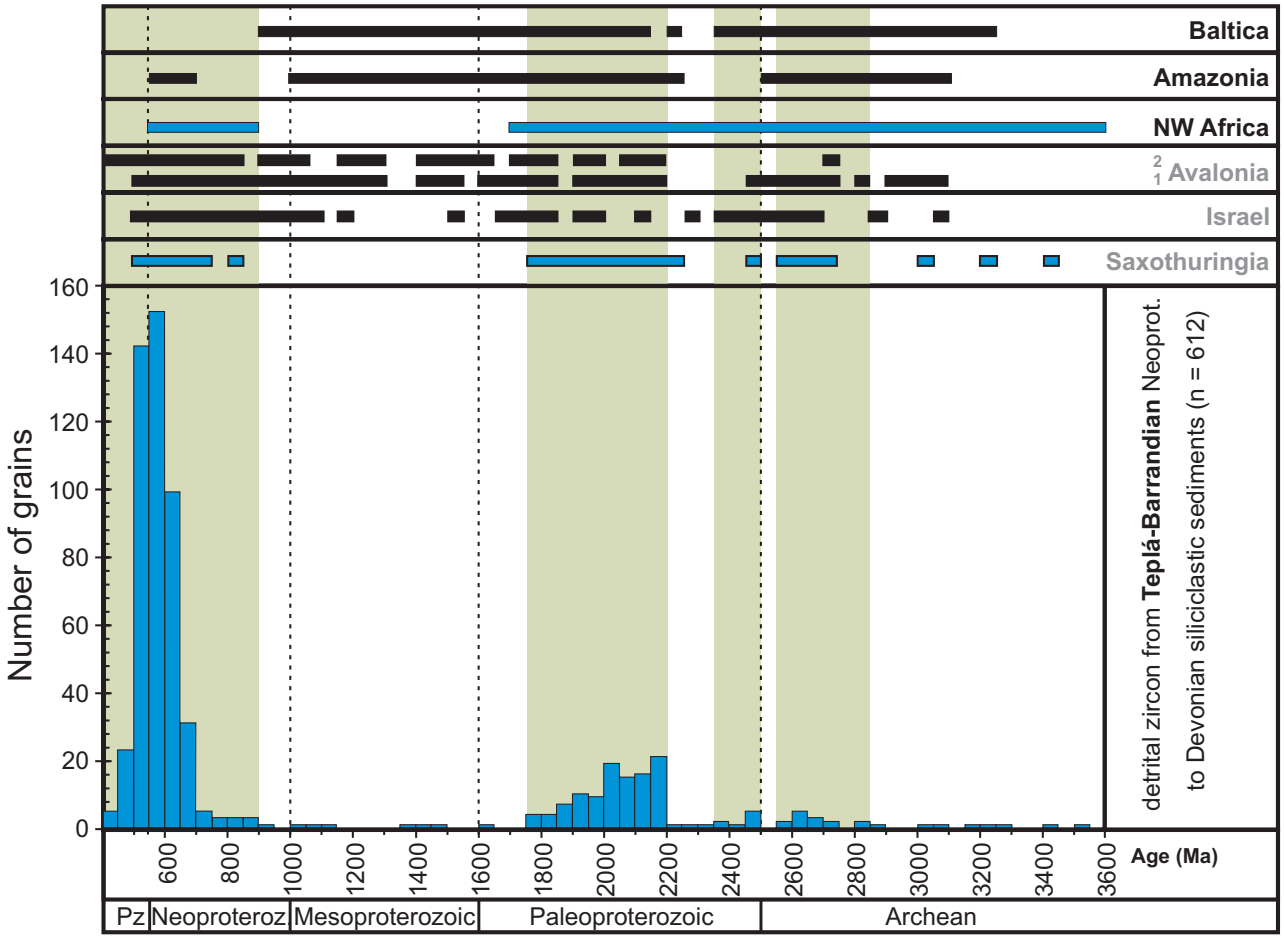

Fig. 7.16: Summarized frequency distribution plot for detrital zircon ages of Neoproterozoic to Devonian samples and comparison with the age spectra of **a**) potential source areas (Baltica, Amazonia, NW-Africa) and **b**) other Gondwanan or Gondwana-derived units (Avalonia, Israel, Saxothuringia). Bars show 50 Ma intervals. Shaded areas highlight time intervals that are represented by a number of zircon ages in the Barrandian samples. Data sources: Baltica – Åhäll et al. (1998), Bingen et al. (2001, 2003); and from the compilations of Gaál & Gorbatschev (1987), Hanski et al. (2001), Romer (in press); Amazonia – from the compilations of Teixeira et al. (1989) and Tassinari & Macambira (1999); NW Africa – see Fig. 7.18 (1–3); Avalonia – detrital zircon ages from (1) Cambro-Ordovician and (2) Silurian to Devonian siliciclastics, Collins & Buchan (2004), Murphy et al. (2004a, 2004b); Saxothuringia – detrital and inherited zircon ages from Neoproterozoic to Ordovician siliciclastic and igneous rocks, Linnemann et al. (2004).

Abb. 7.16: Zusammenfassung der Häufigkeitsverteilungen der neoproterozoischen bis devonischen Proben und Vergleich mit den Altersspektren von **a**) potentiellen Liefergebieten (Baltica, Amazonia, NW-Africa) und **b**) anderen gondwanischen bzw. perigondwanischen Einheiten (Avalonia, Israel, Saxothuringia). Die Balken entsprechen Intervallen von 50 Mio. Jahren. Datenquellen: Baltica – Åhäll et al. (1998), Bingen et al. (2001, 2003); und aus den Zusammenstellungen von Gaál & Gorbatschev (1987), Hanski et al. (2001), Romer (in press); Amazonia – aus den Zusammenstellungen von Teixeira et al. (1989) und Tassinari & Macambira (1999); NW Africa – siehe Abb. 7.18 (1–3); Avalonia – Alter detritischer Zirkone aus (1) kambro-ordovizischen sowie (2) silurischen und devonischen Siliziklastika, Collins & Buchan (2004), Murphy et al. (2004a, 2004b); Saxothuringia – Alter detritischer und ererbter Zirkone aus neoproterozoischen bis ordovizischen Siliziklastika und Magmatiten, Linnemann et al. (2004).

Mesoproterozoic events have not been recognized hitherto. Consequently the absence of 0.9–1.6 Ga old detrital zircon is an indicator for northwest African provenance. However, a number of detrital zircon grains with 0.9–1.2 Ga and Mesoproterozoic ages was discovered in the NE African Arabian-Nubian Shield and its cover sequence (Fig. 7.18). Yet crust-forming events between 0.9 and 1.6 Ga are not known from

GEOLOGICA SAXONICA
Journal of Central European Geology 54 (2008) 1–168

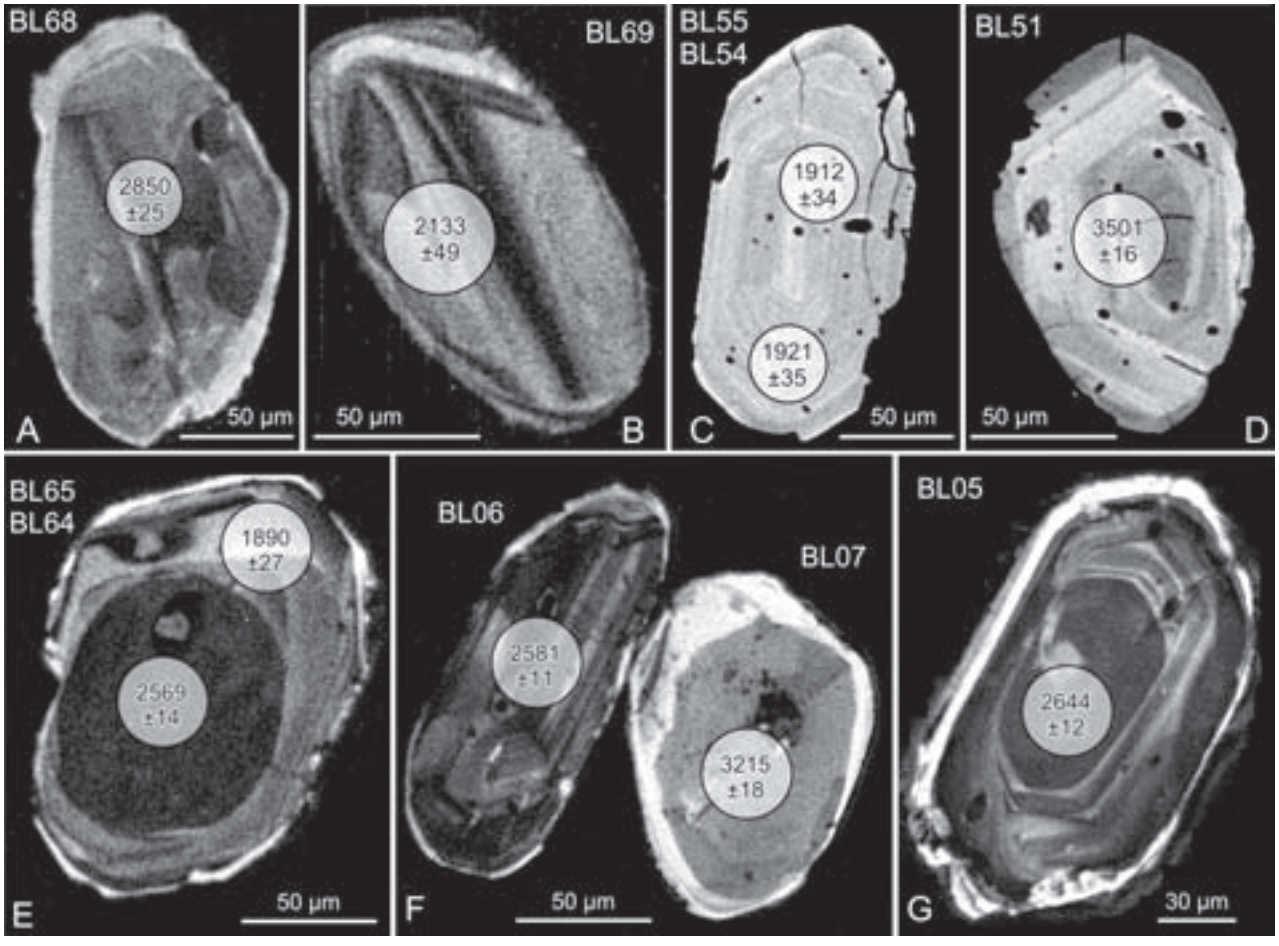

Fig. 7.17: Images of detrital zircon of sample BL (Neoproterozoic Blovice Fm.) showing that many of the pre-Neoproterozoic grains are composed of core and overgrowth zone(s). Particularly the grains yielding Archean ages are not derived from pristine Archean terranes but from reworked Archean crust. The same seems to apply to some of the Palaeoproterozoic zircon crystals: **A**: CL image of an Archean grain with narrow rim, **B**: CL image of Palaeoproterozoic core with narrow rim, **C**: BSE image of a Palaeoproterozoic grain showing magmatic zoning, **D**: BSE image of a grain with Archean core and younger rim – the spot straddles the core and a distinctly younger overgrowth zone resulting in a discordant analyses. However, the core has a $^{207}Pb/^{206}Pb$ minimum age of 3501±16 Ma, **E**: CL image revealing Archean core and Palaeoproterozoic rim, F) CL image of two Archean grains with narrow rims, **G**: CL image of an Archean grain with narrow rim.

Abb. 7.17: Mikrosondenaufnahmen detritischer Zirkone aus Probe BL (Neoproterozoikum, Blovice Formation) zeigen, dass viele der prä-neoproterozoischen Körner aus Kern und Anwachszone(n) zusammengesetzt sind. Vor allem die Körner mit archaischen Altern stammen nicht von unberührten Komplexen sondern von überprägter archaischer Kruste. Das Gleiche scheint für die Paläoproterozoischen Zirkone zu gelten: **A**: Kathodolumineszenz-Aufnahme eines archaischen Korns mit schmalem Rand. **B**: KL-Aufnahme eies paläoproterozoischen Korns mit schmalem Rand. **C**: BSE-Aufnahme eines paläoproterozoischen Korns mit magmatischer Zonierung. **D**: BSE-Aufnahme eines Korns mit archaischem Kern und jüngerem Rand – der Spot hat sowohl den Kern als auch den deutlich jüngeren Anwachssaum getroffen, was in einer diskordanten Analyse resultiert. Der Kern hat ein $^{207}Pb/^{206}Pb$-Minimum-Alter von 3501±16 Ma. **E**: KL-Aufnahme, die einen archaischen Kern mit paläoproterozoischem Anwachssaum zeigt. **F**: KL-Aufnahme von zwei archaischen Körnern mit schmalem Rand. **G**: KL-Aufnahme eines archaischen Korns mit schmalem Rand.

the Arabian-Nubian Shield, too. Nevertheless, during Precambrian and Cambrian times there must have been a source for such detritus. Avigdad et al. (2003) found a distinct number of detrital zircon crystals with ages between 0.9 and 1.2 Ga in Cambrian sandstones from southern Israel and conclude that either rocks

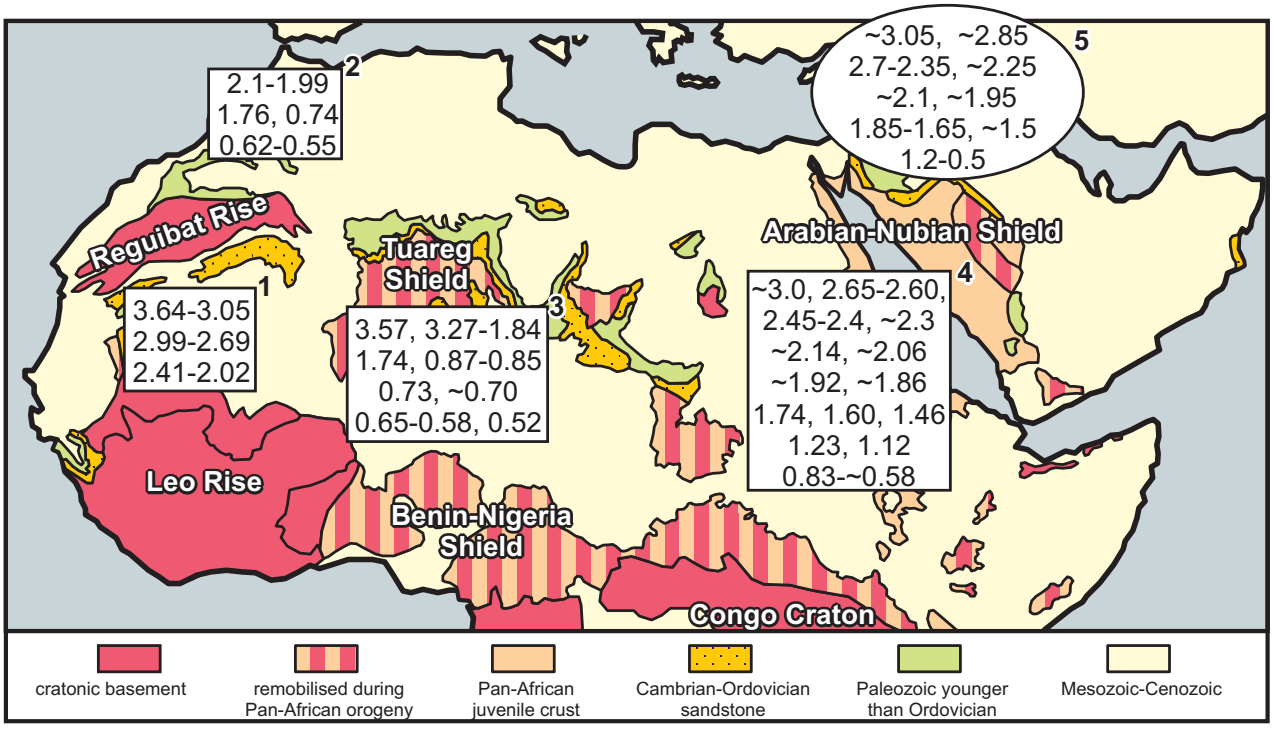

Fig. 7.18: Compilation of detrital, magmatic and metamorphic U-Pb and Pb-Pb zircon ages known from the northern part of the African continent. Data sources: **1** (West African craton) – Barth et al. (2002), Bossière et al., (1996), Doumbia et al. (1998), Egal et al. (2002), Hirdes et al. (1996), Hirdes & Davis (2002), Kouamelan et al. (1997), Oberthür et al. (1998), Peucat et al. (2005), Potrel et al. (1996, 1998), Thiéblemont et al. (2001, 2004); and references therein. **2** (Anti-Atlas, Morocco) – Barbey et al. (2004), Gasquet et al. (2004), Inglis et al. (2004), compilation of Soulaimani & Piqué (2004), Thomas et al. (2002). **3** (Tuareg Shield, Benin-Nigeria Shield) – Affaton et al. (2000), compilation of Caby (2003), Kröner et al. (2001), Peucat et al. (1996, 2003), Paquette et al. (1998); and references therein. **4** (Arabian-Nubian Shield) – compilation of Abdelsalam et al. (2002), Kröner et al. (1994), Stern et al. (1994), Sultan et al. (1994); and references therein. **5** (detrital zircon from Cambrian sandstone in Israel) – Avigdad et al. (2003).

Abb. 7.18: Zusammenstellung von U-Pb- und Pb-Pb-Altern detritischer, magmatischer und metamorpher Zirkone, die aus dem nördlichen Teil Afrikas bekannt sind. Datenquellen: **1** (Westafrikanischer Kraton) – Barth et al. (2002), Bossière et al. (1996), Doumbia et al. (1998), Egal et al. (2002), Hirdes et al. (1996), Hirdes & Davis (2002), Kouamelan et al. (1997), Oberthür et al. (1998), Peucat et al. (2005), Potrel et al. (1996, 1998), Thiéblemont et al. (2001, 2004); und Referenzen darin. **2** (Anti-Atlas, Marokko) – Barbey et al. (2004), Gasquet et al. (2004), Inglis et al. (2004), Zusammenstellung von Soulaimani & Piqué (2004), Thomas et al. (2002). **3** (Tuareg-Schild, Benin-Nigeria-Schild) – Affaton et al. (2000), Zusammenstellung von Caby (2003), Kröner et al. (2001), Peucat et al. (1996, 2003), Paquette et al. (1998); und Referenzen darin. **4** (Arabisch-Nubischer Schild) – Zusammenstellung von Abdelsalam et al. (2002), Kröner et al. (1994), Stern et al. (1994), Sultan et al. (1994); und Referenzen darin. **5** (detritische Zirkone aus einem kambrischen Sandstein Israels) – Avigdad et al. (2003).

of these ages are present but not recognized hitherto in the Arabian-Nubian shield or that detritus of this age was transported by glaciers over a long distance during the Neoproterozoic and became reworked/redeposited afterward.

The age spectra of the analysed samples show (Fig. 7.14, Fig. 7.16) prominent input from sources younger than 0.9 Ga and from rocks that were formed between 1.75 and 2.20 Ga. Even though less frequent – zircon with ages from 2.35 to 2.50 Ga and 2.55 to 2.85 Ga was detected several times. Older Archean grains are rare but present.

Taking sample BL (Neoproterozoic) as an example it can be demonstrated that the analyses yielding Archean ages were obtained from core domains of the grains, which are surrounded by younger overgrowth domains (Fig. 7.17), i.e. there were no pristine Archean terranes in the source area but the

Archean zircon is derived from Archean complexes that were reworked during the Palaeoproterozoic (Fig. 7.17E) and/or during the Neoproterozoic. Also Palaeoproterozoic terranes may have been reworked during later events. Barbey et al. (1989) described migmatites of the Central Hoggar that yielded zircon crystals with polyphase evolution: granodiorite-protoliths of Palaeoproterozoic age (~2.13 Ga) are overgrown by ~610 Ma old metamorphic rims. The core of zircon BL69 (Fig. 7.17B) matches the age of the protolith and shows a narrow rim of unknown age. The rim might correspond to metamorphic overprint as suggested by the roundness of the grain. The absence of indicators for pristine Archean crust and the lack of ages between 0.9 and 1.7 Ga provides clear evidence for the position of the Teplá-Barrandian in the proximity of (present) northwest Africa during the Neoproterozoic. The most probable position of the TBU was in the northern part/continuation of the Trans-Sahara Belt (see chapter 8 for further discussion). Furthermore the similarity with the age distribution patterns of detrital and inherited zircon from Saxo-Thuringia (Linnemann et al. 2004; see Fig. 7.16), the northern Armorican Massif and the Iberian Ossa-Morena Zone (Schäfer et al. 1993, Fernández-Suárez et al. 2002b) suggest a common history of these units with the Barrandian. In contrast Avalonia (Collins and Buchan 2004, Murphy et al. 2004a, 2004b; see Fig. 7.16), the Cantabrian and Westasturian-Leonese Zones of Iberia (Fernández-Suárez et al. 1999, 2000, 2002a) and the Moravo-Silesian domain of the Bohemian Massif (Friedl et al. 2000, 2004) are characterised by age spectra containing prominent proportions of Mesoproterozoic components.

The detrital zircon age spectra of the samples from the Barrandian remain more or less the same from the late Neoproterozoic to the Mid-Devonian, which implies that the source area of the detrital zircon remains more or less the same, too. This source area must have consisted either of Neoproterozoic active margin/magmatic arc sequences and pre-Mesoproterozoic basement complexes (and/)or of Neoproterozoic (and Early Palaeozoic?) siliciclastics and possibly crustally derived igneous rocks with an inherited component. The simplest and most probable explanation for the unchanged zircon age spectra is that the Teplá-Barrandian did not leave its Gondwanan source area prior to the Variscan continent-continent collision but rather drifted together with Gondwana towards lower latitudes. Alternative scenarios would be that the Teplá-Barrandian rifted from the supercontinent and drifted separately towards the north as a constituent of (1) a larger crustal fragment including Gondwanan basement rocks or (2) as a part of Cadomian/Pan-African crust that contained a subaerial part, which was eroded and supplied the basin with reworked (Neoproterozoic?) material. Both interpretations are not very likely because of (1) the scarcity of pre-Neoproterozoic basement rocks in the Variscan and Alpine orogens (only two occurrences of small areal extent are known - the Svetlík gneiss in the Moldanubian Zone and the Icartian gneiss in the northern Armorican Massif) and (2) the lack of Cambrian detrital zircon in the Upper Ordovician samples (if the pre-Neoproterozoic detrital zircon should be derived from reworked Neoproterozoic greywackes, the Cambrian plutons intruding these rocks should also supply detrital material).

Neoproterozoic and Cambrian zircon may have been generated by Cadomian tectono-thermal events at the periphery of Gondwana (in the sense of Murphy & Nance 1989) and/or by Pan-African orogenic processes that amalgamated the individual cratons then forming Gondwana (e.g., Trompette 1994, Dalziel 1997; and references therein). Rocks of appropriate geochemical composition and with suitable formation ages are present in both belts. Furthermore Neoproterozoic and Cambrian zircon may have been derived from local sources. Although Neoproterozoic igneous rocks of the TBU are not or insufficiently dated, their geochemistry and their stratigraphic classification make them suitable source rock candidates, particularly for the Cambrian siliciclastics. Cambrian igneous rocks with ages between 523 and 499 Ma (see chapter 2.2.2 for references) are well known in the Teplá-Barrandian unit. These rocks should have been an important source for the younger Lower Cambrian to Early Ordovician detrital sediments of the TBU.

8 Synthesis

8.1 General initial situation

The late Neoproterozoic amalgamation of Gondwana was realised by continent-continent collision processes and accompanied formation of interior orogens such as the Trans-Saharan mobile belt or the East African orogen (Murphy & Nance 1991). On the other hand subduction and associated orogenic processes occurred at the periphery of Gondwana, too. One of these outboard orogens was represented by the Avalonian-Cadomian tectono-stratigraphic belt that largely formed at around 750–550 Ma at the Amazonian-West African periphery of Gondwana (Murphy & Nance 1989).

The Avalonian terranes, such as West and East Avalonia, Carolina as well as the Brunovistulian block of the Bohemian Massif, show an affinity with Amazonia, whereas the Cadomian terranes, e.g., the Northern Armorican Massif, the Ossa-Morena zone of the Iberian Massif as well as the Saxothuringian and Moldanubian zones of the Bohemian Massif were associated with the West African proportion of Gondwana (e.g., Nance & Murphy 1994, Finger et al. 2000, Fernández-Suárez et al. 2002a, Linnemann & Romer 2002, Friedl et al. 2004, Murphy et al. 2002, 2006). Geotectonic models for the Neoproterozoic to Ordovician development at the Amazonian-West African margin of Gondwana include (e.g., Murphy & Nance 1989, Buschmann 1995, Strachan et al. 1996, Murphy et al. 1999, 2006, Fernández-Suárez et al. 2002b, Gutiérrez Alonso et al. 2003, Nance et al. 2002, Quesada 2006, Sánchez Martínez et al. 2006, Linnemann et al., 2007):

(1) Early arc magmatism in the interval 750–650 Ma.

(2) Accretion of these arc terranes to the Gondwanan margin prior to the main phase of arc magmatism.

(3) Main arc phase recorded by voluminous magmatic arc-related volcanic and plutonic rocks with ages between 635 and 570 Ma. Oblique subduction beneath the Gondwanan margin gave rise to development of a variety of magmatic arc basins.

(4) Cessation of subduction and transition from typical arc-related processes to an intracontinental wrench regime that occurred diachronously between ca. 590 and 540 Ma. Since features of a major collisional event are absent, ridge-trench collision was postulated to have caused termination of subduction, structural inversion of arc-related basins and opening of new rift and wrench-related basins. Lateral displacement processes along the Gondwanan margin played a major role for juxtaposition of units with different basement signatures.

(5) Development of a Latest Neoproterozoic to Ordovician cover sequence and continued transtensional block faulting. Rifting of Avalonia from Gondwana and the Cadomian terranes occurred diachronously and was completed between Early and Middle Ordovician.

Linnemann et al. (2007) modified this general course of the processes for the Saxothuringian zone of the Bohemian Massif. They identified an early arc stage that was characterised by subduction beneath the Andean-type Gondwanan margin (~650–600 Ma) and succeeded by back-arc extension (590–560 Ma). Due to the closure of the back-arc basin (545–540 Ma) a short-lived retro-arc basin developed. Following ridge-trench collision and associated slab breakoff, a magmatic and anatectic event occurred at ~540 Ma. The incision of the ridge into the continent caused formation of Lower and Middle Cambrian rift basins and eventually led to the opening of the Rheic Ocean by the Lower Ordovician.

8.2 Neoproterozoic

The volcanic and sedimentary rocks of the Teplá-Barrandian Neoproterozoic basement are variegated

and indicate a complex setting and/or history, respectively. The presence of several different lithostratigraphic concepts (e.g., Cháb & Pelc 1968, Holubec 1995, Röhlich 2000, Mašek 2000) shows that the Neoproterozoic basement of the Teplá-Barrandian unit is still far from well understood. There is consensus among the majority of the workers that the Neoproterozoic rocks were formed in a magmatic arc setting close to the periphery of Gondwana and were subject to deformation prior to the onset of Cambrian sedimentation (e.g., Jakeš et al. 1979, Pašava & Amov 1993, Waldhausrová 1997a, Zulauf et al. 1999, Kříbek et al. 2000, Dörr et al. 2002). Particularly the geochemical compositions of the volcanic rocks within the Blovice Formation and the older part of the Davle Formation led several authors to favour an intra-oceanic setting for this part of the Neoproterozoic succession (e.g., Waldhausrová 1997b, Kříbek et al. 2000, Pin & Waldhausrová 2007). Other authors (e.g., Zulauf et al. 1999, Dörr et al. 2002), however, rather interpret the Neoproterozoic basement in terms of an Andean-type active continental margin, whereas the Teplá-Barrandian unit belonged to Gondwana during the Late Neoproterozoic.

The new geochemical and isotope data indicate a mixed source for all sampled siliciclastic rocks of Late Neoproterozoic age. The geochemical compositions reveal a low degree of chemical weathering, i.e., mechanical breakdown of the source lithologies and fast transport of the detritus to the place of deposition. Furthermore major and trace element data prove distinct input from rather primitive igneous sources that were most probably represented by island arc complexes. Nevertheless, subordinately varying contributions from crustal sources were detected, too (cf., Jakeš et al. 1979). The results of U-Pb detrital zircon dating suggest an affinity of the Teplá-Barrandian unit with the Cadomian terranes and the Pan-African Trans-Saharan orogen. Nd-Sr-Pb whole rock isotope data are quite variable for the siliciclastics of the Blovice Formation (lower part of the Neoproterozoic succession) but rather homogenous for the samples from the Štěchovice Group (upper part of the Neoproterozoic succession). Considerable input from old continental crust is, however, indicated for both lithostratigraphic units and substantiated by the spectra of U-Pb ages of detrital zircon. Assuming a back-arc position of the basin(s) (e.g., Cháb 1993, Kříbek et al. 2000; and references therein), these signatures are in contrast to the indication of an intra-oceanic setting obtained from geochemical and isotope data of volcanic rocks of the Blovice Formation and the older part of the Davle Formation (e.g., Waldhausrová 1997b, Kříbek et al. 2000, Pin & Waldhausrová 2007).

Among the analysed rocks of different stratigraphic and structural position three groups were recognised. The siliciclastic rocks of the Blovice Formation (= lower part of the Teplá-Barrandian Neoproterozoic succession) may be subdivided into two groups and correspond to an older stage of development:

1) Of all analysed samples, BL01 and BL from the Blovice area (Blovice Formation sensu Mašek 2000) yielded the least radiogenic εNd_{590} value (-11.9) associated with the oldest crustal residence age (2.2 Ga). U-Pb analyses of detrital zircon revealed a considerable proportion of Palaeoproterozoic and Archean ages (~38% of the analysed grains), but show a lack in Mesoproterozoic and pristine Archean zircon, which indicates a relation of the source with the Trans-Saharan mobile belt. The detrital sediments having a maximum sedimentation age of 592±4 Ma are compositionally and texturally immature. They are associated with tholeiitic and alkaline volcanics (Waldhausrová 1997b) as well as with volcanite-hosted cherts (Buschmann 1995). Holubec (1995) concluded from the relatively weak inner deformation of the rocks and the occurrence of primary caldera-like volcanic bodies that the Blovice Formation in the area around the community Blovice was deposited on an older crystalline basement. Furthermore there are indications of temporary subaerial and shallow marine conditions, such as thick pyroclastic deposits, the occurrence of stratovolcanoes, sabkha-type sediments with replacements after anhydrite and stromatolite-like cherts (Kříbek et al. 2000; and references therein). It is, therefore, very likely that this part of the Blovice Formation (Fig. 2.4B, D) reflects a stage of extension

at the Gondwanan margin that eventually led to the opening of a marginal basin. This is in accordance with the geotectonic model of Linnemann et al. (2007), who proposed back-arc extension from ~590 Ma. The source of the siliciclastic material may have been represented by the magmatic arc that developed on NW-African continental crust in front of the basin or by the Trans-Saharan mobile belt behind the basin. Also the latter source is composed of rocks with suitable geochemical and isotopic compositions and involves both Neoproterozoic rocks that originated during various extensional and collisional processes and Archean-Palaeoproterozoic terranes (e.g., Black et al. 1994, Villeneuve and Cornée 1994, Caby 1996, Dostal et al. 2002, Liégeois et al. 2003). Since the frequency distribution pattern of the detrital zircon ages in Fig. 8.1 reveals that the most pronounced maximum at ~635 Ma is >40 m.y. older than the maximum sedimentation age, which is not in good agreement with derivation of the zircon from an active magmatic arc, the siliciclastics are here interpreted to represent recycled Pan-African lithologies deposited at the continent-ward margin of an incipient marginal basin. For the time interval ~625-580 Ma transcurrent movements along roughly N-S-trending major faults (present coordinates) were reported from the Central Saharan Tuareg Shield (Black et al. 1994). Such a fault pattern and a presumably pronounced morphology allow fast transport of fresh detritus to the marginal basin and are in agreement with the relatively low CIA values of the analysed samples. The identification of metamorphic heavy minerals and metamorphic rock fragments within siliciclastics of similar stratigraphic and structural position (Cháb & Pelc 1968, and references therein) supports this option. Alternatively the detritus may have been derived from complexes of an earlier arc stage (prior to back-arc extension when subduction occurred directly beneath the continent) now underlying this part of the basin. This was suggested by Linnemann et al. (2007) for a Neoproterozoic passive margin deposit from the neighbouring Saxothuringian zone. These rocks yielded a detrital zircon spectrum similar to that of sample BL.

2) Samples DB1/1 and DB1/2 taken for whole rock Nd-Sr-Pb isotope analyses were collected from the Blovice Formation sensu Mašek (2000), too, but are assigned to a different unit/facies than samples BL and BL01 in other lithostratigraphic concepts[1]. They have somewhat more radiogenic Nd isotope signatures (εNd_{590} -6.6 and -3.6, T_{DM} 1.8 and 1.5 Ga) than sample BL01, which, nevertheless, point to distinct input from old crustal sources. Unfortunately detrital zircon data of these rocks are not available yet. However, εNd_{600} of -3.0 to -0.1 and T_{DM} of 1.5 to 1.1 Ga obtained by Pin & Waldhausrová (2007) from two greywackes and one black shale of similar stratigraphic and structural position confirm varying input from old crustal sources. The siliciclastics are associated with basalts of the Radnice-Kralupy volcanic belt that was interpreted to correspond to an ancient spreading centre (e.g., Chaloupský et al. 1995, and references therein). Recently obtained geochemical and Nd isotope data of the basalts do not show indications of crustal contamination but are in agreement with generation in an intra-oceanic back arc basin at 605±39 Ma (Sm-Nd isochron age, uncertainty at 95% confidence level; Pin & Waldhausrová 2007). Similar contrasting information of intra-oceanic setting vs. continental crust involvement obtained from volcanic and sedimentary rocks was recognised in the Iberian Ossa-Morena zone, where a sedimentary passive margin sequence derived from a very mature source (Montemolín Formation) forms the immediate basement of a magmatic arc complex (San Jerónimo Formation). Although geochemical and Nd isotope data of arc andesites do not show evidence for significant interaction with continental crust during ascent of the melts, associated detrital

[1] Samples BL01 and BL were collected from a NE-SW trending unit - Rabštejn-Úslava Group of Holubec (1995), monotonous facies of Cháb & Pelc (1968), or the Blovice microsegment of Röhlich (2000) – that is separated from the north-westerly adjoining unit – the Zvíkovec Group of Holubec (1995), the volcanogenic facies of Cháb & Pelc (1968), or West Bohemian microsegment of Röhlich (2000). Samples DB1/1 and DB1/2 were taken from the latter unit/facies. The nature of the boundary is still under debate. Both units are, however, assigned to the Blovice Formation in the lithostratigraphic scheme of Mašek (2000). For a comparison of the different lithostratigraphic concepts see Fig. 2.4 in chapter 2.

sediments gave εNd_{550} of -5.0 to -2.5 and two-stage model ages of 1.3 to 1.6 Ga, clearly indicating involvement of an old crustal component (Pin et al. 2002, Quesada 2006). The succession was eventually interpreted to represent a magmatic arc that developed on continental crust (Quesada 2006, Pin & Waldhausrová 2007). In analogy, the analysed siliciclastics of the Teplá-Barrandian unit represented by samples DB may be interpreted to be derived from the continental magmatic arc in front of the marginal basin and were deposited on newly formed oceanic crust. The relation of these rocks with the adjacent volcano-sedimentary complex in the SE (samples BL and BL01) is uncertain. Either both units were deposited in the same basin but in different temporal and/or spatial positions or they represent fillings of different basins that were juxtaposed by latest Neoproterozoic strike-slip movements.

Assuming that the initial spatial relationships are more or less preserved, the NW unit from which samples DB were collected represents the filling of a back-arc basin that was floored by oceanic crust and the SE complex represented by samples BL was proximal to the continent and deposited on an older crystalline basement. The relation of both units with the Davle Formation (not examined in this study) that crops out in the southeasternmost part of the Teplá-Barrandian unit is not quite clear, too. The magmatic rocks of the Davle Formation were interpreted to represent a Neoproterozoic magmatic arc (Waldhausrová 1984). Both the nature of the boundary of the Davle Formation with the Blovice Formation and the ranges of the absolute ages of both lithostratigraphic units are not well constrained (e.g., Röhlich, 2000). Chaloupský et al. (1995) suggested that the Blovice and Davle formations formed – at least partly – contemporaneously. In case of preservation of the initial spatial relationships the Davle Formation should represent the early arc stage sensu Linnemann et al. (2007) that evolved during roughly S-directed (present coordinates) subduction beneath Gondwanan continental crust. Though in agreement with interpreting these rocks as part of an Andean-type Gondwana margin, Dörr et al. (2002) suggested activity of this arc between ~585 and 565 Ma due to zircon ages from rhyolite pebbles of the overlying Štěchovice Group. In a third concept it is assumed that the magmatic rocks of the Davle Formation represent an intra-oceanic island arc that developed during NW-directed (present coordinates) subduction beneath Teplá-Barrandian crust (Kříbek et al. 2000). This controversy shows that U-Pb zircon and whole rock isotope studies of the magmatic complexes of the Davle Formation would be crucial for the understanding of the Neoproterozoic basement of the Teplá-Barrandian unit.

The top of the Davle Formation is represented by black shales (Lečice Member) and conformably overlain by laminites of the lowermost Štěchovice Group. These sediments are considered to reflect cessation of the arc activity and deposition under calm, hemipelagic conditions (Cháb 1993).

3) The youngest siliciclastic rocks of the Neoproterozoic basement are represented by shale-siltstone-greywacke alternations of the Štěchovice Group. LA-ICP-MS U-Pb ages of detrital zircon provide a maximum sedimentation age of 565±5 for these rocks. The samples from the Štěchovice Group cluster in close ranges with regard to their geochemical and whole rock Nd-Sr-Pb isotope compositions, respectively. Homogenous, relatively unradiogenic εNd_{570} of -7.2 to -5.5 and associated old T_{DM} of 1.7 to 1.6 Ga in combination with the prevalence of greywacke boulders and pebbles within the conglomerates in the middle part of the Štěchovice Group (Klápová & Hyršl 2000, and references therein) indicate that recycling of previously deposited, immature, detrital sediments played a major role for the provenance of the Štěchovice Group siliciclastics. The proportion of Archean and Palaeoproterozoic detrital zircon ages (~21%) is lower than in sample BL from the Blovice Formation and pre-592 Ma (= maximum sedimentation age of sample BL) Neoproterozoic ages show a maximum at ~600–630 Ma (~30%) that is distinctly younger than the maxima of sample BL (630–670 Ma; Fig. 8.1). Additionally to the sedimentary source, young igneous rocks must have contributed to the composition of the Štěchovice Group siliciclastics as is clear from pebbles of volcaniclastic and igneous rocks (Chlupáč 1993, Klápová &

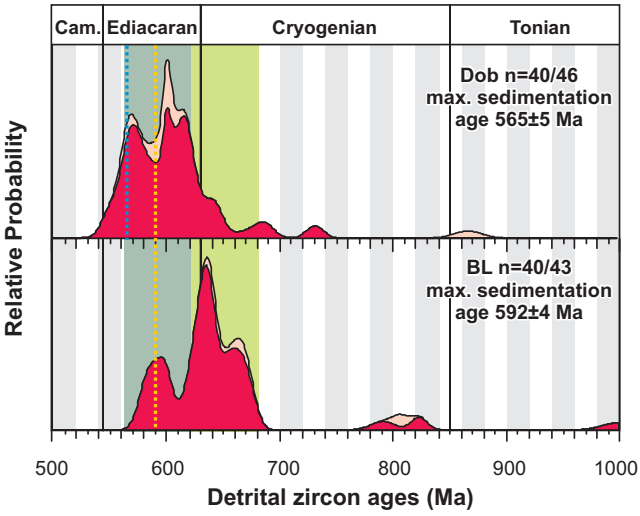

Fig. 8.1: Relative probability plots comparing Neoproterozoic detrital zircon ages of samples BL (Kralupy-Zbraslav Group) and Dob (Štěchovice Group). Red graph represents $^{206}Pb/^{238}U$ ages of analyses that are ≤10% discordant, light graph includes all analyses. Blue line marks the maximum sedimentation age of sample Dob, yellow line that of sample BL.

Abb. 8.1: Plot der reltiven Wahrscheinlichkeit, welcher die neoproterozoischen detritischen Zirkonalter der Proben BL (Kralupy-Zbraslav Group) und Dob (Štěchovice Group) vergleicht. Die roten Kurven zeigen die $^{206}Pb/^{238}U$-Alter der Analysen mit ≤10% Diskordanz. Die hellen Kurven schließen alle Analysen ein. Die blaue Line markiert das maximale Sedimentationsalter von Probe Dob, die gelbe das von Probe BL.

Hyršl 2000, Dörr et al. 2002; and references therein) and the high frequency of Ediacaran detrital zircon (~68%, this study). Furthermore, thin and scarce layers of tuffs and tuffites within the Štěchovice Group report persisting but distant volcanic activity (Cháb 1993). The difference in the detrital zircon age spectra between the sample from the Blovice Formation and the sample from the Štěchovice Group implies that siliciclastics such as those represented by sample BL can neither be considered as a suitable source for the sediments of the Štěchovice Group nor are both units derived from the same, but progressively developping, source. Therefore, it is tentatively assumed that the former unit is made up by detritus derived from Gondwana (roughly to the S of the present Teplá-Barrandian unit), whilst the siliciclastic material composing the Štěchovice Group was delivered by the Cadomian magmatic arc (roughly to the N). The latter is in agreement with NE-SW current direction indicated by sedimentary structures in greywacke layers (references in Chlupáč 1993).

Detrital zircon from the Štěchovice Group indicates Neoproterozoic sedimentation until at least ~565 Ma (this study; Dörr et al. 2002, Drost et al. 2004). In the Saxothuringian zone, dissected continental arc derived siliciclastics of similar age are partly associated with volcanics of varying geochemical compositions and volcanite-hosted cherts. These complexes were interpreted as submarine pull-apart basins floored with oceanic crust and controlled by strike-slip faulting (Buschmann 1995, Buschmann et al. 2001). Detrital zircon ages of these siliciclastics (Linnemann et al. 2007) are similar to those obtained for sample Dob of the Teplá-Barrandian Štěchovice Group. Therefore, the age of ~565 Ma can also be taken as an estimate for the onset of basin inversion in the present Teplá-Barrandian unit. Younger sedimentary rocks are not present or have not been identified so far, which is in contrast to the neighbouring Saxothuringian zone, where Latest Neoproterozoic/Earliest Cambrian siliciclastics (543±4 Ma) exist (Linnemann et al. 2007).

New geochemical and geochronological data from eclogites, high-pressure granulites and amphibolites of the Mariánské Lázně complex (MLC) and the structurally overlying Teplá Crystalline Complex (TCC) in the NW of the Teplá-Barrandian unit indicate a stage of S-directed subduction of late Cadomian ocean floor of the MLC beneath the Teplá-Barrandian unit that gave rise to juxtaposition of the MLC with high-pressure granulites of Teplá-Barrandian lowest crust (Timmermann et al. 2004, 2006). Štědrá et al. (2002) suggested from structural and geochemical data that the high-grade metamorphic rocks of the MLC/TCC area may represent parts of an accretionary wedge or a part of a subducted marginal basin. These units reflect the latest stage of Neoproterozoic convergence in the Teplá-Barrandian unit, which occurred largely contemporaneously with the peak of an LP-HT metamorphic event that occurred at ca. 550-540 Ma and was looked upon as arc-continent collision followed by slab breakoff with associated increase in heat flow (Zulauf et al. 1999).

Intrusions emplaced within the Cadomian basement of the Teplá-Barrandian unit during trans-

tensional movements at 524 Ma and later, postdate the deposition of Cadomian volcano-sedimentary successions and indicate that the change of the geotectonic regime from subduction to transtension/rifting was initiated prior to 524 Ma (Zulauf et al. 1997b, Dörr et al. 1998, 2002).

8.3 Cambrian

Cambrian sedimentation in the Teplá-Barrandian unit started at c. 530 Ma as is indicated by the concordia age obtained from the youngest detrital zircon grains of the basal Žitec-Hluboš Formation. Neoproterozoic detrital zircon ages are similar to those of the sample from the Štěchovice Group (Fig. 8-2). Due to the clast spectra being dominated by greywacke fragments in the Neoproterozoic Štěchovice Group but variegated in the Lower Cambrian Žitec-Hluboš Formation, redeposition of the former sediments is ruled out. The source rocks of the Žitec-Hluboš Formation sandstones and conglomerates are rather represented by the same ultimate source - the Cadomian magmatic arc. Sedimentological studies of Kukal (1971) showed that transport directions of the material making up the Cambrian deposits were approximately to the E and S, which is in agreement with a location of the Cadomian magmatic arc roughly to the NW of the present Teplá-Barrandian unit. The petrographic and geochemical compositions of the Cambrian siliciclastic rocks suggest a rift-related depositional setting. Stable clasts, derived from pre-rift sedimentary and crystalline rocks, are mixed with unstable clasts, chiefly supplied by syn-rift magmatic suites, in highly variable proportions. Nd and Sr isotope signatures clearly identify a source that includes young, primitive, mantle-derived magmatic rocks. In contrast, Pb isotope compositions of the Lower Cambrian samples point to additional involvement of old crustal sources. During deposition of the Middle Cambrian marine sequence this source was, however, not available anymore. U-Pb detrital zircon ages of 3 Cambrian samples substantiate the results obtained from geochemical and whole rock isotope data. The sample taken from the basal Žitec-Hluboš Formation yielded ~35% pre-Neoproterozoic grains confirming the presence of an old crustal source. However, the detrital zircon age spectra of the Cambrian samples show a distinct decrease in pre-Neoproterozoic and Neoproterozoic detritus in combination with a drastic increase in Cambrian ages from the oldest (~530 Ma) to the youngest (~505 Ma) sample. This progressive change in provenance in combination with the results of the whole rock analyses suggests extension associated with volcanism as well as with block tilting and accompanied change of the drainage system.

Plutons emplaced within the Neoproterozoic complexes to the W and NW of the Palaeozoic deposits include gabbros, tonalites, trondjemites, granodiorites, and granites with ages between 524 and 505 Ma (Zulauf et al. 1997a; Dörr et al. 1998, 2002; Venera et al. 2000). These rocks or their extrusive equivalents, respectively, represent suitable sources for the young igneous component detected in the Cambrian detrital sediments. Three of eight dated plutons with Lower to Middle Cambrian emplacement ages yielded inherited zircon with Neoproterozoic (~650 Ma; Pb-Pb single zircon evaporation; Venera et al. 2000) and Palaeoproterozoic (~2.0-2.1 Ga, U-Pb ID-TIMS, upper intercepts; Zulauf et al. 1997a, Dörr et al. 2002) ages. The occurrence of inherited zircon with Palaeoproterozoic age may be interpreted by derivation of these melts from an older crystalline basement with respective ages. However, the findings of inherited zircon in Cambrian magmatic rocks are rare and detrital zircon data of two Middle Cambrian sandstone samples (CB3 and Oh3) show frequent or dominating (36% and 58%) Cambrian ages that correspond to the age of the synsedimentary magmatism, but low (10%) or very low (3%) proportions of pre-Neoproterozoic ages, respectively. In case of a continuous old continental basement beneath the volcano-sedimentary complexes a higher proportion of inheritance may be expected. Therefore, large parts of the Teplá-Barrandian unit should be underlain by rather young, isotopically immature crust that was associated with detrital sedimentary material derived from a source including rocks of different age.

Volcanics of Upper Cambrian age occurring above Neoproterozoic rocks or Cambrian strata range from basaltic andesites to rhyolites (this study; Waldhausrová 1971) and represent the continuation of the Lower and Middle Cambrian magmatism. Rather mafic extrusives represent continental tholeiites. More silicic melts were derived from various sources (cf., Pin et al. 2007). U-Pb SHRIMP dating of zircon from a rhyolite gave an age of 499±4 Ma and revealed one inherited age of 544±14 Ma. The Upper Cambrian volcanic rocks analysed in this study (geochemistry), by Vidal et al. (1975; Sr isotopes) and by Pin et al. (2007; geochemistry and Nd isotopes) do not show indications of significant involvement of old crustal material, neither by melting of such a source nor by contamination of the ascending melts. Thus, these melts have originated from mantle sources and from the lower continental crust, whereas the latter was represented by young, primitive crust plus sedimentary material that were accreted to the Gondwanan margin during Late Neoproterozoic to earliest Cambrian Cadomian orogenic processes.

Magmatism of similar age was also reported from the NW part of the Teplá-Barrandian unit, where gabbros of within-plate basalt geochemistries intruded the MLC at ≤500 Ma and caused monazite growth in the structurally overlying TCC (Bowes & Aftalion 1993, Timmermann et al. 2004, 2006 and references therein). In the TCC rather felsic magmatism of similar age was observed (Dörr et al. 1998, Timmermann et al. 2006).

During the Cambrian, peri-Gondwana underwent an extensional stage commonly associated with block tilting and magmatism (e.g., Jonas et al. 2000, Kemnitz et al. 2002, Kryza & Pin 2002, Sánchez-García et al. 2003, Silva & Pereira 2004, Pin et al. 2007). Sedimentation was largely controlled by tectonic and magmatic activity, which is expressed by extension-related deformational structures, common distribution/preservation of Cambrian deposits in rather isolated basins/basin fragments, witnesses of extension-related magmatism, and a widespread erosional stage during the Upper Cambrian (e.g., Buschmann 1995, Linnemann 2003, Murphy et al. 2004b, Pereira et al. 2006, Buschmann et al. 2006). Although the Lower Cambrian strata of the Teplá-Barrandian unit were largely deposited in continental environments, while those of other peri-Gondwanan terranes are rather marine, there is a strong correspondence with the Cambrian record of the Ossa-Morena Zone[1] (Iberian Massif) and the Saxothuringian Zone[2] (Bohemian Massif).

The Cambrian rifting event is interpreted to be the result of ridge-trench collision, propagation of the MOR into the continental margin and opening of transform linked pull-apart basins that matured into

[1] In the Ossa-Morena Zone, thick rift-related successions unconformably overlie Cadomian basement and include the Lower and Upper Detrital Formations, the intervening Carbonate Formation, volcanics, and volcaniclastics. Cambrian sedimentation started prior to the onset of the Early Igneous Event - that was dated at 530±5 Ma (U-Pb zircon) - and was related to core complex development with associated migmatite formation. The bimodal Main Igneous Event occurred at 517-502 Ma (U-Pb zircon) and is represented by voluminous, chiefly tholeiitic - but also alkaline and calk-alkaline - melts that originated from various sources and were emplaced in upper crustal environments (Sánchez-García et al. 2003, 2006). Likewise, U-Pb SHRIMP data from felsic orthogneisses of the Évora Massif gave Cambrian protolith ages of 527±10, 524±6, 517±6, 505±5 Ma. Among all analyses only one has revealed a Palaeoproterozoic core with an age of 2.0 Ga (Chichorro et al. 2006), which is similar to the Cambrian magmatism in the Teplá-Barrandian unit (see above). Even the Upper Cambrian gap in sedimentation that occurs in the Teplá-Barrandian unit corresponds to a period of erosion/non-deposition in the Ossa-Morena zone (Quesada 2006). Etxebarria et al. (2006) assign the ~530 Ma to ~470 Ma record of the Ossa-Morena zone to the formation of a passive, but volcanically active, margin in northern Gondwana.

[2] Lower Cambrian (~520 Ma) sediments of the Saxothuringian Zone lie unconformably on Neoproterozoic basement (Buschmann et al. 2006). Thick Lower Cambrian carbonaceous and Middle Cambrian siliciclastic sediments yielded faunal assemblages of West Gondwanan affinity and - in combination with palaeontological data from other peri-Gondwanan terranes - report lively faunal exchange between the peri-Gondwanan basins (Elicki & Wotte 2003, Buschmann et al. 2006). The occurrence of Lower Cambrian extension-related volcanics in combination with lithofacies data and structural evidence was interpreted to reflect a transtensional setting on thinned continental crust (Jonas et al. 2000). As well in the Saxothuringian zone the Upper Cambrian is largely characterised by erosion (Linnemann et al. 2000). Only the Vesser complex to the NW of the Saxothuringian zone contains Middle to Upper Cambrian magmatic rocks with MORB affinity and metasedimentary rocks (Kemnitz et al. 2002, Linnemann et al. 2007).

oceanic spreading centres (Murphy et al. 1999, Nance et al. 2002, Keppie et al. 2003). In recent publications, the Cambrian rifting event is considered to represent the birth of the Rheic Ocean (e.g., Robardet et al. 1990, Sánchez-García et al. 2003, Murphy et al. 2006, Linnemann et al. 2007, Pin et al. 2007). Murphy et al. (2006) suggest that rifting of Avalonia and Carolina from other peri-Gondwanan terranes and Gondwana took place along lithospheric structures that were inherited from Neoproterozoic processes and, thus, led to opening of the Rheic Ocean near the suture zone between Neoproterozoic accreted terranes and cratonic Northern Gondwana.

8.4 Ordovician

A major transgression in the Tremadoc initiated another period of marine sedimentation in the Teplá-Barrandian unit. Similarly, an Early (to Middle) Ordovician transgression is traceable over North Africa and the Arabian plate (e.g., Carr 2002) and recognisable within other peri-Gondwanan regions, such as the Saxothuringian Zone of the Bohemian Massif, the Ossa-Morena and Central Iberian zones of the Iberian Massif, the Northern Armorican Massif, and the Moroccan Anti-Atlas (e.g., Beetsma 1995, Linnemann & Buschmann 1995, Waters & Schofield 2004, Quesada 2006). Although not synchronous in the Gondwanan and peri-Gondwanan realm but controlled by local tectonic conditions, this transgression led to widespread Lower and Middle Ordovician siliciclastic deposits.

Initially, Ordovician sedimentation in the Teplá-Barrandian was largely controlled by volcanic activity. Post-magmatic fluids related to the vanishing Upper Cambrian magmatism modified the chemical compositions of siliciclastics from several localities and led to silicification of sandstones and shales of the Třenice and Klabava formations (Lower Ordovician). Fluid activity of Lower Ordovician age is also known from the W part of the Teplá-Barrandian unit and from the Zone of Erbendorf-Vohenstrauss, where it was accompanied with emplacement of pegmatites at c. 487–475 Ma (Glodny et al. 1998).

Lower Ordovician sediments display a volcanic rifted margin provenance. Detritus is derived from reworking of Cambrian volcanics and intensely weathered Neoproterozoic rocks as is indicated by the clast inventory of conglomeratic rocks and detrital zircon age spectra. In comparison to the Cambrian sandstones the sample from the Lower Ordovician Třenice Formation shows a higher proportion of >620 Ma Neoproterozoic detrital zircon ages (Fig. 8.2), which may be taken as the first indicator of a change in the general provenance. This is confirmed by whole rock Nd-Sr-Pb isotope signatures of a shale sample from the overlying Klabava Formation and by detrital zircon age spectra as well as Nd-Sr-Pb isotope signatures of Upper Ordovician siliciclastics, which all show a distinct increase in the proportion of old crustal detritus when compared to the compositions of Cambrian siliciclastics. Trace element data acquired for Ordovician shales, siltstones and sandstones point to a rather felsic provenance, which is in contrast to the rather mafic provenance indicated by the geochemical compositions of the Cambrian detrital sediments. That is, magmatic arc derived detritus that essentially contributed to the composition of the Cambrian detrital sediments is not available anymore. Instead the source of the Ordovician siliciclastics is represented by the NW African proportion of Gondwana. From the Middle Ordovician sediments were chiefly deposited in passive margin shelf environments. Highly mature sediments indicate intense chemical weathering and redeposition processes.

In the Late Lower or Early Middle Ordovician a period of alkaline magmatism started in the Teplá-Barrandian unit. Geochemical compositions of the volcanics are distinctly different from those of the Upper Cambrian volcanic stage and resemble alkaline within-plate basalts that originated from low degrees of partial melting of a relatively shallow garnet peridotite mantle source. Among other arguments, the fact that such intra-plate volcanism in the Teplá-Barrandian unit was not restricted to the Ordovician but occurred episodically until the Devonian, suggests that melt generation was not rift-related. Fairhead & Wilson (2004) proposed a mechanism for formation of volcanic lines/aseismic ridges such as Rio Grande

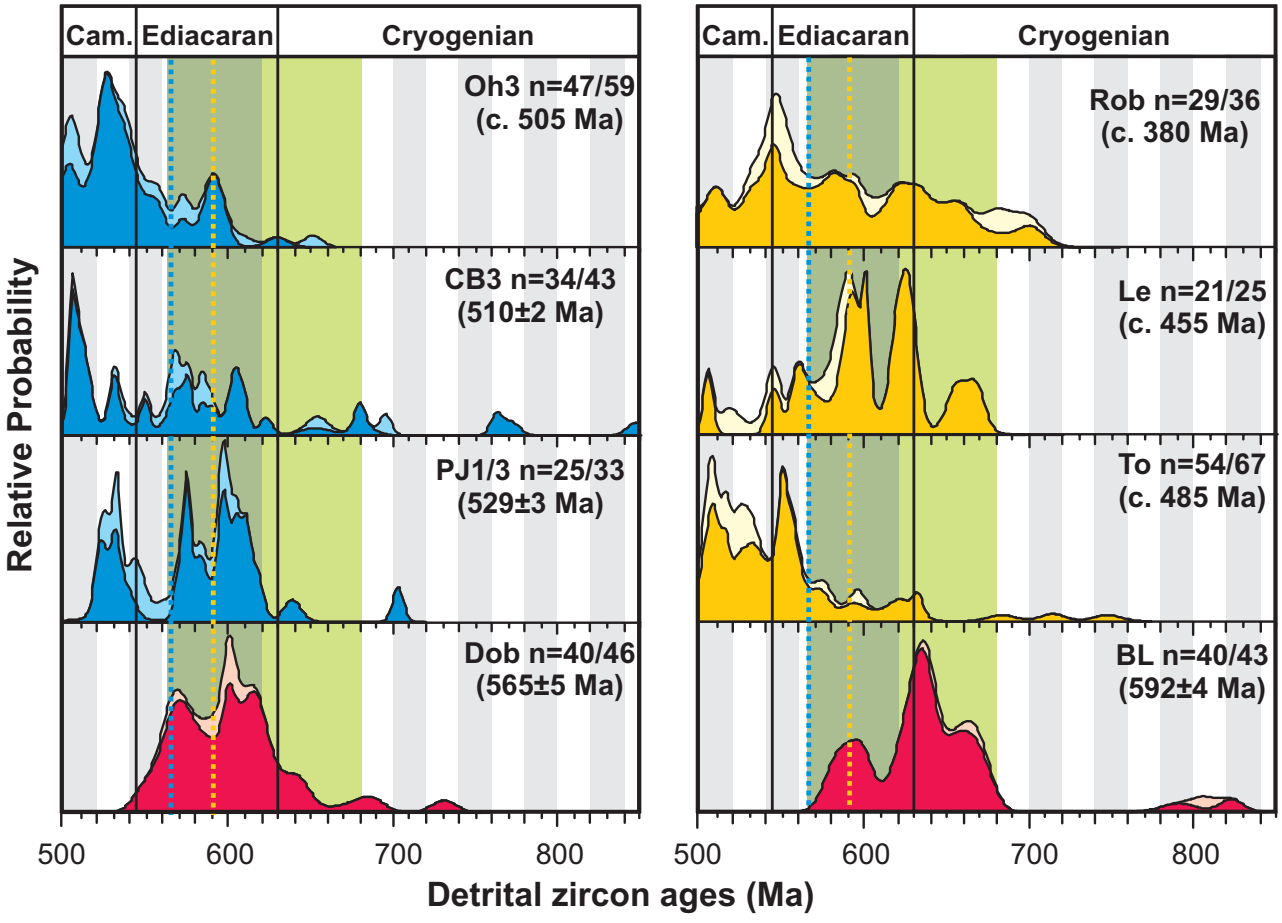

Fig. 8.2: Comparison of Late Neoproterozoic detrital zircon ages of the Palaeozoic samples with those of Neoproterozoic samples. Sample Dob (bottom left) from the ~565 Ma old (blue dotted line) Štěchovice Group is thought to be a good estimate for the Cadomian magmatic arc provenance. Zircon data from the Cambrian samples (blue graphs in the left column) resemble this age pattern very well, i.e. show maxima at c. 560–580 Ma and ca. 600–620 Ma as well as a minimum at ~590 Ma. The pattern of sample BL of the Blovice Formation (bottom right) represents the age spectrum that was available from Gondwanan sources at ~590 Ma (yellow dotted line). Although not unambiguous, because of the short section and the small number of comparable ages (>590 Ma), the Ordovician sandstones and the Devonian greywacke (yellow graphs in right column) tend to resemble the pattern of sample BL, i.e. show characteristic maxima at c. 580–600 Ma, 620–640 Ma and 660 Ma and a distinct minimum at ~610 Ma.

Abb. 8.2: Vergleich der spätneoproterozoischen Zirkonalter der paläozoischen Proben mit denen der neoproterozoischen Proben. Probe Dob (links unten) aus der ~565 Ma alten (blaue Linie) Štěchovice Group repräsentiert höchstwahrscheinlich einen guten Durchschnitt des cadomischen magmatischen Bogens. Die detritschen Zirkonalter der kambrischen Proben (blaue Kurven in der linken Spalte) ähneln diesem Altersverteilungsmuster stark, d. h. sie zeigen Maxima bei ca. 560–580 Ma und 600–620 Ma sowie ein Minimum bei ~590 Ma. Das Muster von Probe BL aus der Blovice Formation (unten rechts) repräsentiert das Altersspektrum, welches bei ~590 Ma (gelbe Linie) von Gondwana bereitgestellt werden konnte. Obwohl nicht ganz eindeutig, da der vergleichbare Zeitabschnitt relativ kurz ist und die Alter daraus (>590 Ma) nicht besonders zahlreich, tendieren die ordovizischen Sandsteine und die devonische Grauwacke dazu, das Muster von Probe BL wiederzuspiegeln, d.h. sie zeigen charakteristische Maxima bei ca. 580–600 Ma, 620–640 Ma und 660 Ma sowie ein deutliches Minimum bei ~610 Ma.

Rise, Walvis Ridge or Cameroon Volcanic Line in the recent South Atlantic Ocean. The CVL even extents into African continental crust and may, therefore, represent a modern analogue of the Ordovician to Devonian volcanic record of the Teplá-Barrandian unit. Fairhead & Wilson (2004) relate the volcanic

chains extending from the Mid Atlantic Ridge to South America and Africa, respectively, to fractures within the lithosphere that form in response to plate interactions elsewhere on the globe (e.g., consumption of oceanic crust resulting in continental collision) and require global adjustments in absolute plate motions. Episodic reactivation of these fractures - in response to global plate dynamics – give rise to development of long-lived volcanic lineaments. Similarly, the huge extent of Gondwana required differential response to such processes, whereas the mobile belts between the cratons are suitable for accommodation of adjusting movements and related alkaline magmatism. In the N African proportion of Gondwana repeated anorogenic, alkaline magmatism occurred in Hoggar since the late Neoproterozoic (Liégeois 2006). It may therefore be proposed that a fracture zone within Gondwanan lithosphere extended from the spreading centre of the Rheic Ocean via the Teplá-Barrandian unit close to the continental margin of Gondwana to the Trans-Saharan mobile belt.

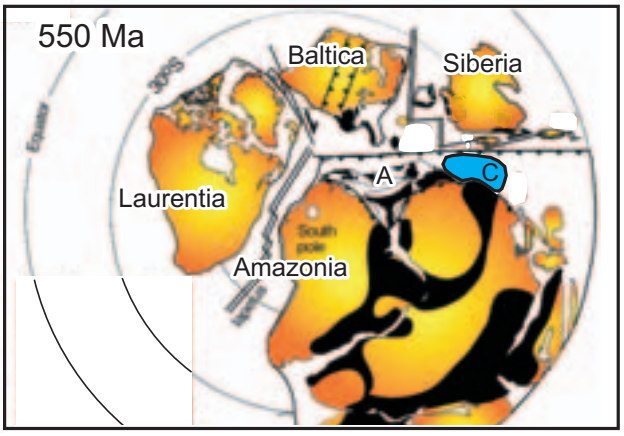

Fig. 8.3: Palaeogeographic reconstruction for the Latest Neoproterozoic showing Siberia and Baltica passing by Gondwana (after Hartz & Torsvik 2002). Late Neoproterozoic interior and peripheral orogens are shown in black, the Cadomian terranes (C) are highlighted in blue.

Abb. 8.3: Paläogeographische Rekonstruktion für das späte Neoproterozoikum, die Sibiria und Baltika zeigt, wie sie am Rand Gondwanas vorbeidriften (nach Hartz & Torsvik 2002). Spätneoproterozoische innere und periphere Orogene sind in schwarz dargestellt, die cadomischen Terrane in blau.

The Ordovician sedimentary record of the Teplá-Barrandian unit shows a clear affinity with the N African proportion of Gondwana and the Cadomian terranes as is clear from the siliciclastic nature of the sediments, faunal assemblages (e.g., Vavrdová 1974, Havlíček & Vaněk 1966, Havlíček & Fatka 1992, Štorch et al. 1993, Havlíček et al. 1994, Fatka 2003), age spectra of detrital zircon (this study), and the occurrence of a glaciomarine diamictite that corresponds to the Hirnantian glaciation (Brenchley & Štorch 1989). Therefore the Teplá-Barrandian unit represented at least until the end of the Ordovician – but probably during the entire pre-Variscan Paleozoic – a part of the southern margin of the Rheic Ocean.

8.5 Concluding remark

Though thick, magmatic arc derived siliciclastics representing the fillings of Neoproterozoic marginal basins are preserved in several units, fragments/slivers of both the largely continental magmatic arc and the Gondwanan continental margin are extremely scarce. In the Teplá-Barrandian unit a small complex – the magmatic rocks of the Davle Formation – was interpreted to represent remnants of a Neoproterozoic magmatic arc (Waldhausrová 1984, Dörr et al. 2002). The high-grade units of the Moldanubian zone obviously contain slivers of Palaeoproterozoic basement (2.0–2.1 Ga, Svetlík gneiss, Wendt et al. 1993) and Cadomian granitoids (c. 610 Ma, Spitz gneiss, Friedl et al. 2004) that are, however, not of large extend. Witnesses of a late Cadomian ~550 Ma magmatic event were identified in the Bavarian part of the Moldanubian zone (Teipel et al. 2004). Though the high-grade units of the Moldanubian zone and the Saxothuringian zone may contain magmatic arc complexes that have not been identified hitherto, the thick, arc derived, Neoproterozoic siliciclastics preserved in the very low-grade to high-grade units of the Bohemian Massif call for more extensive magmatic arc complexes. The continental arc, therefore, must have been removed from the Gondwanan

margin by the Cambro-Ordovician rifting event and the eventual opening of the Rheic Ocean between the back-arc complexes and the magmatic arc itself as postulated by Murphy et al. (2006). This, in turn, implies that the fragments rifting from Gondwana and then forming the N margin of the Rheic Ocean should be found somewhere along the Trans-European suture zone. Terranes with a suitable basement composition (Cadomian magmatic arc, NW African basement signatures) have, however, not been identified there. It is, therefore, possible that large parts of the "Bohemian" magmatic arc complexes were removed by and accreted to Baltica and/or Siberia during their movement along the Avalonian-Cadomian Gondwana margin in Late Neoproterozoic to Cambrian times (Fig. 8.3).

References

Abdelsalam, M. G.; Liégeois, J. P.; Stern, R. J. (2002): The Saharan Metacraton. – J. Afr. Earth Sci., **34**: 119–136.

Affaton, P.; Kröner, A.; Seddoh, K. F. (2000): Pan-African granulite formation in the Kabye Massif of northern Togo (West Africa): Pb-Pb zircon ages. – International Journal of Earth Sciences, **88**: 778–790.

Ahäll, K. I.; Cornell, D. H.; Armstrong, R. (1998): Ion probe zircon dating of metasedimentary units across the Skagerrak: new constraints for early Mesoproterozoic growth of the Baltic Shield. – Precambrian Research, **87**: 117–134.

Álvaro, J. J.; Elicki, O.; Geyer, G.; Rushton, A.; Shergold, J. (2003): Palaeogeographical controls on the Cambrian trilobite immigration and evolutionary patterns reported in the western Gondwana margin. – Palaeogeography, Palaeoclimatology, Palaeoecology, **195**: 5–35.

Andersen, T. (2002): Correction of common lead in U–Pb analyses that do not report ^{204}Pb. – Chem. Geol., **192**: 59–79.

Auvray, B.; Charlot, R.; Vidal, P. (1980): Donnes nouvelles sur le Proterozoique inferieur du domaine nord-Armoricain (France): age et signification. – Canadian Journal of Earth Sciences, **17**: 532–538.

Avigad, D.; Kolodner, K.; McWiliams, M.; Persing, H.; Weissbrod, T. (2003): Origin of northern Gondwana Cambrian sandstone revealed by detrital zircon SHRIMP dating. – Geology, **31**: (3), 227–230.

Azzouni-Sekkal, A.; Liégeois, J. P.; Bechiri-Benmerzoug, F.; Belaidi-Zinet, S.; Bonin, B. (2003): The "Taourirt" magmatic province, a marker of the closing stage of the Pan-African orogeny in the Tuareg Shield: review of available data and Sr-Nd isotope evidence. – Journal of African Earth Sciences, **37**: 331–350.

Bachtadse, V.; Briden, J. C. (1990): Palaeomagnetic constraints on the position of Gondwana during Ordovician to Devonian times. – In: McKerrow, W. S.; Scotese, C. R. (Eds.): Palaeogeography and biogeography. – Geological Society London Memoir, **12**: 43–48,

Bachtadse, V.; Schätz, M. R.; Zwing, A.; Tait, J. A.; Soffel, H. C. (1998): Paleogeography of the Paleozoic terranes in the Variscan and Alpine foldbelts. – Terra Nostra, **98**: (2), 12–15.

Barbey, P.; Oberli, F.; Burg, J.-P.; Nachit, H.; Pons, J.; Meier, M. (2004): The Palaeoproterozoic in western Anti-Atlas (Morocco): a clarification. – Journal of African Earth Sciences, **39**: 239–245.

Barth, M. G.; Rudnick, R. L.; Carlson, R. W.; Horn, I.; McDonough, W. F. (2002): Re-Os and U-Pb geochronological constraints on the eclogite-tonalite connection in the Archean Man Shield, West Africa. – Precambrian Research, **118**: 267–283.

Beetsma, J. J. (1995) The Late Proterozoic / Paleozoic and Hercynian crustal evolution of the Iberian Massif, N Portugal as traced by geochemistry and Sr-Nd-Pb isotope systematics of pre-Hercynian terrigenous sediments and Hercynian granitoids. – Dissertation thesis, Vrije Universiteit Amsterdam: 1–223, Amsterdam.

Bhatia, M. R. (1983): Plate tectonics and geochemical composition of sandstones. – The Journal of Geology, **91**: 611–627.

Bhatia, M. R. (1985): Rare earth element geochemistry of Australian Paleozoic graywackes and mudrocks: provenance and tectonic control. – Sedimentary Geology, **45**: 97–113.

Bhatia, M. R.; Crook, K. A. W. (1986): Trace element characteristics of graywackes and tectonic setting of sedimentary basins. – Contributions to Mineralogy and Petrology, **92**: 181–193.

Bingen, B.; Birkeland, A.; Nordgulen, Ø.; Sigmond, E. M. O. (2001): Correlation of supracrustal sequences and origin of terranes in the Sveconorwegian orogen of SW Scandinavia: SIMS data on zircon in clastic metasediments. – Precambrian Research, **108**: 293–318.

Bingen, B.; Nordgulen, Ø.; Sigmond, E. M. O.; Tucker, R.; Mansfeld, J.; Hogdahl, K. (2003): Relations between

1.19–1.13 Ga continental magmatism, sedimentation and metamorphism, Sveconorwegian province, S Norway. – Precambrian Research, **124**: 215–241.

Black, R.; Latouche, L.; Liégeois, J. P.; Caby, R.; Bertrand, J. M. (1994): Pan-African displaced terranes in the Tuareg shield (central Sahara). – Geology, **22**: (7), 641–644.

Bossière, G.; Bonkoungou, I.; Peucat, J. J.; Pupin, J. P. (1996): Origin and age of Paleoproterozoic conglomerates and sandstones of the Tarkwaian Group in Burkina Faso, West Africa. – Precambrian Research, **80**: (3–4), 153–172.

Boynton, W. V. (1984): Geochemistry of the rare earth elements: meteorite studies. – In Henderson, P. (Ed.): Rare earth element geochemistry: 63–114, Elsevier.

Brenchley, P. J.; Storch, P. (1989): Environmental changes in the Hirnantian (upper Ordovician) of the Prague Basin, Czechoslovakia. – Geological Journal, **24**: 165–181.

Bromley, R. G. (1999): Spurenfossilien: Biologie, Taphonomie und Anwendung: 1–347, Springer (Berlin, Heidelberg).

Buschmann, B. (1995): Geotectonic facies analysis of the Rothstein Formation (Neoproterozoic, Saxothuringian Zone, east Germany). – Unpublished dissertation thesis, TU Bergakademie Freiberg: 1–122, Freiberg.

Buschmann, B.; Elicki, O.; Jonas, P. (2006): The Cadomian unconformity in the Saxo-Thuringian Zone, Germany: Palaeogeographic affinities of Ediacaran (terminal Neoproterozoic) and Cambrian strata. – Precambrian Research, **147**: 387–403.

Buschmann, B.; Nasdala, L.; Jonas, P.; Linnemann, U.; Gehmlich, M. (2001): SHRIMP U-Pb dating of tuff-derived and detrital zircons from Cadomian marginal basin fragments (Neoproterozoic) in the northeastern Saxothuringian Zone (Germany). – N. Jb. Geol. Paläont. Mh., **2001**: (6), 321–342.

Caby, R. (1996): A review of the In Ouzzal granulitic terrane (Tuareg shield, Algeria): its significance within the Pan-African Trans-Saharan belt. – Journal of Metamorphic Geology, **14**: 659–666.

Caby, R. (2003): Terrane assembly and geodynamic evolution of central-western Hoggar: a synthesis. – Journal of African Earth Sciences, **37**: 133–159.

Carr, I. D. (2002): Second-order sequence stratigraphy of the Palaeozoic of North Africa. – Journal of Petroleum Geology, **25**: (3), 259–280.

Cháb, J. (1993): General problems of the TB (Teplá-Barrandian) Precambrian, Bohemian Massif, the Czech Republic. – Vìstník Èeského geologického ústavu, **68**: (4), 1–6.

Cháb, J.; Pelc, Z. (1968): Lithology of Upper Proterozoic in the NE limb of the Barrandian area. – Krystalinikum, **6**: 141–167.

Chaloupský, J.; Chlupáč, I.; Mašek, J.; Waldhausrová, J.; Cháb, J. (1995): VII.B.1 Stratigraphy. – In: Dallmeyer, R. D.; Franke, W.; Weber, K. (Eds.): Pre-Permian geology of central and eastern Europe: 379–391, Berlin (Springer).

Chichorro, M.; Pereira, M. F.; Williams, I.; Silva, J. B. (2006): SHRIMP U-Pb zircon geochronology of felsic of felsic orthogneisses from the Évora Massif: Lower-Middle Cambrian continental rift-related magmatism. – In: Pereira, M. F. & Quesada, C., (Eds.): Evora Meeting 2006. Ediacaran to Viséan crustal growth processes in the Ossa-Morena Zone (SW Iberia) – Conference Abstracts and Field Trip Guide: 13–14, Instituto Geológico y Minero de España (Madrid).

Chlupáč, I. (1993): Geology of the Barrandian – A field trip guide. – Senckenberg-Buch, **69**: 1–163, Frankfurt a. M. (Verlag W. Kramer).

Chlupáč, I. (1995): Lower Cambrian arthropods from the Paseky shale (Barrandian area, Czech Republic). – Journal of the Czech Geological society, **40**: (4), 9–36.

Chlupáč, I. (1998): Devonian. – In: Chlupáč, I.; Havlíček, V.; Kříž, J.; Kukal, Z.; Štorch, P. (Eds.): Palaeozoic of the Barrandian (Cambrian to Devonian). – 101–133, Praha (Czech Geological Survey).

Chlupáč, I.; Havlíček, V.; Kříž, J.; Kukal, Z.; Štorch, P. (1998): Palaeozoic of the Barrandian (Cambrian to Devonian). – 1–183, Prague (Czech Geological Survey).

Chlupáč, I.; Kukal, Z. (1988): Possible global events and the stratigraphy of the Paleozoic of the Barrandian (Cambrian – Middle Devonian, Czechoslovakia). – Sborník geologických věd, 43: (Geologie), 83–146.

Cocks, L. R. M. (2000): The Early Palaeozoic geography of Europe. – Journal of the Geological Society, London, **157**: 1–10.

Collins, A. S.; Buchan, C. (2004): Provenance and age constraints of the South Stack Group, Anglesey, UK: U–Pb SIMS detrital zircon data. – Journal of the Geological Society, London, **161**: (5), 743–746.

Compston, W.; Williams, I. S.; Meyer, C. (1984): U-Pb geochronology of zircons from lunar breccia 73217 using a sensitive high mass-resolution ion microprobe. – J. Geophys. Res., **89**: (Suppl.), B525–534.

Cullers, R. L.; Chaudhuri, S.; Arnold, B.; Lee, M.; Wolf, C. W. J. (1975): Rare earth distributions in clay minerals and in the clay-sized fraction of the Lower Permian Havensville and Eskridge shales of Kansas and Oklahoma. – Geochimica et Cosmochimica Acta, **39**: (12), 1691–1703.

Dallmeyer, R. D.; Franke W., Weber, K. (1995) (Eds.): Pre-Permian geology of Central and Eastern Europe: 1–604, Springer.

David, K.; Schiano, P.; Allegre, C. J. (2000): Assessment of the Zr/Hf fractionation in oceanic basalts and continental materials during petrogenetic processes. – Earth and Planetary Science Letters, 178: (3–4), 285–301.

De Bievre, P.; Taylor, P. D. P. (1993): Table of the isotopic compositions of the elements. – International Journal of Mass Spectrometry and Ion Processes, **123**: (2), 149–166.

DePaolo, D. J. (1988): Neodymium isotope geochemistry – An introduction. – 1–187, Berlin (Springer).

Dickinson, W. R. (1970): Interpreting detrital modes of graywacke and arkose. – Journal of Sedimentary Petrology, **40**: (2), 695–707.

Dickinson, W. R. (1985): Interpreting provenance relations from detrital modes of sandstones. – In: Zuffa, G. G. (Ed.): Provenance of Arenites. – 333–361, Dordrecht (D. Reidel Publishing Company).

Dickinson, W. R.; Suczek, C. A. (1979): Plate tectonics and sandstone compositions. – Am. Ass. Petr. Geol. Bulletin, **63**: 2164–2182.

Dickinson, W. R.; Valloni, R. (1980): Plate settings and provenance of sands in modern ocean basins. – Geology, **8**: 82–86.

Dörr, W.; Fiala, J.; Franke, W.; Haak, U.; Philippe, S.; Schastok, J.; Scheuvens, D.; Vejnar, Z.; Zulauf, G. (1998): Cambrian vs. Variscan tectonothermal evolution within the Teplá-Barrandian: evidence from U-Pb zircon ages of syn-tectonic plutons (Bohemian Massif, Czech Republic). – Acta Universitatis Carolinae – Geologica, **42**: (2), 229–230.

Dörr, W.; Zulauf, G.; Fiala, J.; Franke, W.; Vejnar, Z. (2002): Neoproterozoic to Early Cambrian history of an active plate margin in the Teplá-Barrandian unit – a correlation of U-Pb isotopic-dilution-TIMS ages (Bohemia, Czech Republic). – Tectonophysics, **352**: 65–85.

Dostal, J.; Caby, R.; Keppie, D. F.; Maza, M. (2002): Neoproterozoic magmatism in southwestern Algeria (Sebkha el Melah inlier): a northerly extension of the Trans-Saharan orogen. – Journal of African Earth Sciences, **35**: 213–225.

Dostal, J.; Vozár, J.; Keppie, J. D.; Hovorka, D. (2003): Permian volcanism in the Central Western Carpathians (Slovakia): Basin-and-Range type rifting in the southern Laurussian margin. – International Journal of Earth Sciences, **92**: (1), 27–35.

Doumbia, S.; Pouclet, A.; Kouamelan, A.; Peucat, J. J.; Vidal, M.; Delor, C. (1998): Petrogenesis of juvenile-type Birimian (Paleoproterozoic) granitoids in Central Cote-d'Ivoire, West Africa: geochemistry and geochronology. – Precambrian Research, **87**: (1–2), 33–63.

Drost, K.; Linnemann, U.; McNaughton, N.; Fatka, O.; Kraft, P.; Gehmlich, M.; Tonk, C.; Marek, J. (2004): New data on the Neoproterozoic – Cambrian geotectonic setting of the Teplá-Barrandian volcano-sedimentary successions: geochemistry, U-Pb zircon ages, and provenance (Bohemian Massif, Czech Republic). – International Journal of Earth Sciences, **93**: 742–757.

Drost, K.; Linnemann, U.; Wemmer, K.; Budil, P.; Kraft, P.; Fatka, O.; Marek, J. (2003): Provenance and early genetic processes of the Ordovician Sárka Formation at Praha – Cervený vrch Hill (Barrandian, Czech Republic). – Czech Geological Survey, Bulletin of Geosciences, **78**: (2), 147–156.

Dupuy, C.; Dostal, J. (1984): Trace element geochemistry of some continental tholeiites. – Earth and Planetary Science Letters, **67**: (1), 61–69.

Dupuy, C.; Liotard, J. M.; Dostal, J. (1992): Zr/Hf fractionation in intraplate basaltic rocks: Carbonate metasomatism in the mantle source. – Geochimica et Cosmochimica Acta, **56**: (6), 2417–2423.

Eby, G. N. (1992): Chemical subdivision of the A-type granitoids: Petrogeneric and tectonic implications. – Geology, **20**: 641–644.

Egal, E.; Thiéblemont, D.; Lahondère, D.; Guerrot, C.; Costea, C. A.; Iliescu, D.; Delor, C.; Goujou, J. C.; Lafon, J. M.; Tegyey, M.; Diaby, S.; Kolié, P. (2002): Late Eburnian granitization along the western and northwestern margin of the Archean Kénéma-Man domain (Guinea, West African Craton). – Precambrian Research, **117**: 57–84.

Elderfield, H.; Uppstill-Goddard, R.; Sholkovitz, E. R. (1990): The rare earth elements in rivers, estuaries, and coastal seas and their significance to the composition of ocean waters. – Geochimica et Cosmochimica Acta, **54**: (4), 971–991.

Elicki, O.; Wotte, T. (2003): Cambroclaves from the Cambrian of Sardinia (Italy) and Germany: constraints for the architecture of western Gondwana and the palaeogeographical and palaeoecological potential of cambroclaves. – Palaeogeography, Palaeoclimatology, Palaeoecology, **195**: 55–71.

Etxebarria, M.; Chalot-Prat, F.; Apraiz, A.; Eguiluz, L. (2006): Birth of a volcanic passive margin in Cambrian time: Rift paleogeography of the Ossa-Morena Zone, SW Spain. – Precambrian Research, **147**: (3–4), 366–386.

Fairhead, J. D.; Wilson, M. (2004) Sea-floor spreading and deformation processes in the South Atlantic Ocean: Are hot spots needed? – http://www.mantleplumes.org/SAtlantic.html.

Fatka, O. (2003): Organic-walled microfossils (Chitinozoa and Acritarcha) from Praha – Cervený vrch Hill (Šárka Formation, Middle Ordovician, Prague Basin). – Bulletin of Geosciences, **78**: (2), 119–127.

Fatka, O.; Frýda, J.; Kachlík, V.; Kraft, P.; Dolejš, D. (1998): Sedimentary and volcanic events in the Teplá-Barrandian crustal segment (Bohemia) as a response to dated intracrustal processes. – Schriftenreihe des Staatlichen Museums für Mineralogie und Geologie zu Dresden, **9**: 136–137.

Fatka, O. & Gabriel, Z. (1991): Microfossils from siliceous stromatolitic rocks of the Barrandian Proterozoic (Bohemian Massif). – Časopis pro mineralogii a geologii, **36**: 143–148.

Fedo, C. M.; Nesbitt, H. W.; Young, G. M. (1995): Unraveling the effects of potassium metasomatism in sedimentary rocks and paleosols, with implications for paleoweathering conditions and provenance. – Geology, **23**: (10), 921–924.

Fernández-Suárez, J.; Gutiérrez Alonso, G.; Cox, R.; Jenner, G. A. (2002a): Assembly of the Armorica Microplate: A strike-slip terrane delivery? Evidence from U-Pb ages of detrital zircons. – The Journal of Geology, **110**: 619–626.

Fernández-Suárez, J.; Gutiérrez Alonso, G.; Jeffries, T. E. (2002b): The importance of along-margin terrane transport in northern Gondwana: insights from detrital zircon parentage in Neoproterozoic rocks from Iberia and Brittany. – Earth and Planetary Science Letters, **204**: 75–88.

Fernández-Suárez, J.; Gutiérrez Alonso, G.; Jenner, G. A.; Tubrett, M. N. (1999): Crustal sources in Lower Paleozoic rocks from NW Iberia: insights from laser ablation U-Pb ages of detrital zircons. – Journal of the Geological Society of London, **156**: (6), 1065–1068.

Fernández-Suárez, J.; Gutiérrez Alonso, G.; Jenner, G. A.; Tubrett, M. N. (2000): New ideas on the Proterozoic-Early Palaeozoic evolution of NW Iberia: insights from U-Pb detrital zircon ages. – Precambrian Research, **102**: 185–206.

Fiala, F. (1971): Ordovician diabase volcanism and biotite lamprophyres of the Barrandian. – Sbor. geol. ved, Geologie, **19**: 7–97 (english summary).

Fiala, F. (1977): The Upper Proterozoic volcanism of the Barrandian area and the problem of spilites. – Sborník geologických ved, **30**: 1–247.

Fiala, F. (1978): The TiO_2-K_2O-P_2O_5 diagram and tectonomagmatic relations of the volcanics of the Barrandian area. – Vestník Ústredního Ústavu Geologického, **53**: 333–346.

Finger, F.; Hanžl, P.; Pin, C.; von Quadt, A.; Steyrer, H. P. (2000): The Brunovistulian: Avalonian Precambrian sequence at the eastern end of the Central European Variscides. – In: Franke, W.; Haak, U.; Oncken, O.; Tanner, D. (Eds.): Orogenic processes: quantification and modelling in the Variscan belt. – Geological Society London, Special Publication, **179**: 103–112, London.

Franke, W.; Dallmeyer, R. D.; Weber, K. (1995): XI Geodynamic evolution. – In: Dallmeyer, R. D.; Franke, W.; Weber, K. (Eds.): Pre-Permian geology of Central and Eastern Europe: 579–593, (Springer).

Friedl, G.; Finger, F.; McNaughton, N. J.; Fletcher, I. R. (2000): Deducing the ancestry of terranes: SHRIMP evidence for South America-derived Gondwana fragments in Central Europe. – Geology, **28**: 1035–1038.

Friedl, G.; Finger, F.; Paquette, J. L.; von Quadt, A.; McNaughton, N. J.; Fletcher, I. R. (2004): Pre-Variscan geological events in the Austrian part of the Bohemian Massif deduced from U–Pb zircon ages. – International Journal of Earth Sciences, **93**: 802–823.

Gaál, G.; Gorbatschev, R. (1987): An outline of the Precambrian evolution of the Baltic Shield. – Precambrian Research, **35**: 15–52.

Garzanti, E.; Ando, S.; Vezzoli, G.; Ali Abdel Megid, A.; El Kammar, A. (2006): Petrology of Nile River sands (Ethiopia and Sudan): Sediment budgets and erosion patterns. – Earth and Planetary Science Letters, **252**: (3–4), 327–341.

Garzanti, E.; Vezzoli, G.; Andò, S.; Castiglioni, G. (2001): Petrology of Rifted-Margin Sand (Red Sea and Gulf of Aden, Yemen). – The Journal of Geology, **109**: (3), 277–297.

Gasquet, D.; Chevremont, P.; Baudin, T.; Chalot-Prat, F.; Guerrot, C.; Cocherie, A.; Roger, J.; Hassenforder, B.; Cheilletz, A. (2004): Polycyclic magmatism in the Tagragra d'Akka and Kerdous–Tafeltast inliers (Western Anti-Atlas, Morocco). – Journal of African Earth Sciences, **39**: 267–275.

Gerdes, A.; Zeh, A. (2006): Combined U–Pb and Hf isotope LA-(MC-)ICP-MS analyses of detrital zircons: Comparison with SHRIMP and new constraints for the provenance and age of an Armorican metasediment in Central Germany. – Earth and Planetary Science Letters, **249**: 47–61.

German Stratigraphic Commission (Ed.) (2002): Stratigraphic table of Germany 2002. – Potsdam.

Gerstenberger, H.; Haase, G. (1997): A highly effective emitter substance for mass spectrometric Pb isotope ratio determinations. – Chem. Geol., **136**: 309–312.

Glodny, J.; Grauert, B.; Fiala, J.; Vejnar, Z.; Krohe, A. (1998): Metapegmatites in the western Bohemian massif: ages of crystallisation and metamorphic overprint, as constrained by U-Pb zircon, monazite, garnet, columbite and Rb-Sr muscovite data. – Geologische Rundschau, **87**: 124–134.

Gradstein, F. M.; Ogg, J. G.; Smith, A. G. (Eds.) (2005): Geologic Time Scale 2004: 1–610, Cambridge University Press.

Gutiérrez Alonso, G.; Fernández-Suárez, J.; Collins, A. S.; Abad, I.; Nieto, F. (2005): Amazonian Mesoproterozoic basement in the core of the Ibero-Armorican Arc: 40Ar/39Ar detrital mica ages complement the zircon's tale. – Geology, **33**: (8), 637–640.

Hanski, E.; Huhma, H.; Vaasjoki, M. (2001): Geochronology of northern FInland: a summary and discussion. – In: Vaasjoki, M. (Ed.): Radiometric age determinations from Finish Lapland and their bearing on the timing of Precambrian volcano-sedimentary sequences. – Geological Survey of Finland Special Paper, **33**: 255–279, Espoo.

Hartz, E. H.; Torsvik, T. H. (2002): Baltica upside down: A new plate tectonic model for Rodinia and the Iapetus ocean. – Geology, **30**: (3), 255–258.

Havlíček, V. (1971): Stratigraphy of the Cambrian of Central Bohemia. – Sborník geologických věd, **20**: (rada G), 7–50.

Havlíček, V. (1982): Ordovician in Bohemia: development of the Prague Basin and its benthic communities. – Sbor. geol. ved, Geologie, **37**: 103–136.

Havlíček, V. (1989): Climatic changes and development of benthic communities through the Mediterranean Ordovician. – Sborník geologických vìd – Geologie, **44**: 79–116.

Havlíček, V. (1998a): IV. Příbram-Jince Basin. – In: Chlupáč, I.; Havlíček, V.; Kříž, J.; Kukal, Z.; Štorch, P. (Eds.): Palaeozoic of the Barrandian (Cambrian to Devonian): 19–41, Czech Geological Survey (Prague).

Havlíček, V., 1998b, V. Prague Basin – Ordovician. – In: Chlupáč, I.; Havlíček, V.; Kříž, J.; Kukal, Z.; Štorch, P. (Eds.): Palaeozoic of the Barrandian (Cambrian to Devonian): 41–79, Czech Geological Survey (Prague).

Havlíček, V.; Fatka, O. (1992): Ordovician of the Prague Basin (Barrandian area, Czechoslovakia). – In: Laurie, W. (Ed.): Global perspectives on Ordovician geology: 461–472, Rotterdam (Balkema).

Havlíček, V.; Vaněk, J. (1966): The biostratigraphy of the Ordovician of Bohemia. – Sbor. geol. ved, Paleontologie, **8**: 7–69.

Havlíček, V.; Vaněk, J.; Fatka, O. (1994): Perunica microcontinent in the Ordovician (its position within the mediterranean province, series division, benthic and pelagic associations). – Sborník geologických ved, **46**: (Geologie), 23–56.

Heckman, D. S.; Geiser, D. M.; Eidell, B. R.; Stauffer, R. L.; Kardos, N. L.; Hedges, S. B. (2001): Molecular evidence for the early colonization of land by fungi and plants. – Science, **293**: 1129–1133.

Hirdes, W.; Davis, D. W. (2002): U-Pb geochronology of Paleoproterozoic rocks in the southern part of the Kedougou-Kéniéba inlier, Senegal, West Africa: evidence for diachronous accretionary development of the Eburnian province. – Precambrian Research, **118**: 83–99.

Hirdes, W.; Davis, D. W.; Lüdtke, G.; Konan, G. (1996): Two generations of Birimian (Paleoproterozoic) volcanic belts in northeastern Côte d'Ivoire (West Africa): consequences for the 'Birimian controversy'. – Precambrian Research, **80**: 173–191.

Hladil, J.; Bek, J. (1998): Distances between the Early/ Middle Devonian Gondwana and Laurussia; faunal and spore dispersals as compared with paleomagnetic data on paleolatitude. – Exploration Geophysics, Remote Sensing and Environment, **2**: 29–33.

Holubec, J. (1995): VII.B.2 Structure. – In: Dallmeyer, D. R.; Franke, W.; Weber, K. (Eds.): Pre-Permian geology of Central and Eastern Europe: 392–397, Berlin, Heidelberg (Springer-Verlag).

Horstwood, M. S. A.; Foster, G. L.; Parrish, R. R.; Noble, S. R.; Nowell, G. M. (2003): Common-Pb corrected in situ U–Pb accessory mineral geochronology by LA-MC-ICP-MS. – Journal of Analytical Atomic Spectrometry, **18**: (8), 837–846.

Hoskin, P. W. O.; Schaltegger, U. (2003): The composition of zircon and igneous and metamorphic petrogenesis. – In: Hanchar, J. M.; Hoskin, P. W. O. (Eds.): Zircon. – Reviews in Mineralogy and Geochemistry, **53**: 27–62.

Howell, D. G. (1995): Principles of terrane analysis – New applications for global tectonics: 1–245, London (Chapman & Hall).

Inglis, J. D.; MacLean, J. S.; Samson, S. D.; D'Lemos, R. S.; Admou, H.; Hefferan, K. (2004a): A precise U–Pb zircon age for the Bleïda granodiorite, Anti-Atlas, Morocco: implications for the timing of deformation and terrane assembly in the eastern Anti-Atlas. – Journal of African Earth Sciences, **39**: 277–283.

Inglis, J. D.; Samson, S. D.; D'Lemos, R. S.; Hamilton, M. (2004b): U–Pb geochronological constraints on the tectonothermal evolution of the Paleoproterozoic basement of Cadomia, La Hague, NW France. – Precambrian Research, **134**: 293–315.

Ingram, R. L. (1954): Terminology for the thickness of stratification and parting units in sedimentary rocks. – Geological Society of America Bulletin, **65**: (9), 937–938.

Irvine, T. N. & Baragar, W. R. A. (1971): A guide to the chemical classification of the common volcanic rocks. – Canadian Journal of Earth Sciences, **8**: 523–548.

Jaffey, A. H.; Flynn, K. F.; Glendenin, L.E.; Bentley, W.C.; Essling, A. M. (1971): Precision measurement of half-lives and specific activities of ^{235}U and ^{238}U. – Physics Review, **C4**: 1889–1906.

Jakeš, P.; Zoubek, J.; Zoubková, J.; Franke, W. (1979): Graywackes and metagraywackes of the Teplá-Barrandian Proterozoic area. – Sbor. geol. ved, Geologie, **33**: 83–122.

Janoušek, V.; Gerdes, A.; Vrána, S.; Finger, F.; Erban, V.; Friedl, G.; Braithwaite, C. J. R. (2006): Low-pressure Granulites of the Lišov Massif, Southern Bohemia: Viséan Metamorphism of Late Devonian Plutonic Arc Rocks. – Journal of Petrology, **47**: 705–744.

Jeffries, T. E.; Fernández-Suárez, J.; Corfu, F.; Gutiérrez Alonso, G. (2003): Advances in U-Pb geochronology using a frequency quintupled Nd:YAG based laser ablation system (λ = 213 nm) and quadrupole based ICP-MS. – Journal of Analytical Atomic Spectrometry, **18**: 847–855.

Jensen, L. S. (1976): A new cation plot for classifying subalkalic volcanic rocks. – Ontario Division of Mines Miscellaneous Publications, **66**: 1–22.

Johnsson, M. J.; Ellen, S. D.; McKittrick, M. A. (1993): Intensity and duration of chemical weathering: An example from soil clays of the southeastern Koolau Mountains, Oahu, Hawaii. – In: Johnsson, M. J.; Basu, A. (Eds.): Processes controlling the composition of clastic sediments. – Geological Society of America, Special Paper, **284**: 147–170, Boulder, Colorado.

Jonas, P.; Buschmann, B.; Gaitzsch, B. (2000): Unterkambrischer und unterkarboner Vulkanismus der Torgau-

Doberlug Synklinale (NE Saxothuringische Zone). – Zeitschrift für geologische Wissenschaften, **28**: (1–2), 157–175.

Kemnitz, H.; Romer, R. L.; Oncken, O. (2002): Gondwana break-up and the northern margin of the Saxothuringian belt (Variscides of Central Europe). – International Journal of Earth Sciences, **91**: (2), 246–259.

Keppie, D. F.; Nance, R. D.; Murphy, J. B.; Dostal, J. (2003): Tethyan, Mediterranean, and Pacific analogues for the Neoproterozoic birth and development of peri-Gondwanan terranes and their transfer to Laurentia and Laurussia. – Tectonophysics, **365**: 195–219.

Kettner, R. (1918): Versuch einer stratigraphischen Einteilung des böhmischen Algonkiums. – Geologische Rundschau, **8**: (5–8), 169–188.

Kinny, P. D. (1986): 3820 Ma zircons from a tonalitic Amitsoq gneiss in the Godthab district of southern West Greenland. – Earth and Planetary Science Letters, **79**: 337–347.

Klápová, H.; Hyršl, J. (2000): Correlation of Neoproterozoic conglomerates of the Barrandian, Saxothuringian and Moldanubian units. – Bulletin of the Czech geological survey, **75**: (3), 217–228.

Konzalová, M. (1981): Some late Precambrian microfossils from the Bohemian Massif and their correlation. – Precambrian Research, **15**, 4–62.

Konzalová, M. (2000): Organic-walled microbiota from the greywackes and other siliciclastic sediments of the Barrandian Neoproterozoic (Bohemian Massif, Czech Republic). – Bulletin of the Czech geological survey, **75**: (3), 319–337.

Kouamelan, A.; Delor, C.; Peucat, J. J. (1997): Geochronological evidence for reworking of Archean terrains during the Early Proterozoic (2,1 Ga) in the western Côte d'Ivoire (Man Rise – West African Craton). – Precambrian Research, **86**: 177–199.

Kraft, P.; Linnemann, U.; Mazur, S. (Eds.) (2004): Gondwanan-margin of the Rheic ocean in the Bohemian Massif: Excursion guide books and abstracts. – In: Opening meeting 2004 of the International Geoscience Program IGCP 497 „The Rheic Ocean: its Origin, Evolution and Correlatives": 1–108, Faculty of Science, Charles University Prague, Prague.

Kříbek, B.; Pouba, Z.; Skoček, V.; Waldhausrová, J. (2000): Neoproterozoic of the Teplá-Barrandian Unit as a part of the Cadomian orogenic belt: A review and correlation aspects. – Bulletin of the Czech geological survey, **75**: (3), 175–196.

Kříž, J. (1998): V. Prague Basin – Silurian. – In: Chlupáč, I.; Havlíček, V.; Kříž, J.; Kukal, Z.; Štorch, P. (Eds.): Palaeozoic of the Barrandian (Cambrian to Devonian): 79–101, Czech Geological Survey (Prague).

Kröner, A.; Ekwueme, B. N.; Pidgeon, R. T. (2001): The Oldest Rocks in West Africa: SHRIMP Zircon Age for Early Archean Migmatitic Orthogneiss at Kaduna, Northern Nigeria. – The Journal of Geology, **109**: 399–406.

Kröner, A.; Krüger, J.; Rashwan, A. A. A. (1994): Age and tectonic setting of granitoid gneisses in the Eastern Desert of Egypt and south-west Sinai. – Geologische Rundschau, **83**: 502–513.

Kröner, A.; Wendt, I.; Liew, T. C.; Compston, W.; Todt, W.; Fiala, J.; Vanková, V.; Vaněk, J. (1988): U-Pb zircon and Sm-Nd model ages of high-grade Moldanubian metasediments, Bohemian Massif, Czechoslovakia. – Contributions to Mineralogy and Petrology, **99**: (2), 257–266.

Krs, M.; Krsová, M.; Pruner, P. (1997): D.4. Palaeomagnetism and palaeogeography of the Variscan and pre-Variscan formations of the Bohemian Massif. – In: Vrána, S.; Štedrá, V. (Eds.): Geological model of western Bohemia related to the KTB borehole in Germany. Journal of Geological Sciences **47**: 162–173, Prague (Czech Geological Survey).

Krs, M.; Krsová, M.; Pruner, P.; Chvojka, R.; Havlíèč, V. (1987): Palaeomagnetism, palaeogeography and the multicomponent analysis of middle and upper Cambrian rocks of the Barrandian in the Bohemian Massif. – Tectonophysics, **139**: 1–20.

Krs, M.; Krsová, M.; Pruner, P.; Havlíček, V. (1986): Paleomagnetism, paleogeography and multi-component analysis of magnetization of Ordovician rocks from the Barrandian area of the Bohemian Massif. – Sbor. geol. ved, Uzitá geofyzika, **20**: 9–45.

Krs, M.; Pruner, P.; Man, O. (2001): Tectonic and paleogeographic interpretation of the paleomagnetism of Variscan and pre-Variscan formations of the Bohemian Massif, with special reference to the Barrandian terrane. – Tectonophysics, **332**: 93–114.

Kryza, R.; Pin, C. (2002): Mafic rocks in a deep-crustal segment of the Variscides (the Góry Sowie, SW Poland): evidence for crustal contamination in an extensional setting. – International Journal of Earth Sciences, **91**: 1017–1029.

Kukal, Z. (1963): Composition and Origin of the Ordovician sediments of the Trenice and Mílina Beds. – Sborník ústredního ústavu geologického: 265–307 (english summary).

Kukal, Z. (1966): The source of clastic material in the sediments of the Príbram-Jince Cambrian. – Sborník geologických věd, **10**: (rada G), 83–116.

Kukal, Z. (1971): Sedimentology of Cambrian deposits of the Barrandian area (Central Bohemia). – Sborník geologických věd, **20**: (rada G), 53–100.

Kukal, Z. (1995): The Lower Cambrian Paseky shale: sedimentology. – Journal of the Czech Geological society, **40**: (4), 67–78.

Lang, M. (2000): Composition of Proterozoic greywackes in the Barrandian. – Bulletin of the Czech geological survey, **75**: (3), 205–216.

LeMaître, R. W. (1988): A classification of igneous rocks and glossary of terms: 1–129, Oxford (Blackwell Scientific Publications).

Liégeois, J. P.; Black, R.; Navez, J.; Latouche, L. (1994): Early and late Pan-African orogenies in the Air assembly of terranes (Tuareg shield, Niger). – Precambrian Research, **67**: 59–88.

Liégeois, J. P.; Latouche, L.; Boughrara, M.; Navez, J.; Guiraud, M. (2003): The LATEA metacraton (Central Hoggar, Tuareg shield, Algeria): behaviour of an old passive margin during the Pan-African orogeny. – Journal of African Earth Sciences, **37**: 161–190.

Liew, T. C.; Hofmann, A. W. (1988): Precambrian crustal components, plutonic associations, plate environment of the Hercynian Fold Belt of central Europe: indications from a Nd and Sr isotopic study. – Contributions to Mineralogy and Petrology, **98**: 129–138.

Linnemann, U. (2003): Sedimentation und geotektonischer Rahmen der Beckenentwicklung im Saxothuringikum (Neoproterozoikum – Unterkarbon. – In: Linnemann, U. (Ed.): Das Saxothuringikum. – Geologica Saxonica, **48/49**: 71–110, Dresden.

Linnemann, U.; Buschmann, B. (1995): Die cadomische Diskordanz im Saxothuringikum (oberkambrisch-tremadocische overlap-Sequenzen). – Zeitschrift für geologische Wissenschaften, **23**: (5/6), 707–727.

Linnemann, U.; Romer, R. L. (2002): The Cadomian orogeny in Saxo-Thuringia, Germany: geochemical and Nd-Sr-Pb isotopic characterization of marginal basins with constraints to geotectonic setting and provenance. – Tectonophysics, **352**: 33–64.

Linnemann, U.; McNaughton, N. J.; Romer, R. L.; Gehmlich, M.; Drost, K.; Tonk, C. (2004): West African provenance for Saxo-Thuringia (Bohemian Massif): Did Armorica ever leave pre-Pangean Gondwana? – U/Pb-SHRIMP zircon evidence and the Nd-isotopic record. – International Journal of Earth Sciences, **93**: 683–705.

Linnemann, U.; Gerdes; A., Drost, K.; Buschmann, B. (2007): The continuum between Cadomian orogenesis and opening of the Rheic Ocean: Constraints from LA-ICP-MS U-Pb zircon dating and analysis of plate-tectonic setting (Saxo-Thuringian zone, northeastern Bohemian Massif, Germany). – In: Linnemann, U., Nance, R. D., Kraft, P.; Zulauf, G. (Eds.): The evolution of the Rheic Ocean: From Avalonian-Cadomian active margin to Alleghenian-Variscan collision. – Geological Society of America Special Paper **423**: 61–96, Boulder, Colorado.

Linnen, R. L.; Keppler, H. (2002): Melt composition control of Zr/Hf fractionation in magmatic processes. – Geochimica et Cosmochimica Acta, **66**: (18), 3293–3301.

Ludwig, K. R. (1998): On the treatment of concordant uranium-lead ages. – Geochimica et Cosmochimica Acta, **62**: 665–676.

Ludwig, K. R. (2001): Users Manual for Isoplot/Ex rev. 2.49. – Berkeley Geochronology Center Special Publication, **1a**: 1–56.

Lyons, D. J.; van de Kamp, P. C. (1980): Subsurface geological and geophysical study of the Cerro Prieto geothermal field Baja California, Mexico. – Lawrence Berkeley Laboratory: 1–95.

Mange, M. A.; Maurer, H. F. W. (1991): Schwerminerale in Farbe. – 1–148, Stuttgart (Enke).

Manhes, G.; Minster, J. F.; Allegre, C. J. (1978): Comparative uranium-thorium-lead and rubidium-strontium study of the Saint Severin amphoterite: consequences for early solar system chronology. – Earth and Planetary Science Letters, **39**: (1), 14–24.

Maniar, P. D.; Piccoli, P. M. (1989): Tectonic discrimination of granitoids. – GSA Bulletin, **101**: (5), 635–643.

Martínez Catalán, J. R.; Fernández-Suárez, J.; Jenner, G. A.; Belousova, E.; Díez Montes, A. (2004): Provenance constraints from detrital zircon U–Pb ages in the NW Iberian Massif: implications for Palaeozoic plate configuration and Variscan evolution. – Journal of the Geological Society, London, **161**: 463–476.

Mašek, J. (2000): Stratigraphy of the Proterozoic of the Barrandian area. – Bulletin of the Czech geological survey, **75**: (3), 197–200.

Matte, P.; Maluski, H.; Rajlich, P.; Franke, W. (1990): Terrane boundaries in the Bohemian Massif: Result of large-scale Variscan shearing. – Tectonophysics, **177**: 151–170.

Mazur, S.; Aleksandrowski, P.; Szczepanski, J. (2005): The presumed Tepla-Barrandian/Moldanubian terrane boundary in the Orlica Mountains (Sudetes, Bohemian Massif): structural and petrological characteristics. – Lithos, **82**: (1–2), 85–112.

McElhinny, M. W.; Powell, C. M.; Pisarevsky, S. A. (2003): Paleozoic terranes of eastern Australia and the drift history of Gondwana. – Tectonophysics, **362**: (1–4), 41–65.

McKerrow, W. S.; van Staal, C. R. (2000): The Palaeozoic time scale reviewed. – In: Franke, W.; Haak, U.; Oncken, O.; Tanner, D. (Eds.): Orogenic processes: quantification and modelling in the Variscan belt. – Geological Society Special Publication **179**: 5–8, London.

McLennan, S. M. (1999): Scandium. – In: Marshall, C. P.; Fairbridge, R. W. (Eds.): Encyclopedia of Geochemistry: 569, Dordrecht, Boston, London (Kluwer Academic Publishers).

McLennan, S. M.; Hemming, S.; McDaniel, D. K.; Hanson, G. N. (1993): Geochemical approaches to sedimentation, provenance, and tectonics. – In: Johnsson, M. J.; Basu, A. (Eds.): Processes controlling the composition of clastic sediments. – Geological Society of America Special Paper **284**: 21–40, Boulder, Colorado.

McLennan, S. M.; Taylor, S. R.; McCulloch, M. T.; Maynard, J. B. (1990): Geochemical and Nd-Sr isotopic composition of deep-sea turbidites: Crustal evolution and plate tectonic associations. – Geochimica et Cosmochimica Acta, **54**: 2015–2050.

Melichar, R. (2004): Tectonics of the Prague Synform: a hundred years of scientific discussion. – Krystalinikum, **30**: 167–187.

Meschede, M. (1986): A method of discriminating between different types of mid-ocean ridge basalts and continental tholeiites with the Nb-Zr-Y diagram. – Chem. Geol., **56**: 207–218.

Mikuláš, R. (1990): Trace Fossils from the Zahořany Formation (Upper Ordovician, Bohemia). – Acta Universitatis Carolinae, Geologica, **3**: 307–335.

Miller, C. F.; Lowery, L. E.; Bea, F. (2005): Zircon and Zr/Hf ratios: Assessing magmatic fractionation in the crust. – Geochimica et Cosmochimica Acta, **69**: (10, Supplement), A10.

Mittlefehldt, D. W. (1999): Alkalis and alkaline earth elements. – In: Marshall, C. P.; Fairbridge, R. W. (Eds.): Encyclopedia of Geochemistry: 198–204, Dordrecht, Boston, London (Kluwer Academic Publishers).

Murphy, J. B.; Fernández-Suárez, J.; Jeffries, T. E. (2004a): Lithogeochemical and Sm-Nd and U-Pb isotope data from the Silurian–Lower Devonian Arisaig Group clastic rocks, Avalon terrane, Nova Scotia: A record of terrane accretion in the Appalachian-Caledonide orogen. – GSA Bulletin, **116**: (9–10), 1183–1201.

Murphy, J. B.; Fernández-Suárez, J.; Jeffries, T. E.; Strachan, R. A. (2004b): U-Pb (LA-ICP-MS) dating of detrital zircons from Cambrian clastic rocks in Avalonia: erosion of a Neoproterozoic arc along the northern Gondwanan margin. – Journal of the Geological Society of London, **161**: 243–254.

Murphy, J. B.; Gutiérrez Alonso, G.; Nance, R. D.; Fernández-Suárez, J.; Keppie, J. D.; Quesada, C.; Strachan, R. A.; Dostal, J. (2006): Origin of the Rheic Ocean: Rifting along a Neoproterozoic suture? – Geology, **34**: (5), 325–328.

Murphy, J. B.; Keppie, J. D.; Dostal, J.; Nance, R. D. (1999): Neoproterozoic – early Paleozoic evolution of Avalonia. – In: Ramos, V. A.; Keppie, J. D. (Eds.): Laurentia-Gondwana Connections before Pangea. – Geological Society of America Special Paper **336**: 253–266, Boulder, Colorado.

Murphy, J. B.; Nance, R. D. (1989): Model for the evolution of the Avalonian-Cadomian belt. – Geology, **17**: (7), 735–738.

Murphy, J. B.; Nance, R. D. (1991): Supercontinent model for the contrasting character of Late Proterozoic orogenic belts. – Geology, **19**: (5), 469–472.

Murphy, J. B.; Nance, R. D. (2002): Sm-Nd isotopic systematics as tectonic tracers: an example from West Avalonia in the Canadian Appalachians. – Earth-Science Reviews, **59**: 77–100.

Nance, R. D.; Murphy, J. B. (1994): Contrasting basement isotopic signatures and the palinspastic restoration of peripheral orogens: Example from the Neoproterozoic Avalonian-Cadomian belt. – Geology, **22**: (7), 617–620.

Nance, R. D.; Murphy, J. B.; Keppie, J. D. (2002): A Cordilleran modell for the evolution of Avalonia. – Tectonophysics, **352**: 11–31.

Nance, R. D.; Murphy, J. B.; Strachan, R. A.; D'Lemos, R. S.; Taylor, G. K. (1991): Late Proterozoic tectonostratigraphic evolution of the Avalonian and Cadomian terranes. – Precambrian Research, **53**: 41–78.

Nelson, D. R. (1997) Compilation of SHRIMP U-Pb zircon geochronology data, 1996. – Geological Survey of Western Australia Records, **1997/2**: 1–189 Perth.

Nesbitt, H. W.; MacRae, N. D.; Kronberg, B. I. (1990): Amazon deep-sea fan muds: light REE enriched products of extreme chemical weathering. – Earth and Planetary Science Letters, **100**: 118–123.

Nesbitt, H. W.; Markovics, G.; Price, R. C. (1980): Chemical processes affecting alkalis and alkaline earths during continental weathering. – Geochimica et Cosmochimica Acta, **44**: (11), 1659–1666.

Nesbitt, H. W.; Young, G. M. (1982): Early Proterozoic climates and plate motions inferred from major element chemistry of lutites. – Nature, **299**: 715–717.

Oberthür, T.; Vetter, U.; Davis, D. W.; Amanor, J. A. (1998): Age constraints on gold mineralization and Paleoproterozoic crustal evolution in the Ashanti belt of southern Ghana. – Precambrian Research, **89**: 129–143.

Pacltová, B. (1990): Late Proterozoic organic remains from the Mítov locality. – In: Chanda, S. (Ed.): Silver Jubilee commemoration. – Journal of Palynology, **91**: 261–276.

Pacltová, B. (2000): Thalloid algae with reproductive organs and other fossils in limestones and solid bitumens: Neoproterozoic, Czech Republic. – Bulletin of the Czech geological survey, **75**: (3), 339–349.

Paquette, J. L.; Caby, R.; Djouadi, M. T.; Bouchez, J. L. (1998): U-Pb dating of the end of the Pan-African orogeny in the Tuareg shield: the post-collisional syn-shear Tioueine pluton (Western Hoggar, Algeria). – Lithos, **45**: (1–4), 245–253.

Paris, F.; Robardet, M. (1990): Early Palaeozoic palaeobiogeography of the Variscan regions. – Tectonophysics, **177**: 193–213.

Pašava, J.; Amov, B. (1993): Isotopic composition of lead in Proterozoic anoxic metasedimentary and volcanogenic rocks from the Bohemian Massif (Czech Republic) with metallogenetic implications. – Chemical Geology (Isotope Geoscience Section), **109**: (1–4), 293–304.

Patočka, F.; Vlašímský, P.; Blechová, K. (1993): Geochemistry of early Paleozoic volcanics of the Barrandian basin (Bohemian Massif, Czech Republic): Implications for paleotectonic reconstructions. – Jb. Geol. B.-A., **136**: (4), 873–896.

Pearce, J. A.; Harris, N. B. W.; Tindle, A. G. (1984): Trace element discrimination diagrams for the tectonic interpretation of granitic rocks. – Journal of Petrology, **24**: No. 4, 956–983.

Pearce, J. A. (1983): Role of sub-continental lithosphere in magma genesis at active continental margins. – In: Hawkesworth, C. J.; Norry, M. J. (Eds.): Continental basalts and xenoliths: 230–249, Shiva, Nantwich.

Pearce, J. A.; Norry, M. J. (1979): Petrogenetic implications of Ti, Zr, Y, and Nb variations in volcanic rocks. – Contributions to Mineralogy and Petrology, **69**: 33–47.

Pelc, Z.; Waldhausrová, J. (1994): Geochemical characteristics of volcanites of the Barrandian Upper Proterozoic in the Chudenice-Nepomuk region (Bohemia) – (engl. summary). – Sborník geologických ved, **46**: (Geologie), 5–21.

Pereira, M. F.; Chichorro, M.; Linnemann, U.; Eguiluz, L.; Silva, J. B. (2006): Inherited arc signature in Ediacaran and Early Cambrian basins of the Ossa-Morena Zone (Iberian Massif, Portugal): Paleogeographic link with European and North African Cadomian correlatives. – Precambrian Research, **144**: 297–315.

Peucat, J. J.; Capdevila, R.; Drareni, A.; Choukroune, P.; Fanning, C. M.; Bernard-Griffiths, J.; Fourcade, S. (1996): Major and trace element geochemistry and isotope (Sr, Nd, Pb, O) systematics of an Archaean basement involved in a 2.0 Ga very high-temperature (1000 °C) metamorphic event: In Ouzzal Massif, Hoggar, Algeria. – Journal of Metamorphic Geology, **14**: 667–692.

Peucat, J. J.; Capdevila, R.; Drareni, A.; Mahdjoub, Y.; Kahoui, M. (2005): The Eglab massif in the West African Craton (Algeria), an original segment of the Eburnean orogenic belt: petrology, geochemistry and geochronology. – Precambrian Research, **136**: 309–352.

Peucat, J. J.; Drareni, A.; Latouche, L.; Deloule, E.; Vidal, P. (2003): U-Pb zircon (TIMS and SIMS) and Sm-Nd whole-rock geochronology of the Gour Oumelalen granulitic basement, Hoggar massif, Tuareg shield, Algeria. – Journal of African Earth Sciences, **37**: 229–239.

Pin, C.; Linán, E.; Pascual, E.; Donaire, T.; Valenzuela, A. (2002): Late Neoproterozoic crustal growth in the European Variscides: Nd isotope and geochemical evidence from the Sierra de Córdoba Andesites (Ossa-Morena Zone, Southern Spain). – Tectonophysics, **352**: 133–151.

Pin, C.; Kryza, R.; Oberc-Dziedzic, T.; Mazur, S.; Turniak, K.; Waldhausrová, J. (2007): The diversity and geodynamic significance of Late Cambrian (ca. 500 Ma) felsic anorogenic magmatism in the northern part of the Bohemian Massif: a review based on Sm-Nd isotope and geochemical data. – In: Linnemann, U.; Nance, R. D.; Kraft, P.; Zulauf, G. (Eds.): The Evolution of the Rheic Ocean: From Avalonian-Cadomian Active Margin to Alleghenian-Variscan Collision. – Geological Society of America Special Paper **423**: 209–229, Boulder, Colorado.

Pin, C.; Waldhausrová, J. (2007): Sm-Nd isotope and trace element study of the Late Proterozoic metabasalts ("spilites") from the Central Barrandian Domain (Bohemian Massif, Czech Republic). – In: Linnemann, U.; Nance, R. D.; Kraft, P.; Zulauf, G. (Eds.): The Evolution of the Rheic Ocean: From Avalonian-Cadomian Active Margin to Alleghenian-Variscan Collision. – Geological Society of America Special Paper **423**: 231–247, Boulder, Colorado.

Plant, J. A.; Simpson, P. R.; Smith, B.; Windley, B. F. (1999): Uranium ore deposits – Products of the radioactive earth. – In: Burns, P. C.; Finch, R. (Eds.): Uranium – Mineralogy, Geochemistry and the Environment. – Reviews in Mineralogy, **38**: 255–319.

Plusquellec, Y.; Hladil, J. (2001): Tabulate corals of Ibarmaghian affinities in the Upper Emsian of Bohemia. – Geologica et Palaeontologica, **35**: 31–51.

Potrel, A.; Peucat, J. J.; Fanning, C. M.; Auvray, B.; Burg, J.; Caruba, C. (1996): 3.5 Ga old terranes in the West African Craton, Mauritania. – Journal of the Geological Society, London, **153**: 507–510.

Potrel, A.; Peucat, J. J.; Fanning, M. (1998): Archean crustal evolution of the West African Craton: example of the Amsaga Area (Reguibat Rise). U-Pb and Sm-Nd evidence for crustal growth and recycling. – Precambrian Research, **90**: 107–117.

Pouclet, A.; Bellon, H. (1992): 47. Geochemistry and isotopic composition of volcanic rocks from the Yamato Basin: Hole 794D, Sea of Japan. – In: Tamaki, K.; Suyehiro, K.; Allan, J.; McWilliams, M. (Eds.): Proceedings of the Ocean Drilling Program, Scientific Results: 779–789, College Station, TX (Ocean Drilling Program).

Pupin, J. P. (1980): Zircon and granite petrology. – Contributions to Mineralogy and Petrology, **73**: 207–220.

Quesada, C. (1990): Precambrian terranes in the Iberian Variscan Foldbelt. – In: Strachan, R. A.; Taylor, G. K. (Eds.): Avalonian and Cadomian Geology of the North Atlantic: 109–133, Glasgow, London (Blackie).

Quesada, C. (2006): The Ossa-Morena Zone – From Neoproterozoic arc through Early Palaeozoic rifting to late Palaeozoic orogeny. – In: Pereira, M. F.; Quesada, C. (Eds.): Evora Meeting 2006. Ediacaran to Viséan crustal growth processes in the Ossa-Morena Zone (SW Iberia) – Conference Abstracts and Field Trip Guide: 27–48, Madrid (Instituto Geológico y Minero de Espana).

Quesada, C. (2006): The Ossa-Morena Zone of the Iberian Massif: a tectonostratigraphic approach to its evolution. – Z. dt. Ges. Geowiss., 157: 585–595.

Rankenburg, K.; Lassiter, J. C.; Brey, G. (2005): The Role of Continental Crust and Lithospheric Mantle in the Genesis of Cameroon Volcanic Line Lavas: Constraints from Isotopic Variations in Lavas and Megacrysts from the Biu and Jos Plateaux. – Journal of Petrology, **46**: (1), 169–190.

Redecker, D.; Kodner, R.; Graham, L. E. (2000): Glomalean fungi from the Ordovician. – Science, **289**: 1920–1921.

Robardet, M. (2003): The Armorica 'microplate': fact or fiction? Critical review of the concept and contradictory palaeobiogeographical data. – Palaeogeography, Palaeoclimatology, Palaeoecology, **195**: 125–148.

Robardet, M.; Paris, F.; Racheboeuf, P. R. (1990): Palaeogeographic evolution of southwestern Europe during Early Palaeozoic times. – In: McKerrow, W. S.; Scotese, C. R.

(Eds.): Palaeogeography and biogeography. – Geological Society Memoir **124**: 11–419, London.

Röhlich, P. (1965): Geologische Probleme des mittelböhmischen Algonkiums. – Zschr. Geologie, **17**: (4), 373–403.

Röhlich, P. (2000): Some stratigraphic problems of the Barrandian Neoproterozoic. – Bulletin of the Czech geological survey, **75**: (3), 201–204.

Rollinson, H. (1993): Using geochemical data: evaluation, presentation, interpretation: 1–352 (Longman Group UK Ltd.).

Romer, R. L.; Förster, H.-J.; Breitkreuz, C. (2001): Intracontinental extensional magmatism with a subduction fingerprint: the late Carboniferous Halle Volcanic Complex (Germany). – Contributions to Mineralogy and Petrology, **141**: 201–221.

Romer, R. L.; Heinrich, W.; Schröder-Smeibidl, B.; Meixner, A.; Fischer, C.-O.; Schulz, C. (2005): Elemental dispersion and stable isotope fractionation during reactive fluid-flow and fluid immiscibility in the Bufa del Diente aureole, NE-Mexico: evidence from radiographies and Li, B, Sr, Nd, and Pb isotope systematics. – Contributions to Mineralogy and Petrology, **149**: (4), 400–429.

Rudnick, R. L. (1999): Large-ion lithophile elements. – In: Marshall, C. P.; Fairbridge, R. W. (Eds.): Encyclopedia of Geochemistry: 214, Dordrecht, Boston, London (Kluwer Academic Publishers).

Rudnick, R. L.; Gao, S. (2003): 3.01 Composition of the continental crust. – In: Holland, H. D.; Turekian, K. K. (Eds.): Treatise on Geochemistry: 1–64, (Elsevier).

Samson, S. D.; D'Lemos, R. S. (1998): U-Pb geochronology and Sm-Nd isotopic composition of Proterozoic gneisses, Channel Islands, UK. – Journal of the Geological Society, London, **155**: 609–618.

Samson, S. D.; D'Lemos, R. S.; Blichert-Toft, J.; Vervoort, J. (2003): U-Pb geochronology and Hf-Nd isotope compositions of the oldest Neoproterozoic crust within the Cadomian orogen: new evidence for a unique juvenile terrane. – Earth and Planetary Science Letters, **208**: 165–180.

Sanchez Martinez, S.; Jeffries, T.; Arenas, R.; Fernandez-Suarez, J.; Garcia-Sanchez, R. (2006): A pre-Rodinian ophiolite involved in the Variscan suture of Galicia (Cabo Ortegal Complex, NW Spain). – Journal of the Geological Society, **163**: (5), 737–740.

Sánchez-García, T.; Bellido, F.; Quesada, C. (2003): Geodynamic setting and geochemical signatures of Cambrian-Ordovician rift-related igneous rocks (Ossa-Morena Zone, SW Iberia). – Tectonophysics, **365**: 233–255.

Schmidt, V. A. (1990): Circularity of paleomagnetic data sets: an aid in the recognition of contaminating secondary overprints. – Tectonophysics, **184**: (1), 11–20.

Scotese, C. R.; Barrett, S. F. (1990): Gondwana's movement over the south Pole during the Palaeozoic: evidence from lithological indicators of climate. – In: McKerrow, W. S.; Scotese, C. R. (Eds.): Palaeogeography and biogeography. – Geological Society Memoir **12**: 75–85, London.

Servais, T.; Fatka, O. (1997): Recognition of the Trans-European suture zone (TESZ) by the palaeobiogeographical distribution pattern of early to middle Ordovician. – Geological Magazine, **134**: (5), 617–625.

Shervais, J. W. (1982): Ti – V plots and the petrogenesis of modern and ophiolitic lavas. – Earth and Planetary Science Letters, **59**: (1), 101–118.

Silva, J. B.; Pereira, M. F. (2004): Transcurrent continental tectonics model for the Ossa-Morena Zone Neoproterozoic–Paleozoic evolution, SW Iberian Massif, Portugal. – International Journal of Earth Sciences, **93**: 886–896.

Sircombe, K. N. (2004): AgeDisplay: an EXCEL workbook to evaluate and display univariate geochronological data using binned frequency histograms and probability density distributions. – Computers & Geosciences, **30**: 21–31.

Sláma, J.; Kachlík, V.; Košler, J. (2003): Neoproterozoic metaconglomerates of the Sedlcany-Krásná Hora Metamorphic Islet. – GeoLines, **16**: 96–97.

Soreghan, M. J.; Cohen, A. S. (1993): The effects of basin asymmetry on sand composition: Examples from Lake Tanganyika, Africa. – In: Johnsson, M. J.; Basu, A. (Eds.): Processes controlling the composition of clastic sediments. – Geological Society of America Special Paper **284**: 285–301, Boulder, Colorado.

Soulaimani, A.; Piqué, A. (2004): The Tasrirt structure (Kerdous inlier, Western Anti-Atlas, Morocco): a late Pan-African transtensive dome. – Journal of African Earth Sciences, **39**: 247–255.

Štedrá, V. (1997): C.2.1. Geophysics of the Mariánské Lázne Complex. – In: Vrána, S.; Štedrá, V. (Eds.): Geological model of western Bohemia related to the KTB borehole in Germany. – Journal of Geological Sciences **47**: 61–63, Prague (Czech Geological Survey).

Štedrá, V.; Kachlik, V.; Kryza, R. (2002): Coronitic metagabbros of the Mariánské Lázne Complex and Teplá Crystalline Unit: inferences for the tectonometamorphic evolution of the western margin of the Teplá-Barrandian Unit, Bohemian Massif. – In: Winchester, J. A.; Pharaoh, T. C.; Verniers, J. (Eds.): Palaeozoic Amalgamation of Central Europe. – Geological Society Special Publications **201**: 217–236, London.

Steiger, R. H.; Jäger, E. (1977): Subcommission on geochronology: Convention on the use of decay constants in geo- and cosmochronology. – Earth and Planetary Science Letters, **36**: (3), 359–362.

Stern, R. J.; Kröner, A.; Bender, R.; Reischmann, T.; Dawoud, A. S. (1994): Precambrian basement around Wadi Halfa, Sudan: a new perspective on the evolution of the East Saharan Craton. – Geologische Rundschau, **83**: 564–577.

Štorch, P. (1986): Ordovician-Silurian boundary in the Prague basin (Barrandian area, Bohemia). – Sborník geologických ved, Geologie, **41**: 69–103.

Štorch, P.; Fatka, O.; Kraft, P. (1993): Lower Paleozoic of the Barrandian area (Czech Republic) – a review. – Editorial Complutense, Coloquios de Paleontología **45**: 163–191.

Štorch, P. (1998): VIII. Volcanism. – In: Chlupáč, I.; Havlíček, V.; Kříž, J.; Kukal, Z.; Štorch, P. (Eds.): Palaeozoic of the Barrandian (Cambrian to Devonian): 149–164, Prague (Czech Geological Survey).

Strachan, R. A.; D'Lemos, R. S.; Dallmeyer, D. R. (1996): Neoproterozoic evolution of an active plate margin: North Armorican Massif, France. – In: Nance, R. D.; Thompson, M. D. (Eds.): Avalonian and related peri-Gondwanan terranes of the circum-North Atlantic: – Geological Society of America Special Paper **304**: 319–332, Boulder, Colorado.

Strnad, L.; Mihaljevič, M. (2005): Sedimentary provenance of Mid-Devonian clastic sediments in the Teplá-Barrandian Unit (Bohemian Massif): U–Pb and Pb–Pb geochronology of detrital zircons by laser ablation ICP-MS. – Mineralogy and Petrology, **84**: 47–68.

Sturesson, U.; Dronov, A.; Saadre, T. (1999): Lower Ordovician iron ooids and associated oolitic clays in Russia and Estonia: a clue to the origin of iron oolites ? – Sedimentary Geology, **123**: 63–80.

Sturesson, U.; Heikoop, J. M.; Risk, N. J. (2000): Modern and Palaeozoic iron ooids – a similar volcanic origin. – Sedimentary Geology, **136**: (137–146).

Sultan, M.; Tucker, R. D.; El Alfy, Z.; Attia, R.; Ragab, A. G. (1994): U-Pb (zircon) ages for the gneissic terrane west of the Nile, southern Egypt. – Geologische Rundschau, **83**: 514–522.

Sun, S.-s.; McDonough, W. F. (1989): Chemical and isotopic systematics of oceanic basalts: implications for mantle composition and processes. – In: Saunders, A. D.; Norry, M. J. (Eds.): Magmatism in the ocean basins. – Geological Society Special Publication **42**: 313–345, London.

Tait, J.; Bachtadse, V.; Soffel, H. (1994a): New palaeomagnetic constraints on the position of central Bohemia during Early Ordovician times. – Geophys. J. Int., **116**: 131–140.

Tait, J.; Bachtadse, V.; Soffel, H. (1994b): Silurian paleogeography of Armorica: New paleomagnetic data from central Bohemia. – Journal of Geophysical Research, **99**: (B2), 2897–2907.

Tait, J.; Bachtadse, V.; Soffel, H. (1995): Upper Ordovician palaeogeography of the Bohemian Massif: implications for Armorica. – Geophys. J. Int., **122**: 211–218.

Tait, J. A.; Bachtadse, V.; Franke, W.; Soffel, H. C. (1997): Geodynamic evolution of the European Variscan fold belt: paleomagnetic and geological constraints. – Geologische Rundschau, **86**: 585–598.

Tait, J. A.; Schätz, M.; Bachtadse, V.; Soffel, H. C. (2000): Palaeomagnetism and Palaeozoic palaeogeography of Gondwana and European terranes. – In: Franke, W.; Haak, U.; Oncken, O.; Tanner, D. (Eds.): Orogenic processes: Quantification and modelling in the Variscan belt. – Geological Society Special Publications **179**: 21–34, London.

Tamaki, K.; Suyehiro, K.; Allan, J.; Ingle, J. C. J.; Pisciotto, K. A. (1992): 83. Tectonic synthesis and implications of Japan Sea ODP Drilling. – In: Tamaki, K.; Suyehiro, K.; Allan, J.; McWilliams, M. (Eds.): Proceedings of the Ocean Drilling Program, Scientific Results: 1333–1348, College Station, TX (Ocean Drilling Program).

Tassinari, C. C. G.; Macambira, M. J. B. (1999): Geochronological provinces of the Amazonian Craton. – Episodes, **22**: (3), 174–182.

Taylor, S. R.; McLennan, S. M. (1985): The continental crust: its composition and evolution. – pp. 1–312 Oxford, London, Edinburgh, Boston, Palo Alto, Melbourne (Blackwell Scientific Publications).

Teipel, U.; Eichhorn, R.; Loth, G.; Rohrmüller, J.; Höll, R.; Kennedy, A. (2004): U-Pb SHRIMP and Nd isotopic data from the western Bohemian Massif (Bayerischer Wald, Germany): Implications for Upper Vendian and Lower Ordovician magmatism. – International Journal of Earth Sciences, **93**: 782–801.

Teixeira, W.; Tassinari, C. C. G.; Cordani, U. G.; Kawashita, K. (1989): A review of the geochronology of the Amazonian craton: Tectonic implications. – Precambrian Research, **42**: 213–227.

Thiéblemont, D.; Delor, C.; Cocherie, A.; Lafon, J. M.; Goujou, J. C.; Baldé, A.; Bah, M.; Sané, H.; Fanning, M. (2001): A 3,5 Ga granite-gneiss basement in Guinea: further evidence for early Archean accretion within the West African Craton. – Precambrian Research, **108**: (3–4), 179–194.

Thiéblemont, D.; Goujou, J. C.; Egal, E.; Cocherie, A.; Delor, C.; Lafon, J. M.; Fanning, C. M. (2004): Archean evolution of the Leo Rise and its Eburnean reworking. – Journal of African Earth Sciences, **39**: 97–104.

Thomas, R. J.; Chevallier, L. P.; Gresse, P. G.; Harmer, R. E.; Eglington, B. M.; Armstrong, R. A.; de Beer, C. H.; Martini, J. E. J.; de Kock, G. S.; Macey, P. H.; Ingram, B. A. (2002): Precambrian evolution of the Sirwa Window, Anti-Atlas Orogen, Morocco. – Precambrian Research, **118**: 1–57.

Thompson, R. N. (1982): British Tertiary volcanic province. – Scottish Journal of Geology, **18**: 49–107.

Tilton, G. R. (1973): Isotopic lead ages of chondritic meteorites. – Earth and Planetary Science Letters, **19**: (3), 321–329.

Timmermann, H.; Dörr, W.; Krenn, E.; Finger, F.; Zulauf, G. (2006): Conventional and in situ geochronology of the Teplá Crystalline unit, Bohemian Massif: implications for the processes involving monazite formation. – International Journal of Earth Sciences, **95**: 629–647.

Timmermann, H.; Štedrá, V.; Gerdes, A.; Noble, S. R.; Parrish, R. R.; Dörr, W. (2004): The Problem of Dating High-pressure Metamorphism: a U–Pb Isotope and Geo-

chemical Study on Eclogites and Related Rocks of the Mariánske Lázne Complex, Czech Republic. – Journal of Petrology, **45**: (7), 1311–1338.

Vavrdová, M. (1974): Geographical differentiation of Ordovician acritarch assemblages in Europe. – Review of Palaeobotany and Palynology, **18**: 171–175.

Vavrdová, M. (2000): Microfossils in carbonaceous cherts from Barrandian Neoproterozoic (Blovice Formation, Czech Republic). – Bulletin of the Czech geological survey, **75**: (3), 351–360.

Vecoli, M.; Le Hérissé, A. (2004): Biostratigraphy, taxonomic diversity and patterns of morphological evolution of Ordovician acritarchs (organic-walled microphytoplankton) from the northern Gondwana margin in relation to palaeoclimatic and palaeogeographic changes. – Earth-Science Reviews, **67**: 267–311.

Vejnar, Z. (1966): The petrogenetic interpretation of kyanite, silimanite and andalusite in the Southwestern Bohemian crystalline complexes. – Neues Jahrbuch für Mineralogie, Abhandlungen, 104: 172–189.

Venera, Z.; Schulmann, K.; Kröner, A. (2000): Intrusion within a transitional tectonic domain: the Cistá granodiorite (Bohemian Massif) – structure and rheological modelling. – Journal of Structural Geology, **22**: 1437–1454.

Vidal, P.; Auvray, B.; Charlot, R.; Fediuk, F.; Hameurt, J.; Waldhausrová, J. (1975): Radiometric age of volcanics of the Cambrian "Krivoklat-Rocycany" complex (Bohemian Massif). – Geologische Rundschau, **64**: (2), 563–570.

Villeneuve, M.; Cornee, J. J. (1994): Structure, evolution and palaeogeography of the West African craton and bordering belts during the Neoproterozoic. – Precambrian Research, 69: (1–4), 307–326.

Vokurka, K.; Frýda, J. (1997): The neodymium isotopes in Lower Paleozoic basalts from the Barrandian (Teplá-Barrandian Unit, Bohemian Massif). – Zprávy o geologických výzkumech v roce **1996**: 87.

Waldhausrová, J. (1971): The chemistry of the Cambrian volcanics in the Barrandian area. – Krystalinikum, **8**: 45–75.

Waldhausrová, J. (1984): Proterozoic volcanics and intrusive rocks of the Jílové zone in central Bohemia. – Krystalinikum, **17**: 77–97.

Waldhausrová, J. (1997a): Geochemistry of volcanites (metavolcanites) in the western part of the TBU Precambrian and their original geotectonic setting. – In: Vrána, S.; Stedra, V. (Eds.): Geological model of western Bohemia related to the KTB borehole in Germany. – Journal of Geological Sciences **47**: 85–90, Prague (Czech Geological Survey).

Waldhausrová, J. (1997b): Proterozoic volcanics geochemistry and mineral chemistry: a contribution to the Barrandian upper Proterozoic stratigraphy (Bohemian Massif, Czech Republic). – Krystalinikum, **23**: 151–180.

Waters, C. N.; Schofield, D. I. (2004): Contrasting late Neoproterozoic to Ordovician successions of the Taoudeni Basin, Mauritania and Souss Basin, Morocco. – Journal of African Earth Sciences, **39**: 301–309.

Wendt, J. I.; Kröner, A.; Fiala, J.; Todt, W. (1993): Evidence from zircon dating for existence of approximately 2.1 Ga old crystalline basement in southern Bohemia, Czech Republic. – Geologische Rundschau, **82**: 42–50.

Weyer, S.; Münker, C.; Mezger, K. (2003): Nb/Ta, Zr/Hf and REE in the depleted mantle: implications for the differentiation history of the crust-mantle system. – Earth and Planetary Science Letters, **205**: (3–4), 309–324.

Whalen, J. B.; Currie, K. L.; Chappell, B. W. (1987): A-type granites: geochemical characteristics, discrimination and petrogenesis. – Contributions to Mineralogy and Petrology, **95**: 407–419.

Wiedenbeck, M.; Allé, P.; Corfu, F.; Griffin, W. L.; Meier, M.; Oberli, F.; von Quadt, A.; Roddick, J. C.; Spiegel, W. (1995): Three natural zircon standards for U-Th-Pb, Lu-Hf, trace element and REE analyses. – Geostandards Newsletter, **19**: (1), 1–23.

Williams, I. S.; Compston, W.; Black, L. P.; Ireland, T. R.; Foster, J. J. (1984): Unsupported radiogenic Pb in zircon: a cause of anomalously high Pb-Pb, U-Pb and Th-Pb ages. – Contributions to Mineralogy and Petrology, **88**: (4), 322–327.

Winchester, J. A.; Floyd, P. A. (1977): Geochemical discrimination of different magma series and their differentiation products using immobile elements. – Chem. Geol., **20**: 325–343.

Wood, D. A.; Joron, J. L.; Treuil, M.; Norry, M.; Tarney, J. (1979): Elemental and Sr isotope variations in basic lavas from Iceland and the surrounding ocean floor – The nature of mantle source inhomogeneities. – Contributions to Mineralogy and Petrology, **70**: (3), 319–339.

Wronkiewicz, D. J.; Condie, K. C. (1987): Geochemistry of Archean shales from the Witwatersrand Supergroup, South Africa: Source-area weathering and provenance. – Geochimica et Cosmochimica Acta, **51**: (9), 2401–2416.

Zulauf, G. (1997): Von der Anchizone bis zur Eklogitfazies: Angekippte Krustenprofile als Folge der cadomischen und variscischen Orogenese im Teplá-Barrandium (Böhmische Masse). – Geotektonische Forschungen, **89**: 1–302.

Zulauf, G.; Bues, C.; Dörr, W.; Vejnar, Z. (2002a): 10 km minimum throw along the West Bohemian shear zone: Evidence for dramatic crustal thickening and high topography in the Bohemian Massif (European Variscides). – International Journal of Earth Sciences, **91**: 850–864.

Zulauf, G.; Dörr, W.; Fiala, J.; Kotková, J.; Maluski, H.; Valverde-Vaquero, P. (2002b): Evidence for high-temperature diffusional creep preserved by rapid cooling of lower crust (North Bohemian shear zone, Czech Republic). – Terra Nova: **14**, 343–354.

Zulauf, G.; Dörr, W.; Fiala, J.; Vejnar, Z. (1997a): Late Cadomian crustal tilting and Cambrian transtension in the Teplá-Barrandian unit (Bohemian Massif, Central European Variscides). – Geologische Rundschau, **86**: 571–584.

Zulauf, G.; Dörr, W.; Fiala, J.; Vejnar, Z. (1997b): Lower Carboniferous lift tectonics in the Bohemian Massif: a special kind of gravitational collapse in thickened orogenic crust. – Terra Nostra, **97**: (5), 216–218.

Zulauf, G.; Schitter, F.; Riegler, G.; Finger, F.; Fiala, J.; Vejnar, Z. (1999): Age constraints on the Cadomian evolution of the Teplá Barrandian unit (Bohemian Massif) through electron microprobe dating of metamorphic monazite. – Z. dt. geol. Ges., **150**: (4), 627–639.

Acknowledgements

The present study represents a part of the results obtained within the project "Plate tectonic facies and palaeobiogeography of Cambro-Ordovician successions of the Barrandian in comparison to equivalent complexes of the Saxothuringian Zone" that was funded by the Deutsche Forschungsgemeinschaft (grants Li 521/14-1 and Li 521/14-2).

Sincere thanks are to my supervisor Dr. Ulf Linnemann for entrusting me with the interesting research topic and for providing the scientific environment at the Staatliche Naturhistorische Sammlungen Dresden. His encouragement throughout the last years, the enabling of making use of the applied techniques, the possibility to attend several international meetings, and our numerous discussions promoted my scientific and personal development considerably and are gratefully appreciated.

I feel much obliged to Dr. Rolf L. Romer, who co-supervised the thesis and enabled access to the isotope laboratory facilities of the GeoForschungsZentrum Potsdam. His support and advice concerning the isotope work and administrative, stylistic, and general subjects are thankfully acknowledged.
The cooperation with Oldřich Fatka, Petr Kraft, and Jaroslav Marek from the Institute of Geology and Palaeontology of the Charles University Prague contributed essentially to successful field work and literature survey.

I am thankful to Axel Gerdes and Gerhard Brey for giving me the opportunity of U-Pb zircon dating by the LA-ICP-MS equipment of the Institut für Mineralogie of the J.W. Goethe Universität Frankfurt. Axel Gerdes is furthermore sincerely thanked for generously sharing his "U-Th-Pb isotope knowledge". The technical assistance of Kai Klama, Heidi Höfer, and Jan Heliosch as well as the cordial atmosphere and hospitality at the Institut für Mineralogie of the J.W. Goethe Universität Frankfurt are gratefully acknowledged.

I am indebted to Teresa Jeffries for providing access to the LA-ICP-MS equipment at the Natural History Museum London. Her friendly and competent cooperation is greatly appreciated. Craig Storey (The Open University, Milton Keynes) is thanked for assistance with processing of a part of the U-Pb data acquired at NHM London.

I wish to thank Neal McNaughton (University of Western Australia, Perth) for giving me the opportunity of U-Pb zircon dating using the SHRIMP equipment, which is located at Curtin University in Perth and operated by a university-government consortium with support from the Australian Research Council.

The regional geological and methodical knowledge I acquired during the meetings and field trips of IGCP 453 "Modern and Ancient Orogens" and IGCP 497 "The Rheic Ocean - Its Origin, Evolution and Correlatives" were essential for the realisation of the present study. The participants of these projects, but particularly Cecilio Quesada (Instituto Geologico y Minero de España, Madrid), Christian Pin (Université Blaise Pascal, Clermont-Ferrand), Brendan Murphy (St. Francis Xavier University, Antigonish, Nova Scotia), and Maarten de Wit (University of Cape Town) are thanked for invaluable advice and fruitful discussions. Furthermore, I am very thankful to Cecilio Quesada for the invitation to a very inspiring field trip through Cadomian and Variscan units of SW-Spain in March 2005.

My friends and colleagues Jens Ulrich, Jan-Michael Lange, Dagmar Denkert, Ronald Winkler, Sigrid Schwarz, Manuel Röthel (all MMG Dresden), Andreas Risse (GFZ Potsdam), Guido Meinhold (Universität Mainz), Bernd Buschmann (TU Freiberg), Christian Tonk, and Michael Gehmlich (both previously MMG Dresden) and the staff of the Staatliche Naturhistorische Sammlungen Dresden are thanked for numerous discussions, their help within the framework of LBM, and/or technical assistance.
Last but definitely not least I want to thank my family and my friends for their moral support and their tolerance during each of the "difficult stages".

GEOLOGICA SAXONICA
Journal of Central European Geology 54 (2008) 1–168

Abbreviations

BCC	bulk continental crust
CL	cathodoluminescence
CIA	chemical index of alteration
CVL	Cameroon Volcanic Line
E-MORB	enriched MORB
HFSE	high field strength elements (in the sense of Rollinson, 1993)
HREE	heavy rare earth elements
HREY	heavy rare earth elements and Yttrium
KRVC	Křivoklát-Rokycany volcanic complex
LA-ICP-MS	laser ablation inductively coupled plasma mass spectrometry
LILE	large ion lithophile elements – Cs, Rb, K, Ba, Sr (sensu Rollinson, 1993)
LREE	light rare earth elements
MLC	Mariánské Lázně Complex
MOR	mid-ocean ridge
MORB	mid-ocean ridge basalt
N-MORB	normal MORB
OIB	oceanic island basalt
PAAS	post-Archean average Australian shale
REE	rare earth element(s)
SHRIMP	sensitive high-resolution ion microprobe
SVC	Strašice volcanic complex
T_{DM}	crustal residence age
TBU	Teplá-Barrandian Unit
UCC	upper continental crust

Appendix

Sample preparation and analytical procedures

Whole rock geochemistry

Apparently fresh rocks were cleaned and dried in a drying chamber. After coarse crushing, rock-immanent contaminations (e.g. veins) were removed. The remaining rock fragments were crushed with a jaw crusher.

Pulverisation for analysis and determination of geochemical compositions was accomplished by ACTLABS (Activation Laboratories Ltd., Ancaster, Ontario, Canada). Major elements, Be, and Sc were analysed using lithium metaborate/tetraborate fusion ICP. Trace element and REE contents were measured by ICP-MS. A high quality of the data produced by ACTLABS is ensured by regular analyses of certified reference material and accredited through the International Organization for Standardization/International Electrotechnical Commission.

Analytical results are given in **Tables A3 to A8**.

Whole rock isotope geochemistry

Whole rock powders were dissolved with 52% HF for four days at 160 °C on the hot plate. Digested samples were dried, taken up in 6N HCl, centrifuged and splitted for separation of Pb as well as Nd and Sr. Pb, Sr, and Nd were separated using standard ion exchange techniques.

Strontium: Sr was separated using cation exchange resin Bio Rad AG50 W X 8 (100–200 mesh) and 2.5N HCl. Sr was loaded on single Ta-filaments and its isotopic composition was determined on a VG 54–30 Sector multicollector mass spectrometer using a triple-jump dynamic-multicollection setup. $^{87}Sr/^{86}Sr$ data are normalized with $^{86}Sr/^{88}Sr=0.1194$. Repeated measurement of Sr standard NBS 987 during the measurement period gave 0.710249±0.000004 (2σ, n=mean of 12 measurements). Analytical uncertainties of the individual measurements are reported as $2\sigma_m$. Total procedural blanks are less than 100 pg Sr.

Neodymium: REE were separated after Sr elution and rinsing of the resin with 6N HCL using the same column. Nd separation from other REEs was achieved using standard cation exchange techniques in 0.22N HCl and 0.4N HCl medium, respectively. Nd was loaded on double Re-filaments and its isotopic composition was measured on a Finnigan MAT262 multicollector mass spectrometer using a double-jump dynamic-multicollection experiment. $^{143}Nd/^{144}Nd$ data are normalized with $^{146}Nd/^{144}Nd=0.7219$. Repeated measurement of La Jolla Nd standard during the measurement period gave $^{143}Nd/^{144}Nd=0.511850\pm0.000004$ (2σ, n=mean of 14 measurements). Analytical uncertainties of $^{87}Sr/^{86}Sr$ and $^{143}Nd/^{144}Nd$ are reported as $2\sigma_m$. Total procedural blanks are less than 50 pg Nd.

Lead: Pb was separated using anion exchange resin in Teflon columns and the HCl-HBr ion exchange procedure of Tilton (1973) and Manhès et al. (1978). The resin was cleaned with 6N HCl and conditioned with 2N HCl. Samples were loaded in 2N HCl, rinsed with 2N HCl, 0.8N HBr, and 2N HCl. Pb was eluted in 6N HCl.

Pb was loaded together with H_3PO_4 and silicagel on single Re-filaments (Gerstenberger & Haase, 1997). The isotopic composition of Pb was determined at 1200–1250 °C on a Finnigan MAT262 multicollector mass-spectrometer using dynamic multicollection. Instrumental fractionation was corrected with 0.1%/a.m.u. as determined from repeated measurement of lead reference material NBS 981. Accuracy and precision of the reported Pb ratios are

better than 0.1% at the 2σ level. Total procedural blanks for whole rock samples are 15–30 pg Pb.

Whole rock Nd-Sr-Pb isotopic compositions of the analysed samples are given in **Table A9**.

U-Pb dating of magmatic and detrital zircon

Zircon separation: Zircon concentrates were separated at the Forschungsmuseum für Mineralogie und Geologie in Dresden. Fresh samples were crushed in a jaw crusher and sieved for the fraction 63-400μm. Density separation of this fraction was realized using LST (solution of lithium heteropolytungstates in water) and followed by magnetic separation of the extracted heavy minerals in a Frantz isodynamic separator. Final selection of the zircon grains for U-Pb dating was achieved by hand-picking under a binocular microscope. Zircon grains of all grain sizes and morphological types were selected for single grain analyses by SHRIMP and LA-ICP-MS, respectively. Zircon crystals were set in synthetic resin mounts, polished to approximately half their thickness and cleaned in a warm HNO_3 ultrasonic bath at the institute where the respective analyses were going to be performed.

Sensitive high-resolution ion microprobe (SHRIMP): Uranium, Th, and Pb isotopic analyses of zircon were carried out using SHRIMP II in Perth/Western Australia. The SHRIMP equipment is located at Curtin University. Further preparation of hand-picked zircon grains and SEM imaging were carried out at the University of Western Australia.

Single zircon grains were mounted together with chips of the Perth Consortium zircon standard CZ-3 in epoxy resin. Mounted and polished zircon grains were imaged with a scanning electron microprobe (SEM) in cathodoluminescence (CL) and back-scattered electron (BSE) mode. The CL information was used, in order to select appropriate zircon grains for analysis, to place the ion beam without straddling different zones within the same grain, and to avoid zones which may be typical for zircon domains with disturbed U-Pb systems (Pb loss). BSE images allowed identifying inclusions and cracks cutting the surface of polished zircon grains.

Uranium, Th, and Pb isotopic analyses were achieved at SHRIMP II, applying operating procedures similar to those described by Compston et al. (1984) and Williams et al. (1984). A primary O_2^--beam of about 2 nA was focussed to produce a spot diameter of ~15–20 μm. The resulting secondary ions were accelerated to 10 keV, energy- and mass-filtered, and counted in a single-collector electron multiplier. Pb-U ratios were determined relative to that of the CZ-3 zircon standard (564 Ma, U≈550 ppm - Nelson 1997). Reproducibility of the Pb-U ratio of the standard was better than 1.4% (1σ) during the analysis sessions. Errors of the individual analyses of the unknown zircons are based on counting statistics and include the errors of the U-Pb ages of the standard. For common Pb correction the ^{204}Pb method was used (Kinny 1986). Raw data reduction/age calculation were processed using the Squid software (developed by Ken Ludwig), and the decay constants recommended by the IUGS (Steiger and Jäger, 1977). SHRIMP U-Pb data are listed in **Table A10**.

Laser ablation inductively coupled plasma mass spectrometry (LA-ICP-MS): LA-ICP-MS data were acquired at the Natural History Museum (Department of Mineralogy) in London and at Johann-Wolfgang-Goethe University Frankfurt/Main (Institute of Mineralogy). Both institutes apply different analytical instrumentations and accordingly different methodological approaches followed by specific data reduction routines.

Analytical instrumentation, methodology and data reduction at Natural History Museum in London: Isotopic analyses were achieved at LA-ICP-MS applying operating procedures similar to those described by Fernández-Suárez et al. (2002) and Jeffries et al. (2003). Analytical instrumentation consists of a frequency quintupled Nd:YAG laser ablation system, λ=213 nm (NewWave Research, USA) coupled to a quadrupole based ICP-MS instrument (Plasma Quad 3, Thermo Elemental, UK) with an enhanced sensitivity interface. Samples and standard were placed

in an airtight chamber which was flushed by helium gas carrying the ablated material to the ICP-MS. Data were collected in discrete runs of 20 analyses, comprising 12 unknowns bracketed before and after by 4 analyses of the standard zircon. $^{206}Pb/^{238}U$ and $^{207}Pb/^{206}Pb$ ratios of the unknowns were determined relative to that of the 91500 zircon standard with certified ID-TIMS ages of 1062.4 ± 0.4 Ma for $^{206}Pb/^{238}U$ and 1065.4 ± 0.3 Ma for $^{207}Pb/^{206}Pb$ (Wiedenbeck et al. 1995). Collection of data spanned up to 180s per analysis and includes a gas background taken during the initial ca. 60s.

To reduce the extent of inter-element laser induced fractionation, the sample was moved relative to the laser beam along a line. The nominal diameter of the laser beam was 60μm for the standard and 30μm or 45μm for the unknowns. In very few cases a nominal spot size diameter of 18μm or 60μm was applied to the unknowns. Pulse energy of the laser was 0.01–0.1 mJ per pulse (depending on nominal beam diameter) with an energy density of 3.5 J/cm^2 and a repetition rate of 20 Hz.

Raw data reduction was performed using LAMTRACE, a macro based spreadsheet written by Simon Jackson (Macquarie University, Australia). Calculations and plotting of concordia diagrams were achieved using Isoplot/Ex rev. 2.49 (Ludwig, 2001), probability density plots and histograms were prepared by AgeDisplay (Sircombe, 2004).

The reported ages are not common lead corrected, since, the ^{204}Pb interferes with ^{204}Hg that is a contaminant of the supply gas (Fernández-Suárez et al. 2002) and the ^{202}Hg peak is commonly too small to be used for a reliable overlap correction (Andersen 2002). Corrections by the ^{208}Pb method (Compston et al. 1984) require a simultaneous determination of the ThO^+/UO^+ ratio with acceptable precision – a condition that is not a priori met by the LA-ICP-MS (Fernández-Suárez et al. 2002). LA-ICP-MS U-Pb data obtained at NHM London are listed in **Table A11**.

Analytical instrumentation, methodology and data reduction at Institute of Mineralogy of Johann Wolfgang Goethe University Frankfurt/Main: Zircon grains were imaged with an electron microprobe (Jeol Superprobe JXA-8900) in CL and BSE mode prior to the analyses by LA-ICP-MS to select appropriate grains/parts of grains.

Isotopic analyses were achieved applying operating procedures similar to those described by Gerdes & Zeh (2006) and Janoušek et al (2006). Analytical instrumentation consists of a frequency quintupled Nd:YAG laser ablation system, λ=213 nm (Merchantek/NewWave Research, USA) coupled to a double focusing magnetic sector field ICP-MS instrument (Finnigan Element2, Thermo Electron Corporation, Germany). Samples and standard were placed in a teardrop-shaped, low volume laser cell (NIGL, Nottingham) with a washout time below 1 s (Horstwood et al. 2003) which was flushed by helium gas carrying the ablated material to the ICP-MS. Data were collected in discrete sequences of 36 analyses, comprising 26 unknowns and 10 analyses of the standard zircon. $^{206}Pb/^{238}U$ and $^{207}Pb/^{206}Pb$ ratios of the unknowns were determined relative to those of the GJ1 zircon standard. GJ1 reference values determined by ID-TIMS are 0.060205 for the $^{207}Pb/^{206}Pb$ ratio and 0.097501 for the $^{206}Pb/^{238}U$ ratio (determined by Wolfgang Dörr in the isotopic lab of the Institute of Geosciences at Justus Liebig University Giessen – pers. comm. Axel Gerdes). The masses ^{202}Hg, $^{204}Hg+Pb$, ^{206}Pb, ^{207}Pb, ^{208}Pb, ^{232}Th, ^{235}U and ^{238}U were measured in peak jumping mode during the initial ca. 30 s for the gas background and during up to 90 s for sample/standard ablation. The nominal diameter of the laser beam was 30μm for all analyses (including standards).

Raw data reduction was performed using an Excel spreadsheet written by Axel Gerdes (Johann Wolfgang Goethe University Frankfurt, Germany). Inter-element laser induced fractionation is corrected by a linear regression that is integrated in the spreadsheet. Errors of the individual analyses of the unknowns are based on counting statistics and were propagated with the reproducibility of the standard over the session (Janoušek et al 2006). Due to relatively low counting rates $^{207}Pb/^{235}U$ ratios were calculated using $^{207}Pb/^{206}Pb/(^{238}U/^{206}Pb \times 1/137.88)$. A common lead correction is not applied to the majority of the analyses for the same reasons as discussed in the previous paragraph. However, the spreadsheet

formally calculates ^{204}Pb corrected $^{207}Pb/^{206}Pb^*$ ratios (Gerdes & Zeh 2006), which can be used for identification of common lead contamination. Although the uncertainties of these common lead corrected ratios are rather large, in the case of common lead contamination the calculated $^{207}Pb/^{206}Pb^*$ ages are significantly younger than uncorrected ones and often in the same range as the $^{206}Pb/^{238}U$ age. For analyses with reliable $^{207}Pb/^{206}Pb^*$ ages ^{204}Pb corrected $^{206}Pb/^{238}U^*$ ages are reported.

Calculations and plotting of concordia diagrams were performed using Isoplot/Ex rev. 2.49 (Ludwig 2001), probability density plots and histograms were prepared by AgeDisplay (Sircombe 2004). LA-ICP-MS U-Pb data obtained at Frankfurt University are given in **Table A12**.

Table A1: List of samples.

Tab. A1: Probenliste.

[1] Numbers in brackets are inferred ages. Age estimation was done using (**1**) published biostratigraphic data in combination with the timescale of Gradstein et al. (2005), (**2**) maximum sedimentation ages obtained by U-Pb dating of detrital zircon, (**3**) extrapolation from radiometrically dated samples, and (4) lithostratigraphic criteria.

[2] Coordinates were read from topographic maps (scale partly 1:10,000, partly 1:50,000) and may be somewhat imprecise. Coordinates do not represent GPS data!

Sample	Rock type	Age[1]	Lithostratigraphic unit	Locality	S-JTSK, CZ, Hermannskogel, Bessel[2] Y(west)	X(south)
Neoproterozoic						
BL	greywacke, deformed	Neoproterozoic (590)		Vlčíce, Uslava River	813046	1091003
BL01	greywacke, deformed	Neoproterozoic (590)		Vlčíce, Uslava River	813046	1091003
DB 1/0	volcanic, mafic	Neoproterozoic (590)		road cut N‘ Týřovice	789340	1047300
DB 1/1	greywacke, deformed	Neoproterozoic (590)		road cut N‘ Týřovice	789327	1047320
DB 1/2	greywacke, deformed	Neoproterozoic (590)	Kralupy-Zbraslav Group	road cut N‘ Týřovice	789312	1047354
DB 1/3	greywacke, deformed	Neoproterozoic (590)		road cut N‘ Týřovice	789317	1047384
PK1	shale, deformed	Neoproterozoic (590)		Trhové Dušniky	778491	1079107
DB 6/12	volcanic, mafic	Neoproterozoic (590)		NNE‘ Skryje	790812	1049351
DB 6/13	volcanic, mafic	Neoproterozoic (590)		NNE‘ Skryje	790793	1049354
NP2 Zb C	siltstone	Neoproterozoic (570)	Davle Fm.	Praha-Zbraslav	747914	1058577
NP1 Zb 4	silty shale	Neoproterozoic (570)	Štěchovice Group	Praha-Zbraslav	746698	1058807
NP1 Zb 5	silty shale	Neoproterozoic (570)	Štěchovice Group	Praha-Zbraslav	748286	1059086
Dob	greywacke, fine-grained	Neoproterozoic (570)	Štěchovice Group	Jezírko quarry, Dobříš	765875	1075565
DOBRIS 01	greywacke, fine-grained	Neoproterozoic (570)	Štěchovice Group	Jezírko quarry, Dobříš	765875	1075565
DOBRIS 02B	greywacke, fine-grained	Neoproterozoic (570)	Štěchovice Group	Jezírko quarry, Dobříš	765875	1075565
DOBRIS 04B	greywacke, fine-grained	Neoproterozoic (570)	Štěchovice Group	Jezírko quarry, Dobříš	765875	1075565
Lower Cambrian – Příbram-Jince-Basin						
PJ1/3	sandstone/conglomerate	Lower Cambrian (530)	Žitec-Hluboš-Fm.	E‘ Hluboš	775522	1076598
HL1	sandstone/conglomerate	Lower Cambrian (530)	Žitec-Hluboš-Fm.	NE‘ Hluboš	775375	1076276
HL2	sandstone/conglomerate	Lower Cambrian (530)	Žitec-Hluboš-Fm.	NE‘ Hluboš	774788	1075423
S1	sandstone	Lower Cambrian (525)	Sádek-Fm.	E‘ Bratkovice	777519	1077124
S2	sandstone	Lower Cambrian (525)	Sádek-Fm.	E‘ Bratkovice	777526	1077029
S4	sandstone	Lower Cambrian (525)	Sádek-Fm.	N‘ Hluboš	776571	1076011

Table A1: Continuation.

Tab. A1: Fortsetzung.

Sample	Rock type	Age[1]	Lithostratigraphic unit	Locality	S-JTSK, CZ, Hermannskogel, Bessel[2] Y(west)	X(south)
Lower Cambrian – Příbram-Jince-Basin						
B	sandstone	Lower Cambrian (525)	Sádek-Fm.	Dominikální Paseky	777647	1076325
D1	sandstone	Lower Cambrian (525)	Sádek-Fm.	Dominikální Paseky	777753	1076217
D1-2	sandstone	Lower Cambrian (525)	Sádek-Fm.	Dominikální Paseky	777768	1076183
D2	sandstone	Lower Cambrian (525)	Sádek-Fm.	Dominikální Paseky	777788	1076180
D2-2	sandstone	Lower Cambrian (525)	Sádek-Fm.	Dominikální Paseky	777788	1076180
D2-5	sandstone	Lower Cambrian (525)	Sádek-Fm.	Dominikální Paseky	777788	1076180
D7	sandstone	Lower Cambrian (525)	Sádek-Fm.	Dominikální Paseky	777927	1075879
D10	sandstone	Lower Cambrian (525)	Sádek-Fm.	Dominikální Paseky	777890	1075760
MM2	shale	Lower Cambrian (520)	Holšiny-Hořice-Fm.	Medalův Mlyn (N‘ Hluboš)	777054	1074725
MM7	sandstone	Lower Cambrian (520)	Holšiny-Hořice-Fm.		777054	1074725
MM8	sandstone	Lower Cambrian (520)	Holšiny-Hořice-Fm.		777054	1074725
MM15	sandstone/conglomerate	Lower Cambrian (520)	Holšiny-Hořice-Fm.	NE‘ Hluboš, SE‘ Holý vrch	775203	1074646
SH2	sandstone/conglomerate	Lower Cambrian (520)	Holšiny-Hořice-Fm.	NNW‘ Hluboš	776767	1075546
H2-2	sandstone	Lower Cambrian (520)	Holšiny-Hořice-Fm.	Dominikální Paseky	777775	1075527
CT2	sandstone	Lower Cambrian (515)	Klouček-Čenkov-Fm.	E‘ Čenkov	776523	1072991
CT3-2	volcaniclastic	Lower Cambrian (515)	Klouček-Čenkov-Fm.	E‘ Čenkov	776323	1072864
C2	sandstone	Lower Cambrian (515)	Klouček-Čenkov-Fm.	S‘ Čenkov	776980	1073924
MM11	sandstone/conglomerate	Lower Cambrian (515)	Klouček-Čenkov-Fm.	SE‘ Čenkov, WSW‘ Holý vrch	775870	1074364
MM12	sandstone	Lower Cambrian (515)	Klouček-Čenkov-Fm.		775870	1074364
MM16	sandstone	Lower Cambrian (515)	Klouček-Čenkov-Fm.	S‘ Čenkov	777151	1074274
CB3	sandstone	Lower Cambrian (510)	Chumava-Baština-Fm.	Jince Vinice	777729	1072381
LS1-3	sandstone	Lower Cambrian (510)	Chumava-Baština-Fm.	N‘ Čenkov	777044	1072542
Middle Cambrian – Příbram-Jince-Basin						
J1-2	sandstone	Middle Cambrian (505)	Jince-Fm.	Jince Vinice	777689	1072387
J3	sandstone	Middle Cambrian (505)	Jince-Fm.	Jince Vinice	777749	1072378
J4	shale	Middle Cambrian (505)	Jince-Fm.	Jince Vinice	777889	1072233
J5	sandstone	Middle Cambrian (505)	Jince-Fm.	Jince Vinice	777969	1072222
J6	sandstone	Middle Cambrian (505)	Jince-Fm.	Jince Vinice	778024	1072183
J7	sandstone	Middle Cambrian (505)	Jince-Fm.	Jince Vinice	778363	1072009
J8	siltstone	Middle Cambrian (505)	Jince-Fm.	Jince Vinice	778512	1071645
J9	sandstone	Middle Cambrian (505)	Jince-Fm.	Jince Vinice	778587	1071603
J10	siltstone	Middle Cambrian (505)	Jince-Fm.	Jince Vinice	778479	1071837
Ji MU2	sandstone	Middle Cambrian (505)	Jince-Fm.	Medový Újezd	797592	1070311
Ji MU3	shale	Middle Cambrian (505)	Jince-Fm.	Medový Újezd	797592	1070311
Oh3	sandstone	Middle Cambrian (505)	Ohrazenice-Fm.	Jince Vinice	778688	1071463
Oh MU1	sandstone/conglomerate	Middle Cambrian (505)	Ohrazenice-Fm.	Medový Újezd	797533	1070322
Middle Cambrian – Skryje-Týřovice area						
DB 1/4a	greywacke	Middle Cambrian (505)	Jince-Fm.	road cut N‘ Týřovice	789317	1047384

GEOLOGICA SAXONICA
Journal of Central European Geology 54 (2008) 1–168

Table A1: Continuation.

Tab. A1: Fortsetzung.

Sample	Rock type	Age[1]	Lithostratigraphic unit	Locality	S-JTSK, CZ, Hermannskogel, Bessel[2] Y(west)	X(south)
Middle Cambrian – Skryje-Týřovice area						
DB 1/4b	greywacke	Middle Cambrian (505)	Jince-Fm.	road cut N‘ Týřovice	789317	1047384
DB 1/5	shale	Middle Cambrian (505)	Jince-Fm.	road cut N‘ Týřovice	789291	1047482
DB 1/6	shale	Middle Cambrian (505)	Jince-Fm.	road cut N‘ Týřovice	789291	1047482
DB 1/7	siltstone	Middle Cambrian (505)	Jince-Fm.	road cut N‘ Týřovice	789275	1047515
DB 1/8	conglomerate	Middle Cambrian (505)	Jince-Fm.	road cut N‘ Týřovice	789275	1047515
DB 1/9	conglomerate	Middle Cambrian (505)	Jince-Fm.	road cut N‘ Týřovice	789265	1047579
DB 1/10	shale	Middle Cambrian (505)	Jince-Fm.	road cut N‘ Týřovice	789260	1047549
DB 1/11	shale	Middle Cambrian (505)	Jince-Fm.	road cut N‘ Týřovice	789249	1047613
DB 1/12	conglomerate	Middle Cambrian (505)	Jince-Fm.	road cut N‘ Týřovice	789234	1047646
DB 1/13	greywacke	Middle Cambrian (505)	Jince-Fm.	road cut N‘ Týřovice	789234	1047646
DB 2/1	sandstone	Middle Cambrian (505)	Jince-Fm.	Kamenná hůrka, SW‘ Týřovice	790408	1048786
DB 2/2	sandstone	Middle Cambrian (505)	Jince-Fm.		790408	1048786
DB 3/1	greywacke	Middle Cambrian (505)	Jince-Fm.	road cut SSW‘ Týřovice	789960	1049445
DB 3/3	shale	Middle Cambrian (505)	Jince-Fm.	road cut SSW‘ Týřovice	790122	1049452
DB 3/4	shale	Middle Cambrian (505)	Jince-Fm.	road cut SSW‘ Týřovice	790103	1049455
DB 5/2	greywacke	Middle Cambrian (505)	Jince-Fm.	Pod trnim, SW‘ Týřovice	790121	1048890
DB 6/1	shale	Middle Cambrian (505)	Jince-Fm.	road cut N‘ Skryje	790962	1049548
DB 6/2	shale	Middle Cambrian (505)	Jince-Fm.	road cut N‘ Skryje	790942	1049551
DB 6/3	shale	Middle Cambrian (505)	Jince-Fm.	road cut N‘ Skryje	790964	1049422
DB 6/4	shale	Middle Cambrian (505)	Jince-Fm.	road cut N‘ Skryje	791064	1049283
DB 6/6	sandstone	Middle Cambrian (505)	Jince-Fm.	road cut N‘ Skryje	791025	1049289
DB 6/7	sandstone/conglomerate	Middle Cambrian (505)	Jince-Fm.	road cut N‘ Skryje	790902	1049275
DB 6/8	greywacke	Middle Cambrian (505)	Jince-Fm.	road cut N‘ Skryje	791014	1049353
DB 6/9	greywacke	Middle Cambrian (505)	Jince-Fm.	road cut N‘ Skryje	790902	1049275
DB 6/14	shale	Middle Cambrian (505)	Jince-Fm.	road cut N‘ Skryje	790718	1049396
Upper Cambrian – Křivoklát-Rokycany volcanic complex						
DB 1/14	volcanic, mafic	Upper Cambrian (500)		road cut N‘ Týřovice	789252	1047768
DB 1/15	volcanic, mafic	Upper Cambrian (500)		road cut N‘ Týřovice	789239	1047677
DB 1/16	volcanic, mafic	Upper Cambrian (500)		road cut N‘ Týřovice	789219	1047680
DB 1/17	volcanic, mafic	Upper Cambrian (500)		road cut N‘ Týřovice	789223	1047710
DB 1/18	volcanic, mafic	Upper Cambrian (500)		road cut N‘ Týřovice	789204	1047713
DB 1/19	volcanic, mafic	Upper Cambrian (500)		road cut N‘ Týřovice	789208	1047744
DB 1/20	volcanic, mafic	Upper Cambrian (500)		road cut N‘ Týřovice	789197	1047808
DB 1/22	volcanic, felsic	Upper Cambrian (500)		road cut ENE‘ Týřovice	789236	1048489
DB 1/23	volcanic, mafic	Upper Cambrian (500)		road cut NE‘ Týřovice	789213	1048055
DB 3/2	volcanic, felsic	Upper Cambrian (500)		road cut SSW‘ Týřovice	790182	1049443
DB 3/5	volcanic, felsic	Upper Cambrian (500)		road cut SSW‘ Týřovice	790201	1049440
DB 3/6	volcanic, felsic	Upper Cambrian (500)		road cut SSW‘ Týřovice	790241	1049435
DB 5/1	volcanic, felsic	Upper Cambrian (500)		SW‘ Týřovice	790174	1048976

Table A1: Continuation.

Tab. A1: Fortsetzung.

Sample	Rock type	Age[1]	Lithostratigraphic unit	Locality	S-JTSK, CZ, Hermannskogel, Bessel[2] Y(west)	X(south)
Upper Cambrian – Křivoklát-Rokycany volcanic complex						
KR1A	volcanic, felsic	Upper Cambrian (500)		Mlečice	795851	1054294
KR1B	volcanic, felsic	Upper Cambrian (500)		Mlečice	795851	1054294
KR1C	volcanic, felsic	Upper Cambrian (500)		Mlečice	795851	1054294
KR2A	volcanic, mafic	Upper Cambrian (500)		Roztoky	770233	953121
KR2B	volcanic, mafic	Upper Cambrian (500)		Roztoky	770233	953121
KR4A	volcanic, felsic	Upper Cambrian (500)		Zadní Robce	783399	1049464
KR4B	volcanic, felsic	Upper Cambrian (500)		Zadní Robce	783399	1049464
KR4C	volcanic, felsic	Upper Cambrian (500)		Zadní Robce	783399	1049464
OKR	volcanic, felsic	Upper Cambrian, 500		Třebnuška	795268	1057596
OKR01	volcanic, felsic	Upper Cambrian, 500		Třebnuška	795268	1057596
Ordovician – Prague synform						
Tr To1	conglomerate/sandstone	Lower Ordovician (480)	Třenice Fm.	Točník	783748	1059324
Tr To3	conglomerate/sandstone	Lower Ordovician (480)	Třenice Fm.	Točník	783748	1059324
Tr To7	conglomerate/sandstone	Lower Ordovician (480)	Třenice Fm.	Točník	783748	1059324
Tr To8	conglomerate/sandstone	Lower Ordovician (480)	Třenice Fm.	Točník	783748	1059324
Tocnik	conglomerate/sandstone	Lower Ordovician (480)	Třenice Fm.	Točník	783748	1059324
Tr MU1	conglomerate/sandstone	Lower Ordovician (480)	Třenice Fm.	Medový Újezd	797490	1070324
Mi Mi2	silicified shale	Lower Ordovician (475)	Mílina Fm.	Hrmovka Hill, S‘ Olešná	790652	1071736
Kl RS1	shale	Lower/Middle Ord. (470)	Klabava Fm.	Rokycany stráň	807683	1071834
Kl RS4	shale	Lower/Middle Ord. (470)	Klabava Fm.	Rokycany stráň	807683	1071834
Kl RS6	shale	Lower/Middle Ord. (470)	Klabava Fm.	Rokycany stráň	807683	1071834
Kl RS9	shale	Lower/Middle Ord. (470)	Klabava Fm.	Rokycany stráň	807683	1071834
Kl RS12	shale	Lower/Middle Ord. (470)	Klabava Fm.	Rokycany stráň	807683	1071834
Kl BoA	conglomerate	Lower/Middle Ord. (470)	Klabava Fm.	Borek	804900	1071915
Kl MU1	conglomerate	Lower/Middle Ord. (470)	Klabava Fm.	Medový Újezd	797440	1070325
Kl MU2	shale	Lower/Middle Ord. (470)	Klabava Fm.	Medový Újezd	797440	1070325
CV 03	shale	Middle Ordovician (465)	Šárka Fm.	Praha, Červený vrch		
CV 04	shale	Middle Ordovician (465)	Šárka Fm.	Praha, Červený vrch		
CV 05	shale	Middle Ordovician (465)	Šárka Fm.	Praha, Červený vrch		
CVP 01	concretion, siliceous	Middle Ordovician (465)	Šárka Fm.	Praha, Červený vrch		
CVP 02	concretion, siliceous	Middle Ordovician (465)	Šárka Fm.	Praha, Červený vrch		
Sa Ej2	oolithic iron ore	Middle Ordovician (465)	Šárka Fm.	Ejpovice	812009	1070750
Sa My1	siltstone	Middle Ordovician (465)	Šárka Fm.	Mýto, Svatoštěphánský rybník	794712	1069137
Ko Ze1	volcanic, mafic	Lower/Middle Ord.	All: Komarov Volcanic Complex	N‘ Žebrák	783654	1060505
Ko Ze2	volcanic, mafic	Lower/Middle Ord.		N‘ Žebrák		
Ko Ze3	volcanic, mafic	Lower/Middle Ord.		N‘ Žebrák		
Ko Ze4	volcanic, mafic	Lower/Middle Ord.		N‘ Žebrák		
Ko Ze5	volcanic, mafic	Lower/Middle Ord.		N‘ Žebrák		

GEOLOGICA SAXONICA
Journal of Central European Geology 54 (2008) 1–168

Table A1: Continuation.

Tab. A1: Fortsetzung.

Sample	Rock type	Age[1]	Lithostratigraphic unit	Locality	S-JTSK, CZ, Hermannskogel, Bessel[2] Y(west)	X(south)
Ordovician – Prague synform						
Ko Ze6	volcanic, mafic	Lower/Middle Ord.	All: Komarov Volcanic Complex	N‘ Žebrák		
Ko Ze8	volcanic, mafic	Lower/Middle Ord.		N‘ Žebrák		
Ko Ze9	volcanic, mafic	Lower/Middle Ord.		N‘ Žebrák	783596	1060649
Zebrak1	volcanic, mafic	Lower/Middle Ord.		N‘ Žebrák	783654	1060505
Zebrak2	volcanic, mafic	Lower/Middle Ord.		N‘ Žebrák	783654	1060505
Zebrak3	volcanic, mafic	Lower/Middle Ord.		N‘ Žebrák	783620	1060580
Zebrak4	volcanic, mafic	Lower/Middle Ord.		N‘ Žebrák	783620	1060580
EJP Do1	sandstone	Middle/Upper Ord. (460)	Dobrotivá Fm.	Ejpovice	812239	1070792
Do SP2	sandstone	Middle/Upper Ord. (460)	Dobrotivá Fm.	Starý Plzenec, Černá stráň	815680	1075598
Do SP4	sandstone	Middle/Upper Ord. (460)	Dobrotivá Fm.	Starý Plzenec, Černá stráň	815680	1075598
Do CS1	sandstone	Middle/Upper Ord. (460)	Dobrotivá Fm.		741103	1040000
Do CS3	sandstone	Middle/Upper Ord. (460)	Dobrotivá Fm.	Praha, Jablonka (Černá Skála)		
Do CS4	siltstone	Middle/Upper Ord. (460)	Dobrotivá Fm.			
Do CS5	siltstone	Middle/Upper Ord. (460)	Dobrotivá Fm.			
Do CS6	siltstone	Middle/Upper Ord. (460)	Dobrotivá Fm.		741084	1040054
Li BS0	shale	Upper Ordovician (455)	Libeň Fm.	Praha, Bíla Skála	740138	1040312
Li BS2	sandstone	Upper Ordovician (455)	Libeň Fm.	Praha, Bíla Skála	740092	1040330
Li BS3	sandstone	Upper Ordovician (455)	Libeň Fm.	Praha, Bíla Skála	740071	1040347
Li BS4	siltstone	Upper Ordovician (455)	Libeň Fm.	Praha, Bíla Skála	740028	1040347
Li BS6	siltstone	Upper Ordovician (455)	Libeň Fm.	Praha, Bíla Skála	739932	1040330
Li BS7	sandstone	Upper Ordovician (455)	Libeň Fm.	Praha, Bíla Skála	739911	1040320
LiMo1	shale	Upper Ordovician (455)	Libeň Fm.	Praha-Motol, railway cut	749622	1044886
LiMo2	siltstone	Upper Ordovician (455)	Libeň Fm.	Praha-Motol, railway cut	749622	1044886
Le Zb2	sandstone	Upper Ordovician (455)	Letná Fm.	Praha-Zbraslav, Zavist	745991	1055411
Le Zb3	sandstone	Upper Ordovician (455)	Letná Fm.	Praha-Zbraslav, Zavist	745989	1055401
Le Zb4	shale	Upper Ordovician (455)	Letná Fm.	Praha-Zbraslav, Zavist	745989	1055390
Le Zb5	sandstone	Upper Ordovician (455)	Letná Fm.	Praha-Zbraslav, Zavist	745986	1055366
Le Zb6	sandstone	Upper Ordovician (455)	Letná Fm.	Praha-Zbraslav, Zavist	745986	1055366
Le Zb10	sandstone	Upper Ordovician (455)	Letná Fm.	Praha-Zbraslav, Zavist	754978	1055559
Vi Be1a	shale	Upper Ordovician (455)	Vinice Fm.	Beroun-North	769843	1052242
Vi Be1b	shale	Upper Ordovician (455)	Vinice Fm.	Beroun-North	769843	1052242
Za Vi1	sandstone	Upper Ordovician (450)	Zahořany Fm.	Loděnice - vineyard	763765	1050850
Za Vi3	sandstone	Upper Ordovician (450)	Zahořany Fm.	Loděnice - vineyard	763765	1050850
Za Vi4	siltstone	Upper Ordovician (450)	Zahořany Fm.	Loděnice - vineyard	763765	1050850
Za HV2	siltstone	Upper Ordovician (450)	Zahořany Fm.		761310	1049715
Bo VC1	shale	Upper Ordovician (450)	Bohdalec Fm.	Velká Chuchle	746439	1051269
Bo VC2	shale	Upper Ordovician (450)	Bohdalec Fm.	Velká Chuchle	746439	1051269
KD Le S1	shale	Upper Ordovician (445)	Králův Dvůr Fm.	Levín	774225	1056488
KD Le S2	shale	Upper Ordovician (445)	Králův Dvůr Fm.	Levín	774225	1056488
Ko Le D1d	glaciomarine diamictite	Upper Ordovician (445)	Kosov Fm.	Levín	774265	1056520

Table A1: Continuation.

Tab. A1: Fortsetzung.

Sample	Rock type	Age[1]	Lithostratigraphic unit	Locality	S-JTSK, CZ, Hermannskogel, Bessel[2] Y(west)	X(south)
Ordovician – Prague synform						
Ko Le D1d	glaciomarine diamictite	Upper Ordovician (445)	Kosov Fm.	Levín	774265	1056520
Ko Le S1	shale	Upper Ordovician (445)	Kosov Fm.	Levín	774265	1056520
Ko Le S2	shale	Upper Ordovician (445)	Kosov Fm.	Levín	774265	1056520
Ko Le1	sandstone	Upper Ordovician (445)	Kosov Fm.	Levín	774337	1056544
Carad 1	volcanic, mafic	Upper Ordovician (455)		N‘ Netolice	779499	1063499
Carad 2	volcanic, mafic	Upper Ordovician (455)		N‘ Netolice	779499	1063499
Silurian						
Loden 1	volcanic, mafic	Wenlock (425)		Špicaty Vrch near Loděnice	763149	1051994
Loden 2.1	volcanic, mafic	Wenlock (425)			763149	1051994
Loden 2.2	volcanic, mafic	Wenlock (425)			763149	1051994
Devonian						
Roblin	greywacke (carbonaceous)	Givet (390)	Srbsko Fm.	Praha-Hlubočepy, railway cut		

GEOLOGICA SAXONICA
Journal of Central European Geology 54 (2008) 1–168

Table A2: Detrital modes of Cambrian and Ordovician sandstones and conglomerates. Modal compositions are given in vol.-%. **Q**…quartz, **F**…feldspar, **L**…lithic fragments.

Tab. A2: Modalbestände der kambrischen und ordovizischen Sandsteine und Konglomerate.

Sample	Q	F	L	counted grains
Lower Cambrian				
PJ1/3	80	6	14	415
HL1	68	2	29	391
HL2	83	3	15	432
S1	66	34	0	448
S2	66	32	2	463
S4	61	39	0	429
D1	58	42	0	462
D2-2	51	49	0	439
D2-5	51	49	0	510
MM15	84	9	7	445
H2-2	87	7	6	457
SH2	90	3	7	368
MM11	92	5	3	565
MM12	48	32	20	418
MM16	66	24	10	414
CB3	83	10	7	337
Middle Cambrian				
J3	69	22	10	408
J5	33	46	21	420
J9B	67	32	1	445
DB 1/4a	62	27	11	565
DB 1/4b	64	27	9	449
DB 1/13	61	20	19	445
DB 6/5	79	19	2	413
DB 6/6	76	21	3	406
DB 6/8	71	25	4	477
DB 3/1	63	36	1	381
DB 5/2	75	24	1	404
DB 6/6G	63	29	8	424
DB 6/7	100	0	0	105
OhMU1	88	10	2	282
Oh3	89	4	7	456
Lower/Middle Ordovician				
TrTo1	64	18	18	307
TrTo7	65	8	27	353
TrTo8	58	15	27	357
TrMU1	25	26	49	349
KlMU1	20	24	56	399
KlBoA	28	28	44	205

Table A2: Continuation.

Tab. A2: Fortsetzung.

Sample	Q	F	L	counted grains
Middle/Upper Ordovician				
DoSP2	96	3	1	363
DoSP4	98	2	0	324
LiBS2	98	2	0	353
LiBS3	98	1	1	351
LiBS7	99	1	0	345
LeZb2	87	13	0	319
LeZb6	86	14	0	308
LeZb10	89	10	1	318
KoLe1	93	7	0	253

GEOLOGICA SAXONICA
Journal of Central European Geology 54 (2008) 1–168

Table A3: Major element data of volcanic rocks..

Tab. A3: Hauptelementdaten der vulkanischen Gesteine.

SAMPLE	SiO_2	Al_2O_3	Fe_2O_3	MnO	MgO	CaO	Na_2O	K_2O	TiO_2	P_2O_5	LOI	TOTAL
Neoproterozoic												
DB 1/0	46.8	15.4	9.62	0.256	9.32	8.48	3.24	0.08	0.945	0.09	5.52	99.8
DB 6/11	43.3	14.4	10.4	0.174	7.21	6.75	3.19	0.29	1.72	0.16	11.3	98.9
DB 6/12	49.5	17.4	6.94	0.069	8.81	3.59	4.39	0.66	1.08	0.07	7.28	99.8
Cambrian												
KR1A	66.4	16.0	5.34	0.071	0.47	1.36	4.77	2.11	0.276	0.15	2.84	99.8
KR1B	65.8	15.8	5.02	0.127	0.45	1.95	4.53	2.29	0.271	0.15	3.51	100.0
KR1C	66.0	15.7	4.84	0.090	0.46	2.25	4.65	2.06	0.271	0.15	3.56	100.1
KR2A	48.4	18.1	6.37	0.115	8.82	5.74	3.40	1.01	1.33	0.16	6.77	100.3
KR2B	49.3	16.7	8.00	0.124	5.09	6.32	4.02	1.31	1.23	0.15	7.94	100.2
KR4A	78.1	13.6	0.81	0.004	0.15	0.07	3.17	2.35	0.110	0.06	1.78	100.2
KR4B	78.7	13.1	0.89	0.004	0.16	0.06	2.75	2.41	0.098	0.06	1.82	100.0
KR4C	78.5	12.9	0.90	0.004	0.17	0.08	1.88	2.83	0.098	0.07	2.08	99.5
OKR	75.8	13.1	1.66	0.010	0.16	0.05	2.47	4.94	0.202	0.04	1.41	99.9
OKR 01	76.4	13.0	1.32	0.006	0.13	0.04	2.48	5.23	0.192	0.04	1.10	100.0
DB 1/14	50.3	16.6	7.96	0.125	3.20	8.98	2.86	0.41	1.06	0.14	7.71	99.4
DB 1/15	51.4	17.6	8.59	0.106	3.91	4.36	4.53	1.10	1.12	0.14	6.99	99.8
DB 1/16	49.7	16.7	7.84	0.132	3.54	9.18	3.05	0.28	1.07	0.14	7.34	99.0
DB 1/17	52.0	17.7	7.66	0.110	3.61	8.33	3.34	0.31	1.09	0.13	6.01	100.3
DB 1/18	51.4	17.1	8.82	0.096	4.59	4.34	3.20	1.38	1.09	0.14	7.81	100.0
DB 1/19	49.4	17.2	8.77	0.105	2.91	6.28	3.65	1.46	1.25	0.14	8.83	100.0
DB 1/20	50.6	16.5	8.87	0.104	4.90	6.57	3.70	0.68	1.15	0.15	6.30	99.6
DB 1/22	68.4	14.4	4.18	0.160	0.13	1.63	3.90	2.34	0.118	0.08	3.68	99.1
DB 1/23	53.3	17.1	7.97	0.133	4.99	6.15	4.73	0.94	1.24	0.16	3.15	99.8
DB 3/2	70.4	15.0	3.93	0.079	0.11	0.14	4.61	1.97	0.127	0.10	2.45	99.0
DB 3/5	71.1	15.1	3.47	0.051	0.09	0.10	4.53	2.18	0.113	0.09	2.32	99.1
DB 3/6	71.3	14.9	3.63	0.073	0.12	0.66	4.60	1.98	0.107	0.05	2.58	100.0
DB 5/1	70.2	15.1	4.08	0.077	0.13	0.56	4.61	1.99	0.139	0.08	2.59	99.6
Ordovician												
KoZe1	46.4	12.6	7.26	0.119	4.17	10.5	4.58	0.22	2.21	0.81	10.4	99.3
KoZe2	36.1	15.9	12.4	0.163	8.87	7.77	2.50	0.62	3.01	0.96	10.3	98.5
KoZe3	55.0	10.3	5.26	0.094	4.87	8.55	3.31	0.15	1.66	0.63	9.40	99.2
KoZe4	29.5	12.0	6.85	0.382	6.35	18.9	2.71	0.36	1.69	0.46	19.4	98.6
KoZe5	31.1	8.56	5.25	0.184	3.58	24.1	1.65	0.73	1.28	0.62	21.6	98.6
KoZe6	20.0	7.58	6.27	0.113	5.16	29.5	1.13	0.29	1.22	0.57	26.9	98.7
KoZe8	38.7	13.5	8.27	0.129	8.34	10.2	3.87	0.24	1.78	0.65	13.0	98.6
KoZe9	49.8	10.3	6.08	0.118	5.47	9.82	3.04	0.17	1.68	0.47	12.4	99.4
Zebrak 1	38.4	14.6	9.86	0.126	8.95	8.33	3.56	0.10	2.65	0.61	11.8	99.0
Zebrak 2	40.5	14.6	9.16	0.123	9.15	7.64	3.54	0.17	2.93	0.70	11.1	99.6
Zebrak 3	48.4	11.1	7.72	0.111	7.03	6.98	2.85	0.11	1.85	0.51	12.4	99.1
Zebrak 4	44.1	14.3	10.5	0.118	9.26	3.26	3.48	0.24	2.33	0.65	11.3	99.6
Carad 1	47.1	15.8	12.4	0.076	4.03	4.57	3.72	1.82	1.35	0.67	7.20	98.7
Carad 2	50.8	15.8	11.1	0.068	3.41	3.81	3.80	2.28	1.35	0.68	5.89	99.0
Silurian												
Loden 1	43.2	14.2	13.1	0.167	7.71	10.1	2.34	0.78	2.90	0.52	4.01	99.0
Loden 2.1	35.1	13.9	12.7	0.115	4.19	14.6	2.02	0.39	3.04	0.44	12.1	98.6
Loden 2.2	35.2	13.8	12.9	0.105	4.26	13.0	3.19	0.27	3.06	0.44	12.8	99.0

Table A4: Trace element data of volcanic rocks.

Tab. A4: Spurenelementdaten der vulkanischen Gesteine.

SAMPLE	Sc	Be	V	Cr	Co	Ni	Cu	Zn	Ga	Ge	As	Rb	Sr	Y	Zr	Nb	Mo	Ag	In	Sn	Sb	Cs	Ba	Hf	Ta	W	Tl	Pb	Bi	Th	U
Neoproterozoic																															
DB 1/0	43	0	250	462	38	108	55	118	16	2	0	6	122	25	60	3	0	0	0	0	0	1	101	2	0	0	0	0	0	0.3	0.6
DB 6/11	44	0	280	232	42	88	61	118	17	0	0	12	176	39	117	4	0	0	0	0	5	2	288	3	0	0	0	0	0	0.6	0.3
DB 6/12	40	0	236	559	49	238	70	99	15	0	11	12	253	27	59	0	0	0	0	0	3	3	799	2	0	0	1	0	0	0.2	0.4
Cambrian																															
KR1A	5	3	0	40	4	0	21	134	24	2	0	72	103	46	362	8	0	1	0	4	0	3	383	9	1	0	1	13	0	5.9	4.2
KR1B	5	3	0	0	4	0	24	125	23	2	0	74	102	44	347	8	0	1	0	4	0	3	402	8	1	0	1	14	0	5.5	3.8
KR1C	5	3	0	0	4	0	0	99	22	2	0	62	109	43	340	8	0	0	0	4	0	3	339	8	1	0	0	13	0	5.3	3.8
KR2A	29	0	190	182	38	92	37	118	19	3	0	21	188	31	130	5	0	0	0	0	0	11	652	3	0	0	0	13	0	1.3	1.0
KR2B	28	2	176	167	32	87	0	106	18	3	0	34	324	25	123	4	0	0	0	0	2	3	297	3	0	0	0	15	0	1.1	0.9
KR4A	3	4	12	150	0	0	0	0	22	3	0	94	39	28	109	11	0	0	0	7	1	6	129	4	1	3	1	16	0	6.7	3.3
KR4B	3	4	11	102	0	0	0	61	23	3	0	100	32	27	97	10	0	0	0	8	1	7	94	4	1	2	1	17	0	6.7	3.7
KR4C	3	4	11	123	0	0	0	62	22	3	0	107	30	22	92	10	0	0	0	7	1	8	86	3	1	2	1	11	0	6.0	2.8
OKR	9	3	14	346	3	0	21	88	29	3	0	174	40	86	356	13	0	0	0	7	3	5	1030	11	1	3	1	0	0	12.9	4.6
OKR01	8	3	11	0	2	0	0	89	28	3	0	197	36	81	337	14	0	0	0	11	4	6	1120	11	1	3	2	11	0	13.4	5.2
DB 1/14	22	0	159	97	27	0	21	70	18	2	0	15	194	28	138	4	0	0	0	31	2	3	164	3	0	0	0	0	2	1.5	1.1
DB 1/15	24	0	154	58	28	53	30	121	20	2	0	31	113	28	136	5	0	0	0	2	0	7	160	4	0	0	1	12	0	1.4	1.0
DB 1/16	23	0	154	100	26	0	26	90	18	2	0	7	197	26	134	4	0	0	0	0	1	2	155	3	0	0	0	0	0	1.5	1.0
DB 1/17	23	0	150	103	28	61	32	92	20	2	0	6	218	28	129	5	0	0	0	2	0	3	161	4	0	0	0	0	0	1.5	1.0
DB 1/18	23	0	152	0	34	0	24	102	19	3	0	61	126	25	137	4	7	0	0	0	1	8	271	3	0	0	1	0	0	1.4	1.0
DB 1/19	27	0	164	150	32	88	32	102	19	2	0	43	105	25	127	5	0	0	0	0	1	4	145	3	0	0	1	0	0	1.2	0.9
DB 1/20	25	0	182	183	31	89	29	99	18	2	0	21	151	26	135	4	0	0	0	0	1	11	204	3	0	0	0	0	0	1.4	1.1
DB 1/22	2	2	0	71	2	0	0	243	24	3	0	89	45	33	240	9	0	0	0	5	2	3	293	7	1	2	1	49	0	8.0	4.5
DB 1/23	26	0	163	165	30	77	31	109	21	3	0	22	701	31	151	6	0	0	0	4	1	2	383	4	0	0	0	10	0	1.8	1.2
DB 3/2	0	4	11	130	2	0	39	109	26	3	0	62	59	34	270	9	0	0	0	5	2	4	500	8	1	0	1	15	0	7.3	4.7
DB 3/5	0	4	0	77	2	0	0	145	26	4	0	65	47	32	229	10	0	0	0	5	6	3	314	7	1	0	1	26	0	7.7	4.5
DB 3/6	0	4	0	141	2	0	21	115	28	3	0	68	52	32	237	10	0	0	0	5	5	3	307	7	1	0	1	14	0	8.4	4.3
DB 5/1	3	3	0	98	2	0	0	119	27	3	0	67	48	38	298	10	0	0	0	4	2	3	397	8	1	0	1	20	0	7.3	3.7
Ordovician																															
KoZe1	14	4	84	155	17	65	34	102	15	0	0	5	269	18	194	54	0	1	0	2	0	0	119	5	4	0	0	0	1	4.6	1.3

Table A4: Continuation.

Tab. A4: Fortsetzung.

SAMPLE	Sc	Be	V	Cr	Co	Ni	Cu	Zn	Ga	Ge	As	Rb	Sr	Y	Zr	Nb	Mo	Ag	In	Sn	Sb	Cs	Ba	Hf	Ta	W	Tl	Pb	Bi	Th	U
Ordovician																															
KoZe2	19	4	216	102	38	100	55	149	23	2	0	11	1960	28	236	72	5	2	0	3	0	3	673	6	5	0	0	0	0	5.8	1.8
KoZe3	14	3	131	278	22	77	76	70	13	0	0	0	136	18	147	49	0	0	0	0	0	1	201	4	3	0	0	0	0	3.7	1.7
KoZe4	16	3	147	162	20	92	67	101	14	0	0	6	170	14	143	48	0	0	0	0	0	1	155	4	3	0	0	0	0	3.9	1.4
KoZe5	13	3	106	168	18	163	126	71	11	0	0	15	161	18	110	37	0	0	0	11	0	0	48	3	2	0	0	0	0	2.8	0.9
KoZe6	12	2	99	169	24	189	129	96	13	0	0	7	335	14	108	37	0	0	0	3	0	0	72	3	2	0	0	0	0	2.6	1.1
KoZe8	15	3	135	118	17	93	60	99	19	0	0	5	112	19	150	49	0	0	0	0	0	1	236	4	3	3	0	0	0	4.1	1.3
KoZe9	13	3	143	141	17	89	69	72	15	0	0	7	82	16	140	48	0	0	0	0	0	7	122	4	3	0	0	0	0	3.9	1.7
Zebrak 1	19	3	193	218	36	110	90	108	20	0	0	5	235	21	208	59	0	0	0	0	0	2	294	6	4	0	0	0	0	4.7	1.5
Zebrak 2	20	3	205	218	37	116	158	107	21	0	0	0	275	24	234	71	0	0	0	0	0	1	302	6	5	0	0	0	0	5.1	1.6
Zebrak 3	16	3	166	160	18	159	114	60	17	0	0	6	66	17	160	57	0	0	0	0	0	6	259	4	4	0	0	0	0	4.2	1.4
Zebrak 4	19	3	209	176	28	227	157	104	22	0	13	9	86	21	200	71	0	0	0	0	0	9	1340	5	5	0	1	0	0	5.1	1.8
Carad 1	8	5	74	76	25	66	40	196	30	2	0	30	688	16	388	59	0	0	0	4	0	0	1230	9	4	0	0	14	0	5.2	1.9
Carad 2	8	5	67	96	22	57	35	165	28	2	0	36	675	16	403	61	4	0	0	3	0	0	1130	10	4	0	0	0	0	5.5	1.9
Silurian																															
Loden 1	21	3	232	496	47	173	337	120	24	2	0	7	1090	22	218	39	6	1	0	0	0	0	393	6	2	0	0	0	1	2.2	0.9
Loden 2.1	24	3	242	423	54	251	73	141	23	2	10	0	1090	21	183	27	5	0	0	0	0	0	120	5	2	0	0	0	0	1.7	0.7
Loden 2.2	25	3	262	403	56	269	76	155	24	0	26	0	838	21	187	27	0	0	0	0	0	0	70	5	2	0	0	0	0	1.6	0.7

GEOLOGICA SAXONICA
Journal of Central European Geology
54 (2008) 1–168

Table A5: Rare earth element data of volcanic rocks.

Tab. A5: Seltenerdelementdaten der vulkanischen Gesteine.

SAMPLE	La	Ce	Pr	Nd	Sm	Eu	Gd	Tb	Dy	Ho	Er	Tm	Yb	Lu
Neoproterozoic														
DB 1/0	2.6	6.8	1.19	6.6	2.4	0.90	3.1	0.7	4.1	1.0	2.6	0.43	2.5	0.40
DB 6/11	4.5	12.6	2.32	12.9	4.5	1.36	5.5	1.2	6.9	1.5	4.1	0.64	3.7	0.56
DB 6/12	1.8	5.0	1.01	5.9	2.3	0.89	3.3	0.8	4.7	1.1	3.1	0.48	2.8	0.42
Cambrian														
KR1A	27.3	57.3	7.36	31.0	7.1	1.64	6.9	1.3	8.0	1.7	5.1	0.81	4.9	0.71
KR1B	25.9	54.2	6.97	29.6	6.8	1.60	6.7	1.3	7.5	1.6	4.7	0.76	4.7	0.66
KR1C	24.5	52.0	6.65	27.7	6.5	1.57	6.4	1.2	7.1	1.5	4.6	0.72	4.5	0.64
KR2A	8.4	20.4	2.96	14.5	4.1	1.53	4.7	1.0	5.5	1.2	3.3	0.50	2.9	0.43
KR2B	7.2	16.7	2.41	11.8	3.2	0.99	3.7	0.8	4.6	1.0	2.8	0.45	2.7	0.39
KR4A	13.6	32.2	4.15	16.2	4.0	0.27	3.8	0.9	4.7	0.9	2.3	0.36	1.8	0.25
KR4B	11.2	25.5	3.21	12.0	3.0	0.22	2.8	0.7	4.4	0.9	2.3	0.39	2.0	0.28
KR4C	11.4	25.7	3.21	12.0	2.7	0.19	2.5	0.7	3.7	0.7	1.9	0.31	1.7	0.23
OKR	50.5	98.1	12.8	54.3	12.4	0.94	11.6	2.3	14.2	2.9	8.7	1.36	8.3	1.23
OKR01	47.5	103	12.6	52.9	12.6	0.98	12.6	2.5	14.5	3.0	9.0	1.42	8.6	1.29
DB 1/14	8.4	19.5	2.59	11.9	3.4	1.25	4.0	0.9	4.6	1.0	2.8	0.47	2.7	0.42
DB 1/15	8.5	18.8	2.76	13.2	3.7	1.44	4.3	0.8	4.7	1.0	2.9	0.46	2.7	0.44
DB 1/16	8.5	19.4	2.54	12.0	3.4	1.22	3.9	0.9	4.6	1.0	2.7	0.46	2.6	0.42
DB 1/17	8.9	18.8	2.73	12.8	3.6	1.32	4.0	0.8	4.6	1.0	2.8	0.44	2.6	0.43
DB 1/18	7.5	18.0	2.36	11.0	3.1	0.98	3.6	0.8	4.5	1.0	2.7	0.47	2.6	0.41
DB 1/19	7.3	16.3	2.44	11.9	3.5	1.23	3.8	0.8	4.4	1.0	2.7	0.42	2.4	0.38
DB 1/20	8.2	19.5	2.64	12.3	3.5	1.29	4.0	0.9	4.7	1.0	2.7	0.47	2.7	0.40
DB 1/22	32.0	66.9	7.66	29.5	6.2	1.25	5.5	1.1	5.3	1.1	3.0	0.52	3.3	0.50
DB 1/23	10.0	21.7	3.16	14.7	4.1	1.39	4.6	0.9	5.2	1.1	3.1	0.49	2.9	0.46
DB 3/2	32.0	62.3	7.79	31.4	6.4	1.33	5.3	1.0	5.3	1.1	3.1	0.52	3.2	0.51
DB 3/5	35.1	71.2	8.66	34.8	7.3	1.52	6.3	1.1	5.4	1.1	2.9	0.46	2.9	0.46
DB 3/6	36.2	70.0	8.76	34.6	6.9	1.31	5.4	1.0	5.0	1.0	2.8	0.47	2.8	0.45
DB 5/1	33.8	65.2	8.09	32.7	6.9	1.45	6.1	1.1	6.1	1.3	3.7	0.63	3.8	0.60
Ordovician														
KoZe1	35.1	69.2	8.30	34.4	7.2	2.35	5.8	0.9	3.9	0.8	2.0	0.30	1.6	0.23
KoZe2	58.2	109	12.5	47.9	10.0	3.28	8.6	1.4	6.1	1.2	3.0	0.44	2.4	0.34
KoZe3	29.6	55.8	6.34	24.1	5.2	1.76	4.5	0.8	3.4	0.7	1.8	0.29	1.5	0.23
KoZe4	32.9	58.9	6.57	24.4	5.2	1.72	4.3	0.7	3.2	0.6	1.6	0.26	1.4	0.22
KoZe5	30.5	53.2	5.77	22.4	4.8	1.63	4.4	0.7	3.4	0.7	1.8	0.29	1.5	0.22
KoZe6	23.6	40.7	4.75	18.1	3.9	1.30	3.5	0.6	2.7	0.6	1.4	0.24	1.2	0.20
KoZe8	38.8	68.9	7.47	27.4	5.8	1.75	5.0	0.8	3.7	0.8	1.9	0.30	1.6	0.25
KoZe9	30.0	54.4	6.01	23.9	4.9	1.36	4.2	0.7	3.2	0.7	1.7	0.27	1.4	0.21
Zebrak 1	31.0	63.7	7.47	30.4	6.8	2.31	6.3	1.1	5.0	0.9	2.3	0.34	1.7	0.26
Zebrak 2	44.9	88.0	9.81	37.8	7.7	2.60	6.9	1.2	5.4	1.0	2.5	0.35	1.9	0.28
Zebrak 3	34.4	63.6	7.16	27.5	5.5	1.58	4.9	0.8	3.8	0.8	1.9	0.31	1.6	0.25
Zebrak 4	40.0	77.2	8.53	33.3	6.7	1.87	6.0	1.0	4.7	0.9	2.3	0.35	2.0	0.29
Carad 1	43.0	86.4	9.80	38.1	7.5	2.45	6.0	0.9	4.0	0.7	1.5	0.23	1.1	0.16
Carad 2	43.5	88.2	9.81	37.4	7.5	2.52	6.0	0.9	4.0	0.7	1.5	0.22	1.1	0.17
Silurian														
Loden 1	26.4	58.2	7.13	30.4	6.9	2.37	6.4	1.0	5.0	1.0	2.4	0.35	1.9	0.28
Loden 2.1	20.4	46.3	5.87	25.6	6.2	2.15	5.9	1.0	4.8	0.9	2.3	0.34	1.8	0.28
Loden 2.2	20.2	45.7	5.76	25.2	6.1	2.25	6.0	1.0	4.7	0.9	2.3	0.33	1.8	0.27

Table A6: Major element data of sedimentary rocks.

Tab. A6: Hauptelementdaten der sedimentären Gesteine.

* CIA (Chemical Index of Alteration) after Nesbit and Young (1982) was not calculated for samples containing carbonate.

SAMPLE	SiO_2	Al_2O_3	Fe_2O_3	MnO	MgO	CaO	Na_2O	K_2O	TiO_2	P_2O_5	LOI	TOTAL	CIA*
Neoproterozoic													
BL	62.5	16.3	6.69	0.081	2.66	0.40	3.29	2.97	0.759	0.20	4.08	100.0	65
BL 01	71.1	13.2	3.94	0.051	1.55	0.50	4.02	2.02	0.513	0.15	1.81	98.9	59
DB 1/3	68.6	13.7	5.10	0.073	0.92	0.33	1.54	3.37	0.600	0.19	4.13	98.6	68
DB 1/2	66.7	14.3	6.55	0.097	2.13	0.27	3.41	2.06	0.684	0.16	4.00	100.3	64
DB 1/1	65.9	15.7	5.25	0.097	2.17	0.40	3.95	2.43	0.618	0.17	3.14	99.8	62
DB PK1	58.8	17.5	7.05	0.112	4.06	1.32	4.50	1.76	0.967	0.28	3.55	99.8	61
NP2ZB C	69.6	13.1	5.38	0.057	2.77	0.45	3.26	1.43	0.757	0.16	2.93	99.9	64
NPZB 5	60.2	13.7	6.24	0.125	2.65	4.76	3.36	2.17	0.648	0.28	5.70	99.8	46
NPZB 4	63.9	15.9	6.09	0.100	3.22	0.52	4.15	2.65	0.571	0.09	2.91	100.1	60
DOBRIS 04B	62.4	16.5	6.96	0.103	2.82	0.58	3.35	3.00	0.678	0.17	3.39	100.0	64
DOBRIS 02B	62.3	15.5	7.01	0.107	2.80	1.48	2.94	3.00	0.670	0.15	4.07	99.9	60
DOBRIS 01	69.0	13.7	4.88	0.062	2.02	1.13	3.64	2.31	0.535	0.11	2.49	99.9	57
DOB	68.7	14.3	4.93	0.066	2.12	1.09	3.89	2.20	0.544	0.11	2.52	100.5	58
Lower Cambrian													
PJ1/3	88.0	5.80	2.57	0.010	0.35	0.03	0.18	1.13	0.335	0.04	1.48	99.9	80
DB HL1	80.5	8.71	3.98	0.013	0.73	0.05	0.22	1.48	0.433	0.06	2.63	98.8	82
DB S1	71.5	11.4	3.88	0.087	0.79	2.82	2.86	1.49	0.835	0.13	4.36	100.1	51
DB S2	74.1	10.5	3.04	0.099	0.51	3.32	2.47	1.77	0.457	0.07	4.30	100.6	47
DB B	88.9	5.01	1.19	0.015	0.26	0.18	2.13	0.35	0.310	0.08	0.97	99.4	55
DB D1-2	77.5	11.0	2.91	0.049	0.92	1.10	3.72	1.21	0.592	0.04	1.13	100.2	54
DB D2	57.7	18.3	7.71	0.116	2.92	1.78	3.05	3.22	1.26	0.23	3.77	100.1	62
DB D2-5	76.1	12.0	2.77	0.058	1.11	0.68	4.83	0.84	0.360	0.07	1.21	99.9	55
DB D7	76.1	11.4	2.84	0.073	1.31	0.76	4.74	0.78	0.549	0.06	1.58	100.1	54
DB D10	78.0	10.6	2.20	0.056	1.07	0.84	4.61	0.56	0.528	0.05	1.50	100.1	53
MM2	53.6	20.7	8.97	0.061	2.74	0.37	0.34	4.30	0.851	0.18	6.89	99.1	79
MM7	85.3	7.70	1.71	0.009	0.55	0.04	0.92	0.96	0.459	0.04	2.35	100.1	75
MM8	68.5	14.5	5.57	0.041	1.37	0.19	1.50	2.32	0.765	0.13	4.79	99.7	74
MM15	93.9	3.20	0.58	0.006	0.09	0.05	-	0.73	0.260	0.03	0.64	99.4	80
SH2	96.6	1.64	0.85	0.002	0.07	0.02	-	0.43	0.082	0.02	0.33	99.9	78
H2-2	95.7	2.12	1.04	0.005	0.09	0.01	0.01	0.55	0.115	0.04	0.43	100.1	80
C2	93.6	3.05	1.44	0.009	0.29	0.02	-	0.65	0.142	0.05	0.95	100.2	83
CT2	96.7	1.71	0.59	0.002	0.03	0.02	-	0.26	0.055	0.03	0.58	99.9	87
CT3-2	58.5	15.1	7.86	0.094	2.97	1.88	6.77	0.38	1.28	0.19	4.07	99.1	51
MM16	88.1	5.34	2.50	0.020	0.52	0.07	1.59	0.54	0.347	0.04	0.94	100.0	51
DB LS1-3	92.8	2.99	2.04	0.004	0.07	0.04	0.19	0.82	0.270	0.09	0.59	99.9	74
DB CB3	88.2	6.28	0.60	0.004	0.09	0.02	0.52	0.68	0.627	0.04	1.90	98.9	80
Middle Cambrian													
DB 1/4A	76.1	10.2	5.58	0.057	0.52	0.45	1.94	1.75	0.490	0.10	3.04	100.2	64
DB 1/4B	76.2	9.95	5.43	0.063	0.50	0.65	1.89	1.73	0.472	0.10	3.35	100.3	63
DB 1/5	62.5	17.2	7.25	0.068	2.67	0.30	2.14	3.13	0.773	0.15	3.87	100.0	71

Table A6: Continuation.

Tab. A6: Fortsetzung.

* CIA (Chemical Index of Alteration) after Nesbit and Young (1982) was not calculated for samples containing carbonate.

SAMPLE	SiO_2	Al_2O_3	Fe_2O_3	MnO	MgO	CaO	Na_2O	K_2O	TiO_2	P_2O_5	LOI	TOTAL	CIA*
Middle Cambrian													
DB 1/6	62.5	16.8	7.08	0.077	2.65	0.42	2.40	3.01	0.817	0.17	4.24	100.1	69
DB 1/7	66.2	15.0	6.03	0.075	2.15	0.97	1.87	2.73	0.797	0.15	4.07	100.0	67
DB 1/10	61.9	17.3	7.37	0.071	2.79	0.53	1.74	3.45	0.796	0.16	4.18	100.3	71
DB 1/11	63.1	16.5	7.25	0.078	2.58	0.50	1.73	3.05	0.817	0.21	4.15	99.9	72
DB 1/13	70.6	11.3	6.21	0.068	2.31	1.01	1.47	1.64	0.637	0.09	3.74	99.1	66
DB 3/1	72.8	11.8	4.44	0.088	1.51	1.31	2.37	1.82	0.644	0.11	3.17	100.1	60
DB 2/1	93.5	3.50	1.28	0.008	0.11	0.02	0.12	0.82	0.154	0.02	0.66	100.2	77
DB 2/2	96.9	1.45	0.94	0.008	0.06	0.02	0.06	0.34	0.065	0.01	0.31	100.1	75
DB 3/3	62.9	17.5	6.92	0.063	1.99	0.44	1.95	3.33	0.837	0.16	4.42	100.5	71
DB 3/4	63.0	17.3	6.81	0.057	2.12	0.29	2.05	3.25	0.808	0.13	4.31	100.1	71
DB 5/2	75.0	11.7	3.07	0.060	0.49	0.77	1.33	2.36	0.603	0.10	3.17	98.7	67
DB 6/1	61.1	17.1	7.32	0.063	2.21	0.34	2.24	2.93	0.784	0.14	5.04	99.3	71
DB 6/2	61.4	17.3	6.98	0.058	2.07	0.25	2.08	3.08	0.819	0.14	5.21	99.4	72
DB 6/3	60.5	17.4	7.44	0.085	2.57	0.31	2.29	2.93	0.838	0.18	4.69	99.3	71
DB 6/4	59.8	17.7	7.62	0.057	2.29	0.31	2.13	3.19	0.873	0.14	4.65	98.8	71
DB 6/6	76.9	9.83	5.03	0.089	0.30	0.79	1.75	1.66	0.502	0.08	2.95	99.9	62
DB 6/8	80.1	9.96	3.18	0.023	0.48	0.08	1.96	1.52	0.518	0.09	2.28	100.2	67
DB 6/9	87.8	4.68	2.86	0.032	0.18	0.70	0.22	1.03	0.246	0.05	1.76	99.5	64
DB 6/14	64.6	15.8	6.37	0.047	2.16	0.61	2.37	2.51	0.844	0.15	3.79	99.3	68
J1-2	66.7	13.0	7.89	0.030	1.37	0.89	1.86	1.98	0.824	0.14	4.30	99.0	67
J4	59.4	17.7	7.72	0.070	2.44	0.29	1.81	3.45	0.858	0.10	5.96	99.8	72
J6	68.6	12.1	4.34	0.248	1.63	2.41	3.71	1.48	0.631	0.15	3.76	99.1	51
J7	66.9	13.9	6.34	0.169	2.36	1.14	3.40	1.91	0.680	0.15	3.29	100.3	60
J8	61.4	16.8	7.27	0.056	2.88	0.34	2.79	2.95	0.937	0.19	4.53	100.1	68
J10	65.5	15.3	6.38	0.100	2.55	0.37	3.30	2.43	0.900	0.16	3.12	100.1	65
JIMU2	79.3	10.8	1.57	0.004	0.41	0.21	-	2.36	0.663	0.24	3.20	98.8	82
JIMU3	60.9	17.9	6.83	0.060	1.45	0.29	0.02	5.01	0.944	0.14	6.37	99.9	76
OH3	91.7	4.58	0.47	0.004	0.14	0.10	-	1.07	0.243	0.05	1.33	99.7	79
Ordovician													
KIMU 2	65.0	17.2	5.49	0.029	1.26	0.54	0.12	5.23	0.846	0.41	3.98	100.1	75
KIRS 01	58.1	22.2	6.41	0.012	1.58	0.27	0.53	3.43	0.992	0.16	6.61	100.2	83
KIRS 04	60.5	21.4	5.24	0.014	1.42	0.29	0.62	3.50	0.991	0.15	5.94	100.1	81
KIRS 06	58.5	22.3	6.63	0.015	1.59	0.26	0.60	3.58	0.993	0.14	5.73	100.3	82
KIRS 09	58.8	21.4	6.85	0.014	1.38	0.48	0.60	3.49	0.950	0.18	6.04	100.2	80
KIRS 12	59.3	20.7	7.16	0.032	1.59	0.44	0.79	3.47	0.935	0.22	5.14	99.8	80
SaMy1	65.8	18.2	4.06	0.017	1.26	0.29	1.46	3.65	0.848	0.10	4.38	100.0	73
CV 03	58.6	26.0	1.04	0.004	0.67	0.12	0.71	4.35	1.07	0.11	7.24	99.9	82
CV 04	57.6	25.0	2.81	0.008	0.82	0.29	0.93	3.60	1.07	0.15	7.84	100.1	82
CV 05	56.8	24.7	3.37	0.016	0.82	0.36	0.98	3.53	1.02	0.14	8.09	99.8	81
EJPDO 1	76.6	8.0	6.39	0.082	1.02	0.24	0.07	1.99	0.422	0.09	5.28	100.2	76

Table A6: Continuation.

Tab. A6: Fortsetzung.

* CIA (Chemical Index of Alteration) after Nesbit and Young (1982) was not calculated for samples containing carbonate.

SAMPLE	SiO_2	Al_2O_3	Fe_2O_3	MnO	MgO	CaO	Na_2O	K_2O	TiO_2	P_2O_5	LOI	TOTAL	CIA*
Ordovician													
DoCS1	75.2	14.5	1.30	0.020	0.50	0.08	1.03	3.07	0.805	0.05	3.42	100.0	74
DoCS3	77.9	11.9	3.05	0.010	0.60	0.18	1.41	2.08	0.516	0.14	2.62	100.4	72
DoCS5	64.2	18.2	5.55	0.040	1.41	0.73	1.14	3.85	0.880	0.16	4.13	100.3	72
DoCS6	65.5	17.8	5.01	0.015	1.26	0.35	1.03	3.83	0.888	0.27	3.90	99.9	75
DoSP2	91.9	3.63	2.01	0.010	0.27	0.08	0.07	0.68	0.258	0.11	0.95	100.0	83
DoSP4	84.0	7.43	3.57	0.021	0.64	0.13	0.13	1.11	0.488	0.22	2.22	99.9	87
LIBS 0	56.0	23.8	5.39	0.018	1.32	0.15	0.62	3.61	1.03	0.09	8.07	100.1	83
LIMO 1	59.7	25.1	1.75	0.003	0.59	0.05	0.50	4.28	1.12	0.10	7.10	100.3	83
LIMO 2	67.2	20.1	1.07	0.002	0.48	0.05	0.34	3.64	1.01	0.11	5.90	99.9	82
LiBS2	96.3	1.94	0.58	0.005	0.04	0.04	0.04	0.37	0.190	0.06	0.44	100.0	83
LiBS4	66.0	19.0	1.67	0.003	0.54	0.05	0.21	4.21	1.07	0.20	5.96	98.9	81
LiBS6	72.7	16.3	0.83	0.003	0.44	0.02	0.11	3.47	0.956	0.09	4.29	99.3	81
LiBS7	95.8	2.29	0.66	0.003	0.06	0.09	0.02	0.41	0.230	0.09	0.61	100.3	84
LeZb2	85.5	4.86	2.66	0.063	0.44	2.03	1.36	0.55	0.228	0.14	2.31	100.2	
LeZb3	88.2	4.60	2.36	0.043	0.44	0.84	1.07	0.67	0.200	0.16	1.41	100.0	56
LEZB 4	54.3	24.4	3.90	0.015	1.58	0.27	0.52	6.11	1.38	0.19	6.63	99.3	76
LeZb5	86.4	5.20	2.09	0.048	0.35	1.17	1.52	0.65	0.441	0.14	1.72	99.8	51
LeZb6	79.3	4.10	2.08	0.093	0.36	5.87	1.07	0.53	0.487	0.09	5.21	99.2	
VIBE 1A	59.4	21.2	4.68	0.086	0.88	0.32	0.68	4.67	1.17	0.25	6.79	100.1	77
VIBE 1B	58.7	19.3	7.26	0.102	0.81	0.35	0.72	4.19	1.09	0.26	6.49	99.3	77
ZAHV 2	69.5	14.5	4.82	0.023	1.22	0.44	1.83	2.37	0.992	0.16	3.68	99.5	71
ZaVi1	72.8	8.43	4.02	0.065	0.74	4.54	2.03	0.75	0.567	0.10	5.53	99.6	
ZaVi 3	70.1	7.76	3.89	0.096	0.69	6.82	2.02	0.64	0.644	0.08	7.23	100.0	
ZaVi4	67.7	14.7	4.87	0.022	1.18	0.65	1.76	2.32	1.03	0.17	4.51	98.9	70
BOVC 1	54.5	21.6	7.55	0.830	1.75	0.44	0.65	3.66	1.15	0.10	8.13	100.3	79
BOVC 2	55.9	20.9	7.75	0.079	1.61	0.54	0.71	3.53	1.13	0.24	7.84	100.2	79
KDLE S1	58.3	19.3	6.36	0.032	1.99	0.74	0.92	3.74	1.04	0.37	5.86	98.7	76
KDLE S2	61.9	18.5	5.72	0.104	1.92	0.74	0.88	3.42	1.26	0.11	5.60	100.1	75
KOLE S1	58.6	20.5	6.92	0.060	1.94	0.41	0.65	3.47	1.11	0.14	6.20	100.0	80
KOLE S2	65.0	16.2	6.41	0.094	1.64	0.32	0.87	3.16	1.06	0.12	4.98	99.8	76
KoLe1	73.6	11.0	6.92	0.049	1.22	0.39	1.26	1.48	0.808	0.09	3.06	99.9	73

Table A7: Trace element data of sedimentary rocks.

Tab. A7: Spurenelementdaten der sedimentären Gesteine.

SAMPLE	Sc	Be	V	Cr	Co	Ni	Cu	Zn	Ga	Ge	As	Rb	Sr	Y	Zr	Nb	Mo	Ag	In	Sn	Sb	Cs	Ba	Hf	Ta	W	Tl	Pb	Bi	Th	U
Neoproterozoic																															
BL	16	4	118	197	12	53	58	112	25	2	18	102	77	22	165	13	-	-	-	2	1.6	2.9	750	4.8	1.0	3	1.1	28	3.1	8.5	1.8
BL 01	10	2	65	76	8	42	29	65	16	-	-	66	118	17	181	9	-	-	-	3	1.0	2.2	789	4.9	0.7	-	0.4	10	-	7.0	3.6
DB 1/3	15	3	234	196	10	-	64	102	20	3	-	128	61	23	174	10	-	-	-	4	1.6	5.2	1700	4.4	0.8	-	0.9	17	-	7.1	7.1
DB 1/2	20	2	147	213	20	69	42	111	18	2	12	89	93	25	162	9	5	-	-	2	2.3	3.5	879	4.1	0.8	2	0.7	13	-	5.5	2.6
DB 1/1	19	2	130	197	17	59	36	145	20	2	10	104	115	25	206	10	-	-	-	3	1.7	3.3	881	5.3	0.9	2	0.8	14	-	9.2	2.8
DB PK1	20	3	150	165	20	231	76	120	25	2	21	61	163	28	175	12	-	-	-	3	1.6	1.6	425	4.5	0.9	-	0.4	27	-	7.6	2.7
NP2ZB C	19	3	149	186	11	44	30	84	18	-	-	40	90	30	136	11	-	-	-	2	-	2.1	434	4.2	0.9	-	-	-	-	5.5	2.6
NPZB 5	17	3	124	111	15	46	36	94	18	2	16	74	199	30	130	10	-	-	-	-	1.1	3.5	583	4.2	0.9	2	0.4	13	-	7.9	2.7
NPZB 4	21	3	140	242	21	72	35	115	20	2	29	76	161	16	108	8	-	-	-	-	1.5	4.3	973	3.5	0.6	-	0.8	16	-	6.2	2.3
DOBRIS 04B	17	3	123	100	15	61	58	115	22	2	-	110	126	21	145	12	-	-	-	4	2.8	6.1	556	4.4	1.0	2	0.8	19	-	9.6	2.8
DOBRIS 02B	18	3	121	106	25	57	72	137	22	2	22	111	149	22	173	12	-	-	-	4	3.4	6.6	633	5.0	0.9	2	0.8	25	-	9.3	2.8
DOBRIS 01	17	2	102	115	13	46	43	77	17	2	-	74	164	19	186	10	-	-	-	3	1.1	2.8	719	5.1	0.7	-	0.5	16	-	7.9	2.1
DOB	17	2	99	173	14	52	43	99	17	2	11	71	156	20	198	8	-	-	-	2	1.4	2.9	703	5.1	0.7	-	0.6	16	-	7.1	2.1
Lower Cambrian																															
PJ1/3	5	-	48	195	4	-	-	-	9	2	-	27	24	7	71	8	-	-	-	-	1.3	1.3	181	2.4	0.4	-	0.4	10	-	3.0	1.2
DB HL1	9	-	62	156	4	-	-	102	11	2	-	38	31	14	121	5	-	-	-	-	2.3	2.1	307	3.1	0.5	-	0.3	17	-	3.8	1.5
DB S1	12	2	73	140	7	57	21	81	12	2	-	49	99	24	275	7	-	2.0	-	2	2.5	6.6	329	7.0	0.6	-	0.4	19	-	6.2	1.8
DB S2	9	2	48	82	5	40	20	70	11	2	-	53	67	16	131	5	-	1.0	-	-	2.3	7.6	342	3.3	0.4	-	0.4	-	-	3.8	1.1
DB B	3	-	29	186	-	-	35	-	5	-	-	13	43	8	96	4	-	-	-	2	-	2.9	112	2.3	0.3	-	-	16	-	2.7	0.8
DB D1-2	11	2	59	334	6	66	35	78	13	3	-	37	170	19	176	6	-	1.9	-	2	1.6	2.2	340	4.7	0.6	-	0.3	20	-	4.5	1.9
DB D2	26	3	122	108	16	94	35	124	27	2	-	96	198	39	314	13	-	1.9	-	3	1.9	4.8	943	8.6	1.1	-	0.6	20	-	10.8	2.9
DB D2-5	8	-	44	263	6	163	25	73	11	-	-	25	137	12	89	5	-	-	-	-	1.3	1.8	270	2.4	0.4	-	0.3	16	-	2.8	1.0
DB D7	6	-	40	225	6	46	22	65	12	-	-	20	116	16	187	5	-	1.3	-	-	1.1	1.3	221	4.8	0.5	-	-	11	-	5.6	1.5
DB D10	8	-	53	307	4	66	-	63	10	-	-	16	140	13	210	6	-	1.5	-	-	1.0	1.1	183	5.3	0.6	-	-	11	-	4.6	1.4
MM2	22	3	161	142	23	78	64	168	30	3	-	151	47	37	150	12	-	-	-	3	1.6	16.7	578	4.4	1.0	2	2.4	21	-	10.5	3.4
MM7	6	-	46	98	5	56	24	70	10	2	-	34	38	10	128	8	-	-	-	-	1.3	3.2	183	3.2	0.5	-	0.3	-	-	4.2	1.3
MM8	15	3	102	107	12	61	55	163	20	3	-	77	49	29	184	12	-	-	-	3	1.9	5.8	530	5.6	0.8	-	0.8	21	1.4	7.0	3.0
MM15	3	-	25	431	-	-	-	-	6	2	-	22	19	7	112	5	-	-	-	-	1.0	1.2	251	2.7	0.3	-	0.3	-	-	3.1	0.8
SH2	2	-	23	286	-	-	-	-	4	2	-	15	8	4	40	4	-	-	-	-	1.2	1.1	78	1.1	0.2	-	0.2	11	-	1.3	0.8
H2-2	2	-	26	313	-	-	23	-	4	-	-	19	10	5	54	9	-	-	-	-	1.4	1.1	189	1.6	0.2	-	0.2	-	-	1.6	0.6
C2	4	-	47	201	5	-	-	-	5	2	-	26	8	9	49	4	-	-	-	-	1.2	1.7	154	1.3	0.2	-	0.3	18	-	1.7	0.9

SAMPLE	Sc	Be	V	Cr	Co	Ni	Cu	Zn	Ga	Ge	As	Rb	Sr	Y	Zr	Nb	Mo	Ag	In	Sn	Sb	Cs	Ba	Hf	Ta	W	Tl	Pb	Bi	Th	U
Lower Cambrian																															
CT2	-	-	15	227	-	-	-	-	3	2	-	8	11	4	31	3	-	-	-	-	1.0	0.8	45	0.8	-	-	0.2	-	-	1.1	0.7
CT-3-2	19	2	85	191	21	-	-	107	19	2	-	17	182	37	227	7	-	-	-	3	1.4	3.2	352	6.0	0.7	0	0.2	17	0	5.1	2.4
MM16	5	-	31	538	6	-	61	67	7	2	-	20	48	13	259	6	-	-	-	-	1.0	1.2	160	6.3	0.4	-	0.3	17	0.9	4.1	1.3
DB LS1-3	3	-	20	106	3	-	-	61	4	2	-	21	73	15	275	5	-	1.9	-	-	1.2	-	158	6.8	0.5	-	0.2	15	-	6.5	1.3
DB CB3	4	-	30	203	-	-	-	-	7	2	20	18	41	13	442	6	-	3.2	-	-	2.4	-	66	11.0	0.6	-	0.2	-	-	4.6	1.6
Middle Cambrian																															
DB 1/4A	11	-	95	119	12	-	40	95	13	3	-	69	91	18	146	7	-	-	-	-	1.5	4.7	497	3.9	0.7	3	0.5	-	2.0	6.1	2.1
DB 1/4B	12	2	103	207	13	45	39	129	13	3	-	69	93	18	136	7	-	-	-	2	1.5	4.8	504	3.7	0.6	2	0.4	13	1.0	5.8	2.2
DB 1/5	19	3	152	124	22	58	44	130	22	3	-	136	78	25	188	11	-	-	-	3	1.8	5.9	667	5.0	0.9	2	0.7	17	-	7.6	2.9
DB 1/6	20	3	154	121	21	61	42	135	22	3	-	133	85	30	203	12	-	-	-	3	1.6	5.1	603	5.5	1.0	3	0.7	13	-	8.0	3.1
DB 1/7	17	3	133	126	17	53	38	85	19	3	-	113	84	28	242	12	-	-	-	2	1.7	4.3	536	6.2	1.0	2	0.5	13	-	7.9	2.8
DB 1/10	20	3	151	89	22	73	49	140	24	3	-	135	78	31	184	12	-	-	-	4	1.9	7.2	736	5.0	1.0	3	0.8	17	-	8.7	2.7
DB 1/11	20	3	142	113	20	57	45	133	21	3	-	130	76	38	199	11	-	-	-	3	1.8	6.4	646	5.3	1.0	2	0.8	16	-	7.6	3.0
DB 1/13	16	-	153	167	15	67	55	119	15	3	-	66	57	23	146	7	-	-	-	-	2.2	3.7	479	3.9	0.7	2	0.5	20	-	5.1	2.5
DB 3/1	13	-	100	222	14	57	30	114	15	3	-	69	102	22	234	9	-	-	-	-	2.2	3.0	527	6.5	0.8	2	0.5	15	-	6.9	2.6
DB 2/1	4	-	26	486	2	-	31	121	6	2	-	25	15	8	98	4	4	-	-	-	2.1	1.9	237	2.4	0.3	-	0.3	-	-	2.3	0.9
DB 2/2	2	-	22	242	2	-	-	-	4	2	11	13	9	4	40	3	4	-	-	-	1.6	-	105	0.9	-	-	0.3	-	-	1.1	0.5
DB 3/3	21	3	142	129	18	75	47	119	25	3	-	124	96	27	177	11	-	-	-	3	2.8	7.2	794	4.9	1.0	2	0.9	13	-	8.2	2.9
DB 3/4	20	3	145	130	18	72	45	129	25	3	-	123	94	29	184	12	-	-	-	3	2.5	7.1	776	5.0	1.0	2	0.8	15	-	8.2	2.8
DB 5/2	10	2	81	179	10	48	29	80	16	3	12	86	76	19	237	9	-	-	-	2	3.5	8.8	696	6.0	0.8	-	0.8	16	-	6.0	1.8
DB 6/1	20	3	146	141	20	77	48	149	24	3	-	108	96	28	167	11	-	-	-	3	2.4	5.7	695	4.5	1.0	2	0.7	14	-	7.5	2.5
DB 6/2	20	3	146	152	22	72	50	147	25	3	12	116	91	30	187	12	-	-	-	3	2.6	7.3	759	5.0	1.0	2	0.9	24	0.8	8.0	2.9
DB 6/3	21	3	157	170	25	75	54	143	26	3	11	119	96	31	188	13	-	-	-	3	3.4	8.4	734	5.0	1.0	2	0.8	19	-	8.6	2.9
DB 6/4	21	3	156	167	24	77	58	144	26	3	10	125	103	33	192	13	-	-	-	3	3.9	10.0	751	5.3	1.1	2	0.9	16	-	8.7	2.9
DB 6/6	10	2	77	276	11	49	26	65	13	2	-	56	75	23	206	8	-	-	-	2	5.1	3.2	500	5.2	0.6	-	0.4	-	-	5.2	1.6
DB 6/8	9	2	81	145	7	41	27	88	12	2	-	50	78	13	201	9	-	-	-	-	1.6	3.0	347	4.8	2.0	-	0.4	11	-	5.0	1.9
DB 6/9	6	-	47	329	7	-	31	70	8	3	-	36	27	12	99	5	-	-	-	-	2.6	2.8	286	2.5	0.4	-	0.5	-	-	2.9	1.3
DB 6/14	18	3	130	170	21	83	47	102	21	2	-	95	107	26	239	11	-	-	-	3	2.6	5.6	614	6.3	1.0	2	0.5	14	-	7.9	2.8
J1-2	17	2	126	216	22	62	42	103	18	3	-	76	69	25	131	11	-	-	-	3	1.2	6.5	243	3.5	0.7	-	0.5	12	-	4.4	1.5
J4	22	3	147	161	26	79	57	158	27	3	13	140	57	40	173	13	-	-	-	4	2.1	8.4	560	5.0	1.0	2	1.5	20	-	8.4	3.2
J6	12	3	88	167	15	66	43	110	15	3	-	52	109	29	171	11	-	-	-	4	1.2	2.4	369	4.3	0.7	-	0.4	15	-	6.5	1.8
J7	14	2	110	163	23	67	52	132	19	3	-	70	116	26	155	11	-	-	-	3	1.4	3.7	449	4.2	0.8	-	0.6	28	-	6.8	2.1
J8	21	3	154	173	26	77	53	142	25	3	12	123	101	26	171	13	-	-	-	3	1.3	6.3	547	4.7	1.0	2	0.8	18	-	9.0	2.7
J10	16	2	129	173	26	75	42	126	22	3	12	97	106	25	218	13	-	-	-	3	1.2	5.3	544	6.0	1.0	2	0.7	23	-	9.5	3.0

GEOLOGICA SAXONICA
Journal of Central European Geology
54 (2008) 1–168

Table A7: Continuation.

Tab. A7: Fortsetzung.

SAMPLE	Sc	Be	V	Cr	Co	Ni	Cu	Zn	Ga	Ge	As	Rb	Sr	Y	Zr	Nb	Mo	Ag	In	Sn	Sb	Cs	Ba	Hf	Ta	W	Tl	Pb	Bi	Th	U
Middle Cambrian																															
JIMU2	12	-	93	349	5	-	40	75	14	3	-	79	139	32	218	10	-	-	-	2	8.0	6.7	275	5.2	0.6	2	0.7	35	-	5.9	2.1
JIMU3	21	3	163	198	21	82	51	161	27	3	43	164	132	27	175	13	-	-	-	3	12.2	13.8	435	4.7	1.0	3	1.1	34	0.9	8.9	2.7
OH3	3	-	53	266	3	-	21	-	7	2	-	30	25	8	89	5	-	-	-	-	3.4	1.4	89	2.2	0.3	-	0.3	12	-	2.2	0.8
Ordovician																															
KIMU 2	17	4	66	79	12	41	37	-	26	3	90	210	145	43	148	24	-	-	-	4	8.1	26.7	530	4.8	3.1	3	0.8	-	-	13.2	1.7
KIRS 01	18	5	110	116	14	66	39	119	30	4	10	168	100	34	142	20	-	-	-	5	-	8.3	595	4.4	1.7	3	1.0	23	-	15.8	3.1
KIRS 04	17	4	109	113	17	64	31	83	29	3	13	174	99	34	177	22	-	-	-	5	-	7.7	651	5.4	1.8	3	0.8	17	-	15.2	3.4
KIRS 06	18	4	95	114	16	54	36	108	31	3	19	174	81	26	157	20	-	-	-	5	-	9.1	610	4.6	1.5	3	0.9	19	-	15.4	3.0
KIRS 09	17	4	105	112	15	61	42	107	30	4	17	176	99	33	170	21	-	-	-	5	-	8.2	709	5.2	1.7	3	1.0	19	-	15.1	3.2
KIRS 12	16	4	85	101	15	52	31	86	27	3	-	159	87	34	180	19	-	-	-	4	-	9.3	579	5.5	1.6	3	0.7	18	-	14.9	3.1
SaMy1	14	4	87	124	11	50	25	82	25	3	-	145	95	28	241	18	-	-	-	4	-	6.2	427	6.9	1.2	2	0.9	25	-	14.1	3
CV 03	20	5	139	144	2	-	46	-	37	3	-	186	316	29	128	21	-	-	-	6	4.4	8.6	484	3.9	1.8	3	1.0	13	-	21.0	3.1
CV 04	21	5	143	149	5	-	48	79	37	3	13	190	201	33	139	22	-	-	-	6	1.4	8.7	521	4.2	1.8	3	0.8	13	-	23.3	3.4
CV 05	21	5	140	140	7	41	50	122	35	4	20	185	172	33	135	21	-	-	-	8	1.4	8.7	510	4.0	1.8	3	1.1	17	-	22.1	3.3
EJPDO 1	7	2	31	201	7	-	-	81	11	3	33	63	28	16	301	10	-	-	-	2	1.2	3.7	336	8.4	0.7	-	0.5	21	-	9.5	1.7
DoCS1	9	3	59	138	7	-	25	68	19	2	-	108	54	27	387	13	-	-	-	2	-	2.8	620	10.9	1.3	2	0.7	17	-	15.4	3.1
DoCS3	8	3	47	251	5	-	-	61	17	2	-	80	71	40	208	11	-	-	-	2	1.0	2.3	451	6.3	0.9	-	0.5	23	-	10.1	2.2
DoCS5	14	4	83	165	14	51	33	122	25	3	12	148	102	30	258	16	-	-	-	3	-	6.6	785	8.1	1.4	2	0.9	30	-	16.8	3.2
DoCS6	15	4	84	129	10	49	33	91	28	3	14	151	89	36	320	19	-	-	-	4	-	5.0	810	9.2	1.4	2	0.9	25	-	17.6	3.4
DoSP2	4	-	18	366	4	-	24	-	5	2	-	25	13	11	237	10	-	-	-	-	1.1	1.7	82	6.8	0.4	-	0.3	-	-	5.3	1.0
DoSP4	7	2	41	390	6	-	23	60	11	2	-	48	29	23	481	13	-	-	-	-	1.1	3.0	190	13.2	0.8	-	0.5	10	-	11.3	1.9
LIBS 0	18	5	138	130	12	67	40	-	33	3	13	175	118	23	184	20	-	-	-	4	1.0	8.1	667	5.5	1.6	3	0.5	10	-	16.9	3.2
LIMO 1	18	4	152	127	2	-	24	-	36	3	17	188	334	29	165	20	-	-	-	4	1.3	8.3	735	5.1	1.5	3	1.1	15	-	16.4	3.3
LIMO 2	15	4	178	137	2	-	-	-	30	3	31	156	419	30	279	20	-	-	-	4	2.0	6.4	633	8.3	1.6	3	1.2	27	-	17.2	3.7
LiBS2	3	-	20	434	-	-	-	-	4	-	-	14	146	10	163	6	-	-	-	-	-	-	157	4.8	0.4	-	-	-	-	4.8	0.7
LiBS4	17	4	170	159	-	-	20	-	28	2	13	163	409	29	315	17	-	-	-	4	2.7	5.7	1000	9.6	1.6	3	0.9	19	-	22.1	3.6
LiBS6	13	3	92	170	2	-	32	-	24	2	11	134	230	33	463	18	-	-	-	3	7.0	5.8	517	13.8	1.4	2	0.7	11	-	19.3	4.3
LiBS7	4	-	21	631	-	-	-	-	5	2	10	18	255	18	207	10	-	-	-	-	1.1	-	125	5.8	0.4	-	-	-	-	5.1	1.7
LeZb2	4	-	25	1070	6	44	26	-	6	2	-	23	124	17	184	8	-	-	-	-	-	-	116	5.1	0.4	-	-	-	-	5.2	0.9
LeZb3	3	-	25	1070	5	-	26	-	6	2	-	25	104	15	152	6	-	-	-	-	-	1.2	129	4.5	0.3	-	0.2	-	-	4.8	0.9
LEZB 4	26	5	160	164	8	77	26	-	35	3	12	216	134	45	238	23	-	-	-	4	-	9.7	988	7.0	1.8	3	0.9	-	-	19.3	3.3

SAMPLE	Sc	Be	V	Cr	Co	Ni	Cu	Zn	Ga	Ge	As	Rb	Sr	Y	Zr	Nb	Mo	Ag	In	Sn	Sb	Cs	Ba	Hf	Ta	W	Tl	Pb	Bi	Th	U
Ordovician																															
LeZb5	4	2	26	587	5	-	20	-	6	2	-	24	112	22	393	8	-	2.5	-	-	-	1.1	126	12.2	0.7	-	0.2	-	-	10.2	1.8
LeZb6	6	2	25	817	5	-	22	-	5	2	-	20	185	27	581	9	-	-	-	-	-	-	108	17.1	0.6	-	-	-	-	13.2	2.1
VIBE 1A	19	4	134	127	13	56	40	111	31	3	13	199	217	32	198	23	-	-	-	5	-	9.8	837	6.4	1.7	3	1.4	22	-	15.6	2.9
VIBE 1B	19	4	122	122	19	68	36	99	26	2	12	161	207	36	201	20	-	-	-	4	-	8.1	723	6.2	1.6	3	0.8	16	-	14.5	2.7
ZAHV 2	15	3	126	126	14	61	28	90	21	3	13	105	133	38	459	19	-	-	-	4	-	4.1	471	13.4	1.4	2	0.8	22	-	15.4	2.9
ZaVi1	12	2	59	226	6	43	26	65	10	2	-	32	181	32	364	11	-	-	-	2	-	1.2	248	10.9	0.8	-	0.2	-	-	10.6	1.9
ZaVi 3	10	2	58	132	7	44	23	63	10	3	-	27	250	35	448	13	-	-	-	2	-	1.1	233	12.8	0.9	-	0.3	15	-	10.4	2.1
ZaVi4	15	3	138	163	14	46	39	89	21	3	12	97	153	29	395	17	-	-	-	3	-	3.7	376	12.0	1.3	3	0.6	17	-	16.9	2.8
BOVC 1	22	5	171	134	40	100	42	108	32	4	14	190	157	29	174	22	-	-	-	5	-	9.6	633	5.5	1.8	3	0.9	16	-	15.6	3.1
BOVC 2	22	4	157	128	19	66	47	139	29	4	20	166	149	32	161	21	-	-	0.5	97	-	8.1	544	5.2	1.7	4	1.1	29	-	14.7	3.0
KDLE S1	20	4	152	124	21	71	41	136	26	3	-	151	125	38	178	19	-	-	-	4	-	8.8	424	5.6	1.4	3	0.9	22	-	11.4	4.0
KDLE S2	21	4	179	145	52	88	44	94	28	3	62	154	134	24	235	22	-	-	-	4	1.1	8.9	412	7.1	1.6	3	0.7	18	-	13.1	2.6
KOLE S1	21	4	155	142	29	63	43	121	30	3	19	146	127	27	190	19	-	-	-	3	-	7.8	385	5.7	1.4	3	0.9	20	-	13.1	2.7
KOLE S2	17	4	153	143	27	70	37	137	24	3	25	135	108	24	247	20	-	-	-	4	-	6.5	367	7.5	1.5	3	0.9	26	-	11.2	2.5
KoLe1	10	3	97	221	20	62	33	88	15	3	39	59	73	17	204	15	-	-	-	3	-	2.9	233	6.5	1.0	2	0.4	12	-	8.2	1.7

GEOLOGICA SAXONICA
Journal of Central European Geology
54 (2008) 1–168

Table A8: REE data of sedimentary rocks.

Tab. A8: Seltenerdelementdaten der sedimentären Gesteine.

SAMPLE	La	Ce	Pr	Nd	Sm	Eu	Gd	Tb	Dy	Ho	Er	Tm	Yb	Lu
Neoproterozoic														
BL	35.9	68.3	7.77	29.2	5.6	1.25	4.8	0.9	4.3	0.9	2.5	0.42	2.5	0.38
BL 01	26.8	54.2	5.89	22.2	4.3	1.13	3.4	0.7	3.3	0.7	2.0	0.34	2.0	0.32
DB 1/3	25.9	51.8	5.90	22.9	4.7	1.18	4.0	0.7	3.9	0.8	2.3	0.41	2.4	0.39
DB 1/2	20.7	42.6	5.00	19.8	4.1	1.07	3.9	0.8	4.1	0.9	2.4	0.41	2.3	0.37
DB 1/1	32.5	63.9	6.96	26.6	5.0	1.22	4.4	0.8	4.1	0.9	2.3	0.42	2.4	0.38
DB PK1	25.3	51.0	6.41	25.7	5.6	1.54	5.2	0.9	5.1	1.0	2.9	0.44	2.7	0.39
NP2ZB C	34.9	58.0	6.76	28.5	6.3	1.94	5.2	1.0	5.4	1.0	2.7	0.45	2.7	0.41
NPZB 5	25.2	48.7	5.93	26.2	6.2	1.25	5.5	1.0	5.3	1.0	2.7	0.48	2.8	0.43
NPZB 4	22.0	43.5	5.02	19.3	3.8	0.88	3.5	0.7	3.1	0.7	1.8	0.32	1.7	0.30
DOBRIS 04B	29.0	58.3	6.27	23.9	4.6	1.09	3.9	0.7	3.9	0.8	2.5	0.42	2.5	0.41
DOBRIS 02B	30.7	59.3	6.49	25.0	4.8	1.20	4.1	0.8	4.0	0.9	2.5	0.42	2.4	0.40
DOBRIS 01	17.4	37.4	4.42	16.9	3.6	0.94	3.2	0.6	3.4	0.8	2.1	0.37	2.1	0.35
DOB	19.5	38.2	4.68	18.4	3.9	0.96	3.2	0.7	3.4	0.7	2.0	0.34	2.0	0.32
Lower Cambrian														
PJ1/3	13.3	25.5	2.93	10.8	2.0	0.51	1.7	0.3	1.3	0.3	0.9	0.18	1.0	0.17
DB HL1	15.3	31.8	3.97	15.4	3.0	0.75	2.6	0.5	2.5	0.6	1.6	0.29	1.7	0.27
DB S1	22.5	46.3	5.84	23.4	4.6	1.23	4.3	0.8	4.1	0.9	2.6	0.40	2.4	0.37
DB S2	14.4	27.5	3.37	13.5	2.8	0.85	2.7	0.5	2.7	0.6	1.7	0.28	1.6	0.25
DB B	13.3	24.7	2.72	9.6	1.6	0.47	1.5	0.3	1.3	0.3	0.8	0.16	0.8	0.14
DB D1-2	17.0	35.8	4.66	18.5	3.7	1.02	3.3	0.6	3.3	0.7	2.0	0.33	1.9	0.31
DB D2	30.4	63.5	8.23	34.5	7.2	1.94	6.7	1.2	6.6	1.4	4.1	0.64	4.0	0.60
DB D2-5	8.9	16.9	2.40	9.9	2.2	0.70	2.1	0.4	2.0	0.5	1.3	0.21	1.2	0.20
DB D7	14.0	29.4	3.70	14.7	3.1	1.00	2.7	0.5	2.6	0.6	1.6	0.28	1.6	0.24
DB D10	14.3	30.2	3.88	15.6	3.1	0.94	2.5	0.5	2.4	0.5	1.4	0.25	1.4	0.24
MM2	38.4	73.2	8.45	33.4	6.7	1.77	7.5	1.2	6.3	1.4	3.8	0.61	3.6	0.54
MM7	18.4	36.0	3.60	13.1	2.3	0.59	1.9	0.4	1.7	0.5	1.2	0.22	1.2	0.21
MM8	26.4	55.4	6.99	29.3	6.8	1.63	6.1	1.1	5.2	1.1	3.2	0.53	2.9	0.44
MM15	15.9	32.7	3.27	11.9	2.0	0.52	1.6	0.3	1.2	0.3	0.7	0.15	0.7	0.14
SH2	7.9	17.5	1.64	5.5	0.7	0.17	0.5	-	0.6	0.2	0.4	0.10	0.4	0.09
H2-2	7.6	15.7	1.78	5.9	1.1	0.25	0.7	0.2	0.7	0.2	0.5	0.12	0.5	0.11
C2	5.6	14.0	1.38	5.5	1.3	0.40	1.5	0.3	1.5	0.4	0.9	0.18	0.9	0.15
CT2	4.9	9.8	1.21	4.7	1.0	0.25	0.8	-	0.7	0.2	0.5	0.11	0.5	0.09
CT3-2	21.7	46.8	6.05	26.7	6.6	1.97	7.8	1.3	6.7	1.5	3.9	0.62	3.4	0.53
MM16	15.7	32.5	3.36	12.9	2.5	0.65	2.3	0.4	2.1	0.5	1.3	0.24	1.3	0.22
DB LS1-3	17.9	41.6	4.64	18.0	3.5	0.83	3.2	0.6	2.8	0.6	1.6	0.26	1.5	0.23
DB CB3	13.7	30.2	3.39	13.1	2.6	0.70	2.3	0.5	2.3	0.5	1.5	0.26	1.6	0.27
Middle Cambrian														
DB 1/4A	21.4	44.5	4.64	17.4	3.5	0.90	3.1	0.6	3.1	0.7	1.8	0.32	1.8	0.30
DB 1/4B	20.3	42.4	4.40	16.5	3.3	0.86	3.0	0.6	3.0	0.7	1.8	0.32	1.8	0.29
DB 1/5	28.0	57.6	6.42	25.0	5.0	1.17	4.3	0.8	4.3	0.9	2.6	0.46	2.7	0.44
DB 1/6	31.7	65.1	7.25	28.3	5.8	1.44	5.1	1.0	5.3	1.1	3.0	0.53	3.2	0.48
DB 1/7	30.8	62.8	7.03	27.7	5.7	1.40	5.0	0.9	4.9	1.0	2.9	0.49	3.0	0.47

Table A8: Continuation.

Tab. A8: Fortsetzung.

SAMPLE	La	Ce	Pr	Nd	Sm	Eu	Gd	Tb	Dy	Ho	Er	Tm	Yb	Lu
Middle Cambrian														
DB 1/10	31.2	64.2	7.23	28.0	5.9	1.45	5.2	1.0	5.3	1.2	3.1	0.53	3.2	0.51
DB 1/11	30.3	63.3	7.26	28.9	6.4	1.68	6.6	1.3	6.7	1.4	3.8	0.62	3.7	0.55
DB 1/13	19.4	39.9	4.64	18.3	3.9	1.06	3.5	0.7	3.8	0.9	2.3	0.39	2.3	0.35
DB 3/1	26.8	53.4	5.88	22.0	4.4	1.10	3.8	0.7	3.8	0.8	2.2	0.38	2.2	0.36
DB 2/1	8.0	15.9	1.80	6.8	1.4	0.35	1.2	0.3	1.3	0.3	0.8	0.16	0.8	0.15
DB 2/2	4.3	7.6	0.96	3.5	0.8	0.20	0.6	-	0.6	0.2	0.4	-	0.4	0.09
DB 3/3	31.3	59.4	7.15	28.2	5.7	1.33	4.6	0.9	4.7	1.0	2.8	0.45	2.7	0.45
DB 3/4	30.8	57.9	7.05	27.8	5.5	1.32	4.5	0.9	4.7	1.0	2.8	0.47	2.9	0.46
DB 5/2	27.3	51.6	5.87	22.7	4.3	1.08	3.6	0.7	3.3	0.7	1.8	0.32	1.8	0.30
DB 6/1	30.4	58.1	7.15	28.5	5.8	1.44	5.1	0.9	5.2	1.1	2.9	0.49	3.0	0.45
DB 6/2	33.4	62.5	7.49	29.3	5.8	1.43	5.1	0.9	5.2	1.1	3.1	0.50	3.1	0.47
DB 6/3	35.8	68.3	7.92	30.9	6.1	1.47	5.1	1.0	5.3	1.1	3.2	0.51	3.1	0.48
DB 6/4	37.5	70.4	8.36	32.4	6.6	1.50	5.8	1.1	5.8	1.2	3.4	0.55	3.3	0.52
DB 6/6	24.8	42.0	5.20	20.4	4.1	1.09	3.8	0.7	3.7	0.8	2.1	0.35	1.9	0.32
DB 6/8	18.7	35.5	3.97	14.6	2.6	0.66	2.1	0.4	2.1	0.5	1.4	0.23	1.4	0.22
DB 6/9	12.8	25.9	2.83	10.9	2.4	0.60	2.1	0.4	2.1	0.5	1.2	0.21	1.1	0.19
DB 6/14	34.8	64.9	7.72	30.3	5.9	1.40	4.8	0.9	4.7	1.0	2.7	0.45	2.8	0.44
J1-2	24.3	55.6	6.06	25.3	5.7	1.61	5.8	1.0	4.8	1.1	2.6	0.41	2.4	0.36
J4	35.6	76.2	8.06	32.5	6.9	1.67	7.2	1.3	6.9	1.6	4.4	0.73	4.2	0.63
J6	26.2	52.6	5.61	21.7	4.7	1.28	5.0	0.9	4.8	1.1	2.8	0.45	2.5	0.38
J7	30.1	61.2	6.52	26.2	5.5	1.46	5.4	0.9	4.7	1.1	2.7	0.43	2.3	0.36
J8	34.6	70.5	7.37	28.1	5.6	1.40	5.1	0.9	4.7	1.1	2.8	0.47	2.8	0.43
J10	34.5	70.6	7.39	28.7	5.6	1.45	5.4	0.9	4.7	1.1	2.9	0.48	2.8	0.44
JIMU2	28.0	59.4	6.28	25.9	5.6	1.67	6.4	1.1	5.3	1.2	2.8	0.41	2.2	0.33
JIMU3	36.4	74.0	7.75	29.8	5.6	1.45	5.1	0.9	4.6	1.1	2.9	0.48	2.8	0.44
OH3	12.2	25.1	2.66	10.0	1.8	0.52	1.6	0.3	1.4	0.4	0.9	0.17	0.9	0.15
Ordovician														
KIMU 2	42.5	81.1	10.5	40.2	8.5	2.00	8.2	1.3	6.9	1.4	4.1	0.66	3.5	0.62
KIRS 01	67.7	117	13.0	51.7	9.1	2.00	7.5	1.3	6.3	1.2	3.2	0.51	3.2	0.47
KIRS 04	65.0	112	13.0	52.3	8.8	1.83	7.1	1.2	6.0	1.2	3.3	0.54	3.2	0.48
KIRS 06	55.3	106	12.5	42.2	6.4	1.54	6.3	0.9	4.4	1.0	2.9	0.41	2.4	0.43
KIRS 09	61.9	107	12.6	51.3	8.8	1.88	7.7	1.3	6.2	1.2	3.4	0.54	3.2	0.48
KIRS 12	56.5	107	11.9	45.7	8.3	2.01	7.3	1.2	6.3	1.3	3.3	0.51	3.2	0.50
SaMy1	46.2	93	11.0	38.9	6.4	1.56	6.2	1	4.6	1.1	3	0.44	2.6	0.46
CV 03	62.7	121	13.5	49.4	8.8	1.89	6.3	1.1	5.6	1.2	3.4	0.57	3.3	0.51
CV 04	63.6	123	13.6	50.1	9.3	1.97	6.8	1.2	6.2	1.3	3.7	0.59	3.5	0.53
CV 05	62.0	118	13.4	50.2	9.2	1.99	6.8	1.2	6.5	1.4	3.8	0.59	3.5	0.54
EJPDO 1	23.7	52.5	6.31	23.1	4.1	0.92	4.3	0.7	2.8	0.7	1.8	0.27	1.5	0.29
DoCS1	39.0	76.7	8.90	33.0	6.1	1.30	4.8	1.0	4.9	1.1	2.9	0.50	3.0	0.46
DoCS3	27.5	60.2	6.69	24.3	6.0	1.52	7.8	1.4	8.0	1.6	4.1	0.68	3.8	0.51
DoCS5	52.8	103	12.0	41.7	8.6	1.86	7.4	1.1	6.2	1.3	3.4	0.56	3.4	0.48
DoCS6	56.0	112	13.1	47.4	10.7	2.33	9.6	1.4	7.4	1.5	3.7	0.59	3.4	0.49

Table A8: Continuation.

Tab. A8: Fortsetzung.

SAMPLE	La	Ce	Pr	Nd	Sm	Eu	Gd	Tb	Dy	Ho	Er	Tm	Yb	Lu
Ordovician														
DoSP2	18.5	44.2	4.81	16.9	4.0	0.92	3.4	0.6	2.8	0.6	1.4	0.24	1.3	0.20
DoSP4	38.5	87.5	9.46	33.5	7.9	1.80	6.8	1.1	5.4	1.1	2.6	0.44	2.6	0.38
LIBS 0	58.0	111	12.6	46.0	6.7	1.36	5.2	0.8	3.9	0.9	2.8	0.47	2.6	0.43
LIMO 1	51.5	106	12.2	42.5	6.8	1.68	6.6	1.1	5.0	1.2	3.4	0.51	2.9	0.50
LIMO 2	56.4	113	12.2	47.9	7.7	1.57	6.1	1.1	5.5	1.2	3.6	0.64	3.8	0.59
LiBS2	13.9	33.5	3.72	13.1	3.3	0.80	2.8	0.5	2.2	0.5	1.0	0.19	1.0	0.16
LiBS4	58.1	114	12.6	41.1	8.6	1.82	6.1	1.1	5.8	1.2	3.2	0.58	3.6	0.52
LiBS6	51.8	110	12.7	43.0	9.4	1.99	7.8	1.4	7.2	1.5	3.7	0.62	3.7	0.53
LiBS7	20.1	54.8	6.86	31.2	9.5	2.45	8.8	1.4	5.3	0.9	1.7	0.25	1.3	0.19
LeZb2	20.8	46.8	5.45	19.6	4.9	1.25	4.1	0.8	3.5	0.7	1.7	0.28	1.5	0.22
LeZb3	24.6	53.1	6.03	21.4	5.3	1.31	4.6	0.8	3.5	0.7	1.4	0.22	1.2	0.18
LEZB 4	64.8	137	17.5	63.8	10.6	2.64	11.2	1.6	7.7	1.8	5.0	0.72	4.3	0.74
LeZb5	33.2	70.4	8.00	27.1	5.7	1.38	4.9	0.9	4.5	1.0	2.4	0.41	2.4	0.36
LeZb6	46.7	98.2	11.0	36.8	7.9	1.68	6.1	1.1	5.2	1.0	2.6	0.46	2.8	0.42
VIBE 1A	55.6	104	12.8	50.0	8.2	1.82	7.8	1.3	6.0	1.2	3.6	0.59	3.4	0.52
VIBE 1B	51.6	101	11.4	44.5	8.4	1.92	7.6	1.3	6.7	1.4	3.6	0.58	3.5	0.55
ZAHV 2	51.7	103	12.3	50.5	8.7	1.87	8.0	1.4	6.9	1.4	4.2	0.68	3.9	0.61
ZaVi1	24.9	54.7	6.63	23.4	6.0	1.40	5.6	1.1	5.9	1.3	3.4	0.58	3.4	0.50
ZaVi 3	28.8	61.3	7.77	32.1	5.7	1.30	6.0	1.2	5.6	1.2	3.6	0.57	3.1	0.51
ZaVi4	55.6	119	13.7	46.1	9.3	1.83	6.4	1.1	5.7	1.3	3.3	0.57	3.4	0.51
BOVC 1	59.3	102	11.2	43.0	6.6	1.31	5.4	1.0	5.3	1.2	3.7	0.66	3.8	0.59
BOVC 2	59.3	106	12.0	47.7	8.4	1.84	6.9	1.3	6.4	1.3	3.4	0.57	3.5	0.53
KDLE S1	47.0	105	10.7	45.7	9.4	2.27	8.8	1.6	7.6	1.4	3.6	0.58	3.5	0.53
KDLE S2	43.0	93.6	10.4	37.5	5.6	1.24	4.8	0.8	4.0	1.0	3.0	0.49	2.9	0.51
KOLE S1	45.2	97.4	10.9	38.8	6.0	1.42	5.3	0.9	4.3	1.1	3.1	0.48	2.9	0.51
KOLE S2	42.6	78.7	8.48	34.0	5.1	1.04	4.1	0.8	4.1	0.9	2.8	0.50	2.9	0.45
KoLe1	23.3	48.1	5.31	17.5	4.0	0.90	3.3	0.7	3.4	0.8	2.0	0.36	2.2	0.33

Table A9: Whole rock Nd-Sr-Pb isotope data.

Tab. A9: Gesamtgesteins-Nd-Sr-Pb-Isotopendaten.

[a] Ages estimated using available biostratigraphic and geochronological data and the timescale after Gradstein et al. (2005).
[b] $^{87}Sr/^{86}Sr$ and $^{143}Nd/^{144}Nd$, are normalized to $^{86}Sr/^{88}Sr = 0.1194$ and $^{146}Nd/^{144}Nd = 0.7219$, respectively. Analytical uncertainties are given at $2\sigma_m$ level.
[c] $^{87}Sr/^{86}Sr_{(T)}$ and $\varepsilon Nd_{(T)}$ were calculated for the stratigraphic age using $\lambda^{87}Rb = 1.42\times10^{-11}$ y^{-1} and $\lambda^{147}Sm = 6.54\times10^{-12}$ y^{-1}, $(^{147}Sm/^{144}Nd)^0_{CHUR} = 0.1967$, and $(^{143}Nd/^{144}Nd)^0_{CHUR} = 0.512638$, respectively, and the concentration data given in **Table A7 and A8**.
[d] Two stage model age using the model of Liew & Hofmann (1988).
[e] Lead isotope data recalculated to the biostratigraphic age using the contents of Pb, Th, and U (**Table A7**) and the constants of Jaffey et al (1971) recommended by IUGS (Steiger & Jäger 1977).

Sample [a]		T (Ma)	^{87}Sr [b] / ^{86}Sr	$^{87}Sr_T$ [c] / ^{86}Sr	^{143}Nd [b] / ^{144}Nd	εNd_T [c]	T_{DM} [d] (Ga)	^{206}Pb / ^{204}Pb	^{207}Pb / ^{204}Pb	^{208}Pb / ^{204}Pb	$^{206}Pb_T$ [e] / ^{204}Pb	$^{207}Pb_T$ [e] / ^{204}Pb	$^{208}Pb_T$ [e] / ^{204}Pb
1	**BL 01**	590	0.721829±7	0.7082	0.511733±5	-11.7	2.17	18.152	15.519	38.483	15.73	15.38	37.00
2	**DB 1/1**	590	0.723299±7	0.7013	0.511978±4	-6.6	1.80	19.475	15.628	39.210	18.08	15.55	37.79
3	**DB 1/2**	590	0.723890±7	0.7006	0.512182±5	-3.6	1.49	20.094	15.666	38.721	18.69	15.58	37.81
4	**NPZb 4**	570	0.717642±10	0.7065	0.512069±6	-5.5	1.66	18.597	15.599	38.541	17.63	15.54	37.74
5	**NPZb 5**	570	0.718628±7	0.7098	0.512105±4	-6.5	1.61	18.895	15.616	38.911	17.51	15.53	37.64
6	**Dobris**	570	0.718490±7	0.7078	0.512015±5	-7.2	1.74	18.516	15.603	38.662	17.64	15.55	37.73
7	**Dobris 02B**	570	0.723902±10	0.7064	0.512041±12	-5.7	1.70	18.332	15.587	38.497	17.55	15.54	37.70
8	**DB S1**	525	0.714348±8	0.7037	0.512425±6	1.0	1.12	18.933	15.672	38.800	18.35	15.64	38.17
9	**DB D2**	525	0.715030±7	0.7046	0.512414±4	0.3	1.13	19.003	15.678	38.863	18.09	15.63	37.81
10	**MM2**	520	0.770952±7	0.7018	0.512193±5	-3.7	1.47	19.352	15.708	39.225	18.35	15.65	38.25
11	**DB 1/5**	505	0.736003±18	0.6996	0.512140±5	-5.0	1.55	18.806	15.618	38.679	17.80	15.56	37.84
12	**DB 6/1**	505	0.732287±9	0.7088	0.512162±5	-4.5	1.52	18.857	15.613	38.739	17.80	15.55	37.73
13	**DB 6/3**	505	0.734657±13	0.7088	0.512076±4	-6.0	1.65	18.567	15.595	38.510	17.67	15.54	37.66
14	**J4**	505	0.753715±10	0.7023	0.512323±5	-1.7	1.27	19.150	15.626	38.728	18.18	15.57	37.94
15	**J8**	505	0.731392±10	0.7060	0.512079±6	-6.0	1.65	18.811	15.610	38.862	17.91	15.56	37.92
16	**KlRS 01**	470	0.744340±12	0.7117	0.511876±5	-9.6	1.96	18.561	15.695	39.195	17.80	15.65	37.99
17	**LiBS 0**	455	0.741838±14	0.7139	0.511834±4	-9.4	2.02	18.580	15.693	39.198	16.91	15.60	36.41
18	**LeZb 4**	455	0.738781±18	0.7083	0.511928±4	-8.3	1.88	18.842	15.708	39.654	17.05	15.61	36.35
19	**ViBe 1A**	455	0.727928±13	0.7107	0.511902±5	-8.7	1.92	18.776	15.711	39.282	18.06	15.67	38.09
20	**KDLe S2**	445	0.730318±14	0.7091	0.511869±6	-9.0	1.97	18.723	15.702	39.094	17.94	15.66	37.87
21	**KoLe S1**	445	0.730996±10	0.7099	0.511883±6	-8.9	1.95	18.706	15.688	39.083	17.99	15.65	37.99
22	**KoLe S2**	445	0.734525±7	0.7114	0.511891±5	-8.6	1.93	18.618	15.681	38.915	18.11	15.65	38.19

GEOLOGICA SAXONICA
Journal of Central European Geology
54 (2008) 1–168

Table A10: SHRIMP U-Th-Pb isotopic data for detrital and magmatic zircon.

Tab. A10: SHRIMP-U-Th-Pb-Isotopendaten für detritische und magmatische Zirkone.

[1] One analyses per grain! (Labelling is based on the captions of SEM images used for identification/selection of the individual grains.)
[2] f206(%) is the % of ^{206}Pb attributed to common Pb.
[3] The degree of concordance was calculated using: conc = $^{206}Pb/^{238}U$ age × 100/ $^{207}Pb/^{206}Pb$ age.

grain [1]	Th [ppm]	U [ppm]	Th/U	f206 (%) [2]	$^{207}Pb/^{206}Pb$ ± 1σ	$^{206}Pb/^{238}U$ ± 1σ	$^{207}Pb/^{235}U$ ± 1σ	$^{208}Pb/^{232}Th$ ± 1σ	conc [3] %	$^{207}Pb/^{206}Pb$ age ± 1σ [Ma]	$^{206}Pb/^{238}U$ age ± 1σ [Ma]
Sample Dob (n=17)											
9-1	95	187	0.5	0.37	0.0572 ± 0.0023	0.0979 ± 0.0007	0.7714 ± 0.031	0.0282 ± 0.00113	121	498 ± 88	602 ± 4
10-1	54	72	0.8	0.04	0.1249 ± 0.0013	0.3542 ± 0.0033	6.1013 ± 0.087	0.1022 ± 0.0018	96	2028 ± 19	1954 ± 16
12-1	47	42	1.1	0.93	0.0553 ± 0.0068	0.0984 ± 0.0016	0.7504 ± 0.093	0.0275 ± 0.0017	143	424 ± 275	605 ± 9
13b-1	72	113	0.6	0.14	0.0608 ± 0.0026	0.1005 ± 0.0009	0.8421 ± 0.037	0.0306 ± 0.0007	98	632 ± 94	617 ± 5
14-1	37	120	0.3	0.15	0.0632 ± 0.0017	0.0959 ± 0.0012	0.8353 ± 0.025	0.0323 ± 0.0013	83	714 ± 58	590 ± 7
15-1	187	115	1.6	0.17	0.1249 ± 0.0011	0.3585 ± 0.0027	6.1718 ± 0.073	0.1033 ± 0.0012	97	2027 ± 16	1975 ± 13
15-2	27	18	1.5	0.10	0.0650 ± 0.0012	0.1439 ± 0.0022	1.2901 ± 0.032	0.0426 ± 0.0013	112	774 ± 40	867 ± 13
20-1	35	99	0.4	0.51	0.0604 ± 0.0018	0.0980 ± 0.0009	0.8162 ± 0.025	0.0297 ± 0.0011	98	618 ± 63	603 ± 5
21-1	16	35	0.5	0.08	0.0587 ± 0.0039	0.0918 ± 0.0016	0.7424 ± 0.051	0.0288 ± 0.0020	102	555 ± 146	566 ± 9
23-1	156	253	0.6	0.44	0.0584 ± 0.0015	0.0977 ± 0.0006	0.7870 ± 0.020	0.0287 ± 0.0006	110	545 ± 55	601 ± 3
25-1	23	54	0.4	0.16	0.0629 ± 0.0026	0.0976 ± 0.0013	0.8461 ± 0.037	0.0311 ± 0.0014	85	705 ± 88	600 ± 7
25-2	52	151	0.3	0.15	0.0626 ± 0.0016	0.0915 ± 0.0010	0.7897 ± 0.022	0.0292 ± 0.0011	81	694 ± 53	565 ± 6
28-1	19	14	1.4	0.01	0.0597 ± 0.0012	0.0912 ± 0.0014	0.7509 ± 0.019	0.0279 ± 0.0009	95	594 ± 43	563 ± 8
35-1	23	118	0.2	0.00	0.0603 ± 0.0009	0.0931 ± 0.0020	0.7734 ± 0.020	0.0305 ± 0.0013	94	613 ± 32	574 ± 12
42-1	394	273	1.4	0.46	0.0585 ± 0.0020	0.0924 ± 0.0014	0.7452 ± 0.028	0.0287 ± 0.0006	104	547 ± 75	570 ± 8
42-2	98	99	1.0	0.06	0.0587 ± 0.0013	0.0956 ± 0.0055	0.7732 ± 0.048	0.0300 ± 0.0020	106	555 ± 50	588 ± 32
43-1	79	78	1.0	0.00	0.0600 ± 0.0011	0.0939 ± 0.0014	0.7769 ± 0.019	0.0288 ± 0.0008	96	605 ± 41	578 ± 9
Sample OKR (n=13)											
6-1	55	147	0.4	0.72	0.0562 ± 0.0021	0.0824 ± 0.0011	0.6387 ± 0.025	0.0252 ± 0.0012	111	460 ± 81	511 ± 6
7-1	31	127	0.2	0.08	0.0569 ± 0.0015	0.0791 ± 0.0010	0.6209 ± 0.018	0.0247 ± 0.0010	101	488 ± 58	491 ± 6
9-1	39	152	0.3	0.07	0.0576 ± 0.0011	0.0791 ± 0.0010	0.6281 ± 0.015	0.0244 ± 0.0008	96	514 ± 44	491 ± 6
10-1	89	358	0.2	0.05	0.0580 ± 0.0007	0.0820 ± 0.0010	0.6559 ± 0.011	0.0260 ± 0.0005	96	529 ± 25	508 ± 6
12-1	53	179	0.3	0.12	0.0575 ± 0.0014	0.0791 ± 0.0011	0.6264 ± 0.018	0.0244 ± 0.0009	96	510 ± 55	490 ± 6
13-1	32	98	0.3	0.30	0.0565 ± 0.0011	0.0773 ± 0.0023	0.6023 ± 0.021	0.0229 ± 0.0008	101	474 ± 41	480 ± 14
14-1	60	213	0.3	0.07	0.0566 ± 0.0008	0.0800 ± 0.0010	0.6239 ± 0.012	0.0249 ± 0.0006	104	475 ± 31	496 ± 6
14-2	11	54	0.2	0.00	0.0610 ± 0.0029	0.0802 ± 0.0012	0.6752 ± 0.034	0.0298 ± 0.0031	78	640 ± 102	498 ± 7
15-1	22	94	0.2	0.26	0.0591 ± 0.0015	0.0881 ± 0.0012	0.7183 ± 0.021	0.0257 ± 0.0012	95	571 ± 55	544 ± 7

Table A10: Continuation.

Tab. A10: Fortsetzung.

grain [1]	Th [ppm]	U [ppm]	Th/U	f206 (%) [2]	$^{207}Pb/^{206}Pb$ ± 1σ	$^{206}Pb/^{238}U$ ± 1σ	$^{207}Pb/^{235}U$ ± 1σ	$^{208}Pb/^{232}Th$ ± 1σ	conc [3] %	$^{207}Pb/^{206}Pb$ age ± 1σ [Ma]	$^{206}Pb/^{238}U$ age ± 1σ [Ma]
Sample OKR (n=13)											
15-2	68	253	0.3	0.19	0.0563 ± 0.0011	0.0810 ± 0.0010	0.6284 ± 0.014	0.0247 ± 0.0007	108	464 ± 42	502 ± 6
16-1	118	402	0.3	0.02	0.0569 ± 0.0006	0.0805 ± 0.0010	0.6317 ± 0.011	0.0250 ± 0.0005	103	487 ± 25	499 ± 6
17-1	58	203	0.3	0.17	0.0560 ± 0.0012	0.0808 ± 0.0011	0.6240 ± 0.016	0.0249 ± 0.0008	111	452 ± 47	501 ± 7
23-1	71	230	0.3	0.21	0.0556 ± 0.0012	0.0815 ± 0.0010	0.6245 ± 0.015	0.0249 ± 0.0008	116	436 ± 47	505 ± 6

GEOLOGICA SAXONICA
Journal of Central European Geology
54 (2008) 1–168

Table A11: LA-ICP-MS U-Pb data for detrital zircon obtained at NHM London..

Tab. A11: LA-ICP-MS – U-Pb-Daten gemessen am NHM London.

Analyses that are more than 20% discordant, that showed U-Pb fractionation or features of common lead contamination were rejected. A correction for common lead was not applied.

[a] Corrected for background and within-run Pb/U fractionation and normalised to 91 500 standard zircon.
[b] Mass bias corrected by normalising to 91 500 standard zircon.
[c] The degree of concordance was calculated using: conc = $^{206}Pb/^{238}U$ age × 100/ $^{207}Pb/^{206}Pb$ age.

	Isotopic ratios (1σ errors)			**Apparent ages (2σ errors)**			
spot	$^{207}Pb/^{206}Pb$ [a]	$^{207}Pb/^{235}U$ [a]	$^{206}Pb/^{238}U$ [a]	$^{207}Pb/^{206}Pb$ [b]	$^{207}Pb/^{235}U$ [a]	$^{206}Pb/^{238}U$ [a]	conc [c]
Sample PJ1/3 (n=52)							
ja27a05	0.0603 ± 0.0003	0.6770 ± 0.0031	0.0814 ± 0.0005	614 ± 20	525 ± 4	504 ± 6	82
ja27b05	0.0582 ± 0.0017	0.6630 ± 0.0209	0.0825 ± 0.0017	538 ± 128	516 ± 26	511 ± 20	95
ja27c15	0.0586 ± 0.0003	0.6832 ± 0.0044	0.0845 ± 0.0005	552 ± 24	529 ± 5	523 ± 6	95
ja30c09	0.0591 ± 0.0008	0.6929 ± 0.0083	0.0850 ± 0.0007	570 ± 56	535 ± 10	526 ± 8	92
ja27d06	0.0608 ± 0.0005	0.7148 ± 0.0058	0.0852 ± 0.0005	632 ± 38	548 ± 7	527 ± 6	83
ja30c07	0.0575 ± 0.0017	0.6796 ± 0.0153	0.0856 ± 0.0014	512 ± 128	527 ± 19	530 ± 17	103
ja27e12	0.0581 ± 0.0011	0.6891 ± 0.0179	0.0860 ± 0.0011	532 ± 84	532 ± 22	532 ± 13	100
ja27d05	0.0574 ± 0.0007	0.6818 ± 0.0080	0.0862 ± 0.0004	506 ± 54	528 ± 10	533 ± 5	105
ja27a07	0.0605 ± 0.0005	0.7206 ± 0.0068	0.0864 ± 0.0003	620 ± 40	551 ± 8	534 ± 4	86
ja30c10	0.0584 ± 0.0003	0.7030 ± 0.0076	0.0873 ± 0.0009	544 ± 24	541 ± 9	540 ± 11	99
ja30c14	0.0571 ± 0.0008	0.6940 ± 0.0101	0.0882 ± 0.0007	494 ± 62	535 ± 12	545 ± 8	110
ja27a09	0.0572 ± 0.0006	0.7007 ± 0.0090	0.0889 ± 0.0008	496 ± 48	539 ± 11	549 ± 9	111
ja27e09	0.0610 ± 0.0006	0.7672 ± 0.0089	0.0912 ± 0.0010	638 ± 42	578 ± 10	563 ± 12	88
ja30c08	0.0597 ± 0.0004	0.7616 ± 0.0052	0.0926 ± 0.0004	590 ± 28	575 ± 6	571 ± 5	97
ja27d11	0.0603 ± 0.0005	0.7766 ± 0.0071	0.0933 ± 0.0004	614 ± 38	584 ± 8	575 ± 4	94
ja27d12	0.0605 ± 0.0004	0.7800 ± 0.0053	0.0936 ± 0.0003	618 ± 26	585 ± 6	577 ± 4	93
ja27d16	0.0609 ± 0.0005	0.7870 ± 0.0050	0.0938 ± 0.0006	632 ± 34	589 ± 6	578 ± 8	91
ja27c06	0.0610 ± 0.0005	0.7978 ± 0.0055	0.0948 ± 0.0006	640 ± 32	596 ± 6	584 ± 8	91
ja27b08	0.0627 ± 0.0005	0.8214 ± 0.0143	0.0950 ± 0.0015	696 ± 36	609 ± 16	585 ± 17	84
ja27a06	0.0600 ± 0.0006	0.7878 ± 0.0076	0.0952 ± 0.0006	604 ± 46	590 ± 9	586 ± 7	97
ja27b06	0.0611 ± 0.0005	0.8148 ± 0.0081	0.0967 ± 0.0006	642 ± 34	605 ± 9	595 ± 8	93
ja27b10	0.0576 ± 0.0008	0.7720 ± 0.0074	0.0972 ± 0.0008	514 ± 64	581 ± 8	598 ± 10	116
ja27e05	0.0602 ± 0.0006	0.8064 ± 0.0079	0.0972 ± 0.0006	608 ± 42	600 ± 9	598 ± 7	98
ja27b14	0.0612 ± 0.0006	0.8214 ± 0.0077	0.0973 ± 0.0005	644 ± 42	609 ± 9	599 ± 6	93
ja27d08	0.0609 ± 0.0004	0.8187 ± 0.0063	0.0974 ± 0.0005	636 ± 32	607 ± 7	599 ± 6	94
ja27c16	0.0620 ± 0.0011	0.8339 ± 0.0168	0.0976 ± 0.0008	672 ± 76	616 ± 19	600 ± 10	89
ja30c15	0.0599 ± 0.0009	0.8142 ± 0.0123	0.0986 ± 0.0005	598 ± 66	605 ± 14	606 ± 5	101
ja27c11	0.0606 ± 0.0004	0.8249 ± 0.0050	0.0988 ± 0.0007	624 ± 30	611 ± 6	607 ± 8	97
ja27d10	0.0614 ± 0.0006	0.8364 ± 0.0068	0.0989 ± 0.0006	650 ± 42	617 ± 8	608 ± 7	93
ja27d07	0.0599 ± 0.0005	0.8226 ± 0.0063	0.0996 ± 0.0004	598 ± 36	610 ± 7	612 ± 4	102
ja27e10	0.0600 ± 0.0009	0.8298 ± 0.0113	0.1003 ± 0.0007	602 ± 62	613 ± 13	616 ± 8	102
ja27b07	0.0602 ± 0.0003	0.8367 ± 0.0057	0.1008 ± 0.0007	610 ± 24	617 ± 6	619 ± 8	101
ja30c13	0.0607 ± 0.0006	0.8732 ± 0.0119	0.1044 ± 0.0009	626 ± 40	637 ± 13	640 ± 10	102
ja27d13	0.0644 ± 0.0005	1.0248 ± 0.0096	0.1155 ± 0.0006	752 ± 32	716 ± 10	705 ± 7	94
ja27b09	0.0766 ± 0.0005	1.8473 ± 0.0094	0.1750 ± 0.0013	1108 ± 28	1062 ± 7	1040 ± 15	94

Table A11: Continuation.

Tab. A11: Fortsetzung.

	Isotopic ratios (1σ errors)			Apparent ages (2σ errors)			
spot	$^{207}Pb/^{206}Pb$ [a]	$^{207}Pb/^{235}U$ [a]	$^{206}Pb/^{238}U$ [a]	$^{207}Pb/^{206}Pb$ [b]	$^{207}Pb/^{235}U$ [a]	$^{206}Pb/^{238}U$ [a]	conc [c]
Sample PJ1/3 (n=52)							
ja30c11	0.0919 ± 0.0005	2.9777 ± 0.0292	0.2349 ± 0.0021	1466 ± 22	1402 ± 15	1360 ± 22	93
ja27c05	0.1071 ± 0.0004	4.4796 ± 0.0309	0.3034 ± 0.0020	1750 ± 14	1727 ± 11	1708 ± 20	98
ja27e15	0.1078 ± 0.0014	4.6072 ± 0.0594	0.3101 ± 0.0025	1760 ± 48	1751 ± 22	1741 ± 25	99
ja27e11	0.1161 ± 0.0005	5.2438 ± 0.0320	0.3274 ± 0.0015	1896 ± 16	1860 ± 10	1826 ± 15	96
ja27e06	0.1218 ± 0.0006	5.9128 ± 0.0290	0.3520 ± 0.0015	1982 ± 20	1963 ± 8	1944 ± 14	98
ja30c12	0.1303 ± 0.0005	7.0785 ± 0.0354	0.3939 ± 0.0021	2102 ± 14	2121 ± 9	2141 ± 20	102
ja27b12	0.1309 ± 0.0006	5.6363 ± 0.1110	0.3123 ± 0.0059	2108 ± 18	1922 ± 34	1752 ± 58	83
ja27e13	0.1345 ± 0.0004	6.6777 ± 0.0200	0.3600 ± 0.0012	2156 ± 10	2070 ± 5	1982 ± 11	92
ja27c08	0.1360 ± 0.0004	6.7912 ± 0.0482	0.3621 ± 0.0024	2176 ± 10	2085 ± 13	1992 ± 22	92
ja27a12	0.1368 ± 0.0014	7.2709 ± 0.0858	0.3854 ± 0.0035	2186 ± 36	2145 ± 21	2101 ± 32	96
ja27a13	0.1372 ± 0.0012	6.6918 ± 0.1445	0.3536 ± 0.0052	2192 ± 30	2072 ± 38	1952 ± 49	89
ja27e07	0.1486 ± 0.0008	7.7873 ± 0.0218	0.3801 ± 0.0015	2328 ± 20	2207 ± 5	2077 ± 14	89
ja27a08	0.1539 ± 0.0006	8.3626 ± 0.0652	0.3939 ± 0.0026	2390 ± 14	2271 ± 14	2141 ± 24	90
ja27a14	0.1625 ± 0.0007	9.7617 ± 0.0547	0.4357 ± 0.0029	2480 ± 16	2413 ± 10	2332 ± 26	94
ja27c12	0.1896 ± 0.0011	12.6138 ± 0.1413	0.4823 ± 0.0040	2738 ± 20	2651 ± 21	2537 ± 34	93
ja27a15	0.1997 ± 0.0017	12.9275 ± 0.2715	0.4694 ± 0.0065	2822 ± 26	2674 ± 40	2481 ± 57	88
ja27c10	0.2893 ± 0.0008	25.5976 ± 0.2227	0.6416 ± 0.0046	3412 ± 10	3331 ± 17	3195 ± 36	94
Sample CB3 (n=52)							
ja28a08	0.0580 ± 0.0003	0.6190 ± 0.0095	0.0773 ± 0.0011	530 ± 24	489 ± 12	480 ± 13	91
ja28a15	0.0558 ± 0.0008	0.5980 ± 0.0088	0.0777 ± 0.0006	442 ± 64	476 ± 11	483 ± 7	109
ja28e13	0.0586 ± 0.0004	0.6372 ± 0.0051	0.0789 ± 0.0007	550 ± 30	501 ± 6	490 ± 8	89
ja28b06	0.0576 ± 0.0006	0.6347 ± 0.0067	0.0799 ± 0.0004	514 ± 46	499 ± 8	495 ± 4	96
ja28e06	0.0585 ± 0.0007	0.6568 ± 0.0058	0.0814 ± 0.0005	548 ± 50	513 ± 7	505 ± 6	92
ja28b15	0.0607 ± 0.0008	0.6815 ± 0.0078	0.0814 ± 0.0007	628 ± 56	528 ± 9	505 ± 8	80
ja28a09	0.0585 ± 0.0002	0.6584 ± 0.0030	0.0816 ± 0.0003	548 ± 18	514 ± 4	506 ± 3	92
ja28b14	0.0572 ± 0.0006	0.6464 ± 0.0074	0.0820 ± 0.0006	498 ± 46	506 ± 9	508 ± 8	102
ja28c05	0.0570 ± 0.0005	0.6451 ± 0.0065	0.0820 ± 0.0005	492 ± 38	505 ± 8	508 ± 6	103
ja28c07	0.0568 ± 0.0007	0.6426 ± 0.0076	0.0821 ± 0.0004	482 ± 52	504 ± 9	508 ± 5	105
ja28e12	0.0581 ± 0.0008	0.6589 ± 0.0098	0.0822 ± 0.0006	534 ± 62	514 ± 12	509 ± 7	95
ja28d16	0.0578 ± 0.0006	0.6595 ± 0.0075	0.0827 ± 0.0005	522 ± 42	514 ± 9	512 ± 6	98
ja28a05	0.0578 ± 0.0004	0.6616 ± 0.0048	0.0830 ± 0.0005	520 ± 34	516 ± 6	514 ± 6	99
ja28b16	0.0587 ± 0.0004	0.6741 ± 0.0051	0.0833 ± 0.0006	556 ± 34	523 ± 6	516 ± 7	93
ja28b11	0.0573 ± 0.0004	0.6603 ± 0.0049	0.0836 ± 0.0006	500 ± 34	515 ± 6	518 ± 8	104
ja28b13	0.0595 ± 0.0006	0.7038 ± 0.0075	0.0858 ± 0.0009	584 ± 46	541 ± 9	531 ± 10	91
ja28a10	0.0595 ± 0.0004	0.7063 ± 0.0056	0.0861 ± 0.0005	584 ± 28	543 ± 7	532 ± 5	91
ja28a14	0.0579 ± 0.0007	0.6882 ± 0.0080	0.0863 ± 0.0006	524 ± 50	532 ± 10	533 ± 8	102
ja28e16	0.0600 ± 0.0004	0.7190 ± 0.0077	0.0869 ± 0.0009	602 ± 32	550 ± 9	537 ± 11	89
ja28d06	0.0578 ± 0.0006	0.7052 ± 0.0085	0.0884 ± 0.0012	522 ± 48	542 ± 10	546 ± 14	105
ja28d08	0.0599 ± 0.0004	0.7375 ± 0.0064	0.0892 ± 0.0004	600 ± 32	561 ± 8	551 ± 5	92
ja28b09	0.0625 ± 0.0009	0.7781 ± 0.0129	0.0903 ± 0.0013	690 ± 60	584 ± 15	557 ± 15	81

Table A11: Continuation.

Tab. A11: Fortsetzung.

	Isotopic ratios (1σ errors)			Apparent ages (2σ errors)			
spot	$^{207}Pb/^{206}Pb$ [a]	$^{207}Pb/^{235}U$ [a]	$^{206}Pb/^{238}U$ [a]	$^{207}Pb/^{206}Pb$ [b]	$^{207}Pb/^{235}U$ [a]	$^{206}Pb/^{238}U$ [a]	conc [c]
Sample CB3 (n=52)							
ja28e15	0.0591 ± 0.0008	0.7463 ± 0.0107	0.0915 ± 0.0009	570 ± 58	566 ± 13	565 ± 11	99
ja28c09	0.0619 ± 0.0008	0.7862 ± 0.0091	0.0921 ± 0.0005	670 ± 54	589 ± 10	568 ± 6	85
ja28d10	0.0586 ± 0.0004	0.7460 ± 0.0058	0.0923 ± 0.0006	550 ± 32	566 ± 7	569 ± 8	103
ja28e05	0.0623 ± 0.0004	0.7951 ± 0.0058	0.0925 ± 0.0008	684 ± 28	594 ± 7	570 ± 9	83
ja28c14	0.0600 ± 0.0003	0.7669 ± 0.0056	0.0926 ± 0.0006	604 ± 24	578 ± 6	571 ± 7	95
ja28a12	0.0607 ± 0.0002	0.7828 ± 0.0040	0.0936 ± 0.0004	626 ± 16	587 ± 5	577 ± 5	92
ja28a13	0.0602 ± 0.0005	0.7774 ± 0.0056	0.0937 ± 0.0005	608 ± 32	584 ± 6	577 ± 6	95
ja28b10	0.0624 ± 0.0010	0.8160 ± 0.0105	0.0949 ± 0.0008	686 ± 68	606 ± 12	584 ± 10	85
ja28d13	0.0596 ± 0.0005	0.7819 ± 0.0076	0.0951 ± 0.0004	590 ± 38	587 ± 9	585 ± 5	99
ja28a06	0.0628 ± 0.0006	0.8239 ± 0.0087	0.0952 ± 0.0007	698 ± 42	610 ± 10	586 ± 8	84
ja28d15	0.0590 ± 0.0006	0.7809 ± 0.0080	0.0960 ± 0.0005	566 ± 46	586 ± 9	591 ± 6	104
ja28c11	0.0618 ± 0.0012	0.8300 ± 0.0142	0.0973 ± 0.0010	668 ± 82	614 ± 16	599 ± 11	90
ja28c10	0.0604 ± 0.0005	0.8190 ± 0.0078	0.0984 ± 0.0008	616 ± 36	607 ± 9	605 ± 9	98
ja28d05	0.0607 ± 0.0006	0.8240 ± 0.0084	0.0984 ± 0.0005	628 ± 40	610 ± 9	605 ± 6	96
ja28c12	0.0610 ± 0.0003	0.8312 ± 0.0052	0.0988 ± 0.0006	640 ± 22	614 ± 6	607 ± 7	95
ja28c06	0.0616 ± 0.0004	0.8442 ± 0.0064	0.0994 ± 0.0005	660 ± 26	621 ± 7	611 ± 6	93
ja28c16	0.0598 ± 0.0008	0.8375 ± 0.0106	0.1016 ± 0.0007	594 ± 54	618 ± 12	624 ± 8	105
ja28d09	0.0604 ± 0.0003	0.8891 ± 0.0146	0.1067 ± 0.0016	618 ± 22	646 ± 16	654 ± 19	106
ja28e11	0.0653 ± 0.0018	0.9657 ± 0.0254	0.1072 ± 0.0010	784 ± 112	686 ± 26	656 ± 12	84
ja28c08	0.0632 ± 0.0008	0.9712 ± 0.0125	0.1114 ± 0.0005	714 ± 52	689 ± 13	681 ± 6	95
ja28e10	0.0615 ± 0.0014	0.9487 ± 0.0232	0.1118 ± 0.0012	656 ± 100	677 ± 24	683 ± 14	104
ja28e07	0.0673 ± 0.0008	1.0605 ± 0.0100	0.1142 ± 0.0006	846 ± 48	734 ± 10	697 ± 7	82
ja28b05	0.0645 ± 0.0005	1.1202 ± 0.0083	0.1259 ± 0.0006	758 ± 36	763 ± 8	764 ± 7	101
ja28d14	0.0650 ± 0.0005	1.1427 ± 0.0088	0.1274 ± 0.0009	774 ± 30	774 ± 8	773 ± 10	100
ja28e09	0.0685 ± 0.0011	1.3289 ± 0.0175	0.1407 ± 0.0009	882 ± 66	858 ± 15	849 ± 11	96
ja28c15	0.1111 ± 0.0012	4.3564 ± 0.0823	0.2844 ± 0.0046	1816 ± 40	1704 ± 31	1613 ± 47	89
ja28b08	0.1270 ± 0.0006	6.1233 ± 0.0582	0.3497 ± 0.0029	2056 ± 18	1994 ± 17	1933 ± 28	94
ja28b07	0.1287 ± 0.0005	6.3590 ± 0.0267	0.3583 ± 0.0015	2080 ± 14	2027 ± 7	1974 ± 14	95
ja28d11	0.1616 ± 0.0004	10.0135 ± 0.0551	0.4491 ± 0.0023	2472 ± 8	2436 ± 10	2391 ± 21	97
ja28d12	0.1794 ± 0.0015	12.3202 ± 0.1318	0.4980 ± 0.0034	2646 ± 28	2629 ± 20	2605 ± 30	98
Sample TrTo3 (n=47)							
ja26d10	0.0568 ± 0.0003	0.5215 ± 0.0035	0.0666 ± 0.0003	482 ± 20	426 ± 5	416 ± 3	86
ja26c09	0.0575 ± 0.0003	0.5582 ± 0.0078	0.0704 ± 0.0008	508 ± 24	450 ± 10	439 ± 10	86
ja26b06	0.0577 ± 0.0002	0.5621 ± 0.0049	0.0706 ± 0.0006	518 ± 12	453 ± 6	440 ± 8	85
ja30a14	0.0557 ± 0.0010	0.5467 ± 0.0099	0.0711 ± 0.0007	442 ± 84	443 ± 13	443 ± 8	100
ja26c10	0.0578 ± 0.0003	0.5681 ± 0.0065	0.0713 ± 0.0009	520 ± 22	457 ± 8	444 ± 11	85
ja26b07	0.0572 ± 0.0005	0.5649 ± 0.0053	0.0716 ± 0.0004	500 ± 36	455 ± 7	446 ± 5	89
ja26b13	0.0583 ± 0.0002	0.5808 ± 0.0039	0.0723 ± 0.0006	538 ± 18	465 ± 5	450 ± 7	84
ja26c06	0.0574 ± 0.0003	0.5908 ± 0.0048	0.0746 ± 0.0005	506 ± 24	471 ± 6	464 ± 6	92
ja26c08	0.0575 ± 0.0003	0.5975 ± 0.0038	0.0753 ± 0.0003	512 ± 26	476 ± 5	468 ± 4	91

Table A11: Continuation.

Tab. A11: Fortsetzung.

	Isotopic ratios (1σ errors)			Apparent ages (2σ errors)			
spot	$^{207}Pb/^{206}Pb$ [a]	$^{207}Pb/^{235}U$ [a]	$^{206}Pb/^{238}U$ [a]	$^{207}Pb/^{206}Pb$ [b]	$^{207}Pb/^{235}U$ [a]	$^{206}Pb/^{238}U$ [a]	conc [c]
Sample TrTo3 (n=47)							
ja26b14	0.0578 ± 0.0005	0.6010 ± 0.0071	0.0754 ± 0.0006	522 ± 38	478 ± 9	469 ± 7	90
ja26c07	0.0575 ± 0.0004	0.5987 ± 0.0060	0.0755 ± 0.0007	510 ± 28	476 ± 8	469 ± 8	92
ja26d13	0.0569 ± 0.0006	0.5952 ± 0.0073	0.0758 ± 0.0005	488 ± 48	474 ± 9	471 ± 7	97
ja26d15	0.0566 ± 0.0004	0.5987 ± 0.0054	0.0768 ± 0.0004	472 ± 34	476 ± 7	477 ± 5	101
ja30a16	0.0582 ± 0.0009	0.6169 ± 0.0089	0.0769 ± 0.0004	534 ± 68	488 ± 11	478 ± 5	89
ja26b15	0.0566 ± 0.0004	0.6002 ± 0.0044	0.0769 ± 0.0004	474 ± 30	477 ± 6	478 ± 5	101
ja30b07	0.0598 ± 0.0006	0.6399 ± 0.0127	0.0776 ± 0.0013	594 ± 42	502 ± 16	482 ± 16	81
ja26b10	0.0574 ± 0.0005	0.6160 ± 0.0049	0.0778 ± 0.0004	506 ± 36	487 ± 6	483 ± 5	95
ja26b08	0.0581 ± 0.0005	0.6241 ± 0.0056	0.0779 ± 0.0004	532 ± 34	492 ± 7	484 ± 5	91
ja26d11	0.0552 ± 0.0005	0.6032 ± 0.0051	0.0792 ± 0.0007	422 ± 38	479 ± 6	491 ± 9	116
ja26d07	0.0587 ± 0.0004	0.6424 ± 0.0048	0.0794 ± 0.0004	554 ± 32	504 ± 6	492 ± 5	89
ja30b06	0.0586 ± 0.0003	0.6525 ± 0.0048	0.0807 ± 0.0005	552 ± 20	510 ± 6	500 ± 7	91
ja30a07	0.0605 ± 0.0005	0.6741 ± 0.0086	0.0808 ± 0.0011	620 ± 34	523 ± 10	501 ± 14	81
ja26c11	0.0578 ± 0.0004	0.6471 ± 0.0049	0.0812 ± 0.0004	520 ± 28	507 ± 6	504 ± 5	97
ja26b12	0.0593 ± 0.0005	0.6673 ± 0.0049	0.0816 ± 0.0004	578 ± 34	519 ± 6	506 ± 5	87
ja30a10	0.0581 ± 0.0004	0.6560 ± 0.0050	0.0818 ± 0.0005	534 ± 32	512 ± 6	507 ± 6	95
ja30a15	0.0597 ± 0.0004	0.6757 ± 0.0055	0.0821 ± 0.0004	592 ± 28	524 ± 7	509 ± 5	86
ja30a12	0.0581 ± 0.0005	0.6582 ± 0.0058	0.0822 ± 0.0005	532 ± 36	514 ± 7	509 ± 6	96
ja30b16	0.0578 ± 0.0003	0.6547 ± 0.0040	0.0822 ± 0.0005	520 ± 24	511 ± 5	509 ± 6	98
ja30b12	0.0575 ± 0.0007	0.6534 ± 0.0069	0.0825 ± 0.0005	508 ± 54	511 ± 8	511 ± 6	101
ja26d08	0.0586 ± 0.0002	0.6667 ± 0.0052	0.0825 ± 0.0005	550 ± 18	519 ± 6	511 ± 6	93
ja30a06	0.0590 ± 0.0006	0.6794 ± 0.0090	0.0835 ± 0.0005	568 ± 46	526 ± 11	517 ± 6	91
ja30b11	0.0575 ± 0.0007	0.6616 ± 0.0070	0.0835 ± 0.0004	508 ± 56	516 ± 9	517 ± 5	102
ja30b10	0.0586 ± 0.0008	0.6742 ± 0.0075	0.0835 ± 0.0006	550 ± 62	523 ± 9	517 ± 7	94
ja26d06	0.0604 ± 0.0004	0.6954 ± 0.0053	0.0836 ± 0.0008	616 ± 26	536 ± 6	517 ± 10	84
ja30b13	0.0581 ± 0.0006	0.6797 ± 0.0063	0.0848 ± 0.0005	532 ± 42	527 ± 8	525 ± 6	99
ja30b14	0.0598 ± 0.0006	0.7087 ± 0.0099	0.0859 ± 0.0008	596 ± 40	544 ± 12	531 ± 9	89
ja30b08	0.0581 ± 0.0003	0.6938 ± 0.0095	0.0866 ± 0.0009	532 ± 26	535 ± 11	536 ± 11	101
ja26c05	0.0593 ± 0.0005	0.7291 ± 0.0045	0.0892 ± 0.0004	578 ± 34	556 ± 5	551 ± 4	95
ja26b16	0.0601 ± 0.0004	0.7404 ± 0.0041	0.0894 ± 0.0003	604 ± 26	563 ± 5	552 ± 4	91
ja26b11	0.0597 ± 0.0004	0.7402 ± 0.0056	0.0899 ± 0.0006	592 ± 32	563 ± 6	555 ± 7	94
ja26b05	0.0598 ± 0.0006	0.7437 ± 0.0086	0.0902 ± 0.0007	596 ± 46	565 ± 10	557 ± 8	93
ja26c12	0.0595 ± 0.0003	0.7406 ± 0.0059	0.0902 ± 0.0007	586 ± 22	563 ± 7	557 ± 8	95
ja26c14	0.0597 ± 0.0003	0.7659 ± 0.0061	0.0930 ± 0.0007	594 ± 22	577 ± 7	573 ± 9	96
ja30a09	0.0582 ± 0.0008	0.7526 ± 0.0097	0.0938 ± 0.0007	536 ± 60	570 ± 11	578 ± 9	108
ja30a08	0.0618 ± 0.0005	0.8016 ± 0.0088	0.0940 ± 0.0008	666 ± 34	598 ± 10	579 ± 10	87
ja30a11	0.0620 ± 0.0007	0.8308 ± 0.0088	0.0971 ± 0.0007	674 ± 44	614 ± 10	598 ± 8	89
ja30b09	0.0609 ± 0.0007	0.8679 ± 0.0111	0.1033 ± 0.0005	636 ± 46	634 ± 12	634 ± 6	100
Sample LiBS2 (n=50)							
mr16f05	0.0591 ± 0.0008	0.6791 ± 0.0096	0.0834 ± 0.0005	568 ± 56	526 ± 12	516 ± 6	91
mr16a08	0.0590 ± 0.0008	0.6816 ± 0.0089	0.0838 ± 0.0006	566 ± 58	528 ± 11	519 ± 7	92

Table A11: Continuation.

Tab. A11: Fortsetzung.

	Isotopic ratios (1σ errors)			Apparent ages (2σ errors)			
spot	$^{207}Pb/^{206}Pb$ [a]	$^{207}Pb/^{235}U$ [a]	$^{206}Pb/^{238}U$ [a]	$^{207}Pb/^{206}Pb$ [b]	$^{207}Pb/^{235}U$ [a]	$^{206}Pb/^{238}U$ [a]	conc [c]
Sample LiBS2 (n=50)							
mr16f05	0.0591 ± 0.0008	0.6791 ± 0.0096	0.0834 ± 0.0005	568 ± 56	526 ± 12	516 ± 6	91
mr16a08	0.0590 ± 0.0008	0.6816 ± 0.0089	0.0838 ± 0.0006	566 ± 58	528 ± 11	519 ± 7	92
mr16d05	0.0587 ± 0.0005	0.7158 ± 0.0072	0.0885 ± 0.0005	554 ± 40	548 ± 9	546 ± 5	99
mr16e16	0.0598 ± 0.0017	0.7293 ± 0.0202	0.0884 ± 0.0014	596 ± 126	556 ± 24	546 ± 16	92
mr16b14	0.0615 ± 0.0009	0.7533 ± 0.0099	0.0888 ± 0.0007	656 ± 60	570 ± 11	548 ± 8	84
mr16c15	0.0609 ± 0.0005	0.7515 ± 0.0060	0.0895 ± 0.0005	636 ± 38	569 ± 7	552 ± 6	87
mr16a12	0.0612 ± 0.0005	0.7635 ± 0.0080	0.0905 ± 0.0007	644 ± 34	576 ± 9	558 ± 8	87
mr16d16	0.0609 ± 0.0021	0.7606 ± 0.0224	0.0905 ± 0.0013	636 ± 148	574 ± 26	558 ± 15	88
mr16d08	0.0607 ± 0.0009	0.7584 ± 0.0106	0.0906 ± 0.0006	626 ± 66	573 ± 12	559 ± 8	89
mr16a16	0.0612 ± 0.0010	0.7665 ± 0.0104	0.0908 ± 0.0008	646 ± 70	578 ± 12	560 ± 10	87
mr16c14	0.0596 ± 0.0013	0.7451 ± 0.0165	0.0907 ± 0.0012	586 ± 96	565 ± 19	560 ± 15	96
mr16d11	0.0616 ± 0.0012	0.7755 ± 0.0148	0.0914 ± 0.0014	658 ± 82	583 ± 17	564 ± 16	86
mr16c11	0.0598 ± 0.0013	0.7583 ± 0.0150	0.0919 ± 0.0009	596 ± 94	573 ± 17	567 ± 11	95
mr16e08	0.0588 ± 0.0012	0.7483 ± 0.0144	0.0923 ± 0.0009	558 ± 90	567 ± 17	569 ± 11	102
mr16b06	0.0619 ± 0.0009	0.7883 ± 0.0102	0.0924 ± 0.0008	670 ± 62	590 ± 12	570 ± 9	85
mr16a11	0.0605 ± 0.0006	0.7724 ± 0.0095	0.0925 ± 0.0007	622 ± 44	581 ± 11	571 ± 8	92
mr16e10	0.0574 ± 0.0009	0.7383 ± 0.0137	0.0932 ± 0.0012	508 ± 70	561 ± 16	574 ± 14	113
mr16b12	0.0623 ± 0.0019	0.8085 ± 0.0237	0.0942 ± 0.0012	682 ± 132	602 ± 27	580 ± 14	85
mr16a10	0.0607 ± 0.0012	0.7982 ± 0.0186	0.0954 ± 0.0012	628 ± 86	596 ± 21	587 ± 14	93
mr16d06	0.0586 ± 0.0009	0.7718 ± 0.0114	0.0956 ± 0.0008	550 ± 70	581 ± 13	588 ± 10	107
mr16e14	0.0624 ± 0.0006	0.8257 ± 0.0086	0.0960 ± 0.0005	686 ± 44	611 ± 10	591 ± 5	86
mr16b07	0.0596 ± 0.0011	0.7899 ± 0.0150	0.0961 ± 0.0008	588 ± 82	591 ± 17	592 ± 10	101
mr16d12	0.0609 ± 0.0010	0.8102 ± 0.0124	0.0964 ± 0.0011	636 ± 68	603 ± 14	593 ± 13	93
mr16f08	0.0620 ± 0.0012	0.8234 ± 0.0162	0.0963 ± 0.0008	674 ± 82	610 ± 18	593 ± 10	88
mr16b16	0.0627 ± 0.0013	0.8367 ± 0.0185	0.0968 ± 0.0010	698 ± 92	617 ± 20	595 ± 11	85
mr16a09	0.0616 ± 0.0005	0.8245 ± 0.0077	0.0971 ± 0.0009	658 ± 32	611 ± 9	597 ± 11	91
mr16e11	0.0627 ± 0.0008	0.8389 ± 0.0102	0.0970 ± 0.0008	696 ± 56	619 ± 11	597 ± 9	86
mr16e12	0.0614 ± 0.0010	0.8273 ± 0.0106	0.0978 ± 0.0007	650 ± 68	612 ± 12	601 ± 9	92
mr16e15	0.0614 ± 0.0013	0.8316 ± 0.0171	0.0982 ± 0.0010	652 ± 90	614 ± 19	604 ± 12	93
mr16a05	0.0577 ± 0.0014	0.7853 ± 0.0191	0.0987 ± 0.0010	516 ± 108	588 ± 22	607 ± 12	118
mr16d14	0.0613 ± 0.0008	0.8394 ± 0.0105	0.0993 ± 0.0009	650 ± 58	619 ± 12	610 ± 10	94
mr16c10	0.0626 ± 0.0016	0.8596 ± 0.0225	0.0996 ± 0.0010	692 ± 112	630 ± 25	612 ± 12	88
mr16a15	0.0632 ± 0.0006	0.8715 ± 0.0140	0.1000 ± 0.0013	712 ± 40	636 ± 15	615 ± 15	86
mr16f06	0.0630 ± 0.0012	0.8777 ± 0.0168	0.1010 ± 0.0010	708 ± 82	640 ± 18	620 ± 11	88
mr16a13	0.0629 ± 0.0013	0.8984 ± 0.0277	0.1036 ± 0.0017	704 ± 86	651 ± 30	635 ± 20	90
mr16c16	0.0604 ± 0.0010	0.8837 ± 0.0176	0.1060 ± 0.0011	618 ± 74	643 ± 19	650 ± 13	105
mr16d15	0.0628 ± 0.0014	0.9720 ± 0.0198	0.1123 ± 0.0010	700 ± 98	689 ± 20	686 ± 11	98
mr16b13	0.0696 ± 0.0016	1.3932 ± 0.0307	0.1451 ± 0.0016	916 ± 96	886 ± 26	874 ± 18	95
mr16c09	0.1257 ± 0.0008	5.3543 ± 0.0487	0.3088 ± 0.0024	2038 ± 22	1878 ± 16	1735 ± 24	85
mr16c06	0.1345 ± 0.0018	5.8353 ± 0.0461	0.3145 ± 0.0035	2158 ± 46	1952 ± 14	1763 ± 34	82
mr16e05	0.1267 ± 0.0009	5.6501 ± 0.0441	0.3234 ± 0.0016	2052 ± 24	1924 ± 13	1806 ± 16	88

Table A11: Continuation.

Tab. A11: Fortsetzung.

	Isotopic ratios (1σ errors)			Apparent ages (2σ errors)			
spot	$^{207}Pb/^{206}Pb$ [a]	$^{207}Pb/^{235}U$ [a]	$^{206}Pb/^{238}U$ [a]	$^{207}Pb/^{206}Pb$ [b]	$^{207}Pb/^{235}U$ [a]	$^{206}Pb/^{238}U$ [a]	conc [c]
Sample LiBS2 (n=50)							
mr16b11	0.1244 ± 0.0004	5.7500 ± 0.0247	0.3351 ± 0.0014	2020 ± 12	1939 ± 7	1863 ± 14	92
mr16b08	0.1202 ± 0.0006	5.6378 ± 0.0383	0.3402 ± 0.0018	1958 ± 18	1922 ± 12	1888 ± 17	96
mr16d09	0.1248 ± 0.0014	5.8755 ± 0.0599	0.3414 ± 0.0027	2024 ± 38	1958 ± 18	1893 ± 26	94
mr16c08	0.1290 ± 0.0012	6.1282 ± 0.0423	0.3444 ± 0.0022	2084 ± 32	1994 ± 12	1908 ± 21	92
mr16d10	0.1284 ± 0.0004	6.1859 ± 0.0328	0.3495 ± 0.0017	2074 ± 12	2002 ± 9	1932 ± 16	93
mr16e09	0.1323 ± 0.0013	6.5347 ± 0.0817	0.3581 ± 0.0032	2128 ± 36	2051 ± 22	1973 ± 30	93
mr16b09	0.1544 ± 0.0006	8.0473 ± 0.0451	0.3780 ± 0.0025	2394 ± 14	2236 ± 10	2067 ± 24	86
mr16e13	0.1316 ± 0.0006	6.9394 ± 0.0631	0.3824 ± 0.0034	2118 ± 16	2104 ± 16	2088 ± 32	99
mr16b15	0.2666 ± 0.0018	21.651 ± 0.1732	0.5889 ± 0.0044	3286 ± 22	3168 ± 16	2985 ± 36	91
Sample LeZb6 (n=48)							
mr16h12	0.0575 ± 0.0007	0.6473 ± 0.0073	0.0817 ± 0.0005	508 ± 50	507 ± 9	506 ± 6	100
mr16g08	0.0598 ± 0.0015	0.6919 ± 0.0135	0.0839 ± 0.0011	594 ± 108	534 ± 16	519 ± 14	87
mr16i06	0.0621 ± 0.0015	0.7541 ± 0.0232	0.0881 ± 0.0013	676 ± 106	571 ± 27	544 ± 16	80
mr16j13	0.0585 ± 0.0010	0.7128 ± 0.0117	0.0884 ± 0.0007	546 ± 72	546 ± 14	546 ± 8	100
mr16j07	0.0587 ± 0.0010	0.7341 ± 0.0105	0.0908 ± 0.0007	554 ± 72	559 ± 12	560 ± 8	101
mr16j09	0.0608 ± 0.0013	0.7685 ± 0.0138	0.0917 ± 0.0010	630 ± 96	579 ± 16	566 ± 12	90
mr16i09	0.0581 ± 0.0018	0.7491 ± 0.0172	0.0935 ± 0.0014	532 ± 138	568 ± 20	576 ± 16	108
mr16g05	0.0622 ± 0.0018	0.8079 ± 0.0237	0.0942 ± 0.0010	680 ± 126	601 ± 27	580 ± 12	85
mr16h15	0.0618 ± 0.0014	0.8128 ± 0.0187	0.0953 ± 0.0007	666 ± 94	604 ± 21	587 ± 8	88
mr16h11	0.0603 ± 0.0009	0.7975 ± 0.0147	0.0959 ± 0.0010	614 ± 68	595 ± 17	590 ± 12	96
mr16h13	0.0589 ± 0.0009	0.7811 ± 0.0135	0.0961 ± 0.0006	564 ± 62	586 ± 15	592 ± 8	105
mr16g09	0.0601 ± 0.0016	0.8016 ± 0.0172	0.0967 ± 0.0014	606 ± 116	598 ± 19	595 ± 16	98
mr16g11	0.0612 ± 0.0008	0.8166 ± 0.0100	0.0968 ± 0.0008	644 ± 54	606 ± 11	596 ± 9	93
mr16i08	0.0585 ± 0.0008	0.7872 ± 0.0102	0.0977 ± 0.0010	546 ± 62	590 ± 12	601 ± 12	110
mr16j11	0.0598 ± 0.0009	0.8079 ± 0.0118	0.0979 ± 0.0004	596 ± 64	601 ± 13	602 ± 4	101
mr16i11	0.0616 ± 0.0009	0.8570 ± 0.0132	0.1009 ± 0.0007	658 ± 60	628 ± 14	620 ± 8	94
mr16i12	0.0611 ± 0.0017	0.8520 ± 0.0239	0.1011 ± 0.0013	642 ± 120	626 ± 26	621 ± 15	97
mr16g16	0.0595 ± 0.0008	0.8361 ± 0.0109	0.1019 ± 0.0008	586 ± 58	617 ± 12	625 ± 9	107
mr16j08	0.0609 ± 0.0006	0.8564 ± 0.0102	0.1019 ± 0.0010	636 ± 42	628 ± 11	626 ± 12	98
mr17a14	0.0597 ± 0.0008	0.8451 ± 0.0122	0.1026 ± 0.0008	594 ± 58	622 ± 13	629 ± 9	106
mr17a11	0.0626 ± 0.0012	0.8865 ± 0.0167	0.1027 ± 0.0008	694 ± 80	645 ± 18	630 ± 10	91
mr16f16	0.0624 ± 0.0010	0.9243 ± 0.0161	0.1073 ± 0.0009	688 ± 72	665 ± 17	657 ± 11	95
mr17a05	0.0618 ± 0.0020	0.9188 ± 0.0227	0.1079 ± 0.0018	664 ± 138	662 ± 24	661 ± 21	100
mr16j15	0.0620 ± 0.0007	0.9354 ± 0.0104	0.1093 ± 0.0009	674 ± 46	670 ± 11	669 ± 10	99
mr17a06	0.0750 ± 0.0010	1.6575 ± 0.0287	0.1602 ± 0.0024	1068 ± 52	992 ± 22	958 ± 27	90
mr16g07	0.0888 ± 0.0015	2.8458 ± 0.0316	0.2325 ± 0.0022	1398 ± 64	1368 ± 17	1348 ± 23	96
mr16h05	0.1126 ± 0.0037	4.5692 ± 0.1247	0.2941 ± 0.0053	1842 ± 120	1744 ± 45	1662 ± 53	90
mr16h07	0.1233 ± 0.0010	5.0375 ± 0.1083	0.2962 ± 0.0047	2004 ± 30	1826 ± 36	1672 ± 47	83
mr16h08	0.1346 ± 0.0007	5.8216 ± 0.0419	0.3136 ± 0.0026	2158 ± 16	1950 ± 13	1758 ± 25	81
mr16f11	0.1368 ± 0.0011	5.9265 ± 0.0599	0.3142 ± 0.0029	2186 ± 28	1965 ± 18	1761 ± 28	81
mr16i16	0.1171 ± 0.0010	5.1449 ± 0.0453	0.3186 ± 0.0018	1912 ± 30	1844 ± 15	1783 ± 17	93

Table A11: Continuation.

Tab. A11: Fortsetzung.

	Isotopic ratios (1σ errors)			Apparent ages (2σ errors)			
spot	$^{207}Pb/^{206}Pb$ [a]	$^{207}Pb/^{235}U$ [a]	$^{206}Pb/^{238}U$ [a]	$^{207}Pb/^{206}Pb$ [b]	$^{207}Pb/^{235}U$ [a]	$^{206}Pb/^{238}U$ [a]	conc [c]
Sample LeZb6 (n=48)							
mr17a09	0.1254 ± 0.0013	5.6488 ± 0.0412	0.3266 ± 0.0026	2034 ± 38	1924 ± 13	1822 ± 25	90
mr16h09	0.1339 ± 0.0004	6.1067 ± 0.0379	0.3306 ± 0.0023	2150 ± 10	1991 ± 11	1841 ± 22	86
mr16f15	0.1305 ± 0.0008	5.9717 ± 0.0442	0.3317 ± 0.0022	2104 ± 24	1972 ± 13	1847 ± 22	88
mr16h10	0.1297 ± 0.0007	6.0970 ± 0.0469	0.3410 ± 0.0027	2092 ± 18	1990 ± 13	1891 ± 26	90
mr16i05	0.1243 ± 0.0005	5.9043 ± 0.0514	0.3446 ± 0.0028	2018 ± 14	1962 ± 15	1909 ± 27	95
mr16j16	0.1326 ± 0.0009	6.4109 ± 0.0577	0.3506 ± 0.0023	2132 ± 24	2034 ± 16	1937 ± 22	91
mr16j10	0.1263 ± 0.0007	6.1429 ± 0.0424	0.3528 ± 0.0021	2046 ± 18	1996 ± 12	1948 ± 20	95
mr16j12	0.1356 ± 0.0007	6.6126 ± 0.0727	0.3535 ± 0.0032	2172 ± 18	2061 ± 19	1951 ± 31	90
mr16f14	0.1224 ± 0.0010	6.0365 ± 0.0537	0.3575 ± 0.0019	1992 ± 30	1981 ± 15	1970 ± 18	99
mr16i14	0.1267 ± 0.0014	6.2616 ± 0.0570	0.3584 ± 0.0025	2052 ± 38	2013 ± 16	1974 ± 24	96
mr17a08	0.1346 ± 0.0014	6.8513 ± 0.0733	0.3692 ± 0.0028	2158 ± 36	2092 ± 19	2025 ± 27	94
mr17a12	0.1271 ± 0.0014	6.5192 ± 0.0645	0.3721 ± 0.0028	2056 ± 38	2048 ± 17	2039 ± 26	99
mr16f10	0.1329 ± 0.0018	6.9821 ± 0.0607	0.3811 ± 0.0046	2134 ± 46	2109 ± 15	2081 ± 43	98
mr16g10	0.1307 ± 0.0007	6.8702 ± 0.0447	0.3812 ± 0.0030	2106 ± 20	2095 ± 12	2082 ± 28	99
mr16i13	0.1346 ± 0.0016	7.1006 ± 0.0646	0.3825 ± 0.0026	2158 ± 40	2124 ± 16	2088 ± 24	97
mr16h06	0.1374 ± 0.0009	7.4869 ± 0.0337	0.3952 ± 0.0023	2194 ± 22	2171 ± 8	2147 ± 21	98
mr16g13	0.1598 ± 0.0007	9.9635 ± 0.0468	0.4523 ± 0.0027	2452 ± 16	2431 ± 9	2405 ± 24	98
Sample KoLeD1d (n=54)							
ja29b09	0.0583 ± 0.0004	0.6609 ± 0.0056	0.0822 ± 0.0003	540 ± 32	515 ± 7	509 ± 3	94
ja29e06	0.0589 ± 0.0010	0.6911 ± 0.0106	0.0851 ± 0.0006	560 ± 72	533 ± 13	527 ± 8	94
ja29c16	0.0585 ± 0.0007	0.6878 ± 0.0093	0.0853 ± 0.0008	546 ± 54	531 ± 11	528 ± 9	97
ja29d07	0.0584 ± 0.0008	0.6968 ± 0.0091	0.0865 ± 0.0007	544 ± 58	537 ± 11	535 ± 8	98
ja29b11	0.0603 ± 0.0004	0.7439 ± 0.0024	0.0894 ± 0.0004	614 ± 24	565 ± 3	552 ± 5	90
ja29b05	0.0587 ± 0.0004	0.7264 ± 0.0062	0.0898 ± 0.0006	554 ± 32	554 ± 7	554 ± 7	100
ja29a11	0.0592 ± 0.0007	0.7453 ± 0.0104	0.0913 ± 0.0006	572 ± 50	565 ± 12	563 ± 8	98
ja29c15	0.0585 ± 0.0007	0.7405 ± 0.0087	0.0917 ± 0.0006	548 ± 54	563 ± 10	566 ± 7	103
ja29b06	0.0613 ± 0.0010	0.7904 ± 0.0138	0.0935 ± 0.0009	648 ± 72	591 ± 16	576 ± 11	89
ja29b15	0.0595 ± 0.0005	0.7755 ± 0.0065	0.0946 ± 0.0006	582 ± 36	583 ± 7	583 ± 7	100
ja29c11	0.0579 ± 0.0008	0.7577 ± 0.0107	0.0950 ± 0.0009	524 ± 58	573 ± 12	585 ± 10	112
ja29b13	0.0610 ± 0.0010	0.8002 ± 0.0118	0.0952 ± 0.0006	636 ± 68	597 ± 13	586 ± 7	92
ja29c13	0.0601 ± 0.0008	0.7903 ± 0.0099	0.0953 ± 0.0007	608 ± 54	591 ± 11	587 ± 8	96
ja29e10	0.0602 ± 0.0007	0.7920 ± 0.0107	0.0954 ± 0.0007	610 ± 54	592 ± 12	588 ± 8	96
ja29b07	0.0615 ± 0.0008	0.8118 ± 0.0073	0.0957 ± 0.0008	656 ± 58	603 ± 8	589 ± 9	90
ja29e12	0.0636 ± 0.0010	0.8479 ± 0.0162	0.0966 ± 0.0009	728 ± 64	624 ± 18	595 ± 10	82
ja29e13	0.0601 ± 0.0007	0.8035 ± 0.0112	0.0970 ± 0.0009	604 ± 52	599 ± 13	597 ± 10	99
ja29b16	0.0611 ± 0.0005	0.8186 ± 0.0094	0.0971 ± 0.0006	642 ± 36	607 ± 11	598 ± 7	93
ja29e08	0.0603 ± 0.0013	0.8091 ± 0.0159	0.0973 ± 0.0007	614 ± 96	602 ± 18	599 ± 8	97
ja29c05	0.0594 ± 0.0010	0.8015 ± 0.0133	0.0978 ± 0.0009	582 ± 74	598 ± 15	601 ± 11	103
ja29e15	0.0601 ± 0.0008	0.8129 ± 0.0077	0.0982 ± 0.0008	604 ± 58	604 ± 9	604 ± 9	100
ja29d05	0.0581 ± 0.0014	0.7891 ± 0.0184	0.0984 ± 0.0013	534 ± 102	591 ± 21	605 ± 16	113
ja29d16	0.0600 ± 0.0004	0.8189 ± 0.0061	0.0990 ± 0.0005	600 ± 30	607 ± 7	609 ± 6	101

Table A11: Continuation.

Tab. A11: Fortsetzung.

	Isotopic ratios (1σ errors)			Apparent ages (2σ errors)			
spot	$^{207}Pb/^{206}Pb$ [a]	$^{207}Pb/^{235}U$ [a]	$^{206}Pb/^{238}U$ [a]	$^{207}Pb/^{206}Pb$ [b]	$^{207}Pb/^{235}U$ [a]	$^{206}Pb/^{238}U$ [a]	conc [c]
Sample KoLeD1d (n=54)							
ja29e16	0.0598 ± 0.0011	0.8206 ± 0.0141	0.0994 ± 0.0008	596 ± 84	608 ± 16	611 ± 9	103
ja29a14	0.0604 ± 0.0003	0.8304 ± 0.0049	0.0997 ± 0.0005	618 ± 24	614 ± 5	612 ± 6	99
ja29c07	0.0609 ± 0.0011	0.8385 ± 0.0147	0.0999 ± 0.0014	632 ± 78	618 ± 16	614 ± 17	97
ja30c06	0.0596 ± 0.0005	0.8233 ± 0.0084	0.1002 ± 0.0007	588 ± 40	610 ± 9	616 ± 8	105
ja30c05	0.0595 ± 0.0007	0.8286 ± 0.0100	0.1010 ± 0.0006	584 ± 50	613 ± 11	620 ± 7	106
ja29d10	0.0623 ± 0.0015	0.8755 ± 0.0179	0.1020 ± 0.0008	682 ± 102	639 ± 19	626 ± 10	92
ja29c12	0.0612 ± 0.0007	0.8605 ± 0.0102	0.1020 ± 0.0008	644 ± 52	630 ± 11	626 ± 9	97
ja29a13	0.0625 ± 0.0006	0.8947 ± 0.0080	0.1037 ± 0.0009	692 ± 42	649 ± 9	636 ± 10	92
ja29d11	0.0616 ± 0.0012	0.8844 ± 0.0225	0.1042 ± 0.0013	658 ± 86	643 ± 24	639 ± 15	97
ja29e05	0.0655 ± 0.0015	0.9526 ± 0.0234	0.1055 ± 0.0011	788 ± 98	679 ± 24	647 ± 13	82
ja29a09	0.0625 ± 0.0003	0.9363 ± 0.0079	0.1086 ± 0.0009	690 ± 16	671 ± 8	665 ± 10	96
ja29d06	0.0685 ± 0.0013	1.3364 ± 0.0262	0.1415 ± 0.0011	882 ± 82	862 ± 23	853 ± 13	97
ja29b10	0.0735 ± 0.0004	1.5626 ± 0.0116	0.1542 ± 0.0011	1026 ± 22	955 ± 9	924 ± 12	90
ja29d15	0.1083 ± 0.0007	4.2536 ± 0.0459	0.2847 ± 0.0026	1770 ± 24	1684 ± 18	1615 ± 26	91
ja29a05	0.1125 ± 0.0025	4.6596 ± 0.0326	0.3005 ± 0.0078	1838 ± 80	1760 ± 12	1694 ± 77	92
ja29b14	0.1125 ± 0.0013	4.8227 ± 0.0699	0.3110 ± 0.0034	1838 ± 40	1789 ± 24	1745 ± 33	95
ja29c14	0.1145 ± 0.0007	4.9386 ± 0.0425	0.3127 ± 0.0025	1872 ± 22	1809 ± 15	1754 ± 25	94
ja29e11	0.1146 ± 0.0012	5.0056 ± 0.0486	0.3166 ± 0.0034	1874 ± 38	1820 ± 16	1773 ± 34	95
ja29d09	0.1166 ± 0.0018	5.0693 ± 0.0659	0.3154 ± 0.0024	1904 ± 54	1831 ± 22	1767 ± 24	93
ja29a06	0.1213 ± 0.0004	5.5704 ± 0.0290	0.3331 ± 0.0021	1974 ± 12	1912 ± 9	1853 ± 21	94
ja29c10	0.1250 ± 0.0006	6.0386 ± 0.0236	0.3503 ± 0.0015	2028 ± 16	1981 ± 7	1936 ± 14	95
ja29e07	0.1256 ± 0.0004	6.2028 ± 0.0465	0.3582 ± 0.0022	2082 ± 18	2050 ± 8	2016 ± 20	97
ja29e14	0.1258 ± 0.0008	5.9719 ± 0.0555	0.3442 ± 0.0023	2096 ± 28	2040 ± 16	1984 ± 35	93
ja29c08	0.1289 ± 0.0006	6.5286 ± 0.0281	0.3671 ± 0.0021	2082 ± 18	2050 ± 8	2016 ± 20	97
ja29e09	0.1299 ± 0.0010	6.4547 ± 0.0600	0.3603 ± 0.0037	2096 ± 28	2040 ± 16	1984 ± 35	95
ja29a10	0.1355 ± 0.0005	7.2370 ± 0.0282	0.3874 ± 0.0018	2170 ± 14	2141 ± 7	2111 ± 17	97
ja29c09	0.1361 ± 0.0006	6.4933 ± 0.0617	0.3459 ± 0.0027	2178 ± 16	2045 ± 17	1915 ± 26	88
ja29a08	0.1363 ± 0.0005	6.8683 ± 0.0254	0.3654 ± 0.0016	2180 ± 12	2095 ± 7	2008 ± 15	92
ja29a07	0.1366 ± 0.0004	6.9792 ± 0.0747	0.3706 ± 0.0039	2182 ± 10	2109 ± 19	2032 ± 36	93
ja29d14	0.1781 ± 0.0010	9.8899 ± 0.0841	0.4026 ± 0.0032	2634 ± 18	2425 ± 16	2181 ± 30	83
ja29b12	0.2262 ± 0.0015	15.9969 ± 0.3183	0.5127 ± 0.0074	3024 ± 22	2877 ± 38	2668 ± 63	88

Table A12: LA-ICP-MS U-Pb data for detrital zircon obtained at Frankfurt University.

Tab. A12: LA-ICP-MS-U-Pb-Daten gemessen an der Universität Frankfurt.

Analyses that are more than 20% discordant were rejected.

a: Mass bias corrected by normalising to GJ-1 (c. 0.6% per amu)
b: $^{207}Pb/^{235}U$ calculated using $^{207}Pb/^{206}Pb/(^{238}U/^{206}Pb \times 1/137.88)$.
c: Corrected for background and within-run Pb/U fractionation and normalised to standard zircon GJ-1.
d: The degree of concordance was calculated using: conc = $^{206}Pb/^{238}U$ age × 100/ $^{207}Pb/^{206}Pb$ age.
#: Common lead corrected analyses. Reverse discordant ages ($^{206}Pb/^{238}U$ age older than $^{207}Pb/^{206}Pb$ age and thus conc >100%) with conc >105% chiefly appear in the case of common lead corrected ages younger than 1 Ga, which is due to relatively low count rates of radiogenic ^{207}Pb. This results in over-correction and large errors for the ^{204}Pb-corrected $^{207}Pb/^{206}Pb$ ages. However, the ^{204}Pb-corrected $^{206}Pb/^{238}U$ ages of these analyses are regarded to represent reliable ages.

	Isotopic ratios (1σ errors in %)			Apparent ages (2σ errors)			
spot	$^{207}Pb/^{206}Pb$ [a]	$^{207}Pb/^{235}U$ [b]	$^{206}Pb/^{238}U$ [c]	$^{207}Pb/^{206}Pb$	$^{207}Pb/^{235}U$	$^{206}Pb/^{238}U$	conc[d]
Sample BL (n=69)							
BL74#	0.0579 ± 3.8	0.7499 ± 4.0	0.09394 ± 1.2	526 ± 167	568 ± 35	579 ± 13	110
BL16	0.0599 ± 1.7	0.7852 ± 2.0	0.09502 ± 1.1	601 ± 74	588 ± 18	585 ± 12	97
BL14#	0.0586 ± 6.2	0.7697 ± 6.4	0.09526 ± 1.5	552 ± 270	580 ± 57	587 ± 17	106
BL47#	0.0595 ± 2.9	0.7819 ± 3.2	0.09538 ± 1.3	584 ± 126	587 ± 29	587 ± 15	101
BL57	0.0595 ± 2.2	0.7857 ± 2.5	0.09572 ± 1.2	587 ± 95	589 ± 22	589 ± 14	100
BL58	0.0607 ± 1.5	0.8090 ± 1.8	0.09665 ± 1.0	629 ± 66	602 ± 16	595 ± 11	95
BL12#	0.0599 ± 5.2	0.8062 ± 5.3	0.09759 ± 1.1	601 ± 223	600 ± 49	600 ± 13	100
BL24#	0.0605 ± 2.5	0.8152 ± 2.7	0.09771 ± 1.0	622 ± 109	605 ± 25	601 ± 11	97
BL70	0.0617 ± 1.7	0.8332 ± 2.1	0.09788 ± 1.2	665 ± 74	615 ± 19	602 ± 14	90
BL39	0.0607 ± 1.8	0.8342 ± 2.6	0.09960 ± 1.9	630 ± 77	616 ± 24	612 ± 22	97
BL37	0.0605 ± 1.7	0.8421 ± 2.0	0.10099 ± 1.2	621 ± 73	620 ± 19	620 ± 14	100
BL29	0.0620 ± 1.2	0.8683 ± 1.6	0.10160 ± 1.1	673 ± 52	635 ± 15	624 ± 13	93
BL40	0.0615 ± 1.3	0.8642 ± 1.8	0.10188 ± 1.1	658 ± 57	632 ± 17	625 ± 13	95
BL30#	0.0601 ± 5.4	0.8519 ± 5.6	0.10281 ± 1.2	607 ± 235	626 ± 53	631 ± 14	104
BL44	0.0604 ± 1.5	0.8580 ± 1.9	0.10295 ± 1.1	620 ± 67	629 ± 18	632 ± 13	102
BL38	0.0605 ± 1.3	0.8607 ± 1.8	0.10310 ± 1.2	623 ± 58	631 ± 17	633 ± 14	101
BL43	0.0601 ± 1.9	0.8566 ± 2.3	0.10332 ± 1.3	608 ± 81	628 ± 22	634 ± 16	104
BL27	0.0608 ± 1.9	0.8673 ± 2.4	0.10340 ± 1.5	633 ± 81	634 ± 23	634 ± 18	100
BL22	0.0606 ± 1.7	0.8642 ± 2.1	0.10348 ± 1.2	624 ± 73	632 ± 20	635 ± 15	102
BL21	0.0611 ± 1.4	0.8721 ± 1.8	0.10359 ± 1.2	641 ± 61	637 ± 17	635 ± 15	99
BL50	0.0617 ± 1.2	0.8825 ± 1.6	0.10380 ± 1.0	662 ± 53	642 ± 15	637 ± 12	96
BL25	0.0618 ± 1.2	0.8858 ± 1.7	0.10393 ± 1.2	668 ± 51	644 ± 16	637 ± 15	95
BL41	0.0601 ± 1.5	0.8606 ± 1.9	0.10393 ± 1.1	606 ± 67	630 ± 18	637 ± 13	105
BL75#	0.0609 ± 2.2	0.8736 ± 2.4	0.10403 ± 0.9	636 ± 94	638 ± 23	638 ± 11	100
BL66	0.0606 ± 1.1	0.8740 ± 1.5	0.10466 ± 1.1	624 ± 46	638 ± 14	642 ± 13	103
BL76#	0.0587 ± 2.2	0.8497 ± 2.4	0.10494 ± 1.0	557 ± 97	624 ± 23	643 ± 12	116
BL09#	0.0604 ± 3.0	0.8743 ± 3.2	0.10495 ± 1.1	619 ± 131	638 ± 31	643 ± 13	104
BL61#	0.0602 ± 1.2	0.8770 ± 2.2	0.10560 ± 1.9	612 ± 51	639 ± 21	647 ± 23	106
BL67	0.0613 ± 1.3	0.8956 ± 1.7	0.10591 ± 1.1	651 ± 57	649 ± 16	649 ± 14	100
BL56	0.0624 ± 1.1	0.9194 ± 1.5	0.10694 ± 1.0	686 ± 48	662 ± 15	655 ± 12	95
BL48#	0.0636 ± 3.5	0.9401 ± 3.6	0.10720 ± 1.0	728 ± 147	673 ± 36	656 ± 12	90
BL18	0.0612 ± 1.0	0.9086 ± 1.4	0.10763 ± 1.1	647 ± 42	656 ± 14	659 ± 14	102

Table A12: Continuation.

Tab. A12: Fortsetzung.

	Isotopic ratios (1σ errors in %)			Apparent ages (2σ errors)			
spot	$^{207}Pb/^{206}Pb$ [a]	$^{207}Pb/^{235}U$ [b]	$^{206}Pb/^{238}U$ [c]	$^{207}Pb/^{206}Pb$	$^{207}Pb/^{235}U$	$^{206}Pb/^{238}U$	conc[d]
Sample BL (n=69)							
BL71#	0.0608 ± 3.5	0.9109 ± 3.7	0.10868 ± 1.1	632 ± 153	658 ± 36	665 ± 14	105
BL72#	0.0623 ± 3.3	0.9340 ± 3.4	0.10873 ± 1.0	684 ± 139	670 ± 34	665 ± 13	97
BL23#	0.0611 ± 3.1	0.9178 ± 3.4	0.10888 ± 1.3	644 ± 134	661 ± 33	666 ± 16	103
BL78	0.0612 ± 1.6	0.9201 ± 1.9	0.10911 ± 1.0	645 ± 68	662 ± 19	668 ± 13	104
BL42	0.0596 ± 5.8	0.8977 ± 5.9	0.10920 ± 1.1	590 ± 249	650 ± 57	668 ± 14	113
BL60	0.0619 ± 1.2	0.9392 ± 1.6	0.11001 ± 1.0	671 ± 52	672 ± 16	673 ± 13	100
BL34#	0.0627 ± 2.0	0.9582 ± 2.2	0.11077 ± 1.0	699 ± 84	682 ± 22	677 ± 13	97
BL28	0.0670 ± 2.2	1.2072 ± 2.6	0.13064 ± 1.4	838 ± 90	804 ± 29	792 ± 21	94
BL45#	0.0636 ± 2.1	1.1701 ± 2.4	0.13345 ± 1.0	728 ± 91	787 ± 26	808 ± 15	111
BL49#	0.0685 ± 0.9	1.2884 ± 1.2	0.13643 ± 0.9	883 ± 35	841 ± 14	824 ± 14	93
BL36	0.0723 ± 1.4	1.6679 ± 2.0	0.16737 ± 1.4	994 ± 56	996 ± 26	998 ± 26	100
BL59	0.1073 ± 1.5	4.5858 ± 1.7	0.30999 ± 0.9	1754 ± 53	1747 ± 29	1741 ± 27	99
BL62#	0.1137 ± 1.1	5.2108 ± 1.6	0.33235 ± 1.2	1860 ± 39	1854 ± 27	1850 ± 39	99
BL63	0.1155 ± 0.7	5.5502 ± 1.1	0.34851 ± 0.9	1888 ± 24	1908 ± 19	1927 ± 30	102
BL65	0.1156 ± 0.8	5.3254 ± 1.3	0.33399 ± 1.0	1890 ± 27	1873 ± 22	1858 ± 32	98
BL13	0.1163 ± 1.1	5.3725 ± 1.6	0.33508 ± 1.1	1900 ± 39	1880 ± 28	1863 ± 36	98
BL32	0.1166 ± 1.4	5.2790 ± 1.8	0.32834 ± 1.1	1905 ± 50	1865 ± 31	1830 ± 35	96
BL15	0.1169 ± 0.6	5.8713 ± 1.4	0.36414 ± 1.3	1910 ± 20	1957 ± 24	2002 ± 45	105
BL35	0.1171 ± 0.6	5.2853 ± 1.1	0.32748 ± 1.0	1912 ± 20	1866 ± 19	1826 ± 32	96
BL55	0.1171 ± 1.0	5.4670 ± 1.5	0.33863 ± 1.1	1912 ± 34	1895 ± 26	1880 ± 36	98
BL54	0.1177 ± 1.0	5.6118 ± 1.5	0.34582 ± 1.1	1921 ± 35	1918 ± 26	1915 ± 36	100
BL53#	0.1180 ± 1.2	4.6406 ± 1.5	0.28517 ± 0.9	1927 ± 41	1757 ± 25	1617 ± 26	84
BL04	0.1073 ± 1.5	4.8948 ± 1.5	0.29649 ± 1.3	1952 ± 27	1801 ± 25	1674 ± 38	86
BL03	0.1220 ± 1.0	6.2311 ± 1.8	0.37045 ± 1.5	1986 ± 37	2009 ± 32	2032 ± 52	102
BL26	0.1233 ± 0.5	4.8302 ± 1.5	0.28420 ± 1.4	2004 ± 18	1790 ± 25	1613 ± 40	80
BL20	0.1301 ± 0.9	6.8411 ± 1.4	0.38145 ± 1.1	2099 ± 32	2091 ± 25	2083 ± 39	99
BL69	0.1326 ± 1.4	7.2658 ± 2.0	0.39741 ± 1.4	2133 ± 49	2145 ± 36	2157 ± 51	101
BL46#	0.1336 ± 0.6	6.0929 ± 1.3	0.33086 ± 1.2	2145 ± 22	1989 ± 23	1843 ± 39	86
BL01#	0.1628 ± 0.5	9.7487 ± 1.2	0.43427 ± 1.0	2485 ± 18	2411 ± 22	2325 ± 39	94
BL64	0.1712 ± 0.4	10.2031 ± 1.1	0.43228 ± 1.0	2569 ± 14	2453 ± 20	2316 ± 39	90
BL06	0.1724 ± 0.3	11.5368 ± 1.0	0.48540 ± 1.0	2581 ± 11	2568 ± 19	2551 ± 42	99
BL05	0.1790 ± 0.4	12.3510 ± 1.4	0.50047 ± 1.4	2644 ± 12	2631 ± 26	2616 ± 60	99
BL02	0.1825 ± 1.0	12.8318 ± 1.4	0.51007 ± 1.1	2675 ± 32	2667 ± 27	2657 ± 48	99
BL19	0.2012 ± 0.6	15.5085 ± 1.2	0.55917 ± 1.1	2836 ± 19	2847 ± 23	2863 ± 51	101
BL68	0.2029 ± 0.8	14.8231 ± 1.2	0.52973 ± 1.0	2850 ± 25	2804 ± 23	2740 ± 45	96
BL07	0.2548 ± 0.6	22.5989 ± 1.1	0.64316 ± 1.0	3215 ± 18	3210 ± 22	3201 ± 51	100
BL51	0.3061 ± 0.5	23.0303 ± 1.4	0.54572 ± 1.3	3501 ± 16	3228 ± 27	2807 ± 59	80
Sample Dob (n=41)							
Dob11	0.0591 ± 2.6	0.7223 ± 2.9	0.08868 ± 1.1	570 ± 115	552 ± 25	548 ± 12	96
Dob25	0.0591 ± 4.5	0.7368 ± 4.7	0.09047 ± 1.3	570 ± 196	561 ± 41	558 ± 14	98
Dob63	0.0592 ± 5.0	0.7500 ± 5.1	0.09184 ± 1.0	576 ± 216	568 ± 45	566 ± 11	98

Table A12: Continuation.

Tab. A12: Fortsetzung.

	Isotopic ratios (1σ errors in %)			Apparent ages (2σ errors)			
spot	$^{207}Pb/^{206}Pb$ [a]	$^{207}Pb/^{235}U$ [b]	$^{206}Pb/^{238}U$ [c]	$^{207}Pb/^{206}Pb$	$^{207}Pb/^{235}U$	$^{206}Pb/^{238}U$	conc[d]
Sample Dob (n=41)							
Dob35	0.0603 ± 2.4	0.7637 ± 3.0	0.09188 ± 1.8	614 ± 105	576 ± 27	567 ± 20	92
Dob04	0.0593 ± 4.1	0.7566 ± 4.3	0.09257 ± 1.1	578 ± 178	572 ± 38	571 ± 12	99
Dob03	0.0609 ± 5.9	0.7810 ± 6.0	0.09308 ± 1.1	634 ± 254	586 ± 54	574 ± 12	90
Dob09	0.0598 ± 11.1	0.7776 ± 11.2	0.09425 ± 1.4	598 ± 479	584 ± 102	581 ± 16	97
Dob32	0.0607 ± 4.3	0.7899 ± 4.5	0.09442 ± 1.5	628 ± 184	591 ± 41	582 ± 17	93
Dob23	0.0599 ± 2.5	0.7841 ± 2.9	0.09486 ± 1.5	602 ± 109	588 ± 26	584 ± 17	97
Dob31	0.0592 ± 3.0	0.7747 ± 3.6	0.09495 ± 1.9	574 ± 132	582 ± 32	585 ± 21	102
Dob19	0.0605 ± 2.4	0.8023 ± 2.9	0.09617 ± 1.7	622 ± 102	598 ± 26	592 ± 19	95
Dob15#	0.0604 ± 5.1	0.8029 ± 5.3	0.09635 ± 1.2	619 ± 222	598 ± 49	593 ± 14	96
Dob02	0.0594 ± 1.5	0.7939 ± 1.9	0.09692 ± 1.1	582 ± 65	593 ± 17	596 ± 13	102
Dob61	0.0602 ± 4.2	0.8136 ± 4.3	0.09798 ± 1.1	612 ± 181	604 ± 40	603 ± 13	99
Dob08#	0.0608 ± 5.5	0.8235 ± 5.6	0.09826 ± 0.9	632 ± 237	610 ± 52	604 ± 10	96
Dob60	0.0595 ± 4.3	0.8170 ± 4.5	0.09967 ± 1.3	584 ± 186	606 ± 42	612 ± 15	105
Dob05#	0.0605 ± 7.4	0.8309 ± 7.5	0.09969 ± 1.1	620 ± 319	614 ± 70	613 ± 13	99
Dob22	0.0598 ± 3.1	0.8215 ± 3.4	0.09971 ± 1.3	595 ± 135	609 ± 31	613 ± 15	103
Dob48#	0.0598 ± 3.1	0.8234 ± 3.4	0.09991 ± 1.4	595 ± 134	610 ± 31	614 ± 16	103
Dob49	0.0594 ± 2.3	0.8185 ± 2.7	0.10000 ± 1.4	580 ± 99	607 ± 25	614 ± 16	106
Dob06#	0.0615 ± 4.8	0.8481 ± 4.9	0.10007 ± 1.2	656 ± 204	624 ± 46	615 ± 14	94
Dob10	0.0621 ± 2.4	0.8652 ± 2.6	0.10112 ± 1.0	676 ± 102	633 ± 25	621 ± 12	92
Dob07	0.0597 ± 1.4	0.8351 ± 1.7	0.10147 ± 1.0	592 ± 61	616 ± 16	623 ± 12	105
Dob14#	0.0608 ± 7.1	0.8538 ± 7.2	0.10182 ± 1.5	633 ± 304	627 ± 68	625 ± 18	99
Dob20	0.0603 ± 3.8	0.8568 ± 4.0	0.10313 ± 1.5	613 ± 162	628 ± 38	633 ± 18	103
Dob52	0.0604 ± 4.1	0.8601 ± 4.4	0.10323 ± 1.4	619 ± 179	630 ± 42	633 ± 17	102
Dob44	0.0598 ± 2.6	0.8671 ± 2.8	0.10510 ± 1.1	898 ± 111	634 ± 27	644 ± 13	108
Dob27	0.0618 ± 3.6	0.8978 ± 3.8	0.10535 ± 1.3	668 ± 152	651 ± 37	646 ± 16	97
Dob37	0.0599 ± 3.5	0.9121 ± 4.0	0.11045 ± 1.9	670 ± 107	674 ± 39	675 ± 24	101
Dob66	0.0606 ± 5.5	0.9398 ± 5.6	0.11256 ± 1.2	623 ± 235	673 ± 56	688 ± 16	110
Dob24	0.0637 ± 4.5	1.0566 ± 4.6	0.12027 ± 1.1	732 ± 192	732 ± 49	732 ± 15	100
Dob50	0.1165 ± 2.2	5.6056 ± 2.7	0.34888 ± 1.6	1904 ± 79	1917 ± 47	1929 ± 53	101
Dob45	0.1228 ± 0.8	5.1777 ± 2.4	0.30568 ± 2.3	1998 ± 27	1849 ± 41	1719 ± 70	86
Dob28	0.1235 ± 1.3	6.4154 ± 2.0	0.37667 ± 1.6	2008 ± 45	2034 ± 35	2061 ± 57	103
Dob13#	0.1240 ± 1.2	5.8282 ± 1.9	0.34076 ± 1.4	2015 ± 42	1951 ± 33	1890 ± 46	94
Dob01	0.1243 ± 1.9	6.0649 ± 2.4	0.35391 ± 1.5	2019 ± 67	1985 ± 42	1953 ± 51	97
Dob39	0.1255 ± 3.6	5.1268 ± 3.7	0.29638 ± 1.0	2035 ± 126	1841 ± 64	1673 ± 30	82
Dob21	0.1302 ± 1.1	7.0777 ± 2.0	0.39436 ± 1.6	2100 ± 39	2121 ± 36	2143 ± 58	102
Dob30	0.1362 ± 0.9	6.8836 ± 1.6	0.36660 ± 1.4	2179 ± 30	2097 ± 29	2013 ± 49	92
Dob12	0.1365 ± 1.1	7.9092 ± 1.7	0.42038 ± 1.3	2183 ± 39	2221 ± 31	2262 ± 50	104
Dob51	0.1779 ± 1.5	12.8091 ± 2.4	0.52231 ± 1.8	2633 ± 51	2666 ± 46	2709 ± 80	103
Sample Oh3 (n=66)							
Oh25#	0.0579 ± 4.3	0.5987 ± 4.5	0.07496 ± 1.4	527 ± 187	476 ± 35	466 ± 13	88
Oh76	0.0596 ± 2.0	0.6521 ± 2.1	0.07934 ± 0.7	590 ± 86	510 ± 17	492 ± 7	83

Table A12: Continuation.

Tab. A12: Fortsetzung.

	Isotopic ratios (1σ errors in %)			Apparent ages (2σ errors)			
spot	$^{207}Pb/^{206}Pb$ [a]	$^{207}Pb/^{235}U$ [b]	$^{206}Pb/^{238}U$ [c]	$^{207}Pb/^{206}Pb$	$^{207}Pb/^{235}U$	$^{206}Pb/^{238}U$	conc[d]
Sample Oh3 (n=66)							
Oh75	0.0574 ± 1.9	0.6370 ± 2.2	0.08050 ± 1.0	506 ± 84	500 ± 17	499 ± 10	99
Oh57#	0.0584 ± 3.5	0.6496 ± 3.7	0.08063 ± 0.9	546 ± 154	508 ± 30	500 ± 9	92
Oh17	0.0580 ± 2.3	0.6456 ± 2.6	0.08069 ± 1.3	531 ± 100	506 ± 21	500 ± 13	94
Oh16	0.0583 ± 1.6	0.6490 ± 1.9	0.08076 ± 1.1	540 ± 69	508 ± 15	501 ± 11	93
Oh41#	0.0591 ± 9.6	0.6583 ± 9.7	0.08077 ± 1.6	571 ± 417	514 ± 80	501 ± 15	88
Oh78#	0.0591 ± 6.6	0.6602 ± 6.7	0.08099 ± 1.4	572 ± 285	515 ± 55	502 ± 14	88
Oh11	0.0582 ± 1.6	0.6522 ± 1.8	0.08122 ± 1.0	539 ± 68	510 ± 14	503 ± 10	93
Oh60	0.0581 ± 1.9	0.6536 ± 2.0	0.08163 ± 0.7	533 ± 82	511 ± 16	506 ± 7	95
Oh45#	0.0592 ± 4.2	0.6671 ± 4.3	0.08176 ± 0.9	574 ± 182	519 ± 35	507 ± 9	88
Oh74	0.0586 ± 1.8	0.6607 ± 1.9	0.08182 ± 0.8	551 ± 77	515 ± 15	507 ± 8	92
Oh10	0.0602 ± 1.6	0.6796 ± 1.9	0.08191 ± 1.0	610 ± 71	527 ± 16	508 ± 10	83
Oh01	0.0609 ± 1.8	0.6904 ± 2.1	0.08224 ± 1.1	635 ± 78	533 ± 17	510 ± 11	80
Oh35#	0.0589 ± 4.3	0.6717 ± 4.4	0.08272 ± 0.9	563 ± 188	522 ± 36	512 ± 9	91
Oh23#	0.0578 ± 6.6	0.6609 ± 6.7	0.08291 ± 1.2	523 ± 288	515 ± 55	513 ± 12	98
Oh29#	0.0580 ± 4.2	0.6674 ± 4.3	0.08340 ± 0.8	531 ± 184	519 ± 35	516 ± 8	97
Oh59	0.0578 ± 2.0	0.6714 ± 2.2	0.08429 ± 0.9	521 ± 87	522 ± 18	522 ± 9	100
Oh05	0.0594 ± 4.0	0.6912 ± 4.2	0.08444 ± 1.4	581 ± 175	534 ± 35	523 ± 14	90
Oh20	0.0588 ± 1.1	0.6863 ± 1.5	0.08464 ± 1.0	560 ± 50	531 ± 12	524 ± 10	94
Oh03	0.0581 ± 2.1	0.6789 ± 2.4	0.08477 ± 1.2	533 ± 93	526 ± 20	525 ± 12	98
Oh19#	0.0580 ± 5.9	0.6782 ± 6.0	0.08477 ± 1.2	531 ± 258	526 ± 50	525 ± 12	99
Oh50	0.0594 ± 0.8	0.6942 ± 1.5	0.08479 ± 1.2	581 ± 37	535 ± 13	525 ± 12	90
Oh40	0.0576 ± 2.1	0.6748 ± 2.2	0.08494 ± 0.9	515 ± 90	524 ± 18	526 ± 9	102
Oh24	0.0593 ± 1.5	0.6949 ± 1.8	0.08495 ± 0.9	579 ± 67	536 ± 15	526 ± 9	91
Oh61	0.0587 ± 1.2	0.6886 ± 1.4	0.08509 ± 0.7	556 ± 51	532 ± 12	526 ± 7	95
Oh08	0.0587 ± 1.3	0.6909 ± 1.6	0.08539 ± 1.0	555 ± 56	533 ± 13	528 ± 10	95
Oh32#	0.0576 ± 3.7	0.6790 ± 3.8	0.08550 ± 0.9	514 ± 162	526 ± 31	529 ± 9	103
Oh07	0.0581 ± 1.3	0.6861 ± 1.8	0.08565 ± 1.2	534 ± 57	530 ± 15	530 ± 12	99
Oh42	0.0586 ± 1.6	0.6927 ± 1.8	0.08579 ± 0.9	551 ± 68	534 ± 15	531 ± 9	96
Oh31#	0.0583 ± 3.3	0.6911 ± 3.4	0.08593 ± 0.8	542 ± 143	533 ± 28	531 ± 8	98
Oh39	0.0578 ± 2.1	0.6864 ± 2.5	0.08617 ± 1.3	521 ± 92	531 ± 21	533 ± 13	102
Oh73	0.0580 ± 2.5	0.6901 ± 2.7	0.08627 ± 1.0	530 ± 110	533 ± 23	533 ± 10	101
Oh37	0.0579 ± 1.3	0.6910 ± 1.4	0.08656 ± 0.7	526 ± 55	533 ± 12	535 ± 7	102
Oh63#	0.0597 ± 2.3	0.7156 ± 2.4	0.08697 ± 0.7	592 ± 101	548 ± 20	538 ± 7	91
Oh26	0.0606 ± 1.2	0.7269 ± 1.5	0.08706 ± 1.0	623 ± 50	555 ± 13	538 ± 10	86
Oh52#	0.0578 ± 5.2	0.6943 ± 5.3	0.08712 ± 1.0	522 ± 229	535 ± 45	538 ± 10	103
Oh30	0.0580 ± 1.0	0.6971 ± 1.3	0.08721 ± 0.7	529 ± 44	537 ± 11	539 ± 7	102
Oh34	0.0596 ± 1.3	0.7212 ± 1.5	0.08781 ± 0.8	588 ± 54	551 ± 13	543 ± 8	92
Oh67	0.0584 ± 1.6	0.7088 ± 1.8	0.08797 ± 0.9	546 ± 68	544 ± 15	543 ± 9	100
Oh02	0.0592 ± 2.0	0.7212 ± 2.3	0.08835 ± 1.0	575 ± 88	551 ± 20	546 ± 10	95
Oh15	0.0583 ± 1.5	0.7127 ± 1.9	0.08860 ± 1.2	542 ± 66	546 ± 16	547 ± 13	101
Oh51#	0.0606 ± 4.8	0.7404 ± 5.0	0.08863 ± 1.2	625 ± 209	563 ± 44	547 ± 13	88

Table A12: Continuation.

Tab. A12: Fortsetzung.

	Isotopic ratios (1σ errors in %)			Apparent ages (2σ errors)			
spot	$^{207}Pb/^{206}Pb$ [a]	$^{207}Pb/^{235}U$ [b]	$^{206}Pb/^{238}U$ [c]	$^{207}Pb/^{206}Pb$	$^{207}Pb/^{235}U$	$^{206}Pb/^{238}U$	conc[d]
Sample Oh3 (n=66)							
Oh66#	0.0599 ± 4.5	0.7405 ± 4.7	0.08964 ± 1.1	600 ± 196	563 ± 41	553 ± 12	92
Oh64#	0.0585 ± 3.8	0.7245 ± 4.3	0.08984 ± 2.0	548 ± 165	553 ± 37	555 ± 21	101
Oh18#	0.0593 ± 9.5	0.7360 ± 9.8	0.08996 ± 2.2	579 ± 414	560 ± 86	555 ± 23	96
Oh44	0.0592 ± 1.5	0.7347 ± 1.7	0.08996 ± 0.8	575 ± 65	559 ± 15	555 ± 9	96
Oh72#	0.0626 ± 6.2	0.7806 ± 6.5	0.09043 ± 1.9	695 ± 263	586 ± 59	558 ± 20	80
Oh69#	0.0590 ± 1.5	0.7371 ± 1.7	0.09067 ± 0.7	566 ± 67	561 ± 15	560 ± 8	99
Oh36	0.0572 ± 3.5	0.7205 ± 3.7	0.09138 ± 1.1	499 ± 155	551 ± 32	564 ± 12	113
Oh27	0.0603 ± 1.9	0.7740 ± 2.0	0.09304 ± 0.7	616 ± 81	582 ± 18	573 ± 8	93
Oh46#	0.0612 ± 7.2	0.7857 ± 7.3	0.09305 ± 0.7	648 ± 310	589 ± 66	574 ± 8	89
Oh38#	0.0605 ± 6.8	0.7820 ± 6.9	0.09367 ± 1.1	623 ± 294	587 ± 62	577 ± 12	93
Oh14	0.0613 ± 1.5	0.7992 ± 1.8	0.09448 ± 1.0	651 ± 63	596 ± 16	582 ± 11	89
Oh56#	0.0595 ± 3.4	0.7842 ± 3.6	0.09565 ± 1.1	584 ± 148	588 ± 32	589 ± 12	101
Oh04#	0.0594 ± 1.9	0.7865 ± 2.1	0.09606 ± 1.0	581 ± 80	589 ± 19	591 ± 11	102
Oh09	0.0601 ± 1.3	0.7964 ± 1.7	0.09618 ± 1.1	605 ± 56	595 ± 15	592 ± 12	98
Oh70	0.0606 ± 0.9	0.8036 ± 1.2	0.09619 ± 0.8	625 ± 39	599 ± 11	592 ± 9	95
Oh22#	0.0597 ± 5.5	0.7920 ± 5.6	0.09619 ± 1.0	594 ± 237	592 ± 51	592 ± 11	100
Oh49	0.0601 ± 1.8	0.8027 ± 2.1	0.09688 ± 1.0	607 ± 78	598 ± 19	596 ± 11	98
Oh62	0.0606 ± 1.2	0.8127 ± 1.4	0.09730 ± 0.8	624 ± 51	604 ± 13	599 ± 9	96
Oh47#	0.0624 ± 4.1	0.8537 ± 4.2	0.09924 ± 1.0	688 ± 174	627 ± 40	610 ± 12	89
Oh58#	0.0608 ± 4.5	0.8626 ± 4.6	0.10283 ± 1.1	634 ± 193	632 ± 44	631 ± 13	100
Oh21#	0.0595 ± 2.0	0.8741 ± 2.2	0.10658 ± 0.9	585 ± 85	638 ± 21	653 ± 11	112
Oh77	0.1437 ± 0.7	7.6953 ± 0.9	0.38851 ± 0.6	2272 ± 23	2196 ± 16	2116 ± 22	93
Oh13	0.1812 ± 0.3	11.9578 ± 1.1	0.47872 ± 1.0	2664 ± 12	2601 ± 21	2522 ± 42	95
Sample Tocnik (n=48)							
To24	0.0563 ± 1.9	0.5578 ± 2.7	0.07183 ± 1.8	465 ± 85	450 ± 20	447 ± 16	96
To40	0.0575 ± 2.0	0.6052 ± 2.4	0.07634 ± 1.4	511 ± 89	481 ± 18	474 ± 11	93
To06#	0.0573 ± 3.6	0.6164 ± 3.9	0.07805 ± 1.4	503 ± 160	488 ± 30	484 ± 12	96
To39	0.0570 ± 1.3	0.6181 ± 1.8	0.07859 ± 1.2	493 ± 57	489 ± 14	488 ± 10	99
To20	0.0580 ± 1.0	0.6303 ± 1.7	0.07887 ± 1.4	528 ± 42	496 ± 13	489 ± 13	93
To23	0.0599 ± 1.5	0.6660 ± 2.0	0.08058 ± 1.4	601 ± 63	518 ± 16	500 ± 14	83
To36	0.0572 ± 1.3	0.6444 ± 1.8	0.08177 ± 1.2	498 ± 58	505 ± 14	507 ± 10	102
To25	0.0582 ± 1.2	0.6589 ± 1.8	0.08204 ± 1.3	539 ± 53	514 ± 15	508 ± 12	94
To01	0.0581 ± 1.2	0.6631 ± 1.8	0.08282 ± 1.3	532 ± 52	517 ± 15	513 ± 13	96
To46#	0.0558 ± 7.1	0.6433 ± 7.2	0.08360 ± 1.1	445 ± 317	504 ± 58	518 ± 10	116
To31	0.0578 ± 2.5	0.6716 ± 2.7	0.08422 ± 1.2	524 ± 109	522 ± 22	521 ± 10	100
To49	0.0595 ± 1.4	0.6939 ± 1.9	0.08453 ± 1.2	587 ± 61	535 ± 16	523 ± 11	89
To09	0.0586 ± 1.8	0.6844 ± 3.1	0.08477 ± 2.5	551 ± 78	529 ± 26	525 ± 25	95
To29	0.0603 ± 1.7	0.7066 ± 2.1	0.08492 ± 1.2	616 ± 76	543 ± 18	525 ± 11	85
To03	0.0601 ± 1.5	0.7047 ± 2.1	0.08500 ± 1.4	608 ± 66	542 ± 18	526 ± 15	86
To18	0.0593 ± 1.2	0.6972 ± 1.8	0.08522 ± 1.4	579 ± 51	537 ± 15	527 ± 14	91

Table A12: Continuation.

Tab. A12: Fortsetzung.

	Isotopic ratios (1σ errors in %)			Apparent ages (2σ errors)			
spot	$^{207}Pb/^{206}Pb$ [a]	$^{207}Pb/^{235}U$ [b]	$^{206}Pb/^{238}U$ [c]	$^{207}Pb/^{206}Pb$	$^{207}Pb/^{235}U$	$^{206}Pb/^{238}U$	conc[d]
Sample Tocnik (n=48)							
To41#	0.0584 ± 5.7	0.6918 ± 5.8	0.08585 ± 1.3	546 ± 248	534 ± 49	531 ± 10	97
To44	0.0589 ± 1.6	0.6973 ± 2.0	0.08589 ± 1.3	563 ± 68	537 ± 17	531 ± 12	94
To17	0.0580 ± 1.2	0.6885 ± 1.8	0.08603 ± 1.3	531 ± 54	532 ± 15	532 ± 14	100
To44	0.0589 ± 1.6	0.6986 ± 2.0	0.08604 ± 1.3	563 ± 68	538 ± 17	532 ±	95
To35#	0.0581 ± 4.6	0.6921 ± 6.4	0.08634 ± 4.5	535 ± 200	534 ± 54	534 ± 11	100
To30#	0.0586 ± 5.9	0.7026 ± 6.0	0.08691 ± 1.3	553 ± 255	540 ± 51	537 ± 11	97
To50	0.0583 ± 1.1	0.7065 ± 1.6	0.08789 ± 1.2	541 ± 49	543 ± 13	543 ± 11	100
To19	0.0573 ± 1.7	0.6978 ± 2.2	0.08825 ± 1.4	505 ± 73	537 ± 18	545 ± 15	108
To33#	0.0583 ± 2.5	0.7155 ± 2.8	0.08908 ± 1.2	539 ± 109	548 ± 24	550 ± 12	102
To42	0.0597 ± 1.0	0.7340 ± 1.6	0.08915 ± 1.2	593 ± 45	559 ± 14	551 ± 11	93
To15	0.0588 ± 1.4	0.7241 ± 1.9	0.08925 ± 1.3	561 ± 60	553 ± 16	551 ± 14	98
To07	0.0592 ± 1.4	0.7321 ± 2.0	0.08965 ± 1.4	575 ± 59	558 ± 17	553 ± 15	96
To37	0.0578 ± 1.7	0.7163 ± 2.1	0.08985 ± 1.3	523 ± 73	549 ± 18	555 ± 12	106
To48#	0.0601 ± 6.1	0.7452 ± 6.3	0.08996 ± 1.3	606 ± 265	565 ± 55	555 ± 18	92
To13	0.0588 ± 1.0	0.7317 ± 1.7	0.09017 ± 1.3	562 ± 44	558 ± 15	557 ± 14	99
To27	0.0588 ± 1.2	0.7313 ± 1.8	0.09027 ± 1.3	558 ± 51	557 ± 15	557 ± 13	100
To08	0.0586 ± 1.5	0.7326 ± 2.0	0.09068 ± 1.4	552 ± 67	558 ± 17	560 ± 15	101
To38	0.0617 ± 1.1	0.7759 ± 1.7	0.09115 ± 1.3	665 ± 46	583 ± 15	562 ± 13	85
To05	0.0591 ± 1.7	0.7482 ± 2.1	0.09187 ± 1.3	569 ± 73	567 ± 18	567 ± 14	100
To21	0.0609 ± 1.6	0.7836 ± 2.9	0.09331 ± 2.4	636 ± 71	588 ± 26	575 ± 27	90
To52	0.0610 ± 1.5	0.8084 ± 1.9	0.09613 ± 1.2	639 ± 64	602 ± 17	592 ± 13	93
To28	0.0603 ± 1.0	0.8071 ± 1.7	0.09702 ± 1.3	616 ± 45	601 ± 15	597 ± 13	97
To11	0.0604 ± 1.0	0.8245 ± 1.6	0.09906 ± 1.3	617 ± 42	611 ± 15	609 ± 15	99
To47#	0.0612 ± 3.0	0.8560 ± 3.3	0.10136 ± 1.3	648 ± 128	628 ± 31	622 ± 12	96
To12#	0.0607 ± 4.7	0.8489 ± 4.9	0.10150 ± 1.4	627 ± 202	624 ± 46	623 ± 16	99
To02	0.0608 ± 1.7	0.8608 ± 2.1	0.10263 ± 1.3	633 ± 73	631 ± 20	630 ± 16	99
To10	0.0624 ± 2.1	0.9640 ± 2.5	0.11209 ± 1.4	687 ± 91	685 ± 25	685 ± 18	100
To45	0.0613 ± 2.1	0.9942 ± 2.4	0.11754 ± 1.2	651 ± 88	701 ± 24	716 ± 15	110
To14	0.0649 ± 1.0	1.1020 ± 1.6	0.12320 ± 1.3	770 ± 43	754 ± 17	749 ± 18	97
To51	0.1335 ± 0.6	7.5182 ± 1.3	0.40839 ± 1.2	2145 ± 20	2175 ± 23	2208 ± 40	103
To26	0.1355 ± 0.8	7.1694 ± 1.5	0.38383 ± 1.3	2170 ± 26	2133 ± 27	2094 ± 47	97
Sample Roblin (n=70)							
Rob58	0.0557 ± 1.2	0.4959 ± 1.6	0.06460 ± 1.1	439 ± 54	409 ± 11	404 ± 9	92
Rob16#	0.0548 ± 3.4	0.5012 ± 3.7	0.06634 ± 1.5	404 ± 151	413 ± 25	414 ± 12	103
Rob37	0.0567 ± 1.4	0.5414 ± 2.5	0.06930 ± 2.0	479 ± 64	439 ± 18	432 ± 17	90
Rob59#	0.0556 ± 3.3	0.5723 ± 3.5	0.07470 ± 1.1	435 ± 148	459 ± 26	464 ± 10	107
Rob67	0.0576 ± 1.6	0.5956 ± 1.9	0.07503 ± 1.0	513 ± 69	474 ± 14	466 ± 9	91
Rob17	0.0599 ± 1.8	0.6388 ± 2.4	0.07737 ± 1.5	599 ± 79	502 ± 19	480 ± 14	80
Rob47	0.0576 ± 1.3	0.6222 ± 2.4	0.07829 ± 2.0	516 ± 56	491 ± 19	486 ± 19	94
Rob43	0.0578 ± 1.3	0.6251 ± 2.4	0.07839 ± 2.0	524 ± 59	493 ± 19	487 ± 19	93

Table A12: Continuation.

Tab. A12: Fortsetzung.

	Isotopic ratios (1σ errors in %)			Apparent ages (2σ errors)			
spot	$^{207}Pb/^{206}Pb$ [a]	$^{207}Pb/^{235}U$ [b]	$^{206}Pb/^{238}U$ [c]	$^{207}Pb/^{206}Pb$	$^{207}Pb/^{235}U$	$^{206}Pb/^{238}U$	conc[d]
Sample Roblin (n=70)							
Rob04#	0.0575 ± 5.6	0.6227 ± 5.8	0.07847 ± 1.6	513 ± 245	492 ± 46	487 ± 15	95
Rob21	0.0595 ± 2.7	0.6474 ± 3.0	0.07896 ± 1.3	584 ± 119	507 ± 24	490 ± 12	84
Rob15	0.0579 ± 1.4	0.6572 ± 1.9	0.08229 ± 1.3	527 ± 61	513 ± 15	510 ± 13	97
Rob49	0.0578 ± 1.9	0.6562 ± 2.7	0.08231 ± 2.0	523 ± 82	512 ± 22	510 ± 20	97
Rob08	0.0585 ± 1.3	0.6697 ± 1.9	0.08301 ± 1.3	549 ± 58	521 ± 16	514 ± 13	94
Rob06	0.0575 ± 1.6	0.6826 ± 2.0	0.08603 ± 1.3	513 ± 69	528 ± 17	532 ± 13	104
Rob29	0.0591 ± 1.9	0.7058 ± 2.7	0.08663 ± 2.0	570 ± 81	542 ± 23	536 ± 21	94
Rob22	0.0609 ± 1.8	0.7286 ± 2.4	0.08681 ± 1.6	635 ± 79	556 ± 21	537 ± 16	85
Rob12	0.0592 ± 2.9	0.7106 ± 3.3	0.08703 ± 1.6	575 ± 124	545 ± 28	538 ± 17	94
Rob25#	0.0597 ± 4.4	0.7262 ± 4.6	0.08828 ± 1.3	591 ± 190	554 ± 40	545 ± 14	92
Rob57	0.0598 ± 1.6	0.7301 ± 1.8	0.08849 ± 0.8	598 ± 70	557 ± 15	547 ± 8	91
Rob09	0.0604 ± 2.6	0.7387 ± 2.9	0.08870 ± 1.3	618 ± 114	562 ± 25	548 ± 14	89
Rob60	0.0616 ± 2.4	0.7615 ± 2.6	0.08962 ± 0.9	661 ± 104	575 ± 23	553 ± 10	84
Rob44	0.0593 ± 1.2	0.7358 ± 2.4	0.08992 ± 2.0	580 ± 52	560 ± 21	555 ± 21	96
Rob40	0.0599 ± 2.3	0.7470 ± 3.0	0.09037 ± 2.0	602 ± 100	566 ± 26	558 ± 21	93
Rob23	0.0595 ± 2.0	0.7426 ± 2.4	0.09050 ± 1.3	586 ± 85	564 ± 21	558 ± 14	95
Rob45	0.0615 ± 2.6	0.7736 ± 3.3	0.09117 ± 2.0	658 ± 111	582 ± 29	562 ± 22	85
Rob11	0.0596 ± 1.3	0.7618 ± 1.8	0.09276 ± 1.3	588 ± 57	575 ± 16	572 ± 14	97
Rob39#	0.0600 ± 4.5	0.7705 ± 5.0	0.09307 ± 2.0	605 ± 196	580 ± 45	574 ± 22	95
Rob10	0.0596 ± 1.2	0.7774 ± 1.7	0.09454 ± 1.3	590 ± 51	584 ± 15	582 ± 14	99
Rob55	0.0607 ± 1.7	0.7965 ± 2.0	0.09512 ± 1.0	630 ± 72	595 ± 18	586 ± 11	93
Rob35	0.0597 ± 0.9	0.7877 ± 2.3	0.09567 ± 2.1	593 ± 40	590 ± 21	589 ± 24	99
Rob73#	0.0595 ± 4.0	0.7936 ± 4.1	0.09680 ± 0.8	584 ± 175	593 ± 37	596 ± 9	102
Rob18	0.0624 ± 1.4	0.8469 ± 1.9	0.09842 ± 1.3	688 ± 59	623 ± 18	605 ± 15	88
Rob36#	0.0605 ± 6.7	0.8222 ± 7.0	0.09859 ± 2.0	621 ± 288	609 ± 65	606 ± 23	98
Rob13	0.0619 ± 1.3	0.8537 ± 1.8	0.10008 ± 1.3	669 ± 55	627 ± 17	615 ± 15	92
Rob74#	0.0589 ± 4.4	0.8244 ± 4.5	0.10146 ± 0.9	565 ± 193	611 ± 42	623 ± 11	110
Rob05#	0.0601 ± 5.3	0.8474 ± 5.4	0.10228 ± 1.3	607 ± 228	623 ± 51	628 ± 16	103
Rob63	0.0607 ± 0.9	0.8644 ± 1.3	0.10333 ± 0.9	628 ± 40	633 ± 12	634 ± 11	101
Rob72#	0.0611 ± 1.2	0.8849 ± 1.6	0.10506 ± 1.2	642 ± 50	644 ± 15	644 ± 15	100
Rob38	0.0611 ± 1.9	0.8913 ± 2.8	0.10584 ± 2.0	642 ± 83	647 ± 27	649 ± 25	101
Rob32#	0.0604 ± 4.0	0.8949 ± 4.6	0.10737 ± 2.2	620 ± 172	649 ± 45	657 ± 28	106
Rob68#	0.0606 ± 5.7	0.9009 ± 5.8	0.10783 ± 1.1	625 ± 247	652 ± 57	660 ± 14	106
Rob27	0.0620 ± 1.5	0.9527 ± 2.5	0.11139 ± 2.0	675 ± 62	680 ± 25	681 ± 26	101
Rob19#	0.0600 ± 2.6	0.9243 ± 3.0	0.11163 ± 1.4	605 ± 113	665 ± 29	682 ± 18	113
Rob41	0.0652 ± 1.9	1.0213 ± 2.7	0.11360 ± 2.0	781 ± 80	715 ± 28	694 ± 26	89
Rob02	0.0617 ± 1.2	0.9801 ± 1.7	0.11527 ± 1.2	662 ± 51	694 ± 17	703 ± 16	106
Rob62#	0.0892 ± 0.8	2.8932 ± 1.0	0.23531 ± 0.7	1408 ± 30	1380 ± 15	1362 ± 17	97
Rob51	0.1006 ± 0.8	3.7703 ± 2.1	0.27184 ± 2.0	1635 ± 29	1586 ± 34	1550 ± 55	95
Rob52#	0.1192 ± 0.7	5.1672 ± 2.1	0.31440 ± 2.0	1944 ± 23	1847 ± 36	1762 ± 62	91
Rob42#	0.1205 ± 1.3	5.8194 ± 3.5	0.35035 ± 3.2	1963 ± 48	1949 ± 62	1936 ± 107	99

Table A12: Continuation.

Tab. A12: Fortsetzung.

	Isotopic ratios (1σ errors in %)			Apparent ages (2σ errors)			
spot	$^{207}Pb/^{206}Pb$ [a]	$^{207}Pb/^{235}U$ [b]	$^{206}Pb/^{238}U$ [c]	$^{207}Pb/^{206}Pb$	$^{207}Pb/^{235}U$	$^{206}Pb/^{238}U$	conc[d]
Sample Roblin (n=70)							
Rob24	0.1208 ± 1.1	5.8166 ± 1.7	0.34926 ± 1.3	1968 ± 39	1949 ± 30	1931 ± 43	98
Rob31	0.1230 ± 0.8	6.2381 ± 2.1	0.36774 ± 1.9	2001 ± 30	2010 ± 37	2019 ± 66	101
Rob20#	0.1240 ± 1.6	6.2284 ± 2.1	0.36417 ± 1.4	2015 ± 57	2008 ± 37	2002 ± 48	99
Rob07	0.1275 ± 0.9	6.5678 ± 1.6	0.37349 ± 1.3	2064 ± 32	2055 ± 28	2046 ± 46	99
Rob75#	0.1275 ± 0.9	6.4036 ± 1.3	0.36414 ± 0.9	2064 ± 30	2033 ± 23	2002 ± 31	97
Rob54#	0.1286 ± 0.9	6.0111 ± 1.2	0.33906 ± 0.7	2079 ± 32	1977 ± 21	1882 ± 23	91
Rob01	0.1299 ± 0.7	6.8158 ± 1.5	0.38050 ± 1.3	2097 ± 26	2088 ± 27	2079 ± 46	99
Rob34#	0.1308 ± 0.5	7.4046 ± 2.1	0.41070 ± 2.1	2108 ± 18	2162 ± 38	2218 ± 79	105
Rob53	0.1310 ± 0.8	6.7122 ± 1.3	0.37163 ± 1.0	2111 ± 28	2074 ± 23	2037 ± 35	96
Rob33#	0.1319 ± 0.4	7.3127 ± 2.0	0.40218 ± 2.0	2123 ± 15	2150 ± 36	2179 ± 74	103
Rob65	0.1324 ± 0.7	6.2929 ± 1.3	0.34483 ± 1.1	2129 ± 26	2017 ± 23	1910 ± 36	90
Rob28#	0.1355 ± 1.4	7.6912 ± 2.7	0.41182 ± 2.3	2170 ± 50	2196 ± 49	2223 ± 87	102
Rob66	0.1364 ± 0.5	7.7999 ± 1.0	0.41483 ± 0.8	2182 ± 19	2208 ± 18	2237 ± 30	103
Rob71	0.1395 ± 0.7	7.3786 ± 1.0	0.38348 ± 0.7	2222 ± 23	2158 ± 18	2093 ± 25	94
Rob69#	0.1566 ± 0.9	8.7057 ± 1.4	0.40306 ± 1.1	2420 ± 30	2308 ± 26	2183 ± 41	90
Rob70	0.1620 ± 0.6	10.5151 ± 1.1	0.47086 ± 1.0	2476 ± 21	2481 ± 21	2487 ± 41	100
Rob14	0.1771 ± 0.4	12.4772 ± 1.3	0.51110 ± 1.3	2625 ± 13	2641 ± 25	2661 ± 57	101
Rob61	0.1800 ± 0.3	10.4803 ± 1.3	0.42238 ± 1.2	2652 ± 11	2478 ± 24	2271 ± 46	86
Rob78	0.1858 ± 0.6	13.2796 ± 1.1	0.51825 ± 1.0	2706 ± 19	2700 ± 21	2692 ± 44	99
Rob48	0.2298 ± 0.4	18.7656 ± 2.2	0.59229 ± 2.1	3051 ± 12	3030 ± 43	2999 ± 101	98
Rob46	0.2521 ± 0.6	20.4802 ± 2.2	0.58918 ± 2.1	3198 ± 19	3114 ± 43	2986 ± 101	93

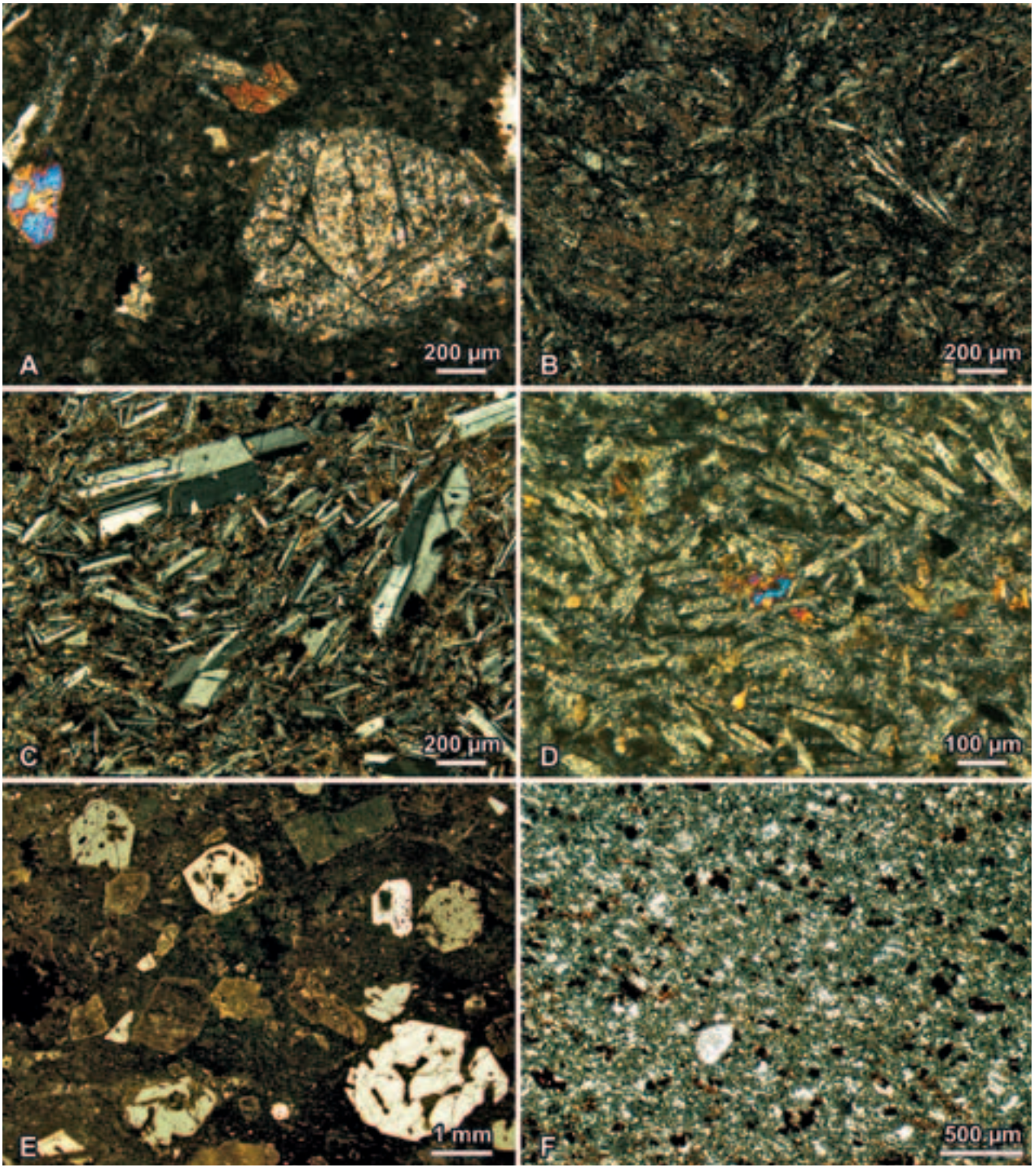
A
200 µm
B
200 µm
C
200 µm
D
100 µm
E
1 mm
F
500 µm

GEOLOGICA SAXONICA
Journal of Central European Geology 54 (2008) 1–168

Plate 1: Photomicrographs of Neoproterozoic and Upper Cambrian volcanic rocks.

Tafel 1: Tafel I: Dünnschliff-Fotos von neoproterozoischen und oberkambrischen vulkanischen Gesteinen.

Neoproterozoic tholeiitic basaltoids from the Kralupy-Zbraslav Group. A: Differently strong altered (micro)phenocrysts (pyroxene, plagioclase) within devitrified matrix. Sample DB1/0, XPL. **B**: Fine-grained rock with tiny plagioclase laths in intensely altered groundmass. Sample DB6/12, XPL.

Upper Cambrian andesites of the Křívoklát-Rokycany volcanic complex. C: Plagioclase (micro)phenocrysts within fine-grained groundmass composed of plagioclase, opaque substance and submicroscopic phases. Sample DB1/17, XPL. **D**: Altered plagioclase and pyroxene. Sample DB1/23, XPL.

Upper Cambrian rhyolites of the Křívoklát-Rokycany volcanic complex. E: Porphyritic rhyolite with large quartz phenocrysts showing effects of resorption as well as strongly kaolinitised or sericitised orthoclase and plagioclase phenocrysts. Sample OKR, XPL. **F**: Fine-grained rhyolite with feldspar microphenocryst and common hematite. Sample DB1/22, XPL.

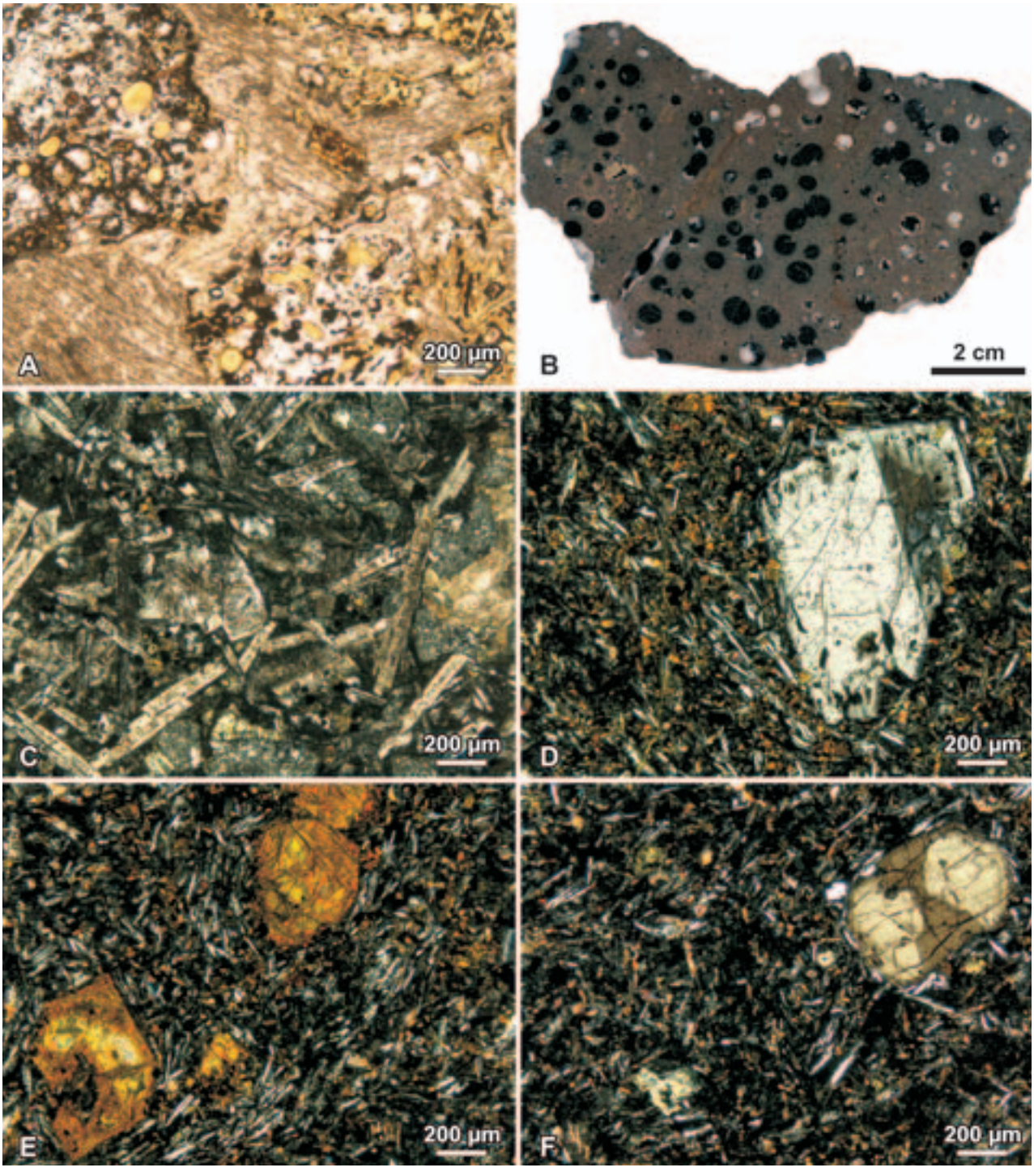
A
200 µm
B
2 cm
C
200 µm
D
200 µm
E
200 µm
F
200 µm

Plate II: Photomicrographs and hand specimen of Ordovician and Silurian volcanics.

Tafel II: Dünnschliff-Fotos und Handstück von ordovizischen und silurischen vulkanischen Gesteinen.

Lower/Middle Ordovician alkaline basaltoids of the Komárov volcanic complex. A: Brecciated rock with angular fragments of scoriaceous lava in carbonate matrix. Sample KoZe4, LPL. **B**: Hand specimen of amygdaloidal basalt. Amygdales are filled with carbonate and/or chlorite. Sample KoZe, hand specimen.

Upper Ordovician trachyandesite. C: Rock with intersertal texture consisting of altered alkali-feldspar and plagioclase within chlorite-carbonate matrix. Sample Carad2, XPL.

Silurian alkali-basalt. D to **E**: Sample Loden1. XPL – **D**: Plagioclase phenocryst showing effects of resorption within a matrix composed of plagioclase, pyroxene and other phases. **E**: Completely altered phenocrysts of olivine and pyroxene. Matrix grains are aligned around phenocrysts. **F**: Pyroxene with sector zoning.

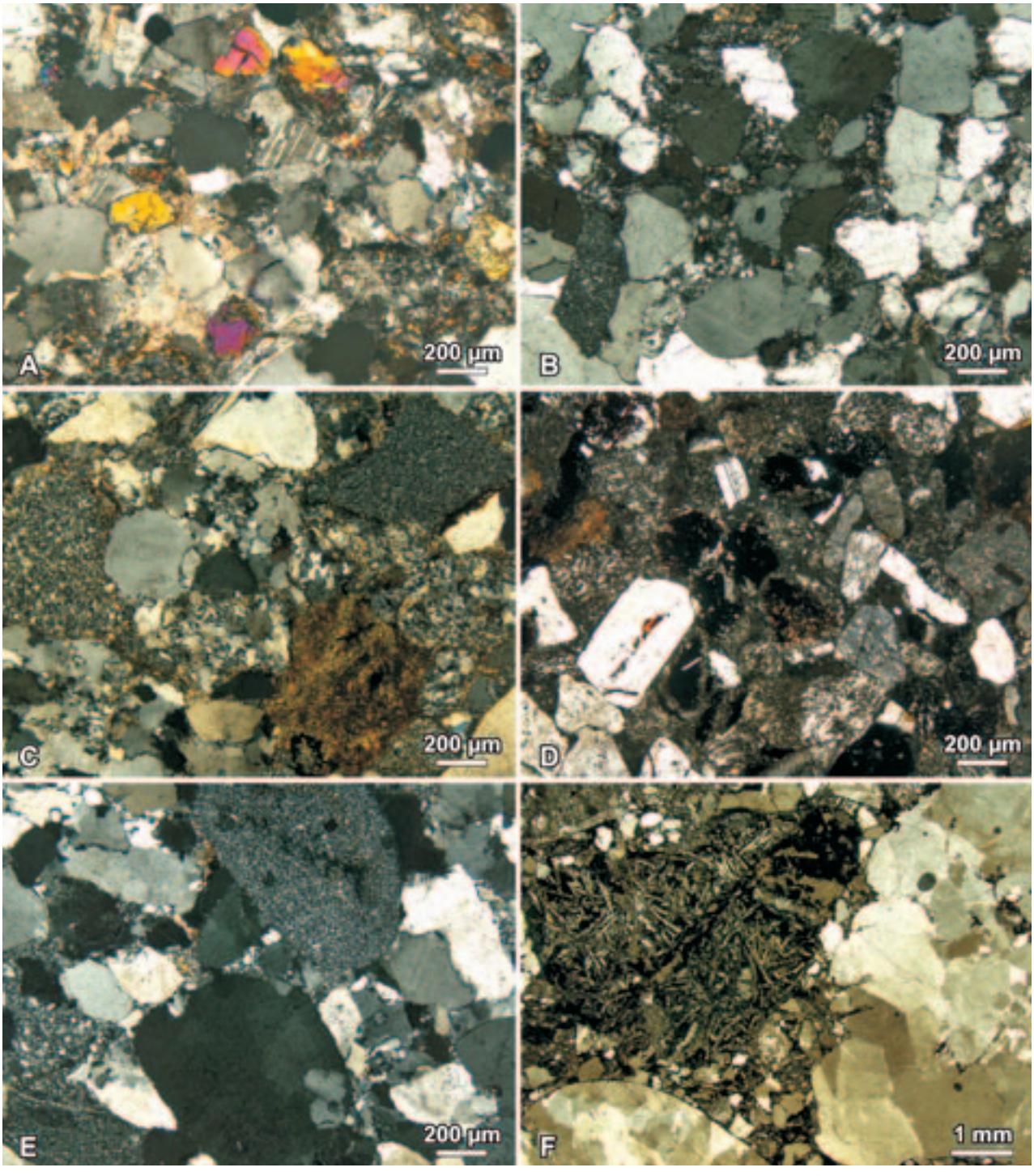
A
200 µm
B
200 µm
C
200 µm
D
200 µm
E
200 µm
F
1 mm

GEOLOGICA SAXONICA
Journal of Central European Geology 54 (2008) 1–168

Plate III: Photomicrographs of Cambrian sedimentary rocks.

Tafel III: Dünnschliff-Fotos von kambrischen sedimentären Gesteinen.

A: Fine-grained sandstone composed of quartz, orthoclase, plagioclase, and transparent heavy minerals. The matrix may be carbonaceous (bottom left) or detrital (top right). Sample DB2-3, Sádek Formation, XPL. **B**: Quartzose sandstone being composed of mono- and polycrystalline quartz, chert and a low proportion of detrital matrix. Arrows indicate beginning reprecipitation of quartz. Sample SH2, Holšíny-Hořice Formation, XPL. **C**: Coarse-grained sandstone containing fragments of chert (top right), altered volcanic rocks (bottom right, left side), quartz, and detrital matrix. Sample MM11, Klouček-Čenkov Formation, XPL. **D**: Sandstone almost entirely composed of volcanic detritus that is represented by feldspars and volcanic rock fragments. Sample CT3, Klouček-Čenkov Formation, XPL. **E**: Highly mature sandstone being made up by quartz and chert. Sample DB2/0, Jince Formation, XPL. **F**: Conglomerate containing stable (e.g., polycrystalline quartz - right, bottom left) and unstable (e.g., fragment of mafic volcanic rock – top right) clasts. Sample DB1/9, Jince Formation, XPL.

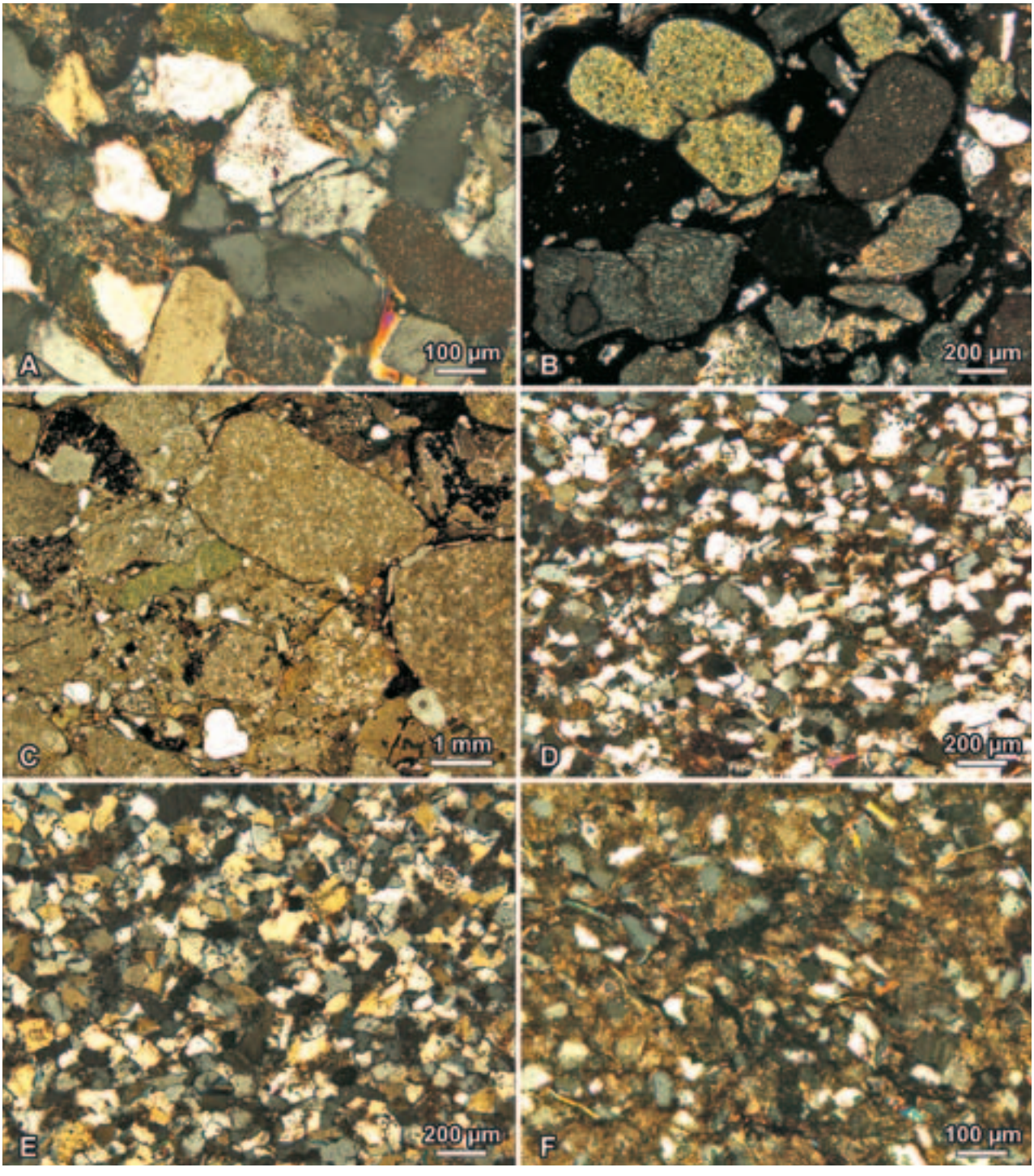
A
100 µm
B
200 µm
C
1 mm
D
200 µm
E
200 µm
F
100 µm

Plate IV: Photomicrographs of Ordovician sedimentary rocks.

Tafel IV: Dünnschliff-Fotos von ordovizischen sedimentären Gesteinen.

A: Sandstone containing quartz, groundmass fragments of volcanic rocks (v), and glauconite (g). Sample TrJi1, Třenice Formation, XPL. **B**: Sandstone with quartz, glauconite (g), volcanic rock fragments (v), quartz and a tectonite clast showing microcrenulation (t). Sample KlBoA, Klabava Formation, XPL. **C**: Conglomerate being composed of groundmass fragments of silicic volcanics (v), quartz, altered feldspar, and glauconite (g). Sample KlMU1, Klabava Formation, XPL. **D**: Highly mature fine-grained sandstone with large proportions of mono-crystalline quartz and a distinct amount of detrital white mica. Sample DoSP4, Dobrotivá Formation, XPL. E: Sandstone consisting almost entirely of monocrystalline quartz. Note the shape of the quartz grains that resulted from re-crystallisation. Sample LiBS3, Libeň Formation, XPL. **F**: Siltstone with carbonaceous matrix. Grains comprise quartz, plagioclase and white mica. Sample LeZb15, Letná Formation, XPL.

GEOLOGICA SAXONICA
Journal of Central European Geology

Hinweise für Autoren

Allgemeine Hinweise

Die Zeitschrift *Geologica Saxonica* veröffentlicht Originalarbeiten vorzugsweise in deutscher und englischer Sprache aus dem Gesamtbereich der Geologie. Als Artikel (Articles) werden längere wissenschaftliche Abhandlungen von regionaler oder überregionaler Bedeutung publiziert. Kurzmitteilungen (Short Communications) dienen der schnellen Publikation vorläufiger wissenschaftlicher Ergebnisse, Fundmitteilungen, Aufschlußbeschreibungen etc. Es wird ausdrücklich eingeladen, publizierte wissenschaftliche Beiträge unter Diskussionen (Discussions) zu referieren.

Die Manuskripte werden nur dann veröffentlicht, wenn sie in der eingereichten Form oder ähnlicher Fassung nicht anderwärts erschienen sind oder erscheinen werden. Nach Drucklegung stehen die Beiträge unter dem Copyright der *Geologica Saxonica*. Die in der *Geologica Saxonica* publizierten Arbeiten sind im Sinne der „Berliner Erklärung" (http://idw-online.de/pages/de/news193869) über das Internet unter der Adresse http://www.geologica-saxonica.de kostenfrei zugänglich.

Manuskriptabgabe

Manuskripte und alle Korrespondenz die Zeitschrift betreffend sind an den Schriftleiter zu richten: Dr. Jan-Michael Lange, Staatliche Naturhistorische Sammlungen Dresden, Museum für Mineralogie und Geologie, Königsbrücker Landstraße 159, D-01109 Dresden, Telefon: +49-351-8926403, Telefax: +49-351-8926404, E-Mail: editor@geologica-saxonica.de. Das Manuskript ist in elektronischer Form (CD) und als Papierausdruck in vierfacher Ausfertigung einzureichen.

Begutachtung

Alle eingereichten Manuskripte werden vor der Drucklegung begutachtet. Die Gutachter werden von der Schriftleitung bestellt. Vorschläge seitens des/der Verfasser können berücksichtigt werden.

Sprache

Manuskripte können in deutscher und englischer Sprache eingereicht werden. Veröffentlichungen in anderen Sprachen sind mit der Schriftleitung vor der Einreichung abzustimmen. Bei deutschsprachigen Arbeiten sind folgende Manuskriptteile in englischer Übersetzung beizufügen: Titel, Kurzfassung, Abbildungs-, Tabellen- und Tafelerläuterungen. Für englischsprachige Texte wird eine deutsche Übersetzung der vorgenannten Teile empfohlen.

Manuskriptgestaltung

Die Beiträge sind nach den Empfehlungen von Horatschek& Schubert (1998): „Richtlinie für die Verfasser geowissenschaftlicher Veröffentlichungen" (ISBN 3510-95820-9) abzufassen. Manuskripte, die nicht den redaktionellen Anforderungen entsprechen, werden zurückgewiesen.

Umfang

Als Artikel eingereichte Veröffentlichungen sollten 20 Druckseiten (etwa 40 A4-Seiten, doppelzeilig geschrieben in Times12) nicht überschreiten. Kurzmitteilungen und Diskussionen sind auf drei Druckseiten (etwa 6 A4-Seiten, doppelzeilig, Times12) beschränkt.

Aufbau

Es wird empfohlen den Aufbau des Manuskriptes wie folgt zu gliedern: Jeweils auf gesonderten Seiten beginnend:

1. Titel/Title – Name – Anschrift
2. Kurzfassung/Abstract
3. Text (gegliedert in Einleitung/Introduction – Methodik/Methods – Ergebnisse/Results – Zusammenfassung/Summary) – Danksagung/Acknowledgements
4. Schriftenverzeichnis/References
5. Abbildungen
6. Tabellen
7. Tafeln

Titel: Kurz, aber bezeichnend! Bei deutschsprachigen Aufsätzen ist eine Übersetzung des Titels in englischer Sprache beizufügen.
Name: Erbeten wird die vollständige Angabe von Vor- und Zuname. Weitere Vornamen können abgekürzt werden (z. B. Markus M. Mustermann). Anschrift: Vollständige postalische Anschrift (Institution – Straße – Postleitzahl (incl. Länderkürzel) – Ort – Land) und wenn möglich auch E-Mail-Adresse. Kurzfassung: Kurze und klare Zusammenfassung der Problemstellung, Methoden, Ergebnisse und Schlußfolgerungen der Publikation. Der Umfang sollte 200 Wörter nicht zu übersteigen. Bei einer deutschsprachigen Publikation ist der Kurzfassung eine englische Übersetzung (Abstract) hinzuzufügen.

Formatierungen

Akzeptiert werden Manuskripte in gängigen Dateiformaten (Texte: z. B. Microsoft Word; Graphiken: Microsoft PowerPoint, CorelDraw, Adobe Illustrator sowie als TIFF-, JPEG-, GIF- oder PDF-Format. Harte Umbrüche innerhalb eines

Absatzes und Silbentrennungen sind zu vermeiden. Der Papierausdruck (Hardcopy) ist einseitig bedruckt und in doppeltem Zeilenabstand vorzulegen. Der Randabstand darf in allen Richtungen 2,5 cm nicht unterschreiten.

Fußnoten

Fußnoten sollten nach Möglichkeit vermieden werden.

Zitate im Text

Im Text werden Zitate mit Autorname, Jahreszahl und ggf. Fundstelle des Zitates gekennzeichnet. Zwei Autorennamen werden durch „&" verbunden. Drei und mehr Autorennamen können durch Angabe des ersten Autorennamens und dem Zusatz „et al." verkürzt werden.

Zitate im Schriftenverzeichnis

Im Schriftenverzeichnis sind alle im Text zitierten Arbeiten – und nur diese – aufzuführen. Das Verzeichnis ist in alphabetischer und chronologischer Reihenfolge zu erstellen. Abweichend von den Richtlinien nach Horatschek & Schubert (1998) gelten folgende Zitierrregeln:

Einzelwerke (Monographien): Name – Komma – Vorname (Initial) – Punkt – (eventuell weitere Autoren) – Jahr (in Klammern) – Doppelpunkt – Titel – Punkt – Gedankenstrich – Erste Seiten – Gedankenstrich – Letzte Seite – Komma – Verlagsort – Verlag (in Klammern) – Punkt.

Kapitel in Sammelwerken: Name – Komma – Vorname (Initial) – Punkt – (eventuell weitere Autoren) – Jahr (in Klammern) – Doppelpunkt – Titel – Punkt – Gedankenstrich – „In" – Doppelpunkt – Name – Komma – Vorname (Initial) – Punkt – (eventuell weitere Autoren) – „Ed." bzw. „Eds." (in Klammern) – Doppelpunkt – Titel des Sammelwerkes – Punkt – Gedankenstrich – Erste Seiten – Gedankenstrich – Letzte Seite – Komma – Verlagsort – Verlag (in Klammern) – Punkt.

Zeitschriftenartikel: Name – Komma – Vorname (Initial) – Punkt – (eventuell weitere Autoren) – Jahr (in Klammern) – Doppelpunkt – Titel – Punkt – Gedankenstrich – Zeitschrift (abgekürzt) – Komma – Bandzahl bzw. Jahrgang (in Fettdruck) – Doppelpunkt – Erste Seiten – Gedankenstrich – Letzte Seite – Komma – Verlagsort – Punkt.

Karten: Name – Komma – Vorname (Initial) – Punkt – (eventuell weitere Autoren) – Jahr (in Klammern) – Doppelpunkt – Titel der Karte (mit Angabe des Maßstabes, Blattnummer und -name) – Punkt – Gedankenstrich – (eventuell Nummer der Auflage – Komma) – Herausgeber – Komma – Verlagsort – Punkt.

Enthält die Karte keine Autorennamen gilt folgende Zitierweise: Titel der Karte (mit Angabe des Maßstabes, Blattnummer und -name) – Jahr (in Klammern) – Punkt – Gedankenstrich – (eventuell Nummer der Auflage – Komma) – Herausgeber – Komma – Verlagsort – Punkt.

Abbildungen, Tafeln und Tabellen

In den laufenden Text eingefügte Graphiken oder Fotos werden als Abbbildungen (Abb.) geführt. Bildliche Darstellungen auf Tafeln werden als Figuren (Fig.) oder Profile (Profil) bezeichnet. Jede Tafel wird mit Fig./Profil 1 beginnend numeriert.

Alle Abbildungen, Tabellen und Tafeln sind auf separaten Blättern einzureichen. Auf der Rückseite sind Autorenname, Nummer und ggf. eine Pfeilmarkierung „oben" anzugeben. Elektronisch eingereichte Darstellungen sind unbedingt durch einen Ausdruck zu ergänzen.

Bei der Anfertigung der Abbildungen, Tabellen und Tafeln ist der Satzspiegel (16,8 × 21,3 cm) zu beachten. Abbildungen und Tabellen im laufenden Text können auch in Spaltenbreite (8,2 cm) gesetzt werden. Im Manuskript ist ihre ungefähre Position anzugegeben.

Graphiken (Strichzeichnungen) sind als Tuschezeichnung oder Computerausdruck einzureichen. Bei der Wahl von Strichstärke und Schriftgröße sind eventuell nachfolgende Verkleinerungen zu beachten. Scans von Strichzeichnungen sollten eine Auflösung von 600 dpi nicht unterschreiten

Fotos sind als kontrastreiche und scharfe Abzüge einzureichen. Akzeptiert werden Diapositive oder Hochglanzabzüge im Format 13 × 18 cm. Für Scans von Fotos beträgt die optimale Auflösung etwa 300 dpi.

Kosten für Farbabbildungen, Falttafeln und größere Tabellen können dem/den Autor/en in Rechnung gestellt werden.

Autorensonderdrucke

Von den in der Geologica Saxonica publizierten Beiträgen werden dem/den Autor/en insgesamt 50 Sonderdrucke kostenfrei zur Verfügung gestellt. Zusätzliche Sonderdrucke werden in Rechnung gestellt. Darüberhinausgehenden Honorarforderungen kann nicht entsprochen werden.